Spring 5-9-2016

Biochemical and Biophysical Studies of Heme Binding Proteins from the Corynebacterium diphtheriae and Streptococcus pyogenes Heme Uptake Pathways

Elizabeth B. Draganova

BIOCHEMICAL AND BIOPHYSICAL STUDIES OF HEME BINDING PROTEINS FROM THE *CORYNEBACTERIUM DIPHTHERIAE* AND *STREPTOCOCCUS PYOGENES* HEME UPTAKE PATHWAYS

by

ELIZABETH DRAGANOVA

Under the Direction of Dabney Dixon, PhD

ABSTRACT

The Gram-positive pathogens *Corynebacterium diphtheriae* and *Streptococcus pyogenes* both require iron for survival. These bacteria have developed sophisticated heme uptake and transport protein machinery responsible for the import of iron into the cell, in the form of heme from the human host. The heme utilization pathway (hmu) of *C. diphtheriae* utilizes multiple proteins to bind and transport heme into the cell. One of these proteins, HmuT, delivers heme to the ABC transporter HmuUV. The axial ligation of the heme in HmuT was probed by examination of wild-type HmuT and a series of conserved heme pocket residue mutants, H136A, Y235A, R237A, Y272A, M292A, Y349A, and Y349F. Characterization by UV-visible

absorption, resonance Raman, and magnetic circular dichroism spectroscopies indicated that H136 and Y235 are the axial ligands in HmuT. Electrospray ionization mass spectrometry was also utilized to assess the roles of conserved residues in contribution to heme binding.

The *S. pyogenes* streptococcal iron acquisition (sia)/heme transport system (hts) utilizes multiple proteins to bring host heme to the intracellular space. Both the substrate binding protein SiaA and the hemoprotein surface receptor Shr were investigated. The kinetic effects on SiaA heme release were probed through chemical unfolding of axial ligand mutants M79A and H229A, as well mutants thought to contribute to heme binding, K61A and C58A, and a control mutant, C47A. The unfolding pathways showed two processes for protein denaturation. This is consistent with heme loss from protein forms differing by the orientation of the heme in the binding pocket. The ease of protein unfolding is related to the strength of interaction of the residues with the heme.

Shr contains two NEAT (near-iron transporter) domains (Shr-N1 and Shr-N2) which can both bind heme. Biophysical studies of both Shr-N1 and Shr-N2 indicated a new class of NEAT domains which utilize methionine as an axial ligand, rather than a tyrosine. Thermal and chemical unfolding showed ferrous Shr-N1 and Shr-N2 to be most resistant to denaturation. Shr-N2 was prone to autoreduction. Together, sequence alignment, homology modeling, and spectral signatures are all consistent with two methionines as the heme ligands of this novel type of NEAT heme-binding domain.

INDEX WORDS: Heme, Heme uptake, Heme transfer, Unfolding, Axial ligand, Denaturation, UV-visible absorption spectroscopy, Resonance Raman spectroscopy

BIOCHEMICAL AND BIOPHYSICAL STUDIES OF HEME BINDING PROTEINS FROM THE *CORYNEBACTERIUM DIPHTHERIAE* AND *STREPTOCOCCUS PYOGENES* HEME UPTAKE PATHWAYS

by

ELIZABETH DRAGANOVA

A Dissertation Submitted in Partial Fulfillment of the Requirements for the Degree of

Doctor of Philosophy

in the College of Arts and Sciences

Georgia State University

2016

BIOCHEMICAL AND BIOPHYSICAL STUDIES OF HEME BINDING PROTEINS FROM THE *CORYNEBACTERIUM DIPHTHERIAE* AND *STREPTOCOCCUS PYOGENES* HEME UPTAKE PATHWAYS

by

ELIZABETH DRAGANOVA

Committee Chair: Dabney Dixon

Committee: Giovanni Gadda

Markus Germann

Electronic Version Approved:

Office of Graduate Studies

College of Arts and Sciences

Georgia State University

May 2016

DEDICATION

I dedicate this dissertation to my loving and intelligent husband Alexander Draganov who has stood by my side and helped me complete this journey.

ACKNOWLEDGEMENTS

Much love goes out to my family, especially my father, James William Bennett, my mother and stepfather, Nancy and Jeff Ingram, and sister, Emily Bennett, who have each helped shape me into the person I am today. Their sacrifices and hard work to provide me with a life in which not all people get to have is why I have had the drive and perseverance to achieve this dream of mine. Knowing all of you believe in me keeps me going, even when I want to give up.

There are not enough words in the English language to express how sincerely grateful I am for my advisor, mentor, and friend, Dr. Dabney W. Dixon. Her guidance and support has led me to do great things during my career at Georgia State University; things that I never imagined myself accomplishing before my time here. Her belief in my abilities as a scientist and a teacher has always been, and will continue to be, the driving force for my next steps in my career.

I would also like to thank my dissertation committee members, Dr. Giovanni Gadda and Dr. Markus Germann for their advice and expertise throughout the completion of my degree. Additionally, I would like to thank my qualification exam committee members: Dr. Binghe Wang, Dr. Giovanni Gadda, and Dr. Ivano Ivanov.

The work in our lab would not have been possible without our hard working collaborators. Many thanks go out to Dr. Kenton Rodgers, Dr. Gudrun Lukat-Rodgers, and their PhD student Seth Adrian at North Dakota State University for their long hours of hard work completing the resonance Raman and time spent on the phone discussing our work; I learned an amazing amount from those conversations. I would also like to thank our MCD collaborators at the University of South Carolina, Dr. John Dawson and Dr. Daniel Collins. Not only did Dan give me science advice, but also teaching and life advice which I will never forget!

Lastly, but not least, I would like to thank the many friends I am grateful to have surrounding me. Graduate school would not have been the same without Crystal, Rizvan, Jalisa, Sarah Laughlin-Toth, Sarah Zingales, Zeus, and Tyler. Each of you helped me through this journey in one way or another and I am forever grateful! To current and previous lab members, you made working in the lab an enjoyable experience. To my undergraduate students I have had the pleasure of mentoring (Brandford, Stephanie, Briana, Cyrianne, Tiffany, and Andrea); I will never forget you as each of you hold a special place in my heart. Each of you taught me something about myself and I wish you all the successes in life, although I have no doubt you will each achieve everything you set your mind to. Endless thanks to Nydia, Katie, KP, Josh, Susie, and Keri for cheering me on from back home. We have been through so much and have so much more to do in life; you all are my support system!

TABLE OF CONTENTS

LIST OF TABLES

LIST OF FIGURES

1 INTRODUCTION

1.1 Iron and Heme in Bacteria

Iron is an essential nutrient for the majority of living organisms to survive *(1, 2)*. This element is found in the ferric and ferrous oxidation states when at standard physiological conditions. The broad redox potential of iron allows for iron-bound proteins to play a diverse role in biological processes such as energy transducing pathways, gene regulation, and dioxygen transport *(3)*. Ferrous iron is soluble at physiological pH, unlike ferric iron, and can undergo Fenton chemistry which converts ferrous iron and hydrogen peroxide to ferric iron and reactive oxygen species *(1, 4, 5)*. Excess free iron in the cell results in a buildup of reactive species which attacks various cellular components and lead to oxidative damage to the cell *(3, 6)*. Nature has overcome this problem by placing iron in a protoporphyrin IX ring, thus creating the macromolecule heme *(3, 7)*. Commonly, human host heme is bound to proteins such as myoglobin (Mb), hemoglobin (Hb), haptoglobin (Hp), and hemopexin *(1, 2, 6)*. As a result, bacteria have developed various strategies to either synthesize heme or take up the host heme into the bacterial cytoplasm to be used as a nutritional source. It has also been shown that some bacterial species utilize both strategies *(8)*. Pathogenic bacteria which rely on heme uptake have developed sophisticated machinery to obtain the heme using proteins in their cellular membranes *(4, 5, 9)*.

1.2 ABC Tranporters

ABC transporters make up a class of integral membrane proteins that utilize energy provided by ATP to pump various compounds across cellular membranes *(10-12)*. These proteins are found in a wide variety of organisms and participate in import and export mechanisms required for survival of the cell. ABC transporters are found in both prokaryotic

and eukaryotic cells *(12)*. In prokaryotes, the transporter is generally located at the plasma membrane with ATP hydrolysis on the cytoplasmic side. Eukaryotes also have ABC transporters in organellar membranes.

A general ABC transporter is made of two transmembrane (TM) modules and two ATP-binding cassettes [otherwise known as nucleotide binding domains (NBDs)]. Import type ABC transporters are commonly found in prokaryotic systems and are responsible for bringing nutrients, sugars, and amino acids into the cell *(13)*. Importers contain a substrate binding protein which brings the substrate to the ABC transporter *(11, 13)*. The importer TM modules and ATP-binding cassette domains are generally encoded on different genes *(11)*. Exporters are commonly found in eukaryotic systems, and in some prokaryotic systems, and are responsible for pumping out drugs and toxins from the intracellular space *(13)*. Unlike importers, exporter functional domains are encoded on a single gene *(10, 13, 14)*.

Currently, four classes of ABC transporters have been identified based on TMD fold *(12)*. Three of the four classes are importers which are found only in prokaryotes: Type I, Type II, and energy coupling factor (ECF) transporters (also referred to as Type III transporters). The fourth class is the exporter fold which is identified in all characterized exporters to date and is found in both prokaryotes and eukaryotes. Type I and II importers rely on SBDs to bring the substrate to the TMDs. In some instances, the SBD is fused to the TMD. Although differences exist in regards to overall fold of these importers, bacterial heme uptake pathways rely on ABC importers to deliver heme to the cell *(2, 3, 9)*.

1.3 Gram-negative Heme Uptake Pathways

Heme uptake systems exist in both Gram-negative and Gram-positive bacteria and many reviews have been written on the subject *(2, 3, 5, 15-17)*. Due to structural differences between

the two types of bacteria, these pathogens have developed different strategies to bring heme to the intracellular space using protein shuttles including ABC importers. The most widely studied group of pathogenic heme uptake pathways are that of Gram-negative bacteria *(5)*. These pathogens must transport heme through the outer membrane (OM) to the periplasmic space and then through the periplasmic membrane to reach the intracellular space *(2, 3)*. Two types of heme uptake systems have been identified for Gram-negative bacteria: hemophore secretion and direct binding of host heme to OM receptors *(15)*.

1.3.1 Hemophore-mediated heme uptake

Two types of hemophore systems have been identified in Gram-negative bacteria: *has* (*heme acquisition system)* and *hxu* (*heme/hemopexin utilization*) *(2, 17, 18)*. Multiple bacterial species have shown to utilize the *has* system including *Yersinia pestis, Serratia marcescens, Yersinia enterolitica, Pseudomonas aeruginosa,* and *Pseudomonas fluorescens*. The *has* operon encodes for multiple proteins and includes the hemophore HasA, which is secreted from the cell, scavenges heme from Hb, and delivers it to the OM receptor HasR. HasA from *S. marcescens* and *P. aeruginosa* bind heme utilizing a histidine/tyrosine binding motif (H32/Y75) while *Y. pestis* HasA uses a single tyrosine (Y75) to bind the heme in a pentacoordinate fashion. In all species of characterized HasA, studies have shown an additional conserved histidine (H83) which hydrogen-bonds to the axial tyrosine. Once heme is brought to the OM receptor, the heme is transferred to the periplasmic space where it binds to periplasmic heme binding proteins.

HxuA from *Haemophilus influenzae* is another hemophore which is able to scavenge heme by forming a complex with hemopexin *(18)*. HxuA, along with the heme receptor HxuC, induce heme release from hemopexin, allowing HxuC to bind the host heme. This hemophore is

an exception to other known hemophores in that HxuA is not able to bind heme although it has been shown it is essential for heme uptake and transfer.

Mycobacterium turberculosis (*Mtb*) has also been identified as bacteria which utilizes a hemophore system although *Mtb* is not classified as either Gram-negative or positive since it does not have the same membrane chemical aspects seen in either type of bacteria *(19)*. *Mtb* uses the hemophore Rv0203 to scavenge heme from Hb *(2, 18)*. This protein differs from other hemophores in fold, yet is thought to utilize a similar His/Tyr binding motif as seen in HasA. Rv0203 delivers heme to the heme receptors MmpL11 and MmpL3 which then pass the heme to MhuD for degradation *(2)*.

1.3.2 Heme transfer across outer membrane

Once heme has reached the OM, either by a hemophore or received by an OM heme receptor directly, the heme must be transported across the membrane *(2, 3, 15, 17, 18)*. Energy to complete this transfer is coupled with bacterial proton motive force in conjunction with an inner membrane complex, TonB/ExbB/ExbD, also known as the TonB box *(2, 18)*. The majority of known OM heme receptors are members of the TonB-depedent outer transporter (TBDT) family and utilize the energy from the TonB box to bring heme across the membrane into the periplasmic space *(15)*. These transmembrane proteins are comprised of a closed β-barrel structure and made of 22 antiparallel β-sheets *(3)*. Most commonly these receptors recognize and bind host Hb and hemoglobin-haptoglobin (Hb-Hp) *(2, 3)*.

Although over 30 OM heme receptors have been reported, the only crystal structure determined is of apo-ShuA from *Shigella dysenteriae* which has been shown to recognize host methemoglobin and binds heme using two histidines, H86 and H428 *(2, 3)*. Other bis-histidine OM receptors, based on sequence similarity and homology, include *P. aeruginosa* PhuR,

Porphyromonas gingivalis HmuR, *S. marcescens* HasR, and *Y. enterocolitica* HemR *(2, 15)*. Once the heme is passed through the OM receptor, the heme is transferred to periplasmic binding proteins (PBPs) which work alongside ABC importers to bring heme into the cell. The exact mechanism of the transfer from the OM the periplasmic membrane is still unknown *(3)*.

1.3.3 Heme transfer across inner periplasmic membrane

Gram-negative PBPs receive heme from OM receptors and deliver the heme to ABC transport systems within the periplasmic membrane to bring heme into the cell *(2)*. Only a few Gram-negative PBPs have been studied including *S. dysenteriae* ShuT, *P. aeruginosa* PhuT, and *Y. pestis* HmuT (*Yp*HmuT).

1.3.3.1 S. dysenteriae ShuT and P. aeruginosa PhuT

ShuT and PhuT are protein homologs with about ~35% sequence identity *(2)*. PhuT/ShuT both utilize a conserved tyrosine residue to coordinate one heme molecule *(20)*. The proteins share a similar fold although there are differences in the heme pocket environment *(2)*. In the PhuT heme binding site, a R73 is in position to H-bond to the axial tyrosine while this residue is replaced by a lysine pointing away from the axial tyrosine in ShuT. The heme propionates in ShuT are pointed inside the protein while PhuT heme propionates are oriented outside of the heme pocket. The mechanism of ShuT/PhuT heme binding and release is yet to be determined.

Both ShuT and PhuT deliver heme to the inner membrane ABC transporter. Only the *S. dysenteriae* shuttle ShuUV has been studied *(2)*. Due to the nature of ABC transporter proteins, (membrane-bound) these studies were carried out in liposomes. The study was performed using ShuT, ShuUV, and ShuS (cytoplasmic-binding protein), and ATP. The cytoplasmic-binding proteins in Gram-negative bacteria are thought to degrade heme once through the periplasmic membrane, although this has not been completely determined. Complete transfer of heme

through the shuttle required all of the listed proteins and ATP, indicating heme transfer from ShuUV to ShuS, and ATP binding and hydrolysis, are coupled. Additionally, E74 and E207 were required for appropriate binding of holoShuT with ShuU.

1.3.3.2 Y. pestis HmuT

*Yp*HmuT binds heme using a His/Tyr axial ligand pair *(21)*. This protein delivers heme to the HmuUV ABC transport system to be brought into the cellular space. HmuT contains two lobes, similar in structure, which are connected by a single backbone α-helix, a common feature among periplasmic heme binding proteins. A crystal structure of holo-*Yp*HmuT showed the heme pocket to be larger than both ShuT and PhuT with two stacked hemes bound in the pocket *(2)*. The propionate groups of the hemes were arranged in such a way that the propionates from one heme molecule were pointing outside of the protein, while the propionates from the other heme were pointing inward. Isothermal titration calorimetry experiments showed the protein to bind the heme in a 2:1 molar ratio confirming the structural finding. Similar to PhuT, *Yp*HmuT also has an arginine in enough proximity to H-bond to the axial tyrosine although the hydrogen-bonding has not been directly observed.

*Yp*HmuT delivers heme to the HmuUV ABC transporter *(2, 21, 22)*. The crystal structure of HmuUV has been determined *(22)*. The structure reveals a conserved H142 in HmuU and a conserved Y93 in HmuV. It has been proposed the heme could be bound by either both of these residues, or only one, during heme transfer *(2)*. Similar to ShuT, *Yp*HmuT contains two conserved glutamic acid residues which are thought to participate in docking of *Yp*HmuT to HmuUV *(22)*.

1.4 Gram-Positive Heme Uptake Pathways

Contrary to Gram-negative bacteria, Gram-positive cells have a thick peptidoglycan layer composed of proteins, teichoic acids, and carbohydrates *(18)*. Heme can either bind to surface receptor proteins to be shuttled through the membrane to an ABC transporter, or be scavenged by hemophores and then shuttled through the membrane *(2, 3, 18)*. The most commonly studied Gram-positive heme uptake and transfer systems are *Staphylococcus aureus, Bacillus anthracis, Streptococcus pyogenes,* and *Corynebacterium diphtheriae.* The focus of this dissertation will be on heme uptake in *S. pyogenes* and *C. diphtheriae.*

1.4.1 S. aureus Isd System and NEAT domains

S. aureus utilizes the iron-responsive surface determinant (Isd) system heme uptake pathways and is the most extensively studied Gram-positive shuttle. The Isd system is composed of nine proteins, most of which have been structurally determined or characterized *(2, 23)*.

Four of the nine Isd proteins function as cell wall anchored surface receptors and are classified as NEAT-containing proteins: IsdA, IsdB, IsdC, and IsdH. NEAT (near iron transporter) domains are a group of conserved residues, about 125 amino acids long, which are rich in beta-strands, contain a 3_{10} α-helix and bind heme *(2, 24)*. NEAT proteins have been shown to utilize the YXXXY heme binding motif in which the first tyrosine in the sequence is the heme axial ligand and the second tyrosine H-bonds to the first. The number of NEAT domains in a protein can vary and not all NEAT domains with this motif have been shown to bind heme. Additionally, these proteins also utilize a SXXXXY/F motif which assists in the stabilization of the bound heme. The serine extends from the beginning of the 3_{10} α-helix and hydrogen bonds to one of the heme propionates while the tyrosine or phenylalanine at the end of the motif stacks over the heme.

Numerous kinetic heme transfer studies have shown the Isd uptake pathway to proceed via transfer between various partners *(2, 25, 26)*. IsdB and IsdH are the most exposed to the extracellular surroundings and can both remove heme from Hb or Hb-Hp, respectively, and can transfer to either IsdA or IsdC. IsdC then transfers heme to the substrate binding protein IsdE. The ABC transporter IsdDF brings the heme into the cellular space. Once passed through the transport system and into the cytoplasm, IsdG and IsdI degrade the heme and release the iron for use by the organism *(8)*.

1.4.1.1 IsdB

IsdB is exposed to the *S. aureus* extracellular surroundings and transports host heme to IsdA *(23, 27, 28)*. IsdB contains two NEAT domains, IsdB-N1 and IsdB-N2, numbered from N-terminus to C-terminus. It has been shown IsdB-N1 can bind to Hb, but is not able to bind heme. In contrast, IsdB-N2 can bind heme, but not Hb *(28)*. IsdB-N2 has the canonical YXXXY heme binding motif as seen in other NEAT proteins. The IsdB-N2 domain alone is capable of transporting heme to IsdA, but transfers at a faster rate when the full construct IsdB construct is present.

The crystal structure of heme-bound IsdB-N2 showed an eight-stranded β-sandwich fold similar to that in IsdA and IsdC *(28)*. Distinct from other Isd NEAT domains, there is an α-helix at the C-terminus following the eighth β-strand. Y440 coordinates the heme iron in the fifth position and hydrogen bonds with the phenol group of Y444. IsdB-N2 is an exception to the simple tyrosine ligation of other Isd NEAT proteins. The crystal structure shows it utilizes a five-coordinate Tyr/Met ligation system while spectroscopic studies indicate the protein exists as a mixture of five-coordinate and six-coordinate heme. Mutation of residues directly contributing

to heme binding, particularly Y440A, Y444A, S361A, and M362L, showed that binding of heme was disrupted.

1.4.1.2 IsdH

S. aureus IsdH, also referred to as HarA, is responsible for the uptake of heme from Hb, Hp, and Hb-Hp complexes *(29, 30)*. IsdH contains three NEAT domains, each with different binding functions. IsdH-N1 and IsdH-N2 bind Hb, Hp, and Hb-Hp complexes, but not heme, while IsdH-N3 binds either single or multiple hemes *(23, 29-31)*.

The crystal structure of holo IsdH-N3 displays similar structural fold as seen in all other NEAT proteins including eight β-strands *(30)*. A single tyrosine residue, Y642, coordinates the ferric heme in a five-coordinate fashion with Y646 hydrogen-bonding to the axial Y642. The heme propionate groups form hydrogen bonds with S563 and Y646 in the heme pocket. The double mutant Y642A/Y646A resulted in diminished ability of heme-binding.

1.4.1.3 IsdA

IsdA retrieves heme from extracellular proteins IsdB and IsdH and delivers heme to IsdC *(23)*. IsdA contains one NEAT domain which is capable of binding heme. The crystal structure of holo-IsdA NEAT shows the domain is similar in fold to other NEAT proteins, consisting of eight β-strands *(27)*. The heme iron has a five-coordinate ligation with Y166 as the axial ligand hydrogen-bonded to Y170 *(27, 32)*. Reduction of IsdA results in a heme ligand switch with H83 serving as the axial ligand rather than Y166 *(27, 32-34)*. Reoxidation yielded the original ferric heme with tyrosine as the proximal ligand.

Spectroscopic studies of point mutations further demonstrated the participation of specific amino acids in the binding of heme in ferric IsdA *(27)*. Y166A and Y170A both result in almost total loss of heme binding. Other tyrosine residues within the NEAT domain were also

mutated and showed no alteration of heme acquisition. H83A showed no effect on the ability of IsdA to bind heme.

1.4.1.4 IsdC and IsdE

IsdC is responsible for transporting heme to IsdE and contains one NEAT domain *(23)*. The crystal structure of Holo-IsdC shows the protein to be similar in fold to other NEAT proteins *(35)*. IsdC utilizes a five-coordinate ferric heme ligation system with Y132 as the axial ligand *(34, 35)*. As with other NEAT proteins, Y136 is hydrogen bonded to the axial Y132 giving a YXXXY motif.

IsdE is the substrate binding protein which delivers heme to the ABC transporter, IsdDF *(23)*. Apo-IsdE can only accept heme from holo-IsdC *(33, 36)*. Structurally, IsdE has similar fold to other substrate binding proteins with two lobes connected by an α-helix forming a bi-lobed topology *(37)*. Unlike the previously discussed Isd proteins, IsdE utilizes a His/Met (H229/M78) ligation system to bind the heme.

Alanine mutations of H229 and M78 yielded a significant loss in the capability of IsdE to bind heme *(37, 38)*. The double mutant (M78A/H229A) showed a complete loss of IsdE heme binding ability. Reduction and addition of carbon monoxide to IsdE resulted in a low-spin ferrous coordination with His and CO serving as the axial ligands.

1.4.2 Bacillus anthracis hemophore mediated heme uptake

Three different heme uptake systems have been identified in *B. anthracis*: Isd, Hal, and BslK *(2, 18, 39-42)*. All of the pathways utilize NEAT domains to bind and transfer heme although not all of the domains are capable of transfer.

Unlike the *S. aureus* Isd system, the *B. anthracis* system utilizes two hemophores to extract heme from host Hb which then bring heme to the surface-anchored IsdC protein. The

two hemophores IsdX1 and IsdX2 contain one and five NEAT domains, respectively. Similar to the *S. aureus* Isd system, many of the IsdX NEAT domains utilize the YXXXY heme binding motif: IsdX1 and NEAT domains 1, 3, 4 and 5 of IsdX2. IsdX2-N2 has a histidine which replaces the second tyrosine in the motif creating an YXXXH motif. Both IsdX1 and IsdX2-N5 have been structurally determined *(43, 44)*. Crystal structures show both proteins exhibit the canonical β-sandwich fold and the heme is bound by a tyrosine residue. A 3_{10} helix utilizing the conserved SXXXXY motif stabilizes the heme in the pocket.

The *B. anthracis* S-layer protein K (BslK) is a surface localized NEAT protein which transfers heme to IsdC *(42)*. *B. anthracis* contains an outer structure called the S-layer which is a crystalline protein layer surrounding the cell and BslK is proposed via homology to be associated with the S-layer. Heme transfer studies show BslK rapidly transfers heme to apo-IsdC. The crystal structure of this protein is still undetermined.

The heme-acquisition leucine-rich repeat protein, Hal, is another *B. anthracis* NEAT heme transport system *(41)*. Sequence alignment with other NEAT proteins shows Hal has the SXXXXY binding motif, but is lacking the complete YXXXY motif which is replaced with YXXXF. Homology modeling indicated the first tyrosine in the YXXXF motif is in position to bind the heme. Directly opposite of the heme is another tyrosine which could be in position to bind the heme. More studies need to be performed in order to elucidate the contributions of each pathway.

1.4.3 Heme uptake by S. pyogenes

The Group A Streptococcus (GAS) from *S. pyogenes* utilizes the Shr/Shp/HtsABC locus for heme uptake *(2, 45-47)*. The streptococcal hemeoprotein receptor (Shr) and Shp are surface exposed proteins which are anchored to the cell wall. The heme transport *Streptococcus* ABC

importer (HtsA)/streptococcal iron acquisition (SiaA) ABC system delivers heme to the intracellular space. Chapter 5 of this dissertation gives a detailed overview of SiaA heme binding.

Shr contains two NEAT domains (Shr-N1 and Shr-N2), both of which are able to bind heme. The crystal structures of these domains remain unknown. Shr is able to receive heme from methemoglobin *(48)*. The kinetics of heme transfer between the proteins in this pathway has been studied in detail *(49-52)*. Additional kinetic studies of heme transfer between the NEAT domains of Shr to apo-Shp (the next protein in the pathway) showed transfer from Shr-N1 to apo-Shp to be rapid while transfer was much slower for Shr-N2 *(53)*. Chapters 7 and 8 of this dissertation go into detail in regards to heme binding of these proteins.

The crystal structure of Shp has been determined and showed the protein utilized a bismethionine heme axial ligation (M66/M153) *(54)*. Although similar in fold to other NEAT proteins, Shp shares very little sequence similarity with NEAT domains lacking the SXXXXY and YXXXY motifs and is therefore not considered a NEAT protein. Shp heme affinity studies indicated loss of the Fe–M153 bond results in a large reduction of holoShp stability *(49)*. Shp delivers heme to HtsA/SiaA which is a His/Met coordinate protein.

1.4.4 C. diphtheriae heme uptake

C. diphtheriae is the a causative agent of diphtheria, a well-known upper respiratory tract disease that carries a high mortality rate in humans *(55)*. The high virulence factor of this pathogen is due to its ability to secrete diphtheria toxin (DT). DT is encoded by the *tox* gene and is negatively regulated by a DT repressor protein (DtxR) and by iron. DtxR is known to regulate at least 50 genes in *C. diphtheriae (56, 57)*. Although this toxin has attracted much attention, it is also known that the ability of the pathogen to take up heme from its external environment is

critical in determining virulence factors and ultimately survival of the pathogenic organism within the host.

C. diphtheriae has been shown to utilize a siderophore-specific uptake system encoded by *ciuABCDE* genes and genes which encode for an ABC-type hemin transporter system called HmuTUV *(56-60)*. These three genes, *hmuT*, *hmuU*, and *hmuV* are individually DtxR- and iron-regulated transcriptional regions. A fourth gene, *htaA* is on the same operon as the *hmuTUV* genes. Removal of either *hmuTUV*, *htaA*, or the entire *hmu* gene cluster resulted in a decreased ability of the pathogen to utilize hemin and Hb as sources of iron *(59, 60)*. This finding indicated HtaA and the ABC-transport system in *C. diphtheriae* are used for the uptake of hemin into the cell. *HtaB* and *htaC* are additional genes within the *hmu* gene cluster and are transcribed independently *(59, 61)*. *C. diphtheriae* has alternate hemin uptake pathways indicated by the ability of the pathogen to still utilize both hemoglobin and hemin as sources of iron even upon the deletion of the *hmu* gene cluster.

It is currently proposed that heme from the extracellular surroundings initially binds to HtaA and is either passed to HtaB, or directly to HmuT which is the substrate binding protein to the HmuUV ABC transport system *(59, 62)*. HmuU is the ABC permease and HmuV is the ATPase *(56)*. Once imported, HmuO, a heme oxygenase, releases the iron from the porphyrin. HmuO is encoded by *hmuO* and it is not a part of the hemin transport gene cluster, yet it is regulated by DtxR and iron *(59, 60, 63)*.

1.4.4.1 HtaA and HtaB

HtaA, a surface-anchored hemin binding protein, contains a hydrophobic C-terminal region along with an N-terminal leader peptide which is thought to assist in the anchoring to the cellular surface *(59, 60)*. The *htaA* gene, which encodes for HtaA, is part of a six gene cluster

that makes up the hmu cluster of *C. diphtheriae (60).* This protein contains two conserved regions (CR) of about 150 amino acids each in length, both of which can bind heme *(59, 60).* HtaB is also a heme binding protein, anchored to the cell and exposed at the surface in the same manner as HtaA and contains one CR. Mutation of *htaB* showed no affect in the ability of the cell to utilize hemin or Hb as a source of iron. Heme is passed from either HtaA or HtaB to HmuT. Heme binding of HmuT is discussed in detail in Chapters 2 – 4.

1.5 References

[1] Smith, A. D., and Wilks, A. (2012) Extracellular heme uptake and the challenges of bacterial cell membranes. *Curr. Top. Membr. 69*, 359-392.

[2] Rodgers, K. R., and Lukat-Rodgers, G. S. (2014) Biophysical perspectives on the acquisition, transport, and trafficking of heme in bacteria. *Handbook of Porphyrin Science with Applications to Chemistry, Physics, Materials Science, Engineering, Biology and Medicine, Vol. 30: Heme Proteins, Part II 30*, 249-309.

[3] Wilks, A., and O'Neill, M. J. (2014) Extracellular heme uptake and metabolism in bacterial pathogenesis, In *Handbook of Porphyrin Science with Applications to Chemistry, Physics, Materials Science, Engineering, Biology and Medicine, Vol 26: Heme Biochemistry* (Ferreira, G. C., Kadish, K. M., Smith, K. M., and Guilard, R., Eds.), pp 267-315, World Scientific, Hackensack, NJ.

[4] Wandersman, C., and Delepelaire, P. (2004) Bacterial iron sources: From siderophores to hemophores. *Annu. Rev. Microbiol. 58*, 611-647.

[5] Nobles, C. L., and Maresso, A. W. (2011) The theft of host heme by Gram-positive pathogenic bacteria. *Metallomics 3*, 788-796.

[6] Braun, V., and Hantke, K. (2011) Recent insights into iron import by bacteria. *Curr. Opin. Chem. Biol. 15*, 328-334.

[7] Tong, Y., and Guo, M. (2009) Bacterial heme-transport proteins and their heme-coordination modes. *Arch. Biochem. Biophys. 481*, 1-15.

[8] Cavallaro, G., Decaria, L., and Rosato, A. (2008) Genome-based analysis of heme biosynthesis and uptake in prokaryotic systems. *J. Proteome Res. 7*, 4946-4954.

[9] Farrand, A. J., and Skaar, E. P. (2014) Heme and infectious diseases, In *Handbook of Porphyrin Science with Applications to Chemistry, Physics, Materials Science, Engineering, Biology and Medicine, Vol 26: Heme Biochemistry* (Ferreira, G. C., Kadish, K. M., Smith, K. M., and Guilard, R., Eds.) 26 ed., pp 317-377, World Scientific, Hackensack, NJ.

[10] Davidson, A. L., and Maloney, P. C. (2007) ABC transporters: How small machines do a big job. *Trends Microbiol. 15*, 448-455.

[11] Oldham, M. L., Davidson, A. L., and Chen, J. (2008) Structural insights into ABC transporter mechanism. *Curr. Opin. Struct. Biol. 18*, 726-733.

[12] ter Beek, J., Guskov, A., and Slotboom, D. J. (2014) Structural diversity of ABC transporters. *J. Gen. Physiol. 143*, 419-435.

[13] Rees, D. C., Johnson, E., and Lewinson, O. (2009) ABC transporters: The power to change. *Nat. Rev. Mol. Cell Biol. 10*, 218-227.

[14] Jones, P. M., O'Mara, M. L., and George, A. M. (2009) ABC transporters: A riddle wrapped in a mystery inside an enigma. *Trends Biochem. Sci. 34*, 520-531.

[15] Benson, D. R., and Rivera, M. (2013) Heme uptake and metabolism in bacteria. *Met. Ions Life Sci 12*, 279-332.

[16] Honsa, E. S., and Maresso, A. W. (2011) Mechanisms of iron import in anthrax. *BioMetals 24*, 533-545.

[17] Runyen-Janecky, L. J. (2013) Role and regulation of heme on acquisition in gram-negative pathogens. *Front. Cell. Infect. Microbiol. 3*, 55.

[18] Contreras, H., Chim, N., Credali, A., and Goulding, C. W. (2014) Heme uptake in bacterial pathogens. *Curr. Opin. Chem. Biol. 19*, 34-41.

[19] Hoffmann, C., Leis, A., Niederweis, M., Pfeifer, G., Plitzko, J., and Engelhardt, H. (2007) Cryo-electron tomography and vitreous sections reveal the outer membrane of mycobacteria. *Int. J. Med. Microbiol. 297*, 138-139.

[20] Ho, W. W., Li, H. Y., Eakanunkul, S., Tong, Y., Wilks, A., Guo, M. L., and Poulos, T. L. (2007) Holo-and apo-bound structures of bacterial periplasmic heme-binding proteins. *J. Biol. Chem. 282*, 35796-35802.

[21] Mattle, D., Zeltina, A., Woo, J. S., Goetz, B. A., and Locher, K. P. (2010) Two stacked heme molecules in the binding pocket of the periplasmic heme-binding protein HmuT from *Yersinia pestis*. *J. Mol. Biol. 404*, 220-231.

[22] Woo, J. S., Zeltina, A., Goetz, B. A., and Locher, K. P. (2012) X-ray structure of the *Yersinia pestis* heme transporter HmuUV. *Nat. Struct. Mol. Biol. 19*, 1310-1315.

[23] Grigg, J. C., Ukpabi, G., Gaudin, C. F., and Murphy, M. E. (2010) Structural biology of heme binding in the *Staphylococcus aureus* Isd system. *J. Inorg. Biochem. 104*, 341-348.

[24] Honsa, E. S., Maresso, A. W., and Highlander, S. K. (2014) Molecular and evolutionary analysis of NEAr-iron Transporter (NEAT) domains. *PLoS One 9*.

[25] Zhu, H., Xie, G., Liu, M. Y., Olson, J. S., Fabian, M., Dooley, D. M., and Lei, B. F. (2008) Pathway for heme uptake from human methemoglobin by the iron-regulated surface determinants system of *Staphylococcus aureus*. *J. Biol. Chem. 283*, 18450-18460.

[26] Tiedemann, M. T., and Stillman, M. J. (2012) Heme binding to the IsdE(M78A; H229A) double mutant: Challenging unidirectional heme transfer in the iron-regulated surface determinant protein heme transfer pathway of *Staphylococcus aureus*. *J. Biol. Inorg. Chem. 17*, 995-1007.

[27] Grigg, J. C., Vermeiren, C. L., Heinrichs, D. E., and Murphy, M. E. P. (2007) Haem recognition by a *Staphylococcus aureus* NEAT domain. *Mol. Microbiol. 63*, 139-149.

[28] Gaudin, C. F. M., Grigg, J. C., Arrieta, A. L., and Murphy, M. E. P. (2011) Unique heme-iron coordination by the hemoglobin receptor IsdB of *Staphylococcus aureus*. *Biochemistry 50*, 5443-5452.

[29] Pilpa, R. M., Robson, S. A., Villareal, V. A., Wong, M. L., Phillips, M., and Clubb, R. T. (2009) Functionally distinct NEAT (NEAr Transporter) domains within the *Staphylococcus aureus* IsdH/HarA protein extract heme from methemoglobin. *J. Biol. Chem. 284*, 1166-1176.

[30] Watanabe, M., Tanaka, Y., Suenaga, A., Kuroda, M., Yao, M., Watanabe, N., Arisaka, F., Ohta, T., Tanaka, I., and Tsumoto, K. (2008) Structural basis for multimeric heme complexation through a specific protein-heme interaction - The case of the third NEAT domain of IsdH from *Staphylococcus aureus*. *J. Biol. Chem. 283*, 28649-28659.

[31] Pilpa, R. M., Fadeev, E. A., Villareal, V. A., Wong, M. L., Phillips, M., and Clubb, R. T. (2006) Solution structure of the NEAT (NEAr Transporter) domain from IsdH/HarA: The human hemoglobin receptor in *Staphylococcus aureus*. *J. Mol. Biol. 360*, 435-447.

[32] Pluym, M., Muryoi, N., Heinrichs, D. E., and Stillman, M. J. (2008) Heme binding in the NEAT domains of IsdA and IsdC of *Staphylococcus aureus*. *J. Inorg. Biochem. 102*, 480-488.

[33] Muryoi, N., Tiedemann, M. T., Pluym, M., Cheung, J., Heinrichs, D. E., and Stillman, M. J. (2008) Demonstration of the iron-regulated surface determinant (Isd) heme transfer pathway in *Staphylococcus aureus*. *J. Biol. Chem. 283*, 28125-28136.

[34] Vermeiren, C. L., Pluym, M., Mack, J., Heinrichs, D. E., and Stillman, M. J. (2006) Characterization of the heme binding properties of *Staphylococcus aureus* IsdA. *Biochemistry 45*, 12867-12875.

[35] Sharp, K. H., Schneider, S., Cockayne, A., and Paoli, M. (2007) Crystal structure of the heme-IsdC complex, the central conduit of the Isd iron/heme uptake system in *Staphylococcus aureus*. *J. Biol. Chem. 282*, 10625-10631.

[36] Liu, M. Y., Tanaka, W. N., Zhu, H., Xie, G., Dooley, D. M., and Lei, B. F. (2008) Direct hemin transfer from IsdA to IsdC in the iron-regulated surface determinant (Isd) heme acquisition system of *Staphylococcus aureus*. *J. Biol. Chem. 283*, 6668-6676.

[37] Grigg, J. C., Vermeiren, C. L., Heinrichs, D. E., and Murphy, M. E. (2007) Heme coordination by *Staphylococcus aureus* IsdE. *J. Biol. Chem 282*, 28815-28822.

[38] Pluym, M., Vermeiren, C. L., Mack, J., Heinrichs, D. E., and Stillman, M. J. (2007) Heme binding properties of *Staphylococcus aureus* lsdE. *Biochemistry 46*, 12777-12787.

[39] Ekworomadu, M. T., Poor, C. B., Owens, C. P., Balderas, M. A., Fabian, M., Olson, J. S., Murphy, F., Bakkalbasi, E., Honsa, E. S., He, C., Goulding, C. W., and Maresso, A. W. (2012) Differential function of lip residues in the mechanism and biology of an anthrax hemophore. *PLoS Pathog. 8*, e1002559.

[40] Honsa, E. S., Fabian, M., Cardenas, A. M., Olson, J. S., and Maresso, A. W. (2011) The five near-iron transporter (NEAT) domain anthrax hemophore, IsdX2, scavenges heme from hemoglobin and transfers heme to the surface protein IsdC. *J. Biol. Chem. 286*, 33652-33660.

[41] Balderas, M. A., Nobles, C. L., Honsa, E. S., Alicki, E. R., and Maresso, A. W. (2012) Hal is a *Bacillus anthracis* heme acquisition protein. *J. Bacteriol. 194*, 5513-5521.

[42] Tarlovsky, Y., Fabian, M., Solomaha, E., Honsa, E., Olson, J. S., and Maresso, A. W. (2010) A *Bacillus anthracis* S-Layer homology protein that binds heme and mediates heme delivery to IsdC. *J. Bacteriol. 192*, 3503-3511.

[43] Ekworomadu, M. T., Poor, C. B., Owens, C. P., Balderas, M. A., Fabian, M., Olson, J. S., Murphy, F., Balkabasi, E., Honsa, E. S., He, C., Goulding, C. W., and Maresso, A. W. (2012) Differential function of Lip residues in the mechanism and biology of an anthrax hemophore. *PLoS Path. 8*.

[44] Honsa, E. S., Owens, C. P., Goulding, C. W., and Maresso, A. W. (2013) The near-iron transporter (NEAT) domains of the anthrax hemophore IsdX2 require a critical glutamine to extract heme from methemoglobin. *J. Biol. Chem. 288*, 8479-8490.

[45] Eichenbaum, Z., Muller, E., Morse, S. A., and Scott, J. R. (1996) Acquisition of iron from host proteins by the group A *Streptococcus*. *Infect. Immun. 64*, 5428-5429.

[46] Akbas, N., Draganova, E. B., Block, D. R., Sook, B. R., Chan, Y. F., Zhuo, J., Eichenbaum, Z., Rodgers, K. R., and Dixon, D. W. (2015) Heme-bound SiaA from *Streptococcus pyogenes*: Effects of mutations and oxidation state on protein stability. *J. Inorg. Biochem.*

[47] Sook, B. R., Block, D. R., Sumithran, S., Montañez, G. E., Rodgers, K. R., Dawson, J. H., Eichenbaum, Z., and Dixon, D. W. (2008) Characterization of SiaA, a streptococcal heme-binding protein associated with a heme ABC transport system. *Biochemistry 47*, 2678-2688.

[48] Ouattara, M., Cunha, E. B., Li, X., Huang, Y. S., Dixon, D. W., and Eichenbaum, Z. (2010) Shr of Group A streptococcus is a new type of composite NEAT protein involved in sequestering haem from methaemoglobin. *Mol. Microbiol. 78*, 739-756.

[49] Ran, Y. C., Zhu, H., Liu, M. Y., Fabian, M., Olson, J. S., Aranda, R. I., Phillips, G. N., Dooley, D. M., and Lei, B. (2007) Bis-methionine ligation to heme iron in the streptococcal cell surface protein Shp facilitates rapid hemin transfer to HtsA of the HtsABC transporter. *J. Biol. Chem. 282*, 31380-31388.

[50] Ran, Y. C., Malmirchegini, G. R., Clubb, R. T., and Lei, B. F. (2013) Axial ligand replacement mechanism in heme transfer from streptococcal heme-binding protein Shp to HtsA of the HtsABC transporter. *Biochemistry 52*, 6537-6547.

[51] Liu, M. Y., and Lei, B. F. (2005) Heme transfer from streptococcal cell surface protein Shp to HtsA of transporter HtsABC. *Infect. Immun. 73*, 5086-5092.

[52] Nygaard, T. K., Blouin, G. C., Liu, M. Y., Fukumura, M., Olson, J. S., Fabian, M., Dooley, D. M., and Lei, B. F. (2006) The mechanism of direct heme transfer from the streptococcal cell surface protein Shp to HtsA of the HtsABC transporter. *J. Biol. Chem. 281*, 20761-20771.

[53] Ouattara, M., Pennati, A., Devlin, D. J., Huang, Y. S., Gadda, G., and Eichenbaum, Z. (2013) Kinetics of heme transfer by the Shr NEAT domains of Group A Streptococcus. *Arch. Biochem. Biophys. 538*, 71-79.

[54] Aranda, R., Worley, C. E., Liu, M., Bitto, E., Cates, M. S., Olson, J. S., Lei, B. F., and Phillips, G. N. (2007) Bis-methionyl coordination in the crystal structure of the heme-binding domain of the streptococcal cell surface protein Shp. *J. Mol. Biol. 374*, 374-383.

[55] Bibb, L. A., Kunkle, C. A., and Schmitt, M. P. (2007) The ChrA-ChrS and HrrA-HrrS signal transduction systems are required for activation of the *hmuO* promoter and repression of the *hemA* promoter in *Corynebacterium diphtheriae*. *Infect. Immun. 75*, 2421-2431.

[56] Drazek, E. S., Hammack, C. A., and Schmitt, M. P. (2000) *Corynebacterium diphtheriae* genes required for acquisition of iron from haemin and haemoglobin are homologous to ABC haemin transporters. *Mol. Microbiol 36*, 68-84.

[57] Schmitt, M. P. (2014) Iron acquisition and iron-dependent gene expression in *Corynebacterium diphtheriae*, In *Corynebacterium diphtheriae and Related Toxigenic Species: Genomics, Pathogenicity and Applications* (Burkovski, A., Ed.), pp 95-121.

[58] Allen, C. E., Burgos, J. M., and Schmitt, M. P. (2013) Analysis of novel iron-regulated, surface-anchored hemin-binding proteins in *Corynebacterium diphtheriae*. *J. Bacteriol. 195*, 2852-2863.

[59] Allen, C. E., and Schmitt, M. P. (2009) HtaA is an iron-regulated hemin binding protein involved in the utilization of heme iron in *Corynebacterium diphtheriae*. *J. Bacteriol. 191*, 2638-2648.

[60] Allen, C. E., and Schmitt, M. P. (2011) Novel hemin binding domains in the *Corynebacterium diphtheriae* HtaA protein interact with hemoglobin and are critical for heme iron utilization by HtaA. *J. Bacteriol. 193*, 5374-5385.

[61] Kunkle, C. A., and Schmitt, M. P. (2003) Analysis of the *Corynebacterium diphtheriae* DtxR regulon: Identification of a putative siderophore synthesis and transport system that is similar to the *Yersinia* high-pathogenicity island-encoded yersiniabactin synthesis and uptake system. *J. Bacteriol 185*, 6826-6840.

[62] Draganova, E. B., Akbas, N., Adrian, S. A., Lukat-Rodgers, G. S., Collins, D. P., Dawson, J. H., Allen, C. E., Schmitt, M. P., Rodgers, K. R., and Dixon, D. W. (2015) Heme binding by *Corynebacterium diphtheriae* HmuT: Function and heme environment. *Biochemistry 54*, 6598-6609.

[63] Kunkle, C. A., and Schmitt, M. P. (2007) Comparative analysis of *hmuO* function and expression in *Corynebacterium* species. *J. Bacteriol. 189*, 3650-3654.

2 HEME BINDING BY *CORYNEBACTERIUM DIPHTHERIAE* HMUT: FUNCTION AND HEME ENVIRONMENT

This chapter has been published verbatim in Draganova, E. B., Akbas, N., Adrian, S. A., Lukat-Rodgers, G., Collins, D. P., Dawson, J. H., Allen, C. E., Schmitt, M. P., Rodgers, K. R., and Dixon, D. W. (2015), *Biochemistry* 54(43): 6598-60. The expression, purification, and UV-visible spectroscopy of the WT and mutants were performed at Georgia State University.

2.1 Abstract

The heme uptake pathway (hmu) of *Corynebacterium diphtheriae* utilizes multiple proteins to bind and transport heme into the cell. One of these proteins, HmuT, delivers heme to the ABC transporter HmuUV. In this study, the axial ligation of the heme in ferric HmuT is probed by examination of wild-type HmuT and a series of conserved heme pocket residue mutants, H136A, Y235A, and M292A. Characterization by UV-visible absorption, resonance Raman, and magnetic circular dichroism spectroscopies indicate that H136 and Y235 are the axial ligands in ferric HmuT. Consistent with this assignment of axial ligands, ferric WT and H136A HmuT are difficult to reduce while Y235A reduces readily in the presence of dithionite. Raman frequencies of the FeCO distortions in WT, H136A, and Y235A HmuT−CO complexes provide further evidence for the axial ligand assignments. Additionally, these frequencies provide insight into the nonbonding environment of the heme pocket. Ferrous Y235A and the Y235A−CO complex reveal that the imidazole of H136 exists in two forms, one neutral and one with imidazolate character, consistent with a hydrogen-bond acceptor on the H136 side of the heme. The ferric fluoride complex of Y235A reveals the presence of at least one hydrogen-bond donor on the Y235 side of the heme. Hemoglobin utilization assays showed that the axial Y235 ligand is required for heme uptake in HmuT.

2.2 Introduction

Iron is required for infection in essentially all bacterial pathogens (*1*). In vertebrate infections, the most abundant source of iron is heme (iron protoporphyrin IX), which comes primarily from hemoglobin. Bacteria have developed sophisticated approaches to transport heme into the cytoplasm. These pathways have been the focus of recent reviews (*2-6*).

To date, pathogenic bacterial heme uptake pathways that have been characterized in detail have involved ATP-binding cassette (ABC) transporters. These transmembrane systems utilize the energy yield from ATP hydrolysis to pump various compounds across cellular membranes (*7;8*). An ABC transporter comprises two transmembrane modules and two ATPase subunits. Import ABC transporters are commonly found in prokaryotic systems and have an associated substrate binding protein [in this instance a heme binding protein (HBP)] that brings the substrate to the ABC transporter (*9*).

A number of HBP's have been characterized. *Pseudomonas aeruginosa* PhuT (*10*) and *Shigella dysenteriae* ShuT (*10;11*) both contain a conserved tyrosine that binds the heme in a pentacoordinate fashion. *Yersinia pestis* HmuT (*Yp*HmuT) utilizes a His/Tyr ligation and binds heme both as a monomer and as a π-stacked dimer (*12;13*). *Staphylococcus aureus* IsdE (*14*) and *Streptococcus pyogenes* SiaA/HtsA (*15;16*) both form hexacoordinate heme complexes having His/Met axial ligation.

The variety of heme binding motifs leads to an interest in further characterization of other HBP's. One such protein is found in the pathogen *Corynebacterium diphtheriae*, a Gram-positive bacterium which is the causative agent of diphtheria, a well-known upper respiratory tract disease that carries a high mortality rate in humans (*17*). Diphtheria is still common in

developing countries due to low vaccination rates (*18*). *C. diphtheriae* requires iron for survival and for virulence (*19-24*).

C. diphtheriae acquires heme via an ABC-type heme binding protein transporter system (*20*) (Figure 2.1). A variety of heme sources can be used including hemoglobin (Hb), hemoglobin/haptoglobin, and myoglobin (Mb) (*25*). The heme utilization (*hmu*) operon includes *hmuT* (the HBP/substrate binding protein), *hmuU* (the permease) and *hmuV* (the ATPase), which form an ABC transport system (*26*). The *htaA* gene is located immediately upstream of the *hmuTUV* locus. Upstream to the *htaA* gene, is the *htaC* gene and a promoter region. Downstream of the *hmuV* gene is a promoter region and the *htaB* gene. The *hmuTUV* and *htaA* genes form a single operon, while *htaB* and *htaC* are transcribed independently (*27*). HtaA and HtaB are proposed to be anchored to the cytoplasmic membrane through a C-terminal hydrophobic region. Both proteins are exposed to the bacterial surface, suggesting that these heme binding proteins may function as heme receptors (*26*). It has been shown that HtaA passes heme to HtaB (*22*). The next protein in the pathway is the HBP HmuT (*Cd*HmuT), which donates heme to the HmuUV transporter. Once the heme is brought into the cell, the heme oxygenase HmuO catalyzes the O_2–dependent degradation of the heme, which releases its iron for further use in cellular functions (*28;29*).

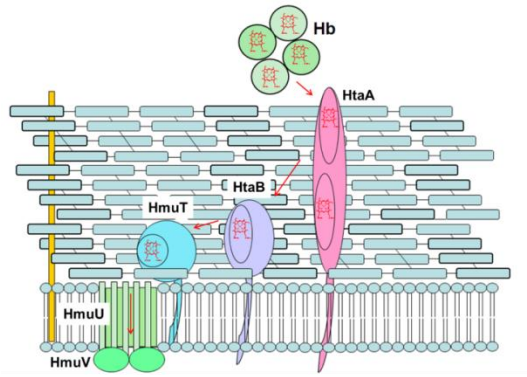

Figure 2.1 Model for heme uptake in C. diphtheriae. Arrows indicate the direction of hemin transfer. It is proposed that hemin would transfer from Hb, a known hemin donor, to the surface exposed hemin binding protein, HtaA, and be transferred to HtaB (membrane-anchored protein) followed by HmuT (substrate binding protein). The hemin would then be passed to the ABC transporter, comprised of HmuU (membrane-bound protease) and HmuV (the ATPase), to bring the hemin into the cytosolic space. Alternatively, HtaA could transfer hemin directly to HmuT.

Sequence alignment studies of *Cd*HmuT with other *Corynebacterium* species reveal two conserved tyrosines: Tyr235 and Tyr349 as well as a conserved histidine (His136) and methionine (Met292) (Figure 2.11 S1). Homology modeling shows that Tyr235 is probably an axial ligand and that either His136 or Met292 could also bind as a sixth ligand. *Cd*HmuT is unique among its homologs in that the proposed axial His and Tyr ligands are reversed with respect to their positions in the structurally characterized proteins ShuT, PhuT and *Yp*HmuT (Figure 2.12 S2). That is, the tyrosines in all proteins in heme uptake pathways known to date come from the N-terminal part of the sequence, but *Cd*HmuT is predicted to have the tyrosine from the C-terminal part of the sequence. As this prediction indicates a key role for tyrosine in heme transfer, it was important to establish the axial ligands in *Cd*HmuT. Herein we report the biophysical characterization of *Cd*HmuT and a number of its mutants. UV-visible absorption, resonance Raman (rR), and magnetic circular dichroism (MCD) studies combine to give a picture of this novel heme uptake protein.

2.3 Materials and Methods

2.3.1 Bacterial strains and media

E. coli strains DH5α and TOP10 (Invitrogen) were used for routine cloning and plasmid maintenance, while XL-1 Gold (Stratagene) was used in the mutagenesis experiments. *E. coli* BL21(DE3) (Novagen) was used for protein expression. *Corynebacterium ulcerans* strain CU77 was previously described (Schmitt & Drazek, 2001) and carries a point mutation that results in premature termination of the *hmuT* gene (Schmitt, unpublished observation). Chromosomal DNA from *C. diphtheriae* strain 1737 (Popovic et al., 1996) was used as the source DNA for PCR. Luria-Bertani (LB) medium was used for culturing *E. coli* and Heart Infusion Broth containing 0.2% Tween 80 (HIBTW) was used for growth of *C. ulcerans* strains. Bacterial stocks were maintained in 20% glycerol at -80º C. Antibiotics were added to LB medium at 50 μg/ml for kanamycin and to HIBTW at 2 μg/ml for chloramphenicol. HIBTW was made low iron by the addition of ethylenediamine di(*o*-hydroxyphenylacetic acid) (EDDA) at 12 μg/ml. Modified PGT is a semi-defined low iron media that has been previously described (Tai et al., 1990). Antibiotics, EDDA, Tween 80, were obtained from Sigma Chemical Co. and hemoglobin (human) was purchased from MP BioMedical.

2.3.2 Plasmid construction

The HmuT expression construct was developed using the pET28a expression vector (Novagen). A PCR-derived DNA fragment containing the *C. diphtheriae hmuT* coding region was initially cloned into the pCR-Blunt II-TOPO vector (Invitrogen). The DNA fragment harboring the *hmuT* gene was subsequently ligated into the NcoI-EcoRI sites in pET28a and the expression plasmid was then transformed into BL21(DE3). The cloned *hmuT* gene in the pET28a vector lacked the 20-amino acid N-terminal secretion signal and contained an N-

terminal Strep-tag, which was used for protein purification. The following primers were used in the PCR: hmuTF; 5'-CC ATGGCA AGC *TGG AGC CAC CCG CAG TTC GAA AAG* GGT GTC CAG GGC ACA TAT-3'; hmuTR; 5'-GAATTC CTA TAC CTG TGG GTC ATAC-3': underlined sequences indicate restriction sites and the sequence in italics encodes the 8-amino acid Strep-tag.

2.3.3 Site-directed mutagenesis and hemoglobin-iron utilization assays

Site-directed mutants were made using the QuikChange Lightning kit (Stratagene) according to the manufacturer's instructions. Briefly, 125 ng of each primer containing the targeted base change and 50 ng of plasmid template were used in the QuikChange reaction. Methylated template DNA was removed from the reaction by digestion with DpnI restriction endonuclease, and mutagenized DNA was recovered by transformation into XL1-Gold competent cells. The presence of the base changes was confirmed by sequence analysis. Plasmids used for site-directed mutagenesis were pET28a containing the cloned Strep-tag-*hmuT* gene, and plasmid pCD842, which harbors the *hmuT* gene on the *E. coli-Corynebacterium* shuttle vector pCM2.6 (*30*). The hemoglobin utilization assay has been described previously (*29*).

2.3.4 Expression and purification of CdHmuT

HmuT was expressed and purified from BL21(DE3) (pET*hmuT*) cells. The N-terminal leader sequence was deleted and replaced with a Strep-tag. The native construct started at residue 21 (Gly) and extended to the native stop codon. The culture was prepared in LB medium containing 50 μg/mL kanamycin. Inoculation was done with an overnight pre-culture and cells were grown at 37 °C. When the OD_{600} of the culture reached 0.5 – 0.6, protein expression was induced by adding isopropyl β-D-1-thiogalactopyranoside (IPTG) to a final concentration of 1.0

mM. The culture was incubated for 3 h at 27 °C. Cells were harvested by centrifugation at 8000 x *g*. The cell pellet was resuspended in lysis solution (100 mM Tris-Cl, 150 mM NaCl, pH 8.0) containing a protease inhibitor cocktail (Roche Complete Mini, EDTA-free, following the manufacturer protocol). The cells were broken using a cell disrupter or sonication. The lysate was then centrifuged at 8000 x *g*, and the supernatant was syringe-filtered with a 0.45 μm filter.

All of the following purification steps were conducted at 4 °C using fast protein liquid chromatography and all buffer solutions were pH 8.0 unless specified otherwise. The protein sample was loaded onto a Strep-Tactin Superflow column (5 mL, IBA BioTAGnology) equilibrated with buffer A (100 mM Tris-Cl, 150 mM NaCl, pH 8.0). Unbound material was washed out with 5 column volumes of buffer A. HmuT was eluted with 10 column volumes of buffer B containing 100 mM Tris-Cl, 150 mM NaCl, 2.5 mM desthiobiotin, pH 8.0 applied using a linear gradient. The purities of the fractions were evaluated using SDS-PAGE. Native-PAGE did not show dimers, indicating that the protein is monomeric in solution. Minor differences in the optical spectra were observed as a function of the buffer type. Heme loading of the WT and mutants were variable from batch to batch. The following heme loading percentages were estimated to the nearest 10%: WT, 100%; M292A, 100%; H136A, 95%; and Y235A, 20%. For the WT protein, spectral signatures associated with a heme dimer at the binding site were seen in a few instances of impure or damaged protein.

2.3.5 Magnetic circular dichroism spectroscopy

Magnetic circular dichroism (MCD) spectra were measured with a magnetic field strength of 1.41 T by using a JASCO J815 spectrophotometer. This instrument was equipped with a JASCO MCD-1B electromagnet and interfaced with a Silicon Solutions PC through a JASCO IF-815-2 interface unit. Data acquisition and manipulation using Cary or Jasco software

has been previously described (*31*). To ensure homogeneity of ferric oxidation for the various mutants, ferricyanide was used to fully oxidize the heme center, followed by desalting chromatography. The resulting spectra were compared to data from other heme-containing proteins with known binding site structures and optical spectra. All spectral measurements for all proteins were carried out with a 0.2 cm quartz cuvette at 4 °C in 50 mM phosphate buffer (either pH 6.5 or 10).

2.3.6 Resonance Raman spectroscopy

Resonance Raman (rR) spectra were collected using the 441.6-nm emission line from a HeCd laser or either 406.7 nm or 413.1 nm emission from a Kr^+ laser. Spectra were recorded at ambient temperature using the 135° backscattering geometry with the laser beam focused to a line on a spinning 5 mm NMR tube. Toluene, DMSO, and CH_2Br_2 were used as external standards for spectral calibration. UV-visible absorption spectra were recorded before and after rR experiments to verify that the samples were not altered by exposure to the laser beam. The final concentrations of all Fe(III) samples were between 25 and 80 μM protein in 100 mM buffer solution. The buffers used were CHES, pH 10.0, Tris-Cl, pH 8.8 or 8.0, sodium phosphate buffer, pH 7.0 or 5.8, MES, pH 5.1, and sodium acetate buffer, pH 5.0. The D_2O and $H_2{}^{18}O$ samples of the Y235A mutant were made by diluting a concentrated sample of the protein into CHES buffer made with either D_2O or $H_2{}^{18}O$ at pD 10 or pH 10, respectively. Resonance Raman spectra were collected with laser powers between 9 and 12 mW at the sample.

The ferric fluoride adduct of Y235A HmuT was prepared by titration with 0.8 M NaF solution in 0.1 M sodium phosphate buffer at pH 5.8. The final protein and NaF concentrations were 80 μM and 330 mM, respectively. The laser power was 9.7 mW for the 406.7 nm Kr^+ excitation and 4.6 mW for the 441.6 nm HeCd excitation.

Ferrous HmuT(Y235A) samples (36 μM) were prepared anaerobically in 5 mm NMR tubes. The protein samples were prepared in 0.1 M Tris-Cl pH 8.2 and equilibrated with water-saturated, O_2-scrubbed N_2 that had been saturated with water. After equilibration under the N_2 atmosphere, an 86-fold excess of aqueous sodium dithionite, buffered at the same pH, was added using a gas-tight 10 μL syringe. Laser power for the ferrous samples ranged from 4 to 8 mW. Ferrous carbonyl adducts (36 to 75 μM) were prepared by reducing the proteins in 0.1 M Tris-Cl pH 8.8 with a 70- to 180-fold excess of buffered sodium dithionite, as described above, except that the reduction was carried out under an atmosphere of natural abundance CO or ^{13}CO (99 atom % ^{13}C) instead of N_2. Laser power for the heme carbonyl samples was held between 2 and 4.5 mW to minimize CO ligand photolysis.

2.4 Results

2.4.1 Heme ligation in ferric HmuT

An alignment of the HmuT amino acid sequences of various *Corynebacterium* species showed that two tyrosine residues (Y235 and Y349) as well as H136 and M292 were highly conserved in this group of bacteria (Figure 2.11 S1). A homology model of HmuT (Figure 2.2) was created by I-TASSER (*32*) with *Yp*HmuT (26% sequence identity) as one of the templates along with four HBP's for which crystal structures have been solved: PhuT from *P. aeruginosa* (*10*), ShuT from *S. dysenteriae* (*10*), IsdE from *S. aureus* (*14*) and *Yp*HmuT (*12*).

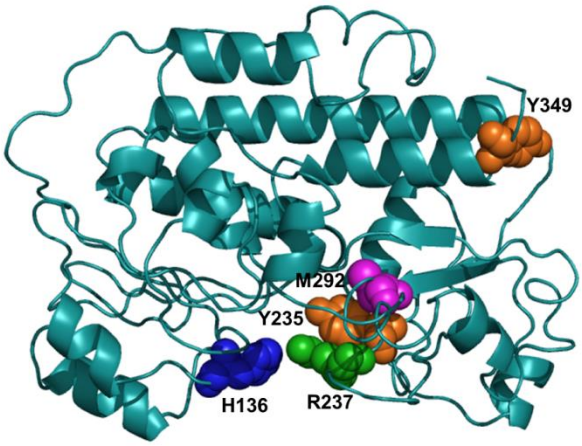

Figure 2.2 I-TASSER homology model of CdHmuT displayed using PyMOL (93). Shown are the locations of H136, Y235, R237, M292, and Y349.

The model indicated that it was probable that *Cd*HmuT would have a Tyr as one axial ligand, and a Met or His as the second. Based on this homology model and sequence alignment, the H136A, Y235A, and M292A mutants were created to probe the heme axial ligation.

2.4.2 Conserved residues and the biological function of HmuT

To determine if H136, Y235, and M292 are important for the biological function of HmuT, the ability of the cloned *hmuT* genes to complement a Hb-iron utilization defect was assessed. It was previously shown that the CU77 mutant strain of *C. ulcerans* HmuT (*Cu*HmuT) was defective for HmuT activity (*20*). The cloned *hmuT* gene from either *Corynebacterium* species could fully restore the wild-type phenotype to this strain. Complementation studies with each of the H136A, Y235A, and M292A *Cd*HmuT mutants revealed that only Y235A was unable to restore growth fully (Figure 2.3). Thus, Y235 is essential for the heme-iron utilization function of HmuT.

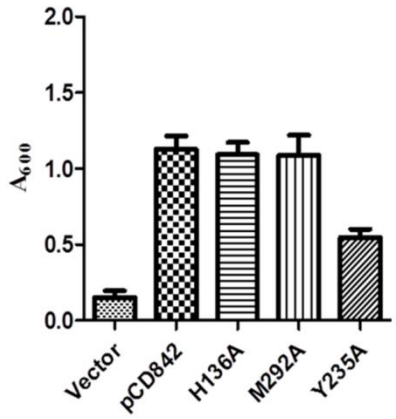

Figure 2.3Hb-iron utilization assay. C. ulcerans CU77 (hmuT) carrying plasmids that encode the wild type (pCD842) and various mutants of the hmuT gene were assessed for their ability to use Hb as the sole iron source for growth in low-iron mPGT medium. Cultures were grown for 36 h at 37 °C in the presence of 25 µg/ml Hb supplemented with 10 µM EDDA, and then cell density was measured by absorbance at A_{600}. Results are the mean of three independent experiments ± standard deviation. The growth difference between WT (pCD842) and Y235A is significant at $p < 0.01$.

2.4.3 Spectroscopy of wild-type CdHmuT

The UV-visible absorption spectrum of ferric wild-type (WT) *Cd*HmuT showed a Soret peak at 407 nm and four peaks in the α,β region at 492, 546, 569, and 616 nm (Figure 2.4). The charge transfer band at 616 nm is characteristic of a high-spin (HS) species, and the two α,β bands at 569 and 546 nm are consistent with the presence of a low-spin (LS) species. Hence, these data suggest an equilibrium mixture of HS and LS WT *Cd*HmuT. This UV-visible absorption spectrum is strikingly similar to that observed for *Serratia marcescens* HasA (*Sm*HasA) (406, 494, 537, 568 and 618 nm) which is known to have His/Tyr axial ligation and exists in a thermal spin equilibrium (*33*).

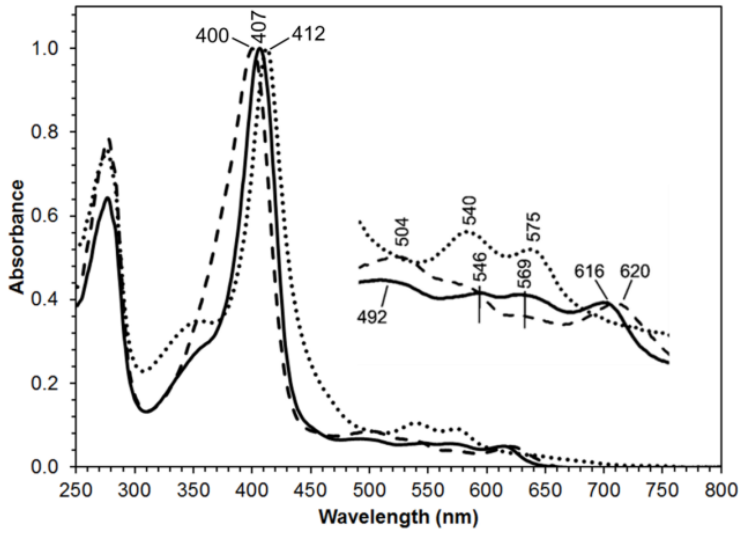

Figure 2.4 UV-visible absorption spectra of the Fe(III) forms of WT CdHmuT (solid line), H136A (dashed line), and Y235A (dotted line) normalized at the Soret. The samples were taken in 50 mM Tris-Cl at pH 7.0.

Ligation of the heme was further probed by the use of MCD. Initial comparisons of the spectra of WT *Cd*HmuT with models having His-only or His/Met axial ligation did not give entirely similar spectral profiles (data not shown). The UV-visible absorption and MCD spectra were then compared with two five-coordinate Tyr-ligated proteins, bovine liver catalase (BLC) (*34-36*) and the H93Y mutant of Mb (*37*) (Figure 2.13 S3). The differences in the spectra indicated that WT *Cd*HmuT does not adopt a five-coordinate, tyrosine-ligated geometry.

WT *Cd*HmuT was then compared to a model for the His/Tyr ligand set: leghemoglobin *a* with exogenous phenol (*38*). This complex adopts a six-coordinate heme binding structure with a histidine axial ligand and a phenol in the *trans* position. Figure 2.5 shows that both the UV-visible absorption and MCD spectra were in agreement with those of the WT *Cd*HmuT supporting the conclusion that *Cd*HmuT is a His/Tyr protein.

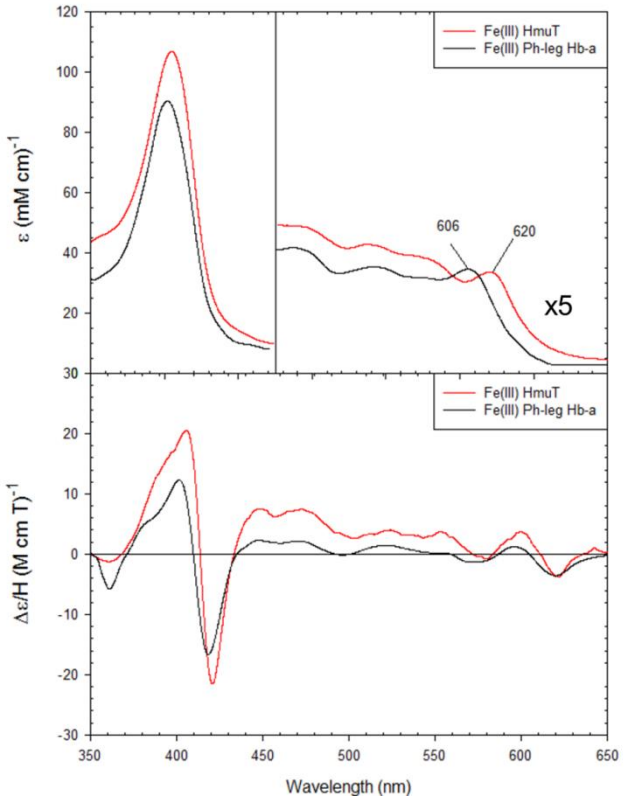

Figure 2.5 The UV-visible absorption and MCD comparison spectra for Fe(III) WT CdHmuT at pH 6.5 with Fe(III) phenol-bound leghemoglobin a. The samples were taken in 50 mM phosphate buffer. Spectra were slightly dependent on buffer conditions. The spectrum of phenol-bound leghemoglobin a was replotted from (38).

Soret-excited rR spectra of WT *Cd*HmuT were recorded over the pH range of 5.0 to 10.0 (Figure 2.14 S4). Two bands are observed in the 1470 – 1510 cm^{-1} region of the rR spectrum. The pair of ν_3 bands observed at 1475 and 1504 cm^{-1} indicates that the protein contains a mixture of six-coordinate high-spin (6cHS) and six-coordinate low-spin (6cLS) hemes. This is consistent with the UV-visible absorption spectra shown in Figure 4. The rR spectra were independent of pH, indicating that the HS/LS equilibrium is not governed by any acid-base speciation of the heme or the protein over this pH range.

2.4.4 Spectroscopy of M292A CdHmuT

The UV-visible absorption (Figure 2.15 S5) and rR (Figure 2.6) spectra for the WT and M292A proteins, as well as the dependence of the rR spectrum on pH (Figure 2.16 S6), were almost identical; the MCD spectra showed only slight differences in absorbance maxima (Figure 2.15 S5). The overall similarities in the spectra indicated that Met is not an axial ligand.

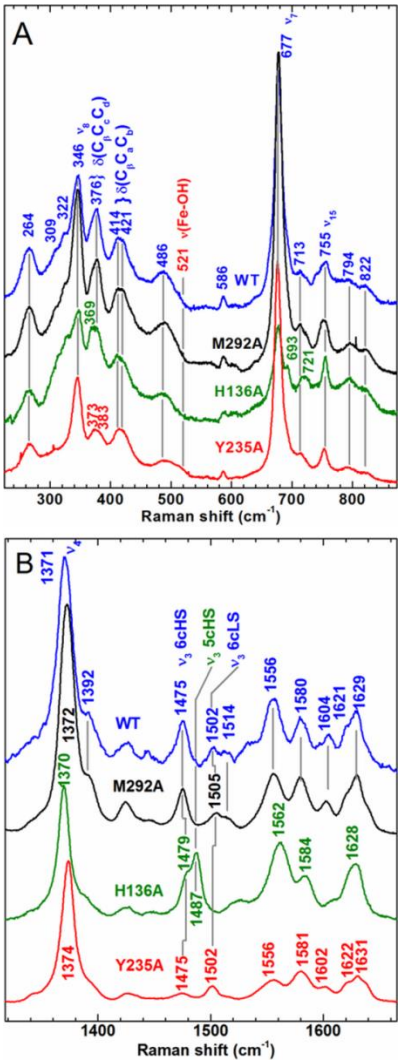

Figure 2.6 Comparison of the Soret-excited rR spectra of WT CdHmuT, M292A, H136A, and Y235A. Protein concentrations were 80, 70, 25 and 36 μM, respectively. All samples were prepared in 50 mM Tris-Cl at pH 7.0. The spectra were recorded with 406.7-nm excitation. A) Low frequency and B) high frequency spectra of WT CdHmuT (blue), M292A (black), H136A (green), and Y235A (red).

2.4.5 Spectroscopy of H136A CdHmuT

In the optical spectrum, H136A *Cd*HmuT gave a broad Soret band that was blue-shifted to 400 nm, compared to the WT, and three defined bands in the α,β region, including one at 620 nm (Figure 2.4). The H136A mutant was compared with three tyrosine models: ShuT (*11*), BLC (*34-36*), and Mb-H93Y (*37*) (Figure 2.17 S7). In the UV-visible absorption spectra, the Soret peaks for all four proteins were similar, with maxima located from 400 to 407 nm. In the visible region, the characteristic high-spin peak located past 600 nm was evident for H136A HmuT, BLC, and ShuT and blue-shifted for H93Y Mb. The peaks and troughs in the visible region of the MCD spectrum are evidence for tyrosinate ligation. Together, the data indicate a ferric five-coordinate tyrosinate-bound heme.

The Soret-excited rR spectrum of H136A HmuT had ν_3 bands at 1479 and 1487 cm^{-1}, indicating the presence of 6cHS and five-coordinate high-spin (5cHS) hemes, respectively (Figure 2.6). The presence of HS species reflects the weakened axial ligand field in the absence of His136 (*39;40*). The bands at 721 and 693 cm^{-1} are assigned to γ_5 (symmetric pyrrole ring fold, A_{2u} in D_{4h}) and γ_{15} (symmetric pyrrole ring fold, B_{2u} in D_{4h}), respectively, by analogy to Mb (*41-43*). Intensification of the bands arising from these modes, which are normally Raman forbidden, reveals lowering of the porphyrin symmetry. Pentacoordination of the heme iron center, as anticipated for H136A mutation and as indicated by the core-size marker band frequencies in Figure 6B, is expected to drive the heme iron out of the mean porphyrin plane toward the Y235 side chain. This type of coordination typically increases the extent of porphyrin doming.

The rR spectrum of H136A does not exhibit a pH dependence over the range of 5.0 to 10.0 (Figure 2.18 S8) suggesting that neither the 5cHS or the 6cHS H136A species binds

hydroxide under alkaline conditions. The inability to form a hydroxide complex has also been reported for *Sm*HasA H32A, wherein tyrosinate is the lone amino acid ligand to the heme (*44*). In fact, there are very few examples of Fe(III) porphyrinates having two anionic axial RO^- ligands, including OH^-, because large overall positive charges are necessary to stabilize such axial ligand sets (*45;46*). Thus, the rR spectra are consistent with an equilibrium mixture of 5cHS Fe−Tyr^- and 6cHS H_2O−Fe−Tyr^- axial ligation.

2.4.6 Spectroscopy of Y235A CdHmuT

Y235A *Cd*HmuT had a Soret band that was red-shifted by 7 nm compared to the WT protein and a significant shoulder near 350 nm, which was absent from the WT and other mutants (Figure 2.4). The α,β region had bands at 575 and 540 nm and no charge transfer band, consistent with a predominantly LS heme.

Figure 2.7 compares the UV-visible absorption and MCD spectra of this mutant in the ferric state at pH 10 with two His/OH^- complexes, alkaline Hb at pH 10 (*47*) and horseradish peroxidase (HRP) at pH 12.5 (*48*). The peaks and troughs in both the Soret and visible regions are located at comparable wavelengths and exhibit similar relative intensities. These similarities indicate that Y235A adopts a His/OH^- ligation set at high pH.

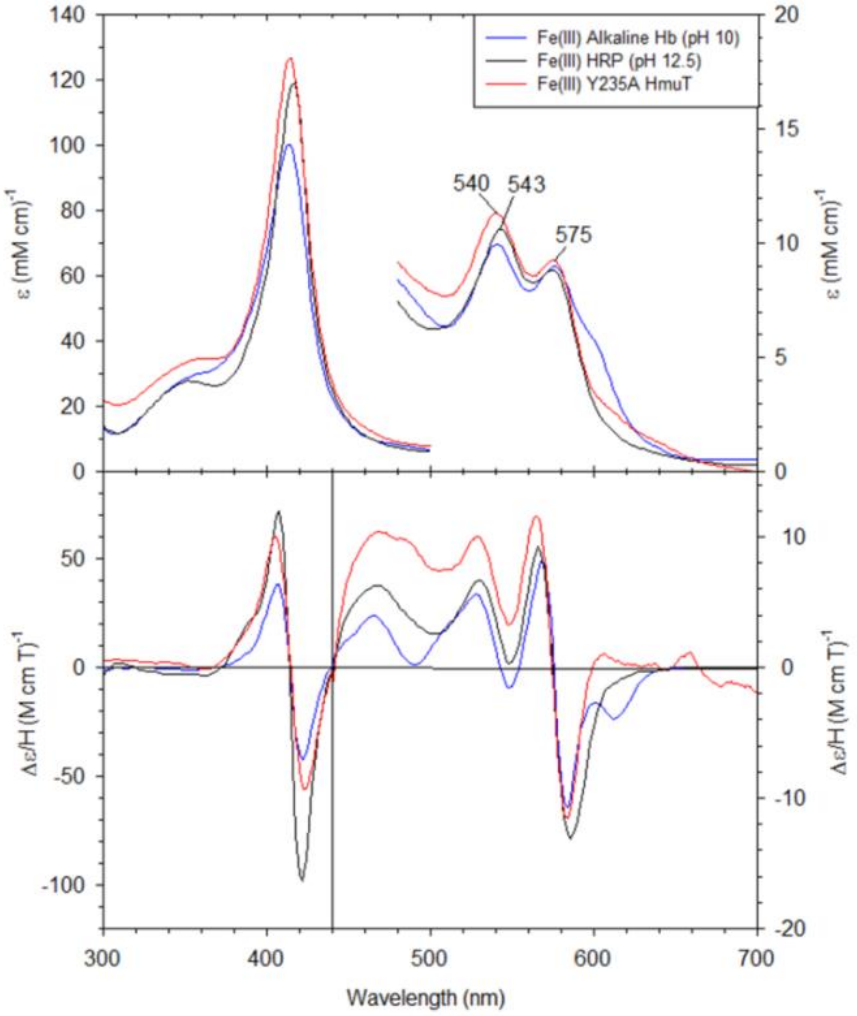

Figure 2.7 The UV-visible absorption and MCD spectra for Fe(III) Y235A CdHmuT at pH 10 with Fe(III) alkaline Hb (pH 10) and Fe(III) HRP (pH 12.5). The samples were prepared in 50 mM phosphate buffer. The spectra of alkaline Hb and HRP were replotted from (47) and (48), respectively.

The heme speciation of Y235A was found to be sensitive to pH in the Raman spectra (Figure 2.8). Y235A was shown to shift from a mixture of 6cHS (1473 cm^{-1}) and 6cLS (1501 cm^{-1}) at pH 10.0 to all 6cHS (1477 cm^{-1}) at pH 5.0 (Figure 2.8C). Based on changes in the relative rR intensities as a function of pH, the pK_a of the acidic form is near 6.

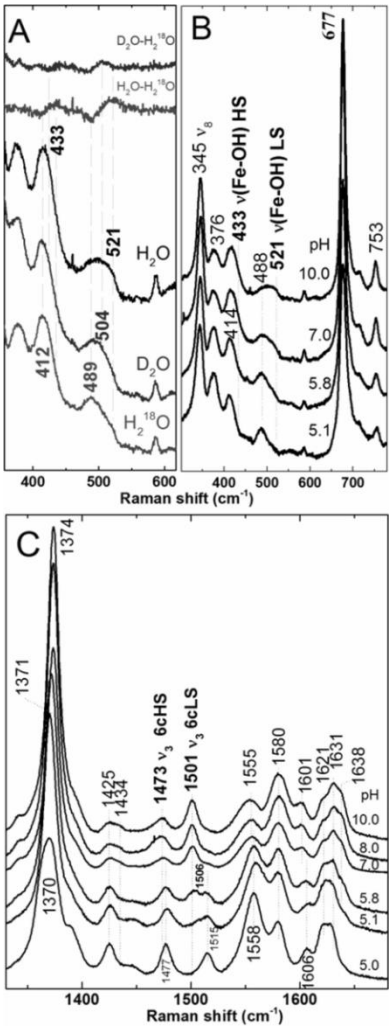

Figure 2.8 The pH dependence of ferric Y235A monitored by 406.7 nm-excited rR spectra (11 mW power at sample). A) Isotopologs of Y235A at pH 10 prepared in H_2O, D_2O, and $H_2{}^{18}O$. Difference spectra of D_2O-$H_2{}^{18}O$ and H_2O-$H_2{}^{18}O$ shown at the top of the figure were generated by subtraction of the respective parent spectra at the bottom of the figure. B) Low frequency and C) high frequency spectra of ferric Y235A as a function of pH. Samples were between 25 and 60 μM.

To determine whether the alkaline species comprising the HS/LS equilibrium are hydroxide complexes, the ^2H and ^{18}O isotopologs were generated in D_2O and $H_2{}^{18}O$, and their Soret-excited rR spectra recorded (Figure 2.8A). Two isotope-sensitive bands were observed. The band at 521 cm^{-1} in H_2O shifted to 504 and 489 cm^{-1} in D_2O and $H_2{}^{18}O$, respectively, and is assigned to the ν_{Fe-OH} mode of LS Y235A−OH. The second isotope-sensitive band appeared at 433 cm^{-1} and shifted to 412 cm^{-1} in $H_2{}^{18}O$ and is tentatively assigned to the ν_{Fe-OH} mode of HS

Y235A−OH component of the mixture. The difference feature for the HS ν_{Fe-OH} observed in the $D_2O - H_2{}^{18}O$ difference spectrum has considerably less amplitude than that of the LS ν_{Fe-OH} making the shift due to deuterium in the HS complex difficult to measure. Y235A is similar to Mb, Hb, and various other heme protein hydroxides (*49-53*) that exist as HS/LS mixtures. Since the alkaline form of Y235A HmuT is a hydroxide complex, it is likely that the 6cHS species that dominates below pH 6 is an aqua complex.

2.4.7 Heme environment in CdHmuT

Useful insight into the distal electrostatic landscape and the σ-donor strength of the *trans* ligand are derived from the position of ferrous heme carbonyl complexes on a ν_{Fe-CO}/ν_{C-O} correlation plot (*54-56*). WT and H136A could be reduced with dithionite only in the presence of CO (which binds to, and stabilizes, the ferrous form of the heme); this has been observed previously for hemes with very low reduction potentials (*57*). The Soret-excited rR spectra are shown in Figure 2.19 S9. Three ^{13}C-sensitive bands were observed for the WT and H136A *Cd*HmuT proteins while four were observed for the Y235A mutant. The spectrum of WT reveals isotope-sensitive bands at 535, 585, and 1920 cm^{-1} which shift to 531, 558, and 1878 cm^{-1}, respectively, in the HmuT−^{13}CO spectrum. They are assigned to the ν_{Fe-C}, δ_{FeCO}, and ν_{C-O} modes, respectively. For the H136A mutant, the isotope–sensitive bands shifted from 530, 574, and 1929 cm^{-1} to 525, 556, and 1884 cm^{-1}, respectively. Thus, its ν_{Fe-C} frequency was 5 cm^{-1} lower than those of WT, and its ν_{C-O} frequency was 9 cm^{-1} greater, consistent with a weakened π-backbonding characteristic of the *trans*-Tyr ligand in this mutant. The largest differences were observed for the Y235A mutant with two ν_{Fe-C} bands occurring at 491 and 509 cm^{-1}, a δ_{FeCO} frequency of 574 cm^{-1}, and ν_{C-O} band at 1943 cm^{-1} which shift to 488, 505, 559, and 1898 cm^{-1}, respectively, with ^{13}C (Figure 2.19 S9).

The inverse correlation between ν_{Fe-C} and ν_{C-O} frequencies is plotted for *Cd*HmuT and its heme pocket mutants along with a number of heme−CO proteins and model complexes for comparison in Figure 2.9. The WT HmuT−CO point falls on the ν_{Fe-C}/ν_{C-O} correlation plot in a position consistent with its proximal ligand being a weaker donor than His, suggesting that WT HmuT−CO contains a weak proximal Fe(II)−O bond, such as Fe(II)−Tyr or Fe(II)−OH_2 (*58*).

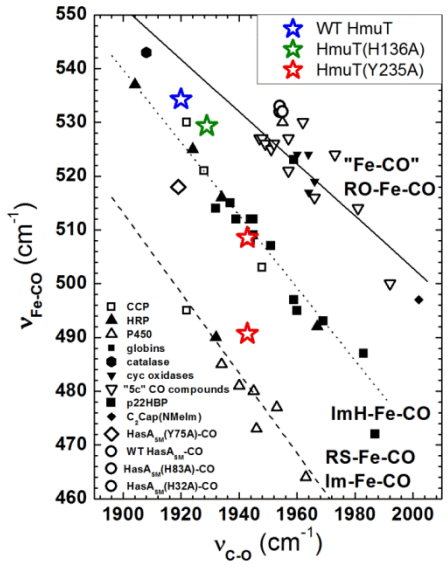

Figure 2.9 Backbonding correlation plot of ν_{Fe-CO} versus ν_{C-O} for ferrous carbonyls of heme proteins showing the dependences of their positions on axial ligation and distal pocket properties. WT (blue), H136A (green), Y235A (red) are shown as stars on the plot. Catalase, hexagon; HasA(Y75A), ◊; HasA(WT), ○; HasA(H83A), ○; HasA(H32A), ○ (57;71). The dashed line is the least squares line for six-coordinate Fe−CO adducts in which the proximal ligand is thiolate or imidazolate; the dotted line is the least squares line for Fe−CO adducts with proximal histidine (neutral imidazole) (53;57;59) (and references therein); and the solid line represents a compilation of "five-coordinate" model complexes (55) (and references therein) and heme proteins which the ligand trans to CO is coordinated through an oxygen atom (61).

Distal H-bond donors to the bound CO ligand and positive charge enhance π-backbonding. Both of these interactions weaken the C−O bond while strengthening the Fe−C bond, placing points high and to the left on the imidazole correlation line (*e.g.*, ν_{Fe-C} 520 cm^{-1} and ν_{C-O} 1935 cm^{-1}) (*59*). Off-axis Fe−C−O distortion and negative charge weaken backbonding which, absent other factors such as hydrogen bonding, is characterized by positions to the low

and to the right on the correlation line. Thus, the positions of WT HmuT−CO and H136A−CO would be interpreted as due to a positive charge near and/or H-bond donation to the bound CO.

The bottom set of spectra in Figure 2.19 S9 reveal that Y235A HmuT−CO has two conformers whose positions on the ν_{Fe-C}/ν_{C-O} correlation plot (Figure 2.9) are distinct from each other and from WT and H136A HmuT−CO. One conformer is located on the imidazole line, indicating neutral histidine axial ligation; its position relative to other proteins on the imidazole correlation line is consistent with a modest distal H-bonding interaction. In contrast, the second conformer is slightly above the imidazolate line suggesting that the proximal histidine (His136) has some imidazolate character, perhaps due to its interaction with an H-bond acceptor in the proximal pocket.

2.4.8 Ferric Y235A CdHmuT−fluoride

Fluoride complexes of heme proteins are sensitive probes of the distal H-bonding environment (*60;61*). The energy of the charge transfer band at 600 – 620 nm (CT1) together with the Fe−F stretching frequency constitutes a sensitive probe of H-bond strength between a distal H-bond donor and the bound F^- ligand. Low ν_{Fe-F} frequencies correlate with red-shifted CT1 bands in complexes having strong hydrogen bonds. The ν_{Fe-F} mode of Y235A HmuT−F was identified by exciting into its CT2 band (450 – 460 nm) with 441.6-nm light (Figure 2.10). Relative enhancement of scattering by the ν_{Fe-F} mode with 441.6-nm excitation is considerably greater than with Soret excitation; peak fitting of the 441.6-nm excited rR spectrum shown in Figure 2.10A revealed that the ν_{Fe-F} band occurs at 392 cm^{-1}. The Y235A HmuT−F CT1 band was observed at 613 nm (16,313 cm^{-1}) (Figure 2.10A inset). Correlation of its ν_{Fe-F} and the CT1 energy places Y235A *Cd*HmuT low on the correlation plot in Figure 2.10B which is consistent with strong hydrogen bonding between the bound F^- ligand and the distal pocket.

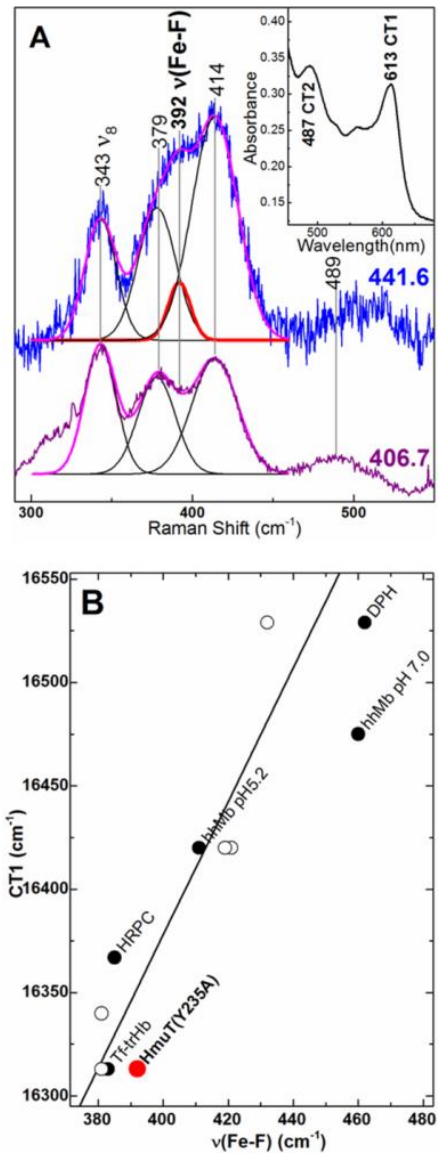

Figure 2.10 Characterization of Y235A−F by correlation of the Fe^{III}−F stretching frequency and CT1 energy. A) Low frequency window of the rR spectra of Y235A−F using Raman excitation into the CT2 (441.6 nm) and Soret (406.7 nm) bands. Protein was 80 μM in 100 mM sodium phosphate buffer in 330 mM sodium fluoride, pH 5.8. Laser power at the sample was 4.6 mW with 441.6-nm excitation and 9.7 mW with 406.7-nm excitation. Peak fitting analyses of both spectra are overlaid on the original spectra with the calculated Fe^{III}−F stretching band shown in red; calculated ν_8 and propionate and vinyl bending bands are shown in black; the overall fit is shown in magenta. Inset: Visible spectrum of Y235A−F rR sample. B) Correlation plot of $\nu_{Fe\text{-}F}$ frequency and the CT1 energy. Y235A is shown in red. Other points are from Nicoletti and coworkers (61). Open circles are for mutants of truncated Hb from Thermobifida fusca (Tf-trHb) with varying number of hydrogen bonds between the distal pocket and the fluoride (60;61).

2.4.9 Ferrous Y235A CdHmuT

Unlike WT and H136A *Cd*HmuT, which are slow to reduce with aqueous buffered $S_2O_4^{2-}$, Y235A *Cd*HmuT was readily converted to a 5cHS ferrous heme (ν_4, 1354 cm^{-1}; ν_3, 1467 cm^{-1}) upon reaction with $S_2O_4^{2-}$ (spectra not shown). The ν_{Fe-His} frequency for 5cHS ferrous hemes has been shown to be significantly enhanced with 441.6 nm laser excitation (*62*) and two ν_{Fe-His} modes for ferrous HmuT-Y235A are tentatively assigned to bands at 221 and 249 cm^{-1} based on comparison of their relative enhancements in the 441.6 and 413.1-nm excited spectra in Figure 2.20 S10. Observation of two ν_{Fe-His} modes is consistent with two proximal pocket conformers in Y235A *Cd*HmuT, which are distinguished by the extent of imidazolate character of the proximal His ligand. These are likely the same conformers responsible for the two ν_{Fe-C} frequencies (491 and 509 cm^{-1}) in the corresponding carbonyl spectrum shown in Figure 2.21 S11.

2.5 Discussion

2.5.1 His/Tyr ligand set identified for HmuT:heme complex

2.5.1.1 Ferric species

Sequence alignment, homology modeling, and UV-visible absorption, MCD, and rR spectroscopies all lead to the conclusion that WT *Cd*HmuT contains a six-coordinate active site with a tyrosine bound to one axial position of the heme and a histidine bound to the other.

H136A *Cd*HmuT exhibited both UV-visible absorption and MCD spectral features of other five-coordinate tyrosine-ligated proteins such as BLC (*36*), *Mycobacterium avium* ssp. *paratuberculosis* (MAP) (*36*), *Plexaura homomalla* coral allene oxide synthase (cAOS) (*35*), *S. dysenteriae* ShuT (*11*), and the *S. aureus* Isd system: IsdA-N1 (*63-65*), IsdB-N2 (*66*), IsdC-N1

(*65;67*), and IsdH-N3 (*66;68*). The ~620 nm charge transfer band appears to be characteristic of a tyrosine bound to the heme.

The Y235A mutant showed loss of the charge transfer band in the UV-visible absorption spectrum, consistent with removal of the axial tyrosine. Both the UV-visible absorption and MCD spectra of Y235A were not comparable with other known 5c His-bound heme proteins, but rather with 6c His/OH^- species, such as HRP (*48*) or alkaline hemoglobin (*47*). It was concluded that the ferric iron was still ligated to H136, but with the axial position vacated by the mutated Y235 occupied by a hydroxide ligand. This His/OH^- motif was seen not only at pH 10, but also at pH 6.5. pK_a values of water *trans* to histidine in ferric heme proteins vary from > 10 down to at least 6.8 (see examples in Table 2.1). The homology model indicates that the Arg237 side chain is found in the heme pocket on the side opposite the axial histidine. Thus, the low pK_a for Y235A may be attributable to the interaction of water with this cationic side chain, which could serve as the H-bond donor to the axial Tyr235 ligand. Consistent with this proposal, in almost all tyrosine-heme proteins studied to date, the axial tyrosine is hydrogen-bonded to a second residue; common examples include Tyr, Arg and His (see examples in Table S2).

For heme proteins having a bound water ligand, a decrease in the Fe−OH stretching frequency relative to Mb and Hb has been attributed to strong hydrogen bond donation to the hydroxide. For example, in hemoglobin from *M. tuberculosis* (HbN) a 35 cm^{-1} decrease in the HS Fe−OH stretching frequency has been attributed to a strong interaction between the bound hydroxide and a distal tyrosine side chain (*52*). Very strong hydrogen bonding in alkaline HRP similarly gives rise to the LS ν_{Fe-OH} frequency of 503 cm^{-1}, 47 cm^{-1} lower than the LS ν_{Fe-OH} Mb frequency of 550 cm^{-1} (*49*). For Y235A *Cd*HmuT, the LS and HS Fe−OH stretching frequencies are 29 and 58 cm^{-1} lower, respectively, than those reported for Mb. This strongly

suggests Tyr235 has a hydrogen bonding partner that upon removal of Tyr235 its normal H-bond partner serves as a H-bond donor to the hydroxide ligand. The presence of a strong hydrogen bonding partner on the Tyr235 side of the heme is further supported by the position of the Y235A HmuT−F on the ν_{Fe-F} frequency/CT1 energy empirical correlation plot (Figure 2.10B). On the correlation plot, it lies very close to the *Thermobifida fusca* (Tf-trHb) fluoride adduct which has two strong hydrogen bonds between the fluoride and the distal heme pocket (*61*).

2.5.1.2 Ferrous Species

The ferrous spectra of the wild-type and the H136A mutant could not be reduced under standard reductive conditions, e.g., sodium dithionite, unless in the presence of CO, which binds to the ferrous heme. This contrasts with reduction of Y235A, which is readily effected. These observations are consistent with His/Tyr heme ligation. Related observations have been made for HasA (*57*), which has a very low reduction potential (−550 mV versus SHE) (*69*). Upon mutation of its axial tyrosine, it is also readily reduced by dithionite (*57*).

Proteins and engineered mutants that can bind CO with either a *trans* His or Tyr have a histidine in some instances and an oxygen ligand (tyrosine or water) in others (*57*). For example, the His/Tyr protein HasA, gives an O−Fe−CO species upon reduction in the presence of CO (*57*). Human heme oxygenase H25Y, with a tyrosine axial ligand in the ferric form, gives an H_2O−Fe−CO species (*70*). Catalase, with an axial tyrosine, is thought to form the Tyr−Fe−CO species (*71*).

The ν_{Fe-CO} band in the Soret-excited rR spectrum of catalase−CO has been reported to be more intense than the totally symmetric ν_7 band (*71*). This signature was correlated with the anionic character of the proximal Tyr whose coordination to heme iron is stabilized by H-bonding to a His residue. Although the ν_{Fe-CO} bands for WT and H136A HmuT CO complexes

are not more intense than their ν_7 bands, they are quite intense relative to the ν_{Fe-CO} band of Y235A HmuT−CO. This is taken as further evidence for a charge neutral Tyr−Fe(II)−CO species in H136A *Cd*HmuT and WT *Cd*HmuT.

Y235A was reduced by aqueous $S_2O_4^{2-}$ in the absence of CO. Based on the two Fe−His stretching frequencies of 221 and 249 cm^{-1}, ferrous Y235A *Cd*HmuT has one conformer with Fe−His proximal bond of strength comparable to that of Mb and Hb (218 – 224 cm^{-1}) (*72;73*) and a second conformer with significant imidazolate character in the proximal histidine similar to that observed for peroxidases (*i.e.*, ν_{Fe-Im^-} occurs at 244 cm^{-1} for HRP) (*74*).

2.5.2 Why tyrosine?

Although not common in heme proteins (*75*), the His/Tyr ligand set has also been observed in *S. marcescens* HasA (*76*), *P. aeruginosa* HasA (*77;78*) and PhuR (*79*), *E. coli* CcmE (*80;81*), *Paracoccus denitrificans* MauG (*82*), and *Y. pestis* HmuT (*12*). Of these, HasA, PhuR, CcmE and HmuT are all involved in heme transfer. MauG, in contrast, appears to use the tyrosinate axial ligand to stabilize a high oxidation center in the mechanistic pathway of this protein (*83*). The His/Tyr ligand set is also known in hemoglobin variants such as Hb M Saskatoon (*84*) and has been created by site-directed mutagenesis of sperm whale Mb (HisE7Tyr) (*85*).

Tyrosine alone is also an axial ligand in a number of proteins in heme uptake pathways characterized to date, including *S. dysenteriae* ShuT (*10*), *P. aeruginosa* PhuT (*10;11*), *Y. pestis* HasA (*86*), *N. meningitidis* HmbR (*87*) and the heme uptake proteins from the *S. aureus* Isd system [IsdA (*64*), IsdB (*88*), IsdC (*67*), and IsdH (*68*)] as well as IsdX1 and IsdX2-N5 of *Bacillus anthracis* (*89;90*). Sequence alignment of the Isd proteins revealed these tyrosine residues are conserved among species, and their role in heme binding is significant. It is possible

that tyrosine favors ligand switching; it has been noted that *S. aureus* IsdA binds heme using Tyr166 in the oxidized state and His83 in the reduced state of the protein (*14;63;65*). IsdB-N2, which has an axial tyrosine, also binds an axial methionine under some circumstances (*88*).

Modulation of H-bond donation to the axial tyrosine may play a role in triggering heme release and transfer. In some instances, the hydrogen bonding residue participates in an extended H-bonding network that also involves the heme propionates (*91*). Disruption of the hydrogen bonding network in these cases could have cooperative effects on the structure of the protein, its affinity for ferric heme, and potentially on the kinetics and mechanism of ferric heme transfer (*33;44;57*).

Tyrosine may also be employed as an axial ligand to ensure heme remains in its ferric form (*57*). Tyrosinate-bound heme proteins are characterized by low reduction potentials, consistent with stabilization of the Fe(III) center by the negative charge of the tyrosinate. For example, the midpoint reduction potential of *Sm*HasA was reported to be −550 mV (*69*), nearly 0.5 V more negative than the potential of −60 mV for the Fe(III)/Fe(II) couple (*92*). The redox potential indicates that tyrosine binds more strongly with the Fe(III) of hemin than with the Fe(II) of heme. Assuming that the His/Tyr axial ligation in HmuT imposes a similarly negative potential as in HasA, estimation of this difference in binding free energy is facilitated by a thermodynamic cycle (Figure 2.22 S12). Based on this cycle, $(\Delta G_{III} - \Delta G_{II}) = nF(E_b^\circ - E_f^\circ) = -4.7\times10^4\ J\cdot mol^{-1}$ where ΔG_{III} and ΔG_{II} are the free energies of apoHmuT complexation with Fe^{III}PPIX to give $HmuT^{III}$ and Fe^{II}PPIX to yield $HmuT^{II}$, respectively. E_b° and E_f° are the reduction potentials of bound ($HmuT^{III}$) and free Fe^{III}PPIX, respectively. Thus, formation of $HmuT^{III}$ is favored by an estimated 47 $kJ\cdot mol^{-1}$ over $HmuT^{II}$. This would strongly favor binding of the ferric form of the protein, thereby favoring uptake of Fe(III) by any bacterium having a

Tyr^{-}-based HBP that delivers Fe^{III}PPIX to the ABC permease. This discrimination could help guard against the damaging effects of Fenton-type chemistry from buildup of free heme in the reducing environment of the cell.

HmuT joins a growing number of extracellular and cell-surface HBP's that use the H-bond assisted axial Tyr ligand motif to bind and stabilize Fe^{III}PPIX. These proteins share high affinities for ferric heme and ostensibly use the free energy of protein-protein complexation to destabilize their Fe^{III}PPIX-bound states, thereby facilitating transfer to the acceptor protein (*5*).

2.6 Conclusions

Multiple lines of spectroscopic evidence have revealed the heme axial ligand set in HmuT from *C. diphtheriae* to be His136/Tyr235 from the N- and C-terminal domains of the protein, respectively. The same axial ligand set is found in *Yp*HmuT, but with the His and Tyr ligands arising from the C- and N-terminal domains of the proteins, respectively. This highlights the variety of binding motifs used by heme binding proteins in bacteria. Solution speciation of the ferric form of *Cd*HmuT is dominated by the 1:1 complex, which, like HasA, exists as a thermal spin state equilibrium between 6cHS and 6cLS complexes. Ferric *Cd*HmuT is slow to reduce with $S_2O_4^{2-}$ in the presence of CO with His136 being replaced by CO upon reduction. The position of the *trans*-Tyr carbonyl complex on the neutral O-bound ligand line of the π-backbonding correlation plot suggests that, as in HasA−CO, the Tyr-based phenol ligand is a charge neutral heme carbonyl. Thus, HmuT reinforces the emerging theme of extracellular and cell surface heme-binding proteins that use H-bond assisted axial Tyr ligands to stabilize hemin-bound states that require a heme-accepting partner for release and transfer of the hemin substrate. Moreover, the axial Tyr ligand (Tyr235 in *Cd*HmuT) is required for full hemin uptake function in *C. diphtheriae*.

2.7 Acknowledgments

We thank Jonathan M. Burgos for technical assistance and Emily Johnson and Dr. Masanori Sono for helpful discussions. We also like to thank the Georgia State University Molecular Basis of Disease Fellowship program for financially supporting E. B. D.

2.8 References

1. Braun, V. and Hantke, K. (2011) Recent insights into iron import by bacteria. *Curr. Opin. Chem. Biol. 15*, 328-334.

2. Smith, A. D. and Wilks, A. (2012) Extracellular heme uptake and the challenges of bacterial cell membranes. *Curr. Top. Membr. 69*, 359-392.

3. Benson, D. R. and Rivera, M. (2013) Heme uptake and metabolism in bacteria. *Met. Ions Life Sci. 12*, 279-332.

4. Farrand, A. J. and Skaar, E. P. (2014) Heme and infectious diseases, in *Handbook of Porphyrin Science with Applications to Chemistry, Physics, Materials Science, Engineering, Biology and Medicine, Vol 26: Heme Biochemistry* (Ferreira, G. C., Kadish, K. M., Smith, K. M., and Guilard, R., Eds.) pp 317-377, World Scientific, Hackensack, NJ.

5. Rodgers, K. R. and Lukat-Rodgers, G. S. (2014) Biophysical perspectives on the acquisition, transport, and trafficking of heme in bacteria, in *Handbook of Porphyrin Science with Applications to Chemistry, Physics, Materials Science, Engineering, Biology and Medicine, Vol. 30: Heme Proteins, Part II* (Ferreira, G. C., Kadish, K. M., Smith, K. M., and Guilard, R., Eds.) pp 251-309, World Scientific, Hackensack, N.J.

6. Wilks, A. and O'Neill, M. J. (2014) Extracellular heme uptake and metabolism in bacterial pathogenesis, in *Handbook of Porphyrin Science with Applications to Chemistry, Physics, Materials Science, Engineering, Biology and Medicine, Vol 26: Heme Biochemistry* (Ferreira, G. C., Kadish, K. M., Smith, K. M., and Guilard, R., Eds.) pp 267-315, World Scientific, Hackensack, NJ.

7. Rice, A. J., Park, A., and Pinkett, H. W. (2014) Diversity in ABC transporters: Type I, II and III importers. *Crit. Rev. Biochem. Mol. Biol. 49*, 426-437.

8. ter Beek, J., Guskov, A., and Slotboom, D. J. (2014) Structural diversity of ABC transporters. *J. Gen. Physiol. 143*, 419-435.

9. Chu, B. C. and Vogel, H. J. (2011) A structural and functional analysis of type III periplasmic and substrate binding proteins: Their role in bacterial siderophore and heme transport. *Biol. Chem. 392*, 39-52.

10. Ho, W. W., Li, H. Y., Eakanunkul, S., Tong, Y., Wilks, A., Guo, M. L., and Poulos, T. L. (2007) Holo-and apo-bound structures of bacterial periplasmic heme-binding proteins. *J. Biol. Chem. 282*, 35796-35802.

11. Eakanunkul, S., Lukat-Rodgers, G. S., Sumithran, S., Ghosh, A., Rodgers, K. R., Dawson, J. H., and Wilks, A. (2005) Characterization of the periplasmic heme-binding protein ShuT from the heme uptake system of *Shigella dysenteriae*. *Biochemistry 44*, 13179-13191.

12. Mattle, D., Zeltina, A., Woo, J. S., Goetz, B. A., and Locher, K. P. (2010) Two stacked heme molecules in the binding pocket of the periplasmic heme-binding protein HmuT from *Yersinia pestis*. *J. Mol. Biol. 404*, 220-231.

13. Woo, J. S., Zeltina, A., Goetz, B. A., and Locher, K. P. (2012) X-ray structure of the *Yersinia pestis* heme transporter HmuUV. *Nature Struc. Mol. Biol. 19*, 1310-1315.

14. Grigg, J. C., Vermeiren, C. L., Heinrichs, D. E., and Murphy, M. E. (2007) Heme coordination by *Staphylococcus aureus* IsdE. *J. Biol. Chem. 282*, 28815-28822.

15. Sook, B. R., Block, D. R., Sumithran, S., Montañez, G. E., Rodgers, K. R., Dawson, J. H., Eichenbaum, Z., and Dixon, D. W. (2008) Characterization of SiaA, a streptococcal heme-binding protein associated with a heme ABC transport system. *Biochemistry 47*, 2678-2688.

16. Ran, Y., Liu, M., Zhu, H., Nygaard, T. K., Brown, D. E., Fabian, M., Dooley, D. M., and Lei, B. (2010) Spectroscopic identification of heme axial ligands in HtsA that are involved in heme acquisition by *Streptococcus pyogenes*. *Biochemistry 49*, 2834-2842.

17. Trost, E., Blom, J., Soares, S. D., Huang, I. H., Al-Dilaimi, A., Schroder, J., Jaenicke, S., Dorella, F. A., Rocha, F. S., Miyoshi, A., Azevedo, V., Schneider, M. P., Silva, A., Camello, T. C., Sabbadini, P. S., Santos, C. S., Santos, L. S., Hirata, R., Mattos-Guaraldi, A. L., Efstratiou, A., Schmitt, M. P., Hung, T. T., and Tauch, A. (2012) Pangenomic study of *Corynebacterium diphtheriae* that provides insights into the genomic diversity of pathogenic isolates from cases of classical diphtheria, endocarditis, and pneumonia. *J. Bacteriol. 194*, 3199-3215.

18. Wagner, K. S., White, J. M., Lucenko, I., Mercer, D., Crowcroft, N. S., Neal, S., and Efstratiou, A. (2012) Diphtheria in the postepidemic period, Europe, 2000-2009. *Emerg. Infect. Dis. 18*, 217-225.

19. Schmitt, M. P. (1997) Utilization of host iron sources by *Corynebacterium diphtheriae*: Identification of a gene whose product is homologous for eukaryotic heme oxygenases and is required for acquisition of iron from heme and hemoglobin. *J. Bacteriol. 179*, 838-845.

20. Drazek, E. S., Hammack, C. A., and Schmitt, M. P. (2000) *Corynebacterium diphtheriae* genes required for acquisition of iron from haemin and haemoglobin are homologous to ABC haemin transporters. *Mol. Microbiol. 36*, 68-84.

21. Schmitt, M. P. and Drazek, E. S. (2001) Construction and consequences of directed mutations affecting the hemin receptor in pathogenic *Corynebacterium species*. *J. Bacteriol. 183*, 1476-1481.

22. Allen, C. E. and Schmitt, M. P. (2011) Novel hemin binding domains in the *Corynebacterium diphtheriae* HtaA protein interact with hemoglobin and are critical for heme iron utilization by HtaA. *J. Bacteriol. 193*, 5374-5385.

23. Allen, C. E., Burgos, J. M., and Schmitt, M. P. (2013) Analysis of novel iron-regulated, surface-anchored hemin-binding proteins in *Corynebacterium diphtheriae*. *J. Bacteriol. 195*, 2852-2863.

24. Schmitt, M. P. (2014) Iron acquisition and iron-dependent gene expression in *Corynebacterium diphtheriae*, in *Corynebacterium diphtheriae and Related Toxigenic Species: Genomics, Pathogenicity and Applications* (Burkovski, A., Ed.) pp 95-121, Springer.

25. Allen, C. E. and Schmitt, M. P. (2015) Utilization of host iron sources by *Corynebacterium diphtheriae*: Multiple hemoglobin-binding proteins are essential for the use of iron from the hemoglobin-haptoglobin complex. *J. Bacteriol. 197*, 553-562.

26. Allen, C. E. and Schmitt, M. P. (2009) HtaA is an iron-regulated hemin binding protein involved in the utilization of heme iron in *Corynebacterium diphtheriae*. *J. Bacteriol. 191*, 2638-2648.

27. Kunkle, C. A. and Schmitt, M. P. (2003) Analysis of the *Corynebacterium diphtheriae* DtxR regulon: Identification of a putative siderophore synthesis and transport system that is similar to the *Yersinia* high-pathogenicity island-encoded yersiniabactin synthesis and uptake system. *J. Bacteriol. 185*, 6826-6840.

28. Bibb, L. A., Kunkle, C. A., and Schmitt, M. P. (2007) The ChrA-ChrS and HrrA-HrrS signal transduction systems are required for activation of the *hmuO* promoter and repression of the *hemA* promoter in *Corynebacterium diphtheriae*. *Infect. Immun. 75*, 2421-2431.

29. Kunkle, C. A. and Schmitt, M. P. (2007) Comparative analysis of *hmuO* function and expression in *Corynebacterium* species. *J. Bacteriol. 189*, 3650-3654.

30. Schmitt, M. P. and Holmes, R. K. (1991) Iron-dependent regulation of diphtheria toxin and siderophore expression by the cloned *Corynebacterium diphtheriae* repressor gene Dtxr in *C. diphtheriae* C7 strains. *Infect. Immun. 59*, 1899-1904.

31. Pond, A. E., Roach, M. P., Thomas, M. R., Boxer, S. G., and Dawson, J. H. (2000) The H93G myoglobin cavity mutant as a versatile template for modeling heme proteins: Ferrous, ferric, and ferryl mixed-ligand complexes with imidazole in the cavity. *Inorg. Chem. 39*, 6061-6066.

32. Roy, A., Kucukural, A., and Zhang, Y. (2010) I-TASSER: A unified platform for automated protein structure and function prediction. *Nat. Protoc. 5*, 725-738.

33. Caillet-Saguy, C., Turano, P., Piccioli, M., Lukat-Rodgers, G. S., Czjzek, M., Guigliarelli, B., Izadi-Pruneyre, N., Rodgers, K. R., Delepierre, M., and Lecroisey, A. (2008) Deciphering the structural role of histidine 83 for heme binding in hemophore HasA. *J. Biol. Chem. 283*, 5960-5970.

34. Browett, W. R. and Stillman, M. J. (1979) Magnetic circular dichroism studies of bovine liver catalase. *Biochim. Biophys. Acta 577*, 291-306.

35. Abraham, B. D., Sono, M., Boutaud, O., Shriner, A., Dawson, J. H., Brash, A. R., and Gaffney, B. J. (2001) Characterization of the coral allene oxide synthase active site with UV-visible absorption, magnetic circular dichroism, and electron paramagnetic resonance spectroscopy: Evidence for tyrosinate ligation to the ferric enzyme heme iron. *Biochemistry 40*, 2251-2259.

36. Bandara, D. M. I., Sono, M., Bruce, G. S., Brash, A. R., and Dawson, J. H. (2011) Coordination modes of tyrosinate-ligated catalase-type heme enzymes: Magnetic circular dichroism studies of *Plexaura homomalla* allene oxide synthase, *Mycobacterium avium* ssp. paratuberculosis protein-2744c, and bovine liver catalase in their ferric and ferrous states. *J. Inorg. Biochem. 105*, 1786-1794.

37. Pond, A. E., Roach, M. P., Sono, M., Rux, A. H., Franzen, S., Hu, R., Thomas, M. R., Wilks, A., Dou, Y., Ikeda-Saito, M., Ortiz de Montellano, P. R., Woodruff, W. H., Boxer, S. G., and Dawson, J. H. (1999) Assignment of the heme axial ligand(s) for the ferric myoglobin (H93G) and heme oxygenase (H25A) cavity mutants as oxygen donors using magnetic circular dichroism. *Biochemistry 38*, 7601-7608.

38. Sievers, G., Gadsby, P. M., Peterson, J., and Thomson, A. J. (1983) Magnetic circular dichroism spectra of soybean leghaemoglobin *a* at room temperature and 4.2 K. *Biochim. Biophys. Acta 742*, 637-647.

39. Spiro, T. G. and Strekas, T. C. (1974) Resonance Raman spectra of heme proteins - Effects of oxidation and spin state. *J. Am. Chem. Soc. 96*, 338-345.

40. Strekas, T. C. and Spiro, T. G. (1974) Resonance Raman evidence for anomalous heme structures in cytochrome *c'* from *Rhodopseudomonas palustris*. *Biochim. Biophys. Acta 351*, 237-245.

41. Hu, S. Z., Smith, K. M., and Spiro, T. G. (1996) Assignment of protoheme resonance Raman spectrum by heme labeling in myoglobin. *J. Am. Chem. Soc. 118*, 12638-12646.

42. Smulevich, G., Hu, S. Z., Rodgers, K. R., Goodin, D. B., Smith, K. M., and Spiro, T. G. (1996) Heme-protein interactions in cytochrome *c* peroxidase revealed by site-directed mutagenesis and resonance Raman spectra of isotopically labeled hemes. *Biospectroscopy 2*, 365-376.

43. Heering, H. A., Jansen, M. A. K., Thorneley, R. N. F., and Smulevich, G. (2001) Cationic ascorbate peroxidase isoenzyme II from tea: Structural insights into the heme pocket of a unique hybrid peroxidase. *Biochemistry 40,* 10360-10370.

44. Caillet-Saguy, C., Piccioli, M., Turano, P., Lukat-Rodgers, G. S., Wolff, N., Rodgers, K. R., Izadi-Pruneyre, N., Delepierre, M., and Lecroisey, A. (2012) Role of the iron axial ligands of heme carrier HasA in heme uptake and release. *J. Biol. Chem. 287,* 26932-26943.

45. Reed, R. A., Rodgers, K. R., Kushmeider, K., Spiro, T. G., and Su, Y. O. (1990) Iron-hydroxide stretching resonance Raman bands of a water-soluble sterically hindered porphyrin. *Inorg. Chem. 29,* 2881-2883.

46. Rodgers, K. R., Reed, R. A., Spiro, T. G., and Su, Y. O. (1992) Fe-OH bond strength in high- and low-spin bis-hydroxides of a model heme from resonance Raman spectroscopy - Implications for heme proteins. *New J. Chem. 16,* 533-535.

47. Sono, M. and Dawson, J. H. (1984) Extensive studies of the heme coordination structure of indoleamine 2,3-dioxygenase and of tryptophan binding with magnetic and natural circular-dichroism and electron paramagnetic resonance spectroscopy. *Biochim. Biophys. Acta 789,* 170-187.

48. Pond, A. E., Sono, M., Elenkova, E. A., McRee, D. E., Goodin, D. B., English, A. M., and Dawson, J. H. (1999) Magnetic circular dichroism studies of the active site heme coordination sphere of exogenous ligand-free ferric cytochrome *c* peroxidase from yeast: Effects of sample history and pH. *J. Inorg. Biochem. 76,* 165-174.

49. Asher, S. A. and Schuster, T. M. (1979) Resonance Raman examination of axial ligand bonding and spin-state equilibria in metmyoglobin hydroxide and other heme derivatives. *Biochemistry 18,* 5377-5387.

50. Feis, A., Marzocchi, M. P., Paoli, M., and Smulevich, G. (1994) Spin state and axial ligand bonding in the hydroxide complexes of metmyoglobin, methemoglobin, and horseradish peroxidase at room and low temperatures. *Biochemistry 33,* 4577-4583.

51. Lukat-Rodgers, G. S., Rexine, J. L., and Rodgers, K. R. (1998) Heme speciation in alkaline ferric FixL and possible tyrosine involvement in the signal transduction pathway for regulation of nitrogen fixation. *Biochemistry 37,* 13543-13552.

52. Yeh, S. R., Couture, M., Ouellet, Y., Guertin, M., and Rousseau, D. L. (2000) A cooperative oxygen finding hemoglobin from *Mycobacterium tuberculosis* - Stabilization of heme ligands by a distal tyrosine residue. *J. Biol. Chem. 275,* 1679-1684.

53. Streit, B. R., Blanc, B., Lukat-Rodgers, G. S., Rodgers, K. R., and DuBois, J. L. (2010) How active-site protonation state influences the reactivity and ligation of the heme in chlorite dismutase. *J. Am. Chem. Soc. 132,* 5711-5724.

54. Vogel, K. M., Kozlowski, P. M., Zgierski, M. Z., and Spiro, T. G. (2000) Role of the axial ligand in heme-CO backbonding; DFT analysis of vibrational data. *Inorg. Chim. Acta 297*, 11-17.

55. Spiro, T. G. and Wasbotten, I. H. (2005) CO as a vibrational probe of heme protein active sites. *J. Inorg. Biochem. 99*, 34-44.

56. Spiro, T. G., Soldatova, A. V., and Balakrishnan, G. (2013) CO, NO and O_2 as vibrational probes of heme protein interactions. *Coord. Chem. Rev. 257*, 511-527.

57. Lukat-Rodgers, G. S., Rodgers, K. R., Caillet-Saguy, C., Izadi-Pruneyre, N., and Lecroisey, A. (2008) Novel heme ligand displacement by CO in the soluble hemophore HasA and its proximal ligand mutants: Implications for heme uptake and release. *Biochemistry 47*, 2087-2098.

58. Linder, D. P., Silvernail, N. J., Barabanschikov, A., Zhao, J. Y., Alp, E. E., Sturhahn, W., Sage, J. T., Scheidt, W. R., and Rodgers, K. R. (2014) The diagnostic vibrational signature of pentacoordination in heme carbonyls. *J. Am. Chem. Soc. 136*, 9818-9821.

59. Smulevich, G., Mauro, J. M., Fishel, L. A., English, A. M., Kraut, J., and Spiro, T. G. (1988) Cytochrome *c* peroxidase mutant active site structures probed by resonance Raman and infrared signatures of the CO adducts. *Biochemistry 27*, 5486-5492.

60. Droghetti, E., Nicoletti, F. P., Bonamore, A., Sciamanna, N., Boffi, A., Feis, A., and Smulevich, G. (2011) The optical spectra of fluoride complexes can effectively probe H-bonding interactions in the distal cavity of heme proteins. *J. Inorg. Biochem. 105*, 1338-1343.

61. Nicoletti, F. P., Droghetti, E., Boechi, L., Bonamore, A., Sciamanna, N., Estrin, D. A., Feis, A., Boffi, A., and Smulevich, G. (2011) Fluoride as a probe for H-bonding interactions in the active site of heme proteins: The case of *Thermobifida fusca* hemoglobin. *J. Am. Chem. Soc. 133*, 20970-20980.

62. Bangcharoenpaurpong, O., Schomacker, K. T., and Champion, P. M. (1984) A Resonance Raman investigation of myoglobin and hemoglobin. *J. Am. Chem. Soc. 106*, 5688-5698.

63. Vermeiren, C. L., Pluym, M., Mack, J., Heinrichs, D. E., and Stillman, M. J. (2006) Characterization of the heme binding properties of *Staphylococcus aureus* IsdA. *Biochemistry 45*, 12867-12875.

64. Grigg, J. C., Vermeiren, C. L., Heinrichs, D. E., and Murphy, M. E. P. (2007) Haem recognition by a *Staphylococcus aureus* NEAT domain. *Mol. Microbiol. 63*, 139-149.

65. Pluym, M., Muryoi, N., Heinrichs, D. E., and Stillman, M. J. (2008) Heme binding in the NEAT domains of IsdA and IsdC of *Staphylococcus aureus*. *J. Inorg. Biochem. 102*, 480-488.

66. Tiedemann, M. T., Muryoi, N., Heinrichs, D. E., and Stillman, M. J. (2009) Characterization of IsdH (NEAT domain 3) and IsdB (NEAT domain 2) in *Staphylococcus aureus* by magnetic circular dichroism spectroscopy and electrospray ionization mass spectrometry. *J. Porph. Phthalo. 13*, 1006-1016.

67. Sharp, K. H., Schneider, S., Cockayne, A., and Paoli, M. (2007) Crystal structure of the heme-IsdC complex, the central conduit of the Isd iron/heme uptake system in *Staphylococcus aureus*. *J. Biol. Chem. 282*, 10625-10631.

68. Watanabe, M., Tanaka, Y., Suenaga, A., Kuroda, M., Yao, M., Watanabe, N., Arisaka, F., Ohta, T., Tanaka, I., and Tsumoto, K. (2008) Structural basis for multimeric heme complexation through a specific protein-heme interaction - The case of the third NEAT domain of IsdH from *Staphylococcus aureus*. *J. Biol. Chem. 283*, 28649-28659.

69. Izadi, N., Henry, Y., Haladjian, J., Goldberg, M. E., Wandersman, C., Delepierre, M., and Lecroisey, A. (1997) Purification and characterization of an extracellular heme-binding protein, HasA, involved in heme iron acquisition. *Biochemistry 36*, 7050-7057.

70. Liu, Y., Moenne-Loccoz, P., Hildebrand, D. P., Wilks, A., Loehr, T. M., Mauk, A. G., and Ortiz de Montellano, P. R. (1999) Replacement of the proximal histidine iron ligand by a cysteine or tyrosine converts heme oxygenase to an oxidase. *Biochemistry 38*, 3733-3743.

71. Hu, S. H. and Kincaid, J. R. (1992) Resonance Raman studies of the carbonmonoxy form of catalase - Evidence for and effects of phenolate ligation. *FEBS Lett. 314*, 293-296.

72. Kitagawa, T., Nagai, K., and Tsubaki, M. (1979) Assignment of the Fe-nitrogen (His F8) stretching band in the resonance Raman spectra of deoxymyoglobin. *FEBS Lett. 104*, 376-378.

73. Nagai, K. and Kitagawa, T. (1980) Differences in Fe(II)-Nε (His-F8) stretching frequencies between deoxyhemoglobins in the two alternative quaternary structures. *Proc. Natl. Acad. Sci. U. S. A. 77*, 2033-2037.

74. Teraoka, J. and Kitagawa, T. (1981) Structural implication of the heme-linked ionization of horseradish peroxidase probed by the Fe-histidine stretching Raman line. *J. Biol. Chem. 256*, 3969-3977.

75. Reedy, C. J., Elvekrog, M. M., and Gibney, B. R. (2008) Development of a heme protein structure-electrochemical function database. *Nucleic Acids Res. 36*, D307-D313.

76. Arnoux, P., Haser, R., Izadi, N., Lecroisey, A., Delepierre, M., Wandersman, C., and Czjzek, M. (1999) The crystal structure of HasA, a hemophore secreted by *Serratia marcescens*. *Nature Struct. Biol. 6*, 516-520.

77. Alontaga, A. Y., Rodriguez, J. C., Schonbrunn, E., Becker, A., Funke, T., Yukl, E. T., Hayashi, T., Stobaugh, J., Monne-Loccoz, P., and Rivera, M. (2009) Structural characterization of the hemophore HasAp from *Pseudomonas aeruginosa*: NMR

spectroscopy reveals protein-protein interactions between holo-HasAp and hemoglobin. *Biochemistry 48*, 96-109.

78. Kumar, R., Matsumura, H., Lovell, S., Yao, H. L., Rodriguez, J. C., Battaile, K. P., Moenne-Loccoz, P., and Rivera, M. (2014) Replacing the axial ligand tyrosine 75 or its hydrogen bond partner histidine 83 minimally affects hemin acquisition by the hemophore HasAp from *Pseudomonas aeruginosa*. *Biochemistry 53*, 2112-2125.

79. Smith, A. D., Modi, A. R., Sun, S. F., Dawson, J. H., and Wilks, A. (2015) Spectroscopic determination of distinct heme ligands in outer-membrane receptors PhuR and HasR of *Pseudomonas aeruginosa*. *Biochemistry 54*, 2601-2612.

80. Couture, M., Das, T. K., Lee, H. C., Peisach, J., Rousseau, D. L., Wittenberg, B. A., Wittenberg, J. B., and Guertin, M. (1999) *Chlamydomonas* chloroplast ferrous hemoglobin - Heme pocket structure and reactions with ligands. *J. Biol. Chem. 274*, 6898-6910.

81. Das, T. K., Couture, M., Lee, H. C., Peisach, J., Rousseau, D. L., Wittenberg, B. A., Wittenberg, J. B., and Guertin, M. (1999) Identification of the ligands to the ferric heme of *Chlamydomonas* chloroplast hemoglobin: Evidence for ligation of tyrosine-63 (B10) to the heme. *Biochemistry 38*, 15360-15368.

82. Jensen, L. M., Sanishvili, R., Davidson, V. L., and Wilmot, C. M. (2010) *In crystallo* post-translational modification within a MauG/pre-methylamine dehydrogenase complex. *Science 327*, 1392-1394.

83. Abu Tarboush, N., Shin, S., Geng, J. F., Liu, A. M., and Davidson, V. L. (2012) Effects of the loss of the axial tyrosine ligand of the low-spin heme of MauG on its physical properties and reactivity. *FEBS Lett. 586*, 4339-4343.

84. Nagai, M., Yoneyama, Y., and Kitagawa, T. (1991) Unusual carbon monoxide bonding geometry in abnormal subunits of hemoglobin M Boston and hemoglobin M Saskatoon. *Biochemistry 30*, 6495-6503.

85. Egeberg, K. D., Springer, B. A., Martinis, S. A., Sligar, S. G., Morikis, D., and Champion, P. M. (1990) Alteration of sperm whale myoglobin heme axial ligation by site-directed mutagenesis. *Biochemistry 29*, 9783-9791.

86. Kumar, R., Lovell, S., Matsumura, H., Battaile, K. P., Moenne-Loccoz, P., and Rivera, M. (2013) The hemophore HasA from *Yersinia pestis* ($HasA_{yp}$) coordinates hemin with a single residue, Tyr75, and with minimal conformational change. *Biochemistry 52*, 2705-2707.

87. Mokry, D. Z., Nadia-Albete, A., Johnson, M. K., Lukat-Rodgers, G. S., Rodgers, K. R., and Lanzilotta, W. N. (2014) Spectroscopic evidence for a 5-coordinate oxygenic ligated high spin ferric heme moiety in the *Neisseria meningitidis* hemoglobin binding receptor. *Biochim. Biophys. Acta 1840*, 3058-3066.

88. Gaudin, C. F., Grigg, J. C., Arrieta, A. L., and Murphy, M. E. (2011) Unique heme-iron coordination by the hemoglobin receptor IsdB of *Staphylococcus aureus*. *Biochemistry 50*, 5443-5452.

89. Ekworomadu, M. T., Poor, C. B., Owens, C. P., Balderas, M. A., Fabian, M., Olson, J. S., Murphy, F., Balkabasi, E., Honsa, E. S., He, C., Goulding, C. W., and Maresso, A. W. (2012) Differential function of Lip residues in the mechanism and biology of an anthrax hemophore. *PLoS Path. 8*.

90. Honsa, E. S., Owens, C. P., Goulding, C. W., and Maresso, A. W. (2013) The near-iron transporter (NEAT) domains of the anthrax hemophore IsdX2 require a critical glutamine to extract heme from methemoglobin. *J. Biol. Chem. 288*, 8479-8490.

91. Grigg, J. C., Ukpabi, G., Gaudin, C. F. M., and Murphy, M. E. P. (2010) Structural biology of heme binding in the *Staphylococcus aureus* Isd system. *J. Inorg. Biochem. 104*, 341-348.

92. Reedy, C. J., Kennedy, M. L., and Gibney, B. R. (2003) Thermodynamic characterization of ferric and ferrous haem binding to a designed four-α-helix protein. *Chem. Commun.* 570-571.

2.9 Supplemental Information

2.9.1 Supplemental Figures

Figure 2.11 S1 Alignment of the amino acid sequence of HmuT from various Corynebacterium species. Species are designated as follows: Cd: C. diphtheriae 1737/NCTC13129; CU: C. ulcerans 712; Cjk: C. jeikeium k411-jk0316; Cglut: C. glutamicum ATCC 13032; Curea: C. urealyticum DSM 7109. Conserved residues that were subjected to site-directed mutagenesis are indicated above the sequence alignment; asterisks indicate sequence identity and colons and periods show sequence similarity.

Figure 2.12 S2 Alignment of the amino acid sequence of CdHmuT with four HBPs with known crystal structures. Square boxes indicate the known axial ligands. Orange: P. aeruginosa PhuT (1) and S. dysenteriae ShuT (1). Green: S. aureus IsdE (2). Blue: Y. pestis HmuT (3). Red: C. diphtheriae HmuT. For CdHmuT, M292 is also shown.

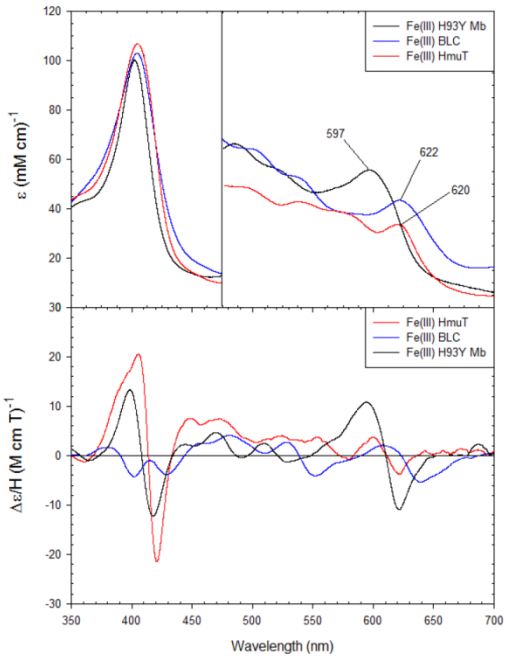

Figure 2.13 S3 Comparison of the UV-visible absorption and MCD spectra for Fe(III) WT CdHmuT at pH 6.5 with Fe(III) bovine liver catalase (BLC) and H93Y myoglobin. The samples were taken in 50 mM phosphate buffer. Spectra were slightly dependent on buffer conditions. The spectra of BLC and H93Y myoglobin were replotted from (4-6) and (7), respectively.

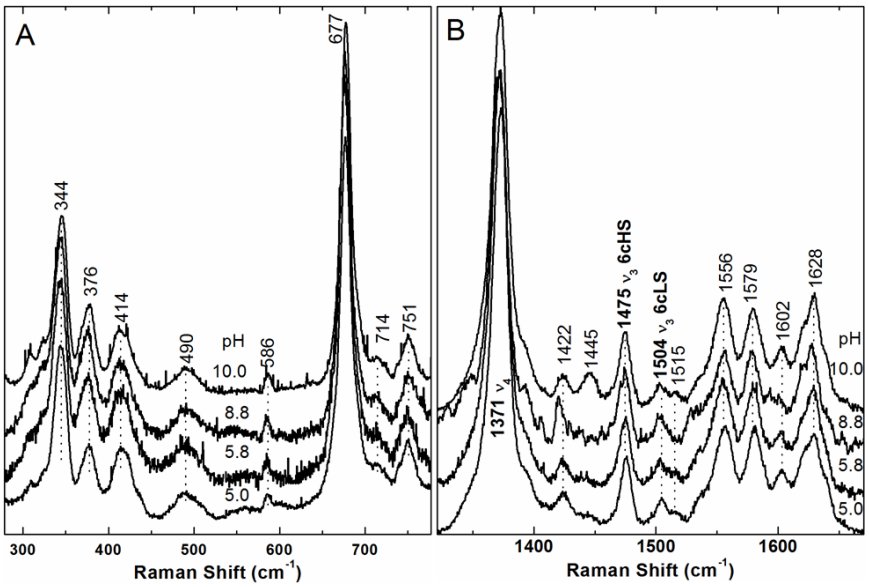

Figure 2.14 S4 The rR spectrum of ferric WT CdHmuT as a function of pH. A) Low frequency window. B) High frequency window. Protein concentration was 40 μM; excitation frequency of 413.1 nm was used with 9.4 mW laser power at the sample. The pH values are as indicated with the buffers described in the experimental section.

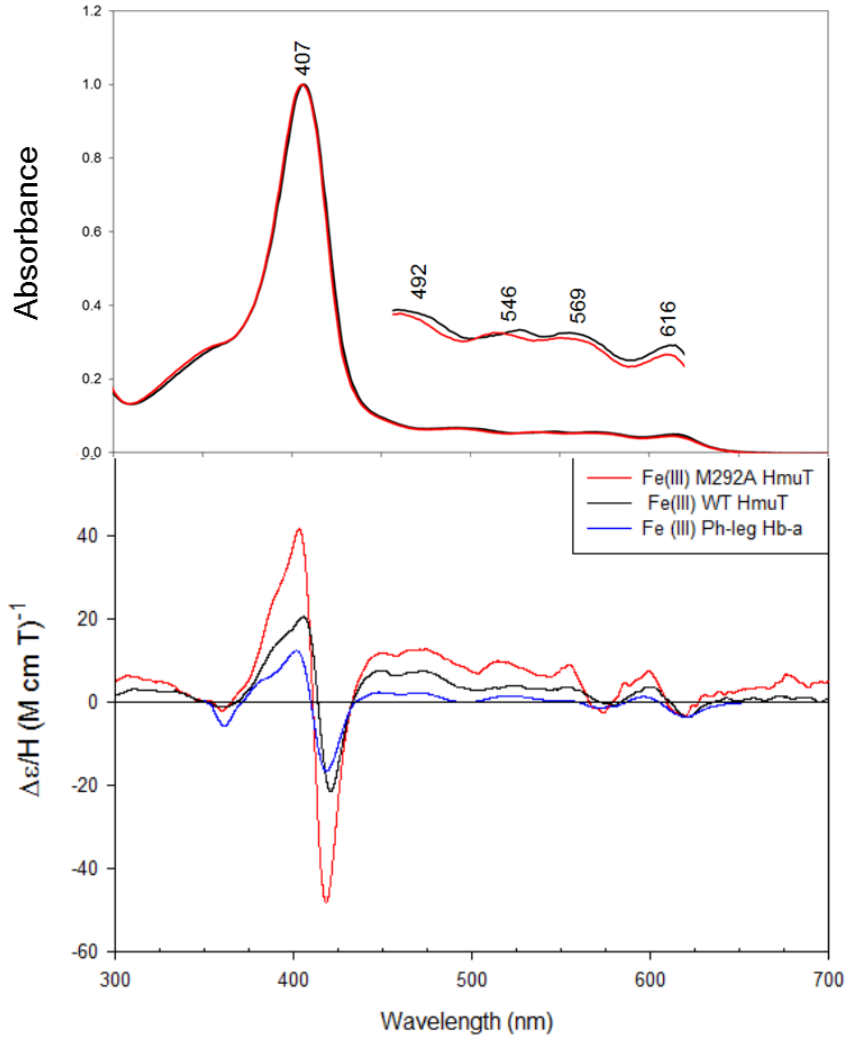

Figure 2.15 S5 Top panel: UV-visible absorption spectrum of WT CdHmuT (black) and M292A CdHmuT (red). The samples were taken in 50 mM Tris-Cl, pH 7.0. Bottom panel: Comparison of the MCD spectra for Fe(III) M292A CdHmuT at pH 6.5 with Fe(III) WT CdHmuT and Fe(III) phenol-leg Hb a. The samples were taken in 50 mM phosphate buffer. The spectrum of phenol-leg Hb a was replotted from (8).

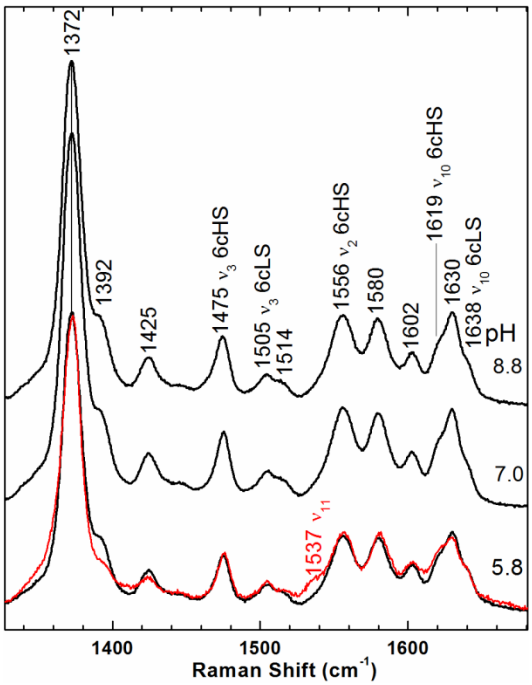

Figure 2.16 S6 The rR spectrum of ferric M292A as a function of pH. Protein concentration was 36 μM; 406.7-nm excitation with 11 mW at the sample was used. The spectrum of ferric WT HmuT at pH 5.0 (red) is overlaid on the M292A pH 5.0 spectrum for comparison purposes. Coordination state and spin state markers ν_3, ν_2 and ν_{10} appear at the same frequencies in both spectra. The only noticeable difference between the WT and M292A spectra is the 1537 cm^{-1} shoulder, which is assigned to ν_{11} (the B_{1g}, C_β-C_β stretching mode) in the WT spectrum, and which is absent in the M292A spectrum.

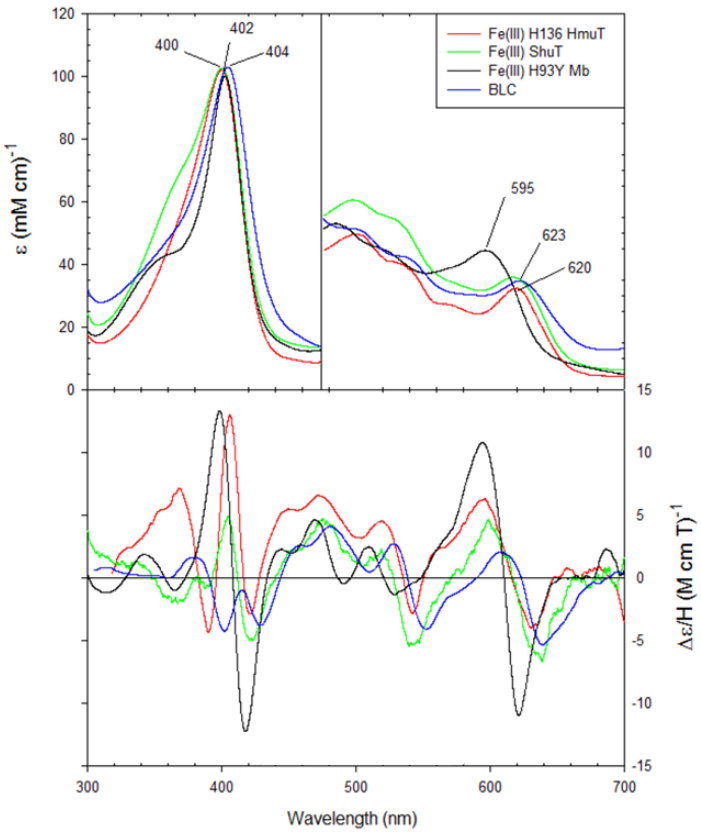

Figure 2.17 S7 The UV-visible absorption and MCD comparison spectra for Fe(III) H136A CdHmuT at pH 6.5. Bottom panel: Comparison of the MCD spectra for Fe(III) H136A CdHmuT with Fe(III) WT CdHmuT, Fe(III) ShuT, Fe(III) H93Y Mb, and Fe(III) BLC. All samples in the work were taken in 50 mM phosphate buffer. Spectra of H93Y, ShuT, and BLC were replotted from (7),(9), and (4-6), respectively.

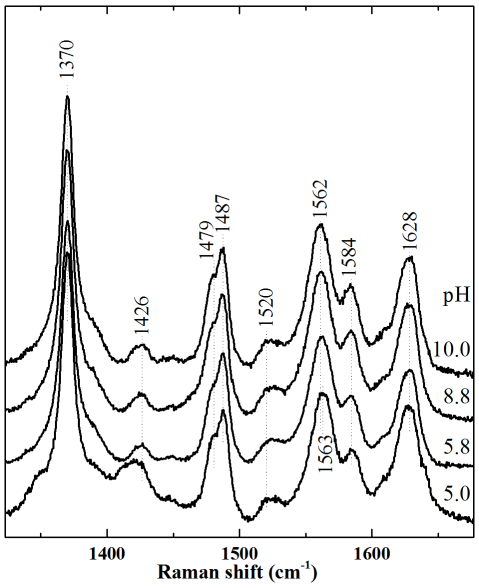

Figure 2.18 S8 The rR spectrum of ferric H136A as a function of pH. Protein concentration was 25 μM; 406.7-nm excitation with 11 mW at the sample was used.

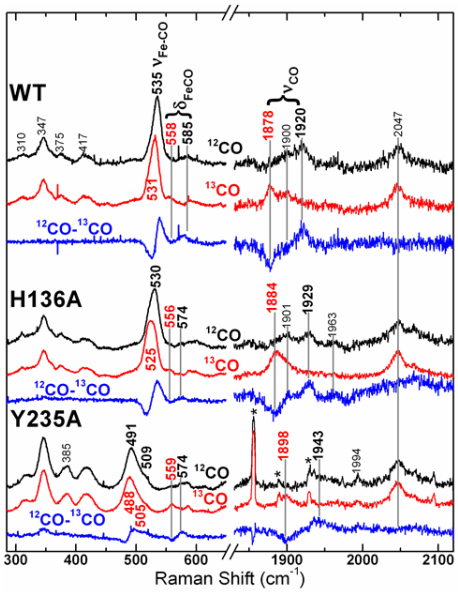

Figure 2.19 S9 Resonance Raman spectra of the ferrous carbonyls of WT CdHmuT, H136A, and Y235A recorded using 413.1-nm excitation. Natural abundance HmuT−CO (black), HmuT−^{13}CO (red) and difference (blue) spectra are shown for each protein. Spectra of WT and H136A were recorded at pH 8.8 and that of Y235A at pH 8.2. The asterisks in the carbonyl stretching region of the Y235A spectrum mark plasma emission lines from the Kr^+ laser.

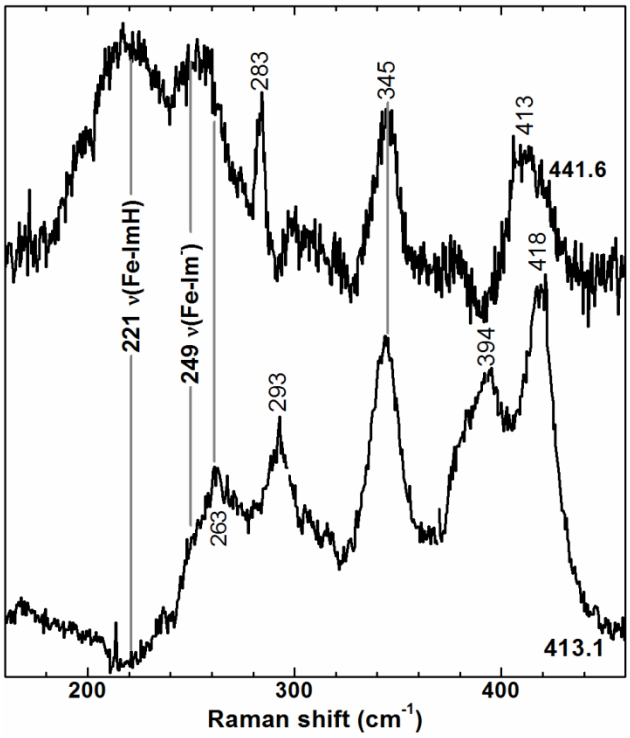

Figure 2.20 S10 Comparison of the low frequency RR window of ferrous Y235A spectra obtained with 413.1-nm and 441.6-nm excitation. Laser powers at the sample were 4.0 mW and 4.6 mW, respectively. The solutions were 38 μM in protein and 100 mM in Tris-Cl, pH 8.8.

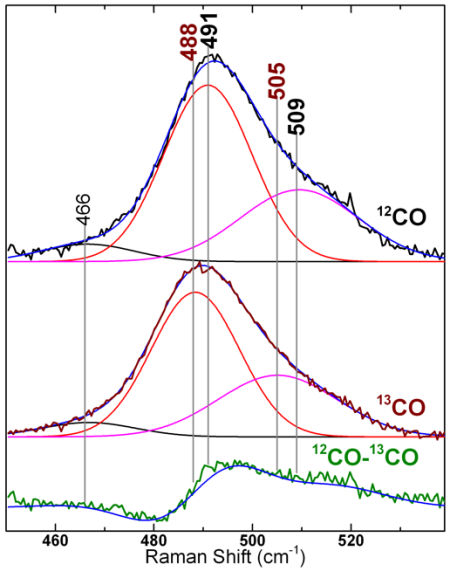

Figure 2.21 S11 The Fe−C stretching region of the Y235A-CO rR spectrum. The experimental data for the natural abundance CO (black) and ^{13}CO (burgundy) complexes are shown with the peak fitting analysis of the 509/505 (magenta) and 491/488 cm^{-1} bands (red). Band widths are 24 and 18 cm^{-1}, respectively. The 466 cm^{-1} band is not ^{13}C sensitive. The simulated spectra are shown in blue; they are the sums of the fit peaks. The difference spectrum, obtained by subtraction of ^{13}CO spectrum from the natural abundance CO spectrum, is shown in green. The simulated ^{12}CO−^{13}CO difference spectrum (blue) is the difference between the simulated spectra for the ^{12}CO and ^{13}CO complexes.

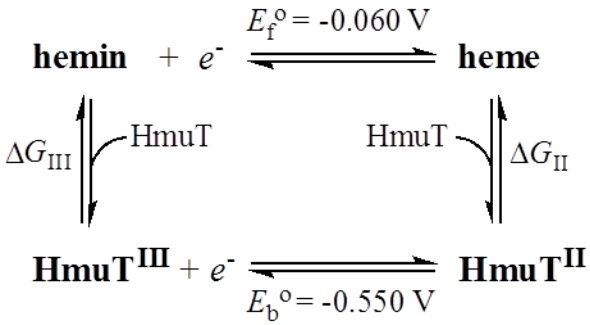

Figure 2.22 S12 Thermodynamic cycle for heme binding and reduction.

2.9.2 Supplemental Tables

Table 2.1 pK_a values of water trans to histidine in selected ferric heme proteins. The pK_a of ferrous microperoxidase 8 is reported as 10.9 (10).

Class	Protein	Fe(III)	Reference
CCOx	Cytochrome *c* oxidase	9.0	(*11*)
ClD	GR-1 chlorite dismutase	8.2	(*12*)
ClD	*Ideonella dechloratans* chlorite dismutase	8.5	(*13*)
ClD	*Dechloromonas aromatica* chlorite dismutase	8.7	(*14*)
FixL	*Rhizobium meliloti* FixL	9.3	(*15*)
FixL	*Bradyrhizobium japonicum* FixL	9.3	(*15*)
FixL	*Rhizobium meliloti* FixL	10	(*15*)
Hb	Leghemoglobin	8.3	(*16*)
Hb	Hemoglobin I (clam)	9.6	(*17*)
H-NOX	*Thermoanaerobacter tengcongensis* H-NOX	6.8	(*18*)
H-NOX	*Thermoanaerobacter tengcongensis* H-NOX I5L	7.9	(*18*)
H-NOX	*Thermoanaerobacter tengcongensis* H-NOX I5L/P115A	>10	(*18*)
H-NOX	*Thermoanaerobacter tengcongensis* H-NOX P115A	>10	(*18*)
HO	Heme oxygenase	7.6	(*19;20*)
HO	Mammalian HO-1	7.6	(*20*)
HO	Rat heme oxygenase-1	7.6	(*20*)
HO	*Pseudomonas aeruginosa* heme oxygenase	8.3	(*21*)
HO	Mammalian HO-2	8.5	(*22*)
HO	Bacterial heme oxygenase HmuO	9.0	(*23*)
HO	*Neisseriae meningitidis* heme oxygenase	9.3	(*24*)
HRP	Horseradish peroxidase	10.9	(*25*) (*26*)
IsdI	*Staphylococcus aureus* IsdI	7.1	(*27*)
Mb	Porcine myoglobin H64V/V68H/H93A/H97F	7.17	(*28*)
Mb	Aplysia myoglobin	7.6	(*25*)
Mb	Porcine myoglobin H64V/V68H/H93G/H97F	7.74	(*28*)
Mb	*Dolabella auricularia* myoglobin	7.8	(*29*)
Mb	Sperm whale myoglobin	8.95	(*25*)
MP	Microperoxidase 8	9.6	(*10;30*)

Table 2.2 Selected His/Tyr and Tyr heme-binding proteins with corresponding residues which are hydrogen-bonded to the axial tyrosine ligand. The examples are ordered by hydrogen bonding motif.

Protein	Axial Ligation	Hydrogen Bonding Residue	Motif[a]	Soret	Q Bands	Reference
S. aureus IsdA	Y166	Y170	Yxxx**Y**	406	502, 535, 628	(*31*)
S. aureus IsdB-N2	Y440	Y444	Yxxx**Y**	406	504, 540, 630	(*32*)
S. aureus IsdC	Y132	Y136	Yxxx**Y**	403	502, 533, 627	(*33*)
S. aureus IsdH-N3	Y642	Y646	Yxxx**Y**	401	504, 537, 630	(*34*)
B. anthracis IsdX1	Y136	Y140	Yxxx**Y**	400	505, 540, 630	(*35*)
B. anthracis IsdX2-N5	Y108	Y112	Yxxx**Y**	404	500, 630	(*36*)
P. aeruginosa HasA	H32/Y75	H83	Yxxxxxxx**H**	407	495, 540, 577, 616	(*37*)
S. marcesans HasA	H32/Y75	H83	Yxxxxxxx**H**	406	494, 537, 568, 618	(*38*)
Y. pestis HasA	Y75	H81	Yxxxxx**H**	403	498, 535, 620	(*39*)
Y. pestis HmuT	Y70/H167	R72[b]	Yx**R**	404		(*3*)
C. diphtheriae HmuT	H136/Y235	R237[c]	Yx**R**	407	492, 546, 569, 616	This work
C. diphtheriae HmuT H136A	Y235	R237[c]	Yx**R**	400	504, 546, 620	This work
C. diphtheriae HmuT Y235A	H136	--	--	412	540, 575	This work
P. aeruginosa PhuT	Y71	R73	Yx**R**	400	500, 534, 624	(*1*)
S. dysenteriae ShuT	Y67	K69[b]	Yx**K**	400	500, 521, 617	(*1*)
P. homomalla cAOS	Y353	R349	**R**xxxY	406	500, 534, 620	(*6*)
Bovine liver catalase	Y357	R353	**R**xxxY	404.5	500, 535, 622	(*6;40*)
M. avium ssp. *paratuberculosis* MAP	Y294	R290	**R**xxxY	406	503, 621	(*6*)

[a] Residues in bold represent the amino acid hydrogen bonded to the axial ligand.
[b] Predicted that the residue could hydrogen bond the axial ligand, but is not directly observed in the crystal structure.
[c] Predicted that the residue could hydrogen bond the axial ligand via homology modeling and spectroscopic studies.

2.9.3 Supplemental References

1. Ho, W. W., Li, H. Y., Eakanunkul, S., Tong, Y., Wilks, A., Guo, M. L., and Poulos, T. L. (2007) Holo-and apo-bound structures of bacterial periplasmic heme-binding proteins. *J. Biol. Chem. 282*, 35796-35802.

2. Grigg, J. C., Vermeiren, C. L., Heinrichs, D. E., and Murphy, M. E. (2007) Heme coordination by *Staphylococcus aureus* IsdE. *J. Biol. Chem. 282*, 28815-28822.

3. Mattle, D., Zeltina, A., Woo, J. S., Goetz, B. A., and Locher, K. P. (2010) Two stacked heme molecules in the binding pocket of the periplasmic heme-binding protein HmuT from *Yersinia pestis*. *J. Mol. Biol. 404*, 220-231.

4. Browett, W. R. and Stillman, M. J. (1979) Magnetic circular dichroism studies of bovine liver catalase. *Biochim. Biophys. Acta 577*, 291-306.

5. Abraham, B. D., Sono, M., Boutaud, O., Shriner, A., Dawson, J. H., Brash, A. R., and Gaffney, B. J. (2001) Characterization of the coral allene oxide synthase active site with UV-visible absorption, magnetic circular dichroism, and electron paramagnetic resonance spectroscopy: Evidence for tyrosinate ligation to the ferric enzyme heme iron. *Biochemistry 40*, 2251-2259.

6. Bandara, D. M. I., Sono, M., Bruce, G. S., Brash, A. R., and Dawson, J. H. (2011) Coordination modes of tyrosinate-ligated catalase-type heme enzymes: Magnetic circular dichroism studies of *Plexaura homomalla* allene oxide synthase, *Mycobacterium avium* ssp. paratuberculosis protein-2744c, and bovine liver catalase in their ferric and ferrous states. *J. Inorg. Biochem. 105*, 1786-1794.

7. Pond, A. E., Roach, M. P., Sono, M., Rux, A. H., Franzen, S., Hu, R., Thomas, M. R., Wilks, A., Dou, Y., Ikeda-Saito, M., Ortiz de Montellano, P. R., Woodruff, W. H., Boxer, S. G., and Dawson, J. H. (1999) Assignment of the heme axial ligand(s) for the ferric myoglobin (H93G) and heme oxygenase (H25A) cavity mutants as oxygen donors using magnetic circular dichroism. *Biochemistry 38*, 7601-7608.

8. Sievers, G., Gadsby, P. M., Peterson, J., and Thomson, A. J. (1983) Magnetic circular dichroism spectra of soybean leghaemoglobin *a* at room temperature and 4.2 K. *Biochim. Biophys. Acta 742*, 637-647.

9. Eakanunkul, S., Lukat-Rodgers, G. S., Sumithran, S., Ghosh, A., Rodgers, K. R., Dawson, J. H., and Wilks, A. (2005) Characterization of the periplasmic heme-binding protein ShuT from the heme uptake system of *Shigella dysenteriae*. *Biochemistry 44*, 13179-13191.

10. Vashi, P. R. and Marques, H. M. (2004) The coordination of imidazole and substituted pyridines by the hemeoctapeptide N-acetyl-ferromicroperoxidase-8 (Fe(II)NAcMP8). *J. Inorg. Biochem. 98*, 1471-1482.

11. Branden, M., Namslauer, A., Hansson, O., Aasa, R., and Brzezinski, P. (2003) Water-hydroxide exchange reactions at the catalytic site of heme-copper oxidases. *Biochemistry 42*, 13178-13184.

12. Hagedoorn, P. L., de Geus, D. C., and Hagen, W. R. (2002) Spectroscopic characterization and ligand-binding properties of chlorite dismutase from the chlorate respiring bacterial strain GR-1. *Eur. J. Biochem. 269*, 4905-4911.

13. Stenklo, K., Thorell, H. D., Bergius, H., Aasa, R., and Nilsson, T. (2001) Chlorite dismutase from *Ideonella dechloratans*. *J. Biol. Inorg. Chem. 6*, 601-607.

14. Streit, B. R., Blanc, B., Lukat-Rodgers, G. S., Rodgers, K. R., and Dubois, J. L. (2010) How active-site protonation state influences the reactivity and ligation of the heme in chlorite dismutase. *J. Am. Chem. Soc. 132*, 5711-5724.

15. Gilles-Gonzalez, M. A., Gonzalez, G., Perutz, M. F., Kiger, L., Marden, M. C., and Poyart, C. (1994) Heme-based sensors, exemplified by the kinase FixL, are a new class of heme protein with distinctive ligand binding and autoxidation. *Biochemistry 33*, 8067-8073.

16. Jones, D. K., Badii, R., Rosell, F. I., and Lloyd, E. (1998) Bacterial expression and spectroscopic characterization of soybean leghaemoglobin *a*. *Biochem. J. 330*, 983-988.

17. Kraus, D. W., Wittenberg, J. B., Lu, J. F., and Peisach, J. (1990) Hemoglobins of the *Lucina pectinata*/bacteria symbiosis. II. An electron paramagnetic resonance and optical spectral study of the ferric proteins. *J. Biol. Chem. 265*, 16054-16059.

18. Olea, C., Kuriyan, J., and Marletta, M. A. (2010) Modulating heme redox potential through protein-induced porphyrin distortion. *J. Am. Chem. Soc. 132*, 12794-12795.

19. Sun, J., Wilks, A., Demontellano, P. R. O., and Loehr, T. M. (1993) Resonance Raman and EPR spectroscopic studies on heme-heme oxygenase complexes. *Biochemistry 32*, 14151-14157.

20. Takahashi, S., Wang, J. L., Rousseau, D. L., Ishikawa, K., Yoshida, T., Host, J. R., and Ikedasaito, M. (1994) Heme-heme oxygenase complex structure of the catalytic site and its implication for oxygen activation. *J. Biol. Chem. 269*, 1010-1014.

21. Caignan, G. A., Deshmukh, R., Zeng, Y. H., Wilks, A., Bunce, R. A., and Rivera, M. (2003) The hydroxide complex of *Pseudomonas aeruginosa* heme oxygenase as a model of the low-spin iron(III) hydroperoxide intermediate in heme catabolism: C-13 NMR spectroscopic studies suggest the active participation of the heme in macrocycle hydroxylation. *J. Am. Chem. Soc. 125*, 11842-11852.

22. Ishikawa, K., Takeuchi, N., Takahashi, S., Matera, K. M., Sato, M., Shibahara, S., Rousseau, D. L., Ikedasaito, M., and Yoshida, T. (1995) Heme oxygenase-2 - Properties of the heme complex of the purified tryptic fragment of recombinant human heme oxygenase-2. *J. Biol. Chem. 270*, 6345-6350.

23. Chu, G. C., Tomita, T., Sonnichsen, F. D., Yoshida, T., and Ikeda-Saito, M. (1999) The heme complex of Hmu O, a bacterial heme degradation enzyme from *Corynebacterium diphtheriae* - Structure of the catalytic site. *J. Biol. Chem. 274*, 24490-24496.

24. Zeng, Y. H., Caignan, G. A., Bunce, R. A., Rodriguez, J. C., Wilks, A., and Rivera, M. (2005) Azide-inhibited bacterial heme oxygenases exhibit an S=3/2 (d(xz),d(yz))(3) (d(xy))(1)(d(z)(2))(1) spin state: Mechanistic implications for heme oxidation. *J. Am. Chem. Soc. 127*, 9794-9807.

25. Brunori, M., Amiconi, G., Antonini, E., Wyman, J., Zito, R., and Fanelli, R. (1968) Transition between acid and alkaline ferric heme proteins. *Biochim. Biophys. Acta 154*, 315-&.

26. Sitter, A. J., Shifflett, J. R., and Terner, J. (1988) Resonance Raman spectroscopic evidence for heme iron-hydroxide ligation in peroxidase alkaline forms. *J. Biol. Chem. 263*, 13032-13038.

27. Takayama, S. J., Ukpabi, G., Murphy, M. E. P., and Mauk, A. G. (2011) Electronic properties of the highly ruffled heme bound to the heme degrading enzyme IsdI. *Proc. Natl. Acad. Sci. USA 108*, 13071-13076.

28. Uno, T., Sakamoto, R., Tomisugi, Y., Ishikawa, Y., and Wilkinson, A. J. (2003) Inversion of axial coordination in myoglobin to create a "proximal" ligand binding pocket. *Biochemistry 42*, 10191-10199.

29. Yamamoto, Y., Chûjô, R., Inoue, Y., and Suzuki, T. (1992) Kinetic characterization of the acid-alkaline transition in *Dolabella auricularia* ferric myoglobin using ^{1}H-NMR saturation transfer experiments. *FEBS Lett. 310*, 71-74.

30. Munro, O. Q. and Marques, H. M. (1996) Heme-peptide models for hemoproteins. 2. N-acetylmicroperoxidase-8 - study of the pi-pi dimers formed at high ionic-strength using a modified version of molecular exciton theory. *Inorg. Chem. 35*, 3768-3779.

31. Grigg, J. C., Vermeiren, C. L., Heinrichs, D. E., and Murphy, M. E. P. (2007) Haem recognition by a *Staphylococcus aureus* NEAT domain. *Mol. Microbiol. 63*, 139-149.

32. Gaudin, C. F., Grigg, J. C., Arrieta, A. L., and Murphy, M. E. (2011) Unique heme-iron coordination by the hemoglobin receptor IsdB of *Staphylococcus aureus*. *Biochemistry 50*, 5443-5452.

33. Sharp, K. H., Schneider, S., Cockayne, A., and Paoli, M. (2007) Crystal structure of the heme-IsdC complex, the central conduit of the Isd iron/heme uptake system in *Staphylococcus aureus*. *J. Biol. Chem. 282*, 10625-10631.

34. Watanabe, M., Tanaka, Y., Suenaga, A., Kuroda, M., Yao, M., Watanabe, N., Arisaka, F., Ohta, T., Tanaka, I., and Tsumoto, K. (2008) Structural basis for multimeric heme complexation through a specific protein-heme interaction - The case of the third NEAT domain of IsdH from *Staphylococcus aureus*. *J. Biol. Chem. 283*, 28649-28659.

35. Ekworomadu, M. T., Poor, C. B., Owens, C. P., Balderas, M. A., Fabian, M., Olson, J. S., Murphy, F., Balkabasi, E., Honsa, E. S., He, C., Goulding, C. W., and Maresso, A. W. (2012) Differential function of Lip residues in the mechanism and biology of an anthrax hemophore. *PLoS Path. 8*.

36. Honsa, E. S., Owens, C. P., Goulding, C. W., and Maresso, A. W. (2013) The near-iron transporter (NEAT) domains of the anthrax hemophore IsdX2 require a critical glutamine to extract heme from methemoglobin. *J. Biol. Chem. 288*, 8479-8490.

37. Alontaga, A. Y., Rodriguez, J. C., Schonbrunn, E., Becker, A., Funke, T., Yukl, E. T., Hayashi, T., Stobaugh, J., Monne-Loccoz, P., and Rivera, M. (2009) Structural characterization of the hemophore HasAp from *Pseudomonas aeruginosa*: NMR spectroscopy reveals protein-protein interactions between holo-HasAp and hemoglobin. *Biochemistry 48*, 96-109.

38. Arnoux, P., Haser, R., Izadi, N., Lecroisey, A., Delepierre, M., Wandersman, C., and Czjzek, M. (1999) The crystal structure of HasA, a hemophore secreted by *Serratia marcescens*. *Nature Struct. Biol. 6*, 516-520.

39. Kumar, R., Lovell, S., Matsumura, H., Battaile, K. P., Moenne-Loccoz, P., and Rivera, M. (2013) The hemophore HasA from *Yersinia pestis* ($HasA_{yp}$) coordinates hemin with a single residue, Tyr75, and with minimal conformational change. *Biochemistry 52*, 2705-2707.

40. Fita, I. and Rossmann, M. G. (1985) The active center of catalase. *J. Mol. Biol. 185*, 21-37.

3 CORYNEBACTERIUM DIPTHERIAE HMUT: A CLOSER LOOK AT CONSERVED RESIDUES

This chapter is additional work on *C. diphtheriae* HmuT, spanning from our work in Chapter 2. The following chapter is intended for publication. Site-directed mutagenesis of R237A, expression, purification, UV-visible absorption spectroscopy, thermal unfolding, and mass spectrometry were performed at Georgia State University.

3.1 Abstract

The heme binding protein HmuT is part of the *Corynebacterium diphtheriae* heme uptake pathway and is responsible for the delivery of heme to the HmuUV ABC transporter. HmuT binds heme with a conserved His/Tyr heme binding motif. Sequence alignment indicated other conserved residues which may be important for heme binding: R237, Y272, M292, and Y349. In this study, a combination of UV-visible and resonance Raman spectroscopies, along with collision-induced dissociation electrospray ionization mass spectrometry and thermal unfolding titrations, are utilized to probe the roles of each conserved residue in regards to heme binding. R237 acts as a hydrogen-bonding partner to the axial tyrosine ligand while Y272 may be participating as a hydrogen-bond partner to another residue in the pocket. M292 appears to buttress the axial tyrosine in the pocket as shown by the detection of multiple Fe(II)-CO species by Raman spectroscopy. Y349, although predicted to not be near the heme-binding pocket, results in a minimally heme-loaded protein and may alter the overall fold of HmuT in some fashion. In addition, the plasticity of the overall HmuT protein was probed using heme reconstitution experiments and showed HmuT has the ability to bind heme in more than one form.

3.2 Introduction

Iron is a necessary element for almost all living organisms, including pathogenic bacteria *(1, 2)*. Studies have shown the availability of iron to a pathogen is linked to not only survival, but also virulence *(2, 3)*. In the human host, the majority of iron is commonly found in the form of heme bound to proteins such as myoglobin and hemoglobin. Although some bacteria are able to synthesize heme, others rely solely on uptake from host heme sources *(1, 4)*. As a result, pathogenic bacteria have developed sophisticated strategies to obtain required iron, in the form of heme, from the host.

Studies of heme uptake pathways in both Gram-negative and Gram-positive bacteria have been the subject of many reviews *(1-3, 5-8)*. Commonly studied Gram-negative pathways involve *Pseudomonas aeruginosa, Shigella dysenteriae,* and *Yersinia pestis (1, 3, 5, 9)*. Gram-positive pathways such as *Staphylococcus aureus (10, 11), Bacillus anthracis (12), Streptococcus pyogenes (13, 14),* and *Corynebacterium diphtheriae (15)* have also been characterized in regards to heme uptake. *C. diphtheriae* is one such pathogen which utilizes a heme uptake pathway in conjunction with an ABC transporter to obtain host heme *(15-18)*.

The heme utilization (*hmu*) operon in *C. diphtheriae* includes the *hmuT* (substrate binding protein), *hmuU* (the permease), and *hmuV* (the ATPase) genes which make up the ABC-type heme binding transporter system *(19)*. The pathway has previously been studied in detail; heme is transferred from HtaA (surface-exposed hemin binding protein) to HtaB (membrane-anchored protein) *(16, 17, 19-21)*. The third protein in the pathway, HmuT (the substrate binding protein), delivers the heme to the ABC transporter.

BLAST analysis and sequence alignment shows that the HmuT heme binding motif is found throughout *Corynebacterium* species *(17)* and extends into other genuses including

Yersinia (22), Bradyrhizobium (23), and *Propionibacterium (24).* Detailed studies on three HmuT protein homologs are available, those from *Y. pestis (22), C. diphtheriae (17)* and *C. glutamicum (25).* These proteins are similar in many respects. All three proteins are involved in heme transfer to the corresponding HmuUV ABC transporter; all three use a His/Tyr binding heme motif. However, these three HmuT proteins also differ in fundamental aspects. Both *Cd*HmuT and *Cg*HmuT utilize a histidine axial ligand from the N-terminal end of the protein and a tyrosine from the C-terminal end of the protein. In contrast, *Yp*HmuT binds heme in a reverse manner with an N-terminal tyrosine and a C-terminal histidine. *Yp*HmuT is also able to bind heme as a dimer; this has not been reported for *Cg*HmuT. In view of both the similarities and differences between these three closely-related proteins, our goal was to establish the roles of various conserved residues in the structure and function of HmuT, specifically by investigating the *C. diphtheriae* protein.

*Cd*HmuT coordinates heme through the conserved residues H136 and Y235 *(17).* Sequence alignment with other *Corynebacterium* species indicated other conserved residues in the HmuT heme pocket, including R237, Y272, M292, and Y349 (Figure S EBalign and Figure EBModel). The homology model indicated that R237 and Y272 were in position to interact with the axial Y235 residue. M292, while recently shown not to be an axial ligand *(17)* is still in the heme pocket and might play a role in the binding of this prosthetic group. Y349, although conserved, was not near the proposed binding pocket as indicated by the x-ray structure of *Cg*HmuT *(25)* and the homology model of *Cd*HmuT (Figure EBModel). Conservation of these residues implies the potential importance of these amino acids to the protein.

Herein we report the roles of these conserved residues using UV-visible and resonance Raman (rR) spectroscopies along with electrospray ionization mass spectrometry (ESI-MS).

Thermal unfolding of these proteins, including the heme axial ligand mutants, is also investigated. Additionally, reconstitution studies on the wild-type protein are performed. The data indicate a protein that uses a number of residues in controlling heme binding and has significant plasticity in its structure.

3.3 Materials and Methods

3.3.1 Bacterial strains and media

E. coli strains DH5α and TOP10 (Invitrogen) were used for routine cloning and plasmid maintenance, while XL-1 Gold (Stratagene) was used in the mutagenesis experiments. Chromosomal DNA from *C. diphtheriae* strain 1737 *(30)* was used as the source DNA for PCR. Luria-Bertani (LB) medium was used for culturing of *E. coli* strains. Bacterial stocks were maintained in 20 % glycerol at -80^{o} C. Kanamycin (Sigma Chemical Co.) was added to LB medium at 50 μg/ml.

3.3.2 Plasmid construction

The HmuT expression construct was developed using the pET28a expression vector (Novagen) and is previously described *(17)*. A PCR-derived DNA fragment containing the *C. diphtheriae hmuT* coding region was initially cloned into the pCR-Blunt II-TOPO vector (Invitrogen). The DNA fragment harboring the *hmuT* gene was subsequently ligated into the NcoI-EcoRI sites in pET28a and the expression plasmid was then transformed into BL21(DE3) cells. The cloned *hmuT* gene in the pET28a vector lacked the 20-amino acid N-terminal secretion signal and contained an N-terminal Strep-tag, which was used for protein purification. The following primers were used in the PCR: hmuTF; 5'-CC ATGGCA AGC *TGG AGC CAC CCG CAG TTC GAA AAG* GGT GTC CAG GGC ACA TAT-3'; hmuTR; 5'-GAATTC CTA TAC

CTG TGG GTC ATAC-3': underlined sequences indicate restriction sites and the sequence in italics encodes the 8-amino acid Strep-tag.

3.3.3 Site-directed mutagenesis

Site-directed mutants were made using the QuikChange Lightning kit (Stratagene) according to the manufacturer's instructions as previously described *(17)*. Briefly, 125 ng of each primer containing the targeted base change and 50 ng of plasmid template were used in the QuikChange reaction. Methylated template DNA was removed from the reaction by digestion with DpnI restriction endonuclease, and mutagenized DNA was recovered by transformation into XL1-Gold competent cells. The presence of the base changes was confirmed by sequence analysis. Plasmids used for site-directed mutagenesis were pET28a containing the cloned Strep-tag-*hmuT* gene, and plasmid pCD842, which harbors the *hmuT* gene on the *E. coli Corynebacterium* shuttle vector pCM2.6 *(27)*.

3.3.4 Expression and purification of CdHmuT

HmuT was expressed and purified from BL21(DE3) (pET*hmuT*) cells as previously described *(17)*. The N-terminal leader sequence was deleted and replaced with a Strep-tag. The native construct started at residue 21 (Gly) and extended through the native stop codon. The culture was prepared in a LB medium containing 50 μg/mL kanamycin. Inoculation was done with an overnight pre-culture and cells were grown at 37 °C with shaking at 220 rpm. When the OD_{600} of the culture reached 0.5 – 0.6, protein expression was induced by adding isopropyl β-D-1-thiogalactopyranoside (IPTG) to a final concentration of 1.0 mM. The culture was incubated for 3 h at 27 °C. Cells were harvested by centrifugation at 8000 *g*. The cell pellet was resuspended in lysis solution (100 mM Tris-Cl, 150 mM NaCl, pH 8.0) containing a protease inhibitor cocktail (Roche Complete Mini, EDTA-free, following the manufacturer protocol). The

cells were broken using a cell disrupter or sonication. The lysate was then centrifuged at 8000 *g*, and the supernatant was syringe-filtered with a 0.45 μm filter.

All of the following purification steps were conducted at 4 °C using fast protein liquid chromatography and all buffer solutions were pH 8.0 unless specified otherwise. The protein sample was loaded onto a Strep-Tactin Superflow column (5 mL, IBA BioTAGnology) equilibrated with buffer A (100 mM Tris-Cl, 150 mM NaCl, pH 8.0). Unbound material was washed out with 5 column volumes (CV) of buffer A. HmuT was eluted with 10 CV of buffer B containing 100 mM Tris-Cl, 150 mM NaCl, 2.5 mM desthiobiotin, pH 8.0 applied via a linear gradient. The purities of the fractions were evaluated using sodium dodecyl sulfate polyacrylamide gel electrophoresis. HmuT and mutants are isolated in the ferric form as a mixture of holo and apoproteins.

3.3.5 Heme extraction and reconstitution studies

Apo-HmuT was prepared using the Teale method *(32)*. HmuT (10 μM) was mixed with cold 2-butanone and cold 1 M HCl was used to adjust the pH of the solution to 2.0. The solution was mixed and the protein layer was dialyzed against 20 mM Tris-Cl, pH 7.0 at 4˚C. The concentration of apo-HmuT was determined using the ExPASy ε_{280} = 15,930 $M^{-1}cm^{-1}$ *(33)*.

Reconstitution was monitored via UV-visible spectroscopy. Hemin solutions were prepared fresh by dissolving 1 mg of hemin in 5 mL of dimethyl sulfoxide (DMSO, EMD Chemicals) to prevent aggregation. Hemin concentration was spectroscopically determined using the extinction coefficient of 188 $M^{-1}cm^{-1}$ at 404 nm *(34)*. The stock hemin solution was then titrated in 1 μL aliquots to the apo-HmuT (~5 μM) protein. The reconstituted HmuT was checked spectrally for heme aggregation. Reconstituted HmuT was then dialyzed using a 13,000 MWCO dialysis bag in the appropriate buffer.

3.3.6 UV-visible absorption spectroscopy

Samples of HmuT and mutants were analyzed by UV-visible absorption spectroscopy using a Varian 50 Bio spectrophotometer in 1 cm quartz cuvettes (Fisherbrand, Inc.) at room temperature.

3.3.7 Resonance Raman spectroscopy

Resonance Raman (rR) spectra were collected using the 441.6-nm emission line from a HeCd laser or either 406.7 nm or 413.1 nm emission from a Kr^+ laser. Spectra were recorded at ambient temperature using the 135° backscattering geometry with the laser beam focused to a line on a spinning 5 mm NMR tube. Toluene, DMSO, and CH_2Br_2 were used as external standards for spectral calibration. UV-visible absorption spectra were recorded before and after rR experiments to verify that the samples were not altered by exposure to the laser beam. The final concentrations of all Fe(III) samples were between 25 and 80 μM protein in 100 mM buffer solution. The buffers used were CHES, pH 10.0, Tris-Cl, pH 8.8 or 8.0, sodium phosphate buffer, pH 7.0 or 5.8, MES, pH 5.1, and sodium acetate buffer, pH 5.0.

3.3.8 Collision-induced heme dissociation via ESI mass spectrometry

Samples (50 μM) of WT, H136A, Y235A, R237A, Y272A, and M292A in 50 mM ammonium acetate, pH 6.8 ESI spectra were obtained using a Waters Micromass Q-TOF Micro mass spectrometer in the positive mode. Samples were run at the following relative heme-loading percentages: WT HmuT, 100%; H136A, 50%; Y235A, 20%; R237A, 25%; Y272A, 100%; and M292A, 90%. Spectra were recorded for each sample at the following collision energy voltages: 5, 10, 15, 20, 25, and 30 volts. All other parameters were held constant. Deconvolution of the charged state was performed using the MaxEnt program with the MassLynx™ software. Peaks were rounded to the nearest Dalton. Peak heights were measured

in order to determine a relative estimation of holo protein percentages at each collision energy voltage.

3.3.9 Thermal Unfolding

Thermal denaturation experiments on WT HmuT and mutants were performed using a Carey 300 Bio Spectrophotometer equipped with automated temperature control. Supracil 1.5 mL screw-top cuvettes (Spectracell) with 1 cm path lengths were utilized. Protein samples were in 50 mM potassium phosphate, pH 7.0 and at the following wavelengths and concentrations: WT HmuT (406 nm; 5 μM), H136A (399 nm; 5 μM), Y235A (412 nm; 7 μM), R237A (407 nm; 8 μM), Y272A (406 nm; 8 μM), Y349A (406 nm; 4 μM), and Y349F (406 nm; 8 μM). Spectra were recorded between 25 ˚C and 80 ˚C.

The data were fit to a two-state unfolding model using Equation 1 *(35)*:

$$Y(Abs) = \frac{(A_F + m_F T) + (A_U + m_U T) exp\left[\frac{\Delta H_m}{R}\left(\frac{1}{T_m} - \frac{1}{T}\right)\right]}{1 + exp\left[\frac{\Delta H_m}{R}\left(\frac{1}{T_m} - \frac{1}{T}\right)\right]} \quad [1]$$

where *y* is the absorbance at any point along the fitted denaturation curve, A_F is the absorbance of the folded state, m_F is the slope of the folded state, A_U is the absorbance of the unfolded state, m_U is the slope of the unfolded state, ΔH_m is the enthalpy of the unfolding, T_m is the temperature at which the protein is half-unfolded, R is the gas constant, and T is the temperature (Kelvin).

3.4 Results and Discussion

3.4.1 Sequence alignment and homology modeling

The heme axial ligands of *Cd*HmuT are H136 and Y235 *(17)*. Sequence alignment of *C. diphtheriae* HmuT with homologs from various *Corynebacterium* species indicated three

conserved residues in the heme pocket which could potentially play a role in heme binding: R237, Y272, and M292 (Figure 3.9 S1). R237 and M292 were conserved across all *Corynebacterium* species aligned (four other species); Y272 was conserved in all species except *C. glutamicum*. Y349 was also conserved in all species, but homology modeling and comparison with the *Y. pestis* and *C. glutamicum* x-ray structures indicated that this residue was not near the heme binding pocket (Figure 3.1).

It is common in tyrosine heme binding proteins for another residue (most frequently His, Tyr, or Arg) in the heme pocket to form a hydrogen bond with the axial tyrosine. The recent study of *Cg*HmuT proposed that R242 hydrogen bonds to the axial Y240 as they are 2.7 Å apart *(25)*. This is in line with earlier studies on *Yp*HmuT, in which R72 was suggested as a potential hydrogen partner of axial ligand Y70 *(2, 22)*. For *Cd*HmuT, R237 is the homologous reside that could hydrogen bond to Y235. However, *Cd*HmuT also has Y272 (not found in *C. glutamicum* and an Arg in *Yp*HmuT) that could potentially serve as a hydrogen bond partner.

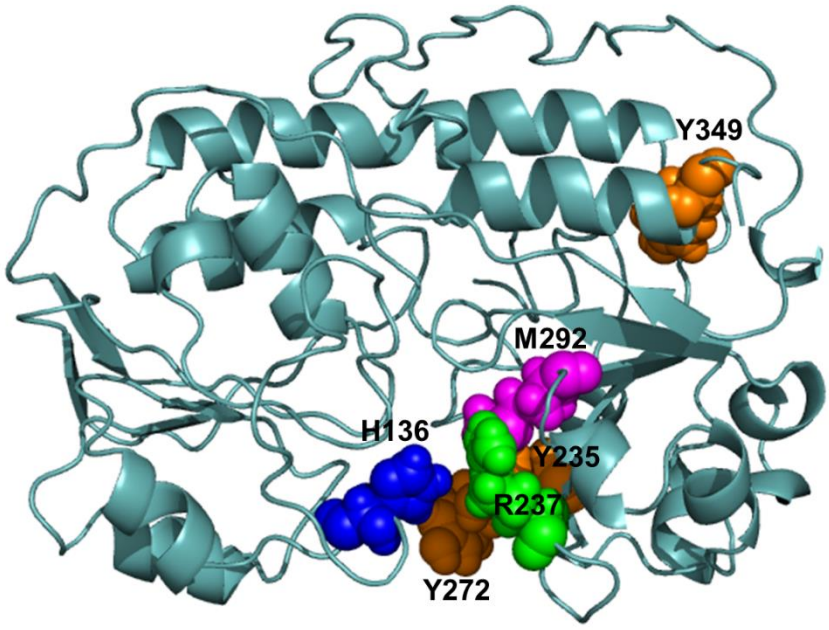

Figure 3.1 I-TASSER homology model of HmuT and heme binding pocket. Shown are the locations of H136 (axial ligand), Y235 (axial ligand), R237, Y272, M292, and Y349.

.

3.4.2 UV-visible absorption spectroscopy and heme loading of HmuT mutants

The heme loading of the as-isolated protein varies with the nature of the mutant. WT HmuT and Y272A are approximately 100% heme loaded as-isolated. M292A is about 90% heme-loaded. R237A and Y349A are both approximately 25% heme loaded and Y349F is about 55% heme loaded.

The UV-visible absorption spectra comparison of WT, Y272A, and R237A are shown in Figure 3.2. WT HmuT has a Soret at 407 nm with bands at 492, 546, 569, and 616 nm. R237A has a Soret at 407 nm, similar to WT, but also gave four bands at 492, 541, 578, and 610 nm which are shifted compared to the WT. Y272A gave a Soret maximum at 406 nm and has an altered α,β-region, with bands at 492, 556, 581, and 616 nm. M292A has previously been shown to have a spectrum almost identical to that of WT *(17)*. Y349A and Y349F have similar UV-visible absorption spectra with a Soret around 406 nm, with Y349A isolated mainly in the apo form of the protein (Figure 3.10 S2). The four α,β-bands at 492, 538, 578, and 613 are in the

same positions for both mutants and are slightly shifted compared to the WT. The observation of four α,β-bands in all of the spectra indicates the protein mutants are isolated as a mixture of high-spin and low-spin heme as seen in the WT *(17)*.

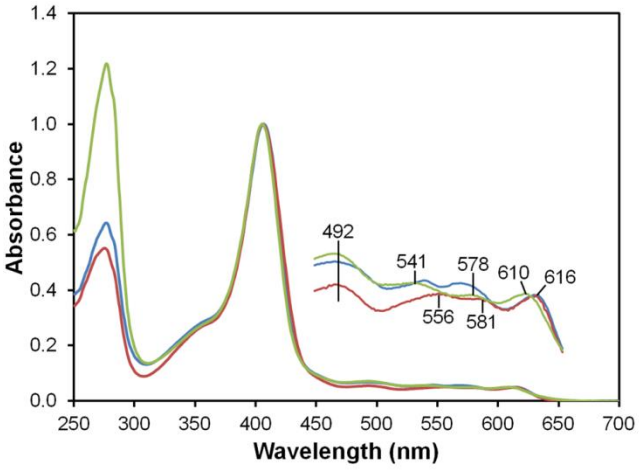

Figure 3.2 UV-visible absorption spectra of Fe(III) WT HmuT (blue), R237A (green), and Y272A (red) normalized at the Soret. The α,β-peaks are labeled for R237A and Y272A. Samples were recorded in 50 mM Tris-Cl, pH 7.0.

3.4.3 Buttressing of the heme pocket by M292

Previous work by our group showed M292 to not be a heme axial ligand based on UV-visible absorption spectroscopy and MCD spectral similarities between WT and M292A *(17)*. However, this residue, essentially in the heme pocket, may still play a role in heme binding. For the CO-bound ferrous forms of heme proteins, an inverse correlation plot of the frequency of the Fe-CO stretch versus that of the bound carbonyl gives insight into the axial ligands of the heme (Figure 3.3). As shown previously *(17)*, the spectrum of Fe(II)-CO WT HmuT is consistent with a single Tyr-Fe(II)-CO motif. In contrast, replacement of M292 by alanine in the M292A mutant results in two Fe(II)-CO species, one of which falls along the Tyr-Fe(II)-CO line (Fe-CO and carbonyl stretches at 537 cm^{-1} and 1932 cm^{-1}, respectively). The second species falls along the His-Fe(II)-CO correlation lines (Fe-CO carbonyl stretch at 504 cm^{-1} and 1950 cm^{-1}, respectively). This indicates a role for M292 in buttressing the heme in the binding pocket.

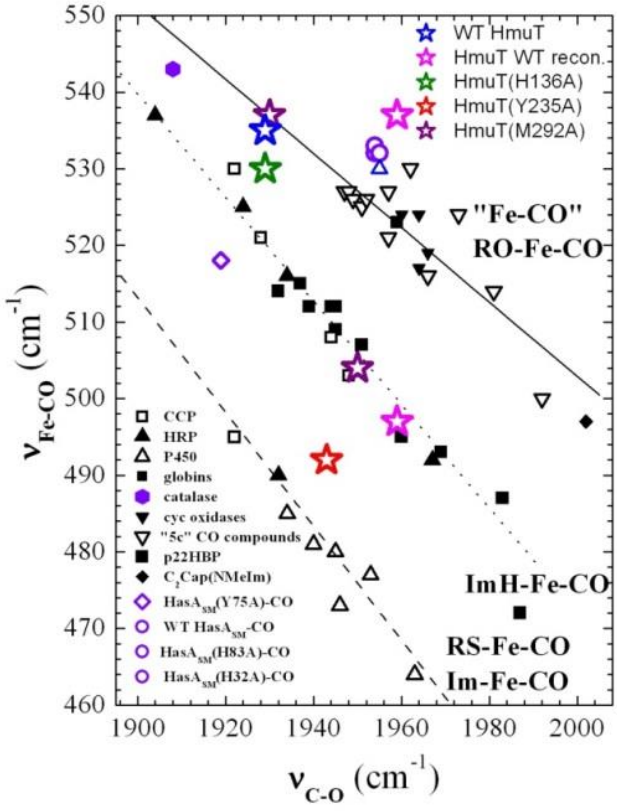

Figure 3.3 Backbonding correlation plot of vFe-CO versus vC-O for ferrous carbonyls of heme proteins showing the dependences of their positions on axial ligation and distal pocket properties. As-isolated WT (blue), reconstituted HmuT (pink), H136A (green), Y235A (red), and M292A (purple) are shown as stars on the plot. Catalase, hexagon; HasA(Y75A), ◊; HasA(WT), ○; HasA(H83A), ○; HasA(H32A), ○. The dashed line is the least squares line for six-coordinate Fe−CO adducts in which the proximal ligand is thiolate or imidazolate; the dotted line is the least squares line for Fe−CO adducts with proximal histidine (neutral imidazole); and the solid line represents a compilation of "five-coordinate" model complexes and heme proteins which the ligand trans to CO is coordinated through an oxygen atom.

3.4.4 Thermal unfolding studies

To assess the roles of each conserved residue of HmuT, thermal unfolding studies were performed on WT HmuT, H136A, Y235A, R237A, Y272A, M292A, Y349A, and Y349F (Figure 3.4 and Table 3.1). After unfolding, samples were cooled to room temperature and folding was shown to be ~90% reversible. The WT protein had a melting temperature (T_m) of 67 ˚C. Mutation of the two axial ligands had very different effects on protein stability. Mutation of

the axial histidine to alanine (H136A) resulted in only about 2 ˚C decrease in the T_m while mutation of the axial tyrosine (Y235A) decreased the T_m by more than 15 ˚C. Mutation of Y272 and M292 to alanine resulted in T_m decreases of only 1 ˚C and 2 ˚C, respectively.

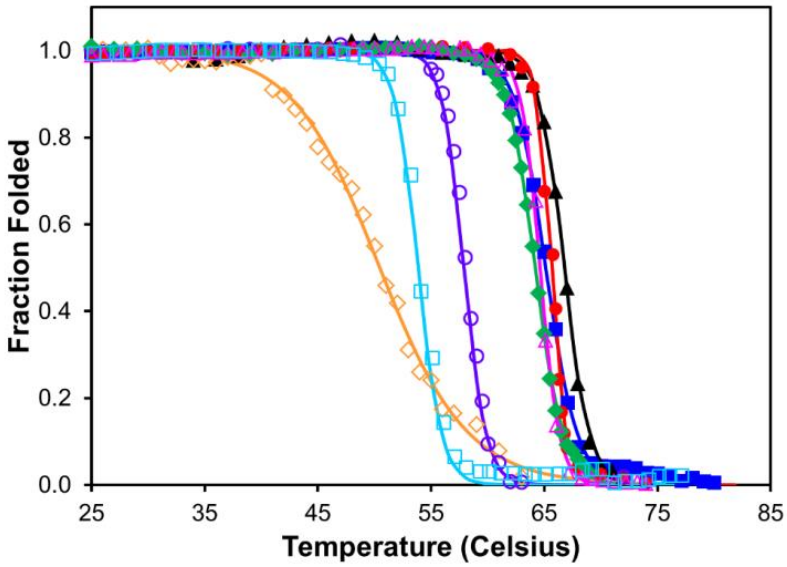

Figure 3.4 Fraction folded thermal unfolding titrations of WT HmuT (black triangles), H136A (dark blues squares), Y235A (orange open diamonds), R237A (cyan open squares), Y272A (red circles), M292A (pink, open triangles), Y349A (purple open circles), and Y349F (green diamonds). Samples were in 50 mM potassium phosphate, pH 7.0. The T_m values are in Table 3.1.

The R237A mutant also showed a significantly reduced T_m, 13 ˚C less than WT. This is in line with the expectation, based on the *C. glutamicum* x-ray structure *(25)* and the Raman studies presented herein, that R237 is the hydrogen bonding partner to the axial tyrosine. Removal of axial ligand hydrogen-bonding partners for tyrosine-bound ferric heme proteins often affects the protein similarly to the removal of an axial ligand *(36-38)*. In the *Y. pestis* HmuT crystal structure, R72 is in position to hydrogen-bond to the axial Y70 ligand using an YxR motif, although this bond is not directly observed *(2, 22)*. In the *C. glutamicum* crystal structure, the imino nitrogen of R242 is 2.7 Å from the oxygen of Y240, indicating a hydrogen bond between these residues *(25)*. Other five-coordinate tyrosine ligated heme proteins utilize

arginine as a hydrogen-bonding partner such as *P. aeruginosa* PhuT *(39)*, *Plexaura homomalla* cAOS *(40)*, bovine liver catalase *(41)*, and *Mycobacterium avium* ssp. *paratuberculosis* MAP *(40)*. With the exception of PhuT, these proteins have the arginine residue preceding the axial tyrosine in the sequence in an RxxxY motif. In contrast, PhuT has an YxR motif, similar to the predicted hydrogen-bonds in *Yp*HmuT, *Cg*HmuT, and *Cd*HmuT.

Table 3.1 Thermal unfolding T_m values of WT HmuT and mutants shown in Figure 3.4.

Protein	**T_m (°C)**
WT	66.8 ± 0.1
Y272A	65.6 ± 0.1
H136A	65.1 ± 0.1
M292A	64.6 ± 0.1
Y349F	64.2 ± 0.1
Y349A	58.1 ± 0.1
R237A	54.0 ± 0.1
Y235A	50.5 ± 1.0

3.4.5 Heme dissociation in the gas phase

Heme dissociation in the gas phase was probed by recording mass spectra at increasing collision energy voltages (5 – 30 V) (Figure 3.5). WT HmuT had the least heme loss over the range of collision energy voltages tested, still retaining approximately 90% of the bound heme even at a collision voltage of 30 V. The axial ligand mutant H136A lost a significant amount of heme at higher collision voltages, being only about 40% heme loaded at 30 V. The second axial ligand mutant, Y235A, had very little heme loading as-isolated, and did not appear as the holoprotein in this experiment, even at the lowest collision voltage.

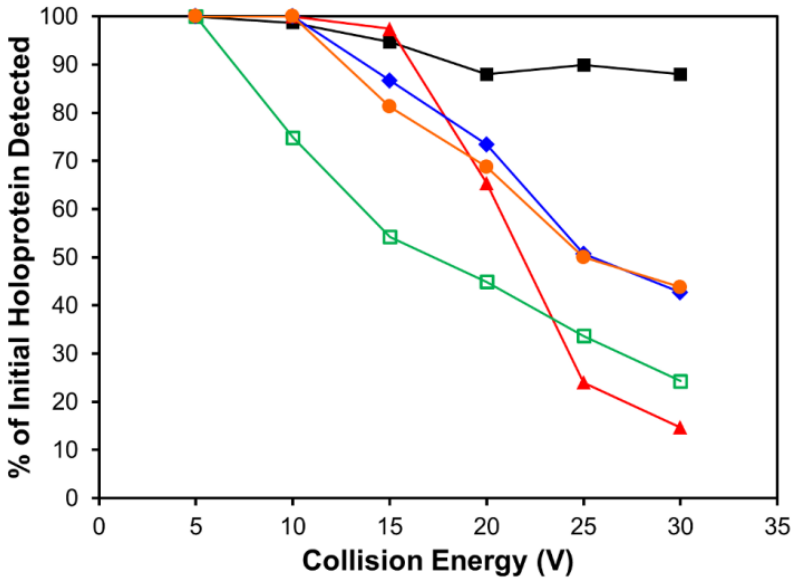

Figure 3.5 Electrospray ionization mass spectrometry detection of heme-bound WT HmuT (black squares), H136A (blue diamonds), R237A (orange circles), Y272A (red triangles), and M292A (green open squares) as a function of collision energy voltage. Holo-Y235A is not detected in the MS due to minimal heme-loading. Samples were recorded in 50 mM ammonium acetate, pH 6.8.

R237A had a very similar pattern to H136A, again starting to lose heme after 10 V, and giving a species that was about 50% heme loaded by 30 V. This significant loss of heme is in line with the expected role of R237A as a hydrogen bonding partner to the axial tyrosine. Y272A retained heme until 15 V and then lost the majority of bound heme, having only about 10% bound heme at 30 V. This residue might serve to buttress the heme in position, or it may play a hydrogen-bonding role in the heme pocket. Although methionine is neither an axial ligand nor, presumably, a hydrogen bonding partner to an axial ligand, this mutant (M292A) was the most susceptible to heme loss at low voltages, beginning to lose heme at 5 V and showing a greater loss at each increasing voltage. Although there are individual differences in the patterns, these data taken together suggest that all of the studied residues have roles in maintaining the integrity of the heme pocket and keeping the heme bound to the protein. A corollary of this is that

binding to a partner protein in the heme uptake process could induce a variety of minor changes in the heme pocket geometry and hydrogen bonding patterns, many of which could promote heme transfer.

The thermal melting and collision-induced mass spectrometry data are complimentary. As expected from previous studies on myoglobin and cytochrome b_5 *(42)*, the gas phase and solution phase data do not show a direct correlation. However, the gas phase data in particular can lead to new insights into residues that may be important in the heme transfer pathway. For example, M292A has a UV-visible absorbance spectrum that is essentially identical to that of WT, with a T_m that is only two degrees lower than WT, leading to the tentative conclusion that it does not play a role in heme binding. However, it shows a collision-induced loss of heme that is significant, indicating a buttressing role for this residue, as observed also in the Raman experiments.

3.4.6 The plasticity of the HmuT structure

It might be expected that heme transfer proteins would demonstrate some plasticity, in that their role is to repeatedly take up and release heme. For HmuT, this possibility is indicated by the observation that the crystal structure of *Yp*HmuT shows heme binding as a dimer *(22)* while that of *Cg*HmuT shows heme binding as a monomer *(25)*. In solution, *Yp*HmuT can bind heme both as a dimer and as a monomer *(22)*. We have observed dimer binding on occasion for *Cd*HmuT, but only for samples of this protein that may have been compromised in terms of conformational stability (e.g., protein from the tails of FPLC peaks).

To probe this further, we looked at reconstitution of *Cd*HmuT with heme. In initial experiments, WT *Cd*HmuT was unfolded with standard protocols and then reconstituted with hemin. UV-visible absorption spectroscopy (Figure 3.6) shows a similar spectral profile for the

two proteins, albeit with slight differences in the position of the α,β-bands. However, the two forms of the protein were not the same. As-isolated WT HmuT took over an hour to reduce in the presence of excess dithionite *(17)*; reduction of reconstituted HmuT occurred within minutes. The inverse correlation plot of the reconstituted WT HmuT Fe(II)-CO species (Figure 3.4) showed two ν_{FeCO} bands at 496 and 533 cm^{-1}, with one ν_{C-O} band at 1959 cm^{-1}. In contrast, as-isolated HmuT has a single ν_{FeCO} band at 535 cm^{-1} and a single ν_{C-O} band at 1920 cm^{1}. In terms of spin-state assignment, as-isolated HmuT has a six-coordinate high-spin (6cHS) band at 1475 cm^{-1} and a six-coordinate low-spin (6cLS) band at 1504 cm^{-1} (Figure 3.7). Reconstituted HmuT has the same bands as-isolated HmuT with one additional five-coordinate high-spin (5cHS) band at 1490 cm^{-1}. These results indicate that heme reconstitution can lead to heme binding in a reconstituted protein that is not the same as when first isolated after purification. The complexity of the system precludes identification of all the individual species, but these experiments, in conjunction with those in the literature, indicate that HmuT can adopt more than one heme-bound form.

Sequence alignment of *C. diphtheriae* HmuT with closely related *Corynebacterium* species showed Y349 to be conserved, although homology modeling and the comparison *C. glutamicum* structure predicted that the residue was not near the binding site (*Y. pestis* does not have an aromatic residue at this sequence position). Expression and purification of both Y349A and Y349F resulted in less heme-loading when compared to the WT, indicating that the ability of the protein to bind heme is somehow altered by these mutations. Thermal unfolding studies gave reductions in T_m by three and nine degrees, respectively, for Y349F and Y349A. Removal of

Y349 may result in altered protein folding, which could in turn result in reduced heme binding.

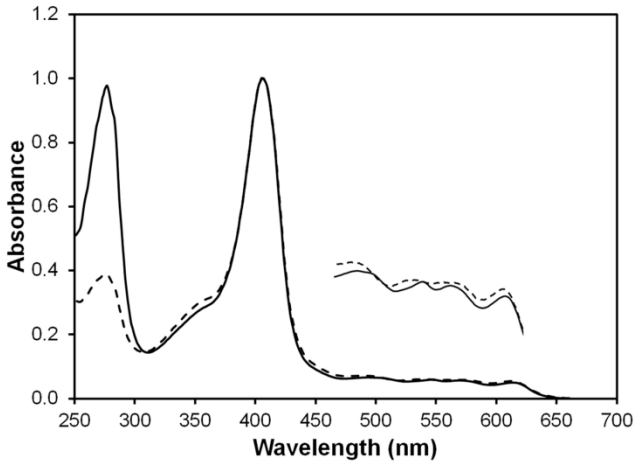

Figure 3.6 UV-visible absorption spectra of Fe(III) as-isolated (solid) and reconstituted WT HmuT (dashed line) normalized at the Soret. Samples were recorded in 50 mM Tris-Cl, pH 7.0.

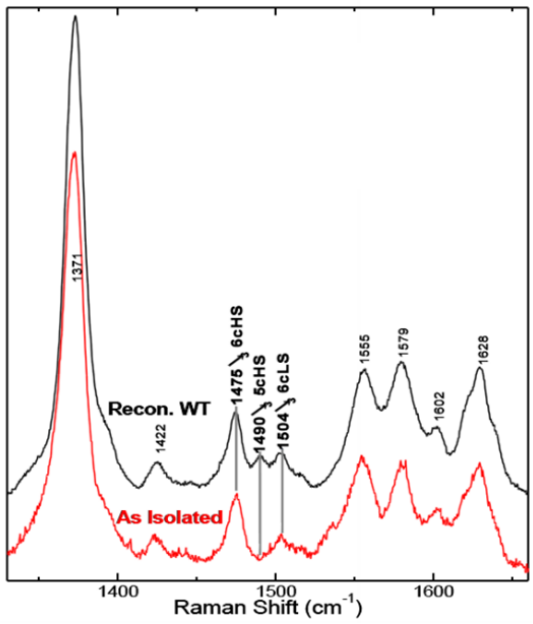

Figure 3.7 High frequency resonance Raman spectra of Fe(III) as-isolated and reconstituted HmuT. Spectra were excited with a 413.1 nm Kr^+ ion laser.

3.5 Conclusions

In the case of *Cd*HmuT, other residues in addition to the heme axial ligands are necessary for efficient heme binding. Following an emerging theme of tyrosine-ligated heme proteins, *Cd*HmuT utilizes R237 to hydrogen-bond to the axial Y235 which was also indicated in previous studies on the *Cg*HmuT and *Yp*HmuT sister proteins. Heme binding of Y272 was affected by collision energy and could be participating as a hydrogen-bonding partner in the pocket. M292, although not an axial ligand, buttresses the heme as shown by resonance Raman and thermal unfolding. Y349 mutations resulted in a much less heme-loaded protein. Reconstitution alters the form of heme bound to HmuT and indicates the overall plasticity of the HmuT structure which could be indicative of *in vivo* function towards the ability of this heme transfer protein to bind and release heme molecules multiple times.

3.6 References

[1] Benson, D. R., and Rivera, M. (2013) Heme uptake and metabolism in bacteria. *Met. Ions Life Sci 12*, 279-332.

[2] Rodgers, K. R., and Lukat-Rodgers, G. S. (2014) Biophysical perspectives on the acquisition, transport, and trafficking of heme in bacteria. *Handbook of porphyrin science with applications to chemistry, physics, materials science, engineering, biology and medicine, vol. 30: Heme proteins, part II 30*, 249-309.

[3] Wilks, A., and O'Neill, M. J. (2014) Extracellular heme uptake and metabolism in bacterial pathogenesis, In *Handbook of porphyrin science with applications to chemistry, physics, materials science, engineering, biology and medicine, vol 26: Heme biochemistry* (Ferreira, G. C., Kadish, K. M., Smith, K. M., and Guilard, R., Eds.), pp 267-315, World Scientific, Hackensack, NJ.

[4] Cavallaro, G., Decaria, L., and Rosato, A. (2008) Genome-based analysis of heme biosynthesis and uptake in prokaryotic systems. *J. Proteome Res. 7*, 4946-4954.

[5] Contreras, H., Chim, N., Credali, A., and Goulding, C. W. (2014) Heme uptake in bacterial pathogens. *Curr. Opin. Chem. Biol. 19*, 34-41.

[6] Smith, A. D., and Wilks, A. (2012) Extracellular heme uptake and the challenges of bacterial cell membranes. *Curr. Top. Membr. 69*, 359-392.

[7] Farrand, A. J., and Skaar, E. P. (2014) Heme and infectious diseases, In *Handbook of porphyrin science with applications to chemistry, physics, materials science, engineering, biology and medicine, vol 26: Heme biochemistry* (Ferreira, G. C., Kadish, K. M., Smith, K. M., and Guilard, R., Eds.) 26 ed., pp 317-377, World Scientific, Hackensack, NJ.

[8] Nobles, C. L., and Maresso, A. W. (2011) The theft of host heme by Gram-positive pathogenic bacteria. *Metallomics 3*, 788-796.

[9] Runyen-Janecky, L. J. (2013) Role and regulation of heme on acquisition in gram-negative pathogens. *Front. Cell. Infect. Microbiol. 3*, 55.

[10] Grigg, J. C., Ukpabi, G., Gaudin, C. F., and Murphy, M. E. (2010) Structural biology of heme binding in the *Staphylococcus aureus* Isd system. *J. Inorg. Biochem. 104*, 341-348.

[11] Haley, K. P., and Skaar, E. P. (2012) A battle for iron: Host sequestration and *Staphylococcus aureus* acquisition. *Microb. Infect. 14*, 217-227.

[12] Honsa, E. S., and Maresso, A. W. (2011) Mechanisms of iron import in anthrax. *BioMetals 24*, 533-545.

[13] Eichenbaum, Z. (2012) The streptococcal hemoprotein receptor. A moonlighting protein or a virulence factor? *Virulence 3*, 553-555.

[14] Akbas, N., Draganova, E. B., Block, D. R., Sook, B. R., Chan, Y. F., Zhuo, J., Eichenbaum, Z., Rodgers, K. R., and Dixon, D. W. (2015) Heme-bound SiaA from *Streptococcus pyogenes*: Effects of mutations and oxidation state on protein stability. *J. Inorg. Biochem.*

[15] Schmitt, M. P. (2014) Iron acquisition and iron-dependent gene expression in *Corynebacterium diphtheriae*, In *Corynebacterium diphtheriae and related toxigenic species: Genomics, pathogenicity and applications* (Burkovski, A., Ed.), pp 95-121.

[16] Allen, C. E., and Schmitt, M. P. (2014) Utilization of host iron sources by *Corynebacterium diphtheriae*: Multiple hemoglobin-binding proteins are essential for the use of iron from the hemoglobin/haptoglobin complex. *J. Bacteriol. 195*, 2413-2414.

[17] Draganova, E. B., Akbas, N., Adrian, S. A., Lukat-Rodgers, G. S., Collins, D. P., Dawson, J. H., Allen, C. E., Schmitt, M. P., Rodgers, K. R., and Dixon, D. W. (2015) Heme binding by *Corynebacterium diphtheriae* HmuT: Function and heme environment. *Biochemistry 54*, 6598-6609.

[18] Drazek, E. S., Hammack, C. A., and Schmitt, M. P. (2000) *Corynebacterium diphtheriae* genes required for acquisition of iron from haemin and haemoglobin are homologous to ABC haemin transporters. *Mol. Microbiol 36*, 68-84.

[19] Allen, C. E., and Schmitt, M. P. (2009) HtaA is an iron-regulated hemin binding protein involved in the utilization of heme iron in *Corynebacterium diphtheriae*. *J. Bacteriol. 191*, 2638-2648.

[20] Allen, C. E., and Schmitt, M. P. (2011) Novel hemin binding domains in the *Corynebacterium diphtheriae* HtaA protein interact with hemoglobin and are critical for heme iron utilization by HtaA. *J. Bacteriol. 193*, 5374-5385.

[21] Allen, C. E., Burgos, J. M., and Schmitt, M. P. (2013) Analysis of novel iron-regulated, surface-anchored hemin-binding proteins in *Corynebacterium diphtheriae*. *J. Bacteriol. 195*, 2852-2863.

[22] Mattle, D., Zeltina, A., Woo, J. S., Goetz, B. A., and Locher, K. P. (2010) Two stacked heme molecules in the binding pocket of the periplasmic heme-binding protein HmuT from *Yersinia pestis*. *J. Mol. Biol. 404*, 220-231.

[23] Nienaber, A., Hennecke, H., and Fischer, H. M. (2001) Discovery of a haem uptake system in the soil bacterium *Bradyrhizobium japonicum*. *Mol. Microbiol 41*, 787-800.

[24] Lodes, M. J., Secrist, H., Benson, D. R., Jen, S., Shanebeck, K. D., Guderian, J., Maisonneuve, J. F., Bhatia, A., Persing, D., Patrick, S., and Skeiky, Y. A. W. (2006) Variable expression of immunoreactive surface proteins of *Propionibacterium acnes*. *Microbiology-SGM 152*, 3667-3681.

[25] Muraki, N., and Aono, S. (2016) Structural basis for heme recognition by HmuT responsible for heme transport to the heme transporter in *Corynebacterium glutamicum*. *Chem. Lett. 45*, 24-26.

[26] Trost, E., Blom, J., Soares, S. D., Huang, I. H., Al-Dilaimi, A., Schroder, J., Jaenicke, S., Dorella, F. A., Rocha, F. S., Miyoshi, A., Azevedo, V., Schneider, M. P., Silva, A., Camello, T. C., Sabbadini, P. S., Santos, C. S., Santos, L. S., Hirata, R., Mattos-Guaraldi, A. L., Efstratiou, A., Schmitt, M. P., Hung, T. T., and Tauch, A. (2012) Pangenomic study of *Corynebacterium diphtheriae* that provides insights into the genomic diversity of pathogenic isolates from cases of classical diphtheria, endocarditis, and pneumonia. *J. Bacteriol. 194*, 3199-3215.

[27] Wagner, K. S., White, J. M., Lucenko, I., Mercer, D., Crowcroft, N. S., Neal, S., and Efstratiou, A. (2012) Diphtheria in the postepidemic period, Europe, 2000-2009. *Emerging Infect. Dis. 18*, 217-225.

[28] Schmitt, M. P. (1997) Utilization of host iron sources by *Corynebacterium diphtheriae*: Identification of a gene whose product is homologous for eukaryotic heme oxygenases and is required for acquisition of iron from heme and hemoglobin. *J. Bacteriol 179*, 838-845.

[29] Schmitt, M. P., and Drazek, E. S. (2001) Construction and consequences of directed mutations affecting the hemin receptor in pathogenic *Corynebacterium species*. *J. Bacteriol 183*, 1476-1481.

[30] Popovic, T., Kombarova, S. Y., Reeves, M. W., Nakao, H., Mazurova, I. K., Wharton, M., Wachsmuth, I. K., and Wenger, J. D. (1996) Molecular epidemiology of diphtheria in Russia, 1985-1994. *J. Infect. Dis. 174*, 1064-1072.

[31] Schmitt, M. P., and Holmes, R. K. (1991) Iron-dependent regulation of diphtheria toxin and siderophore expression by the cloned *Corynebacterium diphtheriae* repressor gene Dtxr in *C. diphtheriae* C7 strains. *Infect. Immun. 59*, 1899-1904.

[32] Teale, F. W. (1959) Cleavage of the heme protein by acid methyl ethyl ketone. *Biochim. Biophys. Acta 35*, 543.

[33] Gasteiger, E., Hoogland, C., Gattiker, A., Duvaud, S., Wilkins, M. R., Appel, R. D., and Bairoch, A. (2005) Protein identification and analysis tools on the ExPASy server, In *The proteomics protocols handbook* (Walker, J. M., Ed.), pp 571-607, Humana Press, Totowa, N.J.

[34] Collier, G. S., Pratt, J. M., De Wet, C. R., and Tshabalala, C. F. (1979) Studies on haemin in dimethyl sulphoxide/water mixtures. *Biochem. J 179*, 281-289.

[35] Swint, L., and Robertson, A. D. (1993) Thermodynamics of unfolding for turkey ovomucoid third domain: Thermal and chemical denaturation. *Protein Sci. 2*, 2037-2049.

[36] Arnoux, P., Haser, R., Izadi, N., Lecroisey, A., Delepierre, M., Wandersman, C., and Czjzek, M. (1999) The crystal structure of HasA, a hemophore secreted by *Serratia marcescens*. *Nature Struct. Biol 6*, 516-520.

[37] Grigg, J. C., Vermeiren, C. L., Heinrichs, D. E., and Murphy, M. E. P. (2007) Haem recognition by a *Staphylococcus aureus* NEAT domain. *Mol. Microbiol. 63*, 139-149.

[38] Caillet-Saguy, C., Piccioli, M., Turano, P., Lukat-Rodgers, G., Wolff, N., Rodgers, K. R., Izadi-Pruneyre, N., Delepierre, M., and Lecroisey, A. (2012) Role of the iron axial ligands of heme carrier HasA in heme uptake and release. *J. Biol. Chem. 287*, 26932-26943.

[39] Ho, W. W., Li, H. Y., Eakanunkul, S., Tong, Y., Wilks, A., Guo, M. L., and Poulos, T. L. (2007) Holo-and apo-bound structures of bacterial periplasmic heme-binding proteins. *J. Biol. Chem. 282*, 35796-35802.

[40] Bandara, D. M. I., Sono, M., Bruce, G. S., Brash, A. R., and Dawson, J. H. (2011) Coordination modes of tyrosinate-ligated catalase-type heme enzymes: Magnetic circular dichroism studies of *Plexaura homomalla* allene oxide synthase, *Mycobacterium avium* ssp. paratuberculosis protein-2744c, and bovine liver catalase in their ferric and ferrous states. *J. Inorg. Biochem. 105*, 1786-1794.

[41] Fita, I., and Rossmann, M. G. (1985) The active center of catalase. *J. Mol. Biol 185*, 21-37.

[42] Hunter, C. L., Mauk, A. G., and Douglas, D. J. (1997) Dissociation of heme from myoglobin and cytochrome *b*(5): Comparison of behavior in solution and the gas phase. *Biochemistry 36*, 1018-1025.

3.7 Supplemental Information

3.7.1 Supplemental Figures

Figure 3.8 S1 Sequence alignment of the HmuT amino acid sequence from various Corynebacterium species. Conserved residues which were subjected to site-directed mutagenesis are labeled: R237, Y272, M292, and Y349.

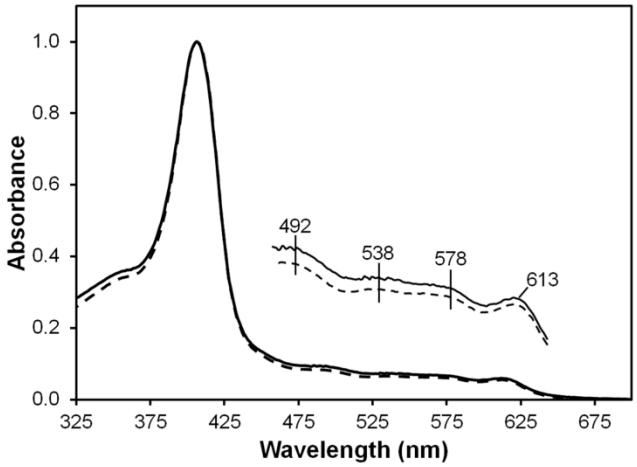

Figure 3.9 UV-visible absorption spectra of Fe(III) Y349A (dashed) and Y349F (solid line) normalized at the Soret. Samples were recorded in 50 mM Tris-Cl, pH 7.0.

4 ADDITIONAL STUDIES ON THE CHARACTERIZATION OF *C. DIPHTHERIAE* HMUT

Chapter 1 gave a detailed overview of heme uptake in some of the most commonly studied pathogenic bacteria. Chapter 2 was published work by our group which determined the heme axial ligands of HmuT. Chapter 3 was additional work for publication expanding on our work of HmuT and other important residues involved in heme binding. This chapter gives additional experimental data and literature discussions related to our previously published and unpublished work on HmuT. All of the following experiments in this chapter were performed at Georgia State University.

4.1 Experimental

4.1.1 Expression and purification of HmuT and mutants

Expression and purification of WT, H136A, Y235A, Y272A, R237A, M292A, Y349A, and Y349F were previously described *(1)*. Protein samples are isolated as a mixture of apo and holo forms. Purity of the samples was evaluated by SDS-PAGE electrophoresis and performed as previously described *(1)*. Approximate heme loading was calculated based on the Soret to 280 nm ratio.

4.1.2 Optical spectroscopy

Samples of apo- and holo-HmuT WT and mutants were analyzed by UV-visible absorption spectroscopy using a Varian 50 Bio spectrophotometer in 1 cm quartz cuvettes at room temperature unless otherwise noted. Circular dichroism (CD) spectra were recorded using a Jasco J-810 Spectropolarimeter in quartz Suprasil cuvettes (Fisherbrand, Inc.) with a 1 mm path length. Protein samples (10 μM) were recorded in 10 mM KH_2PO_4 buffer at pH 7.0 in a spectral window of 190 to 260 nm. The final spectrum represents an average of 10 scans.

Estimations of secondary structure were obtained using the DichroWeb analysis program *(2)*. Both SELCON and CONTIN databases were used to analyze the CD data. Secondary structural content was reported as an average of the two databases.

4.1.3 HmuT Y235A and M292A heme extraction

Apo-Y235A and apo-M292A were prepared using the Teale method *(3)*. All samples during the extraction process were kept on ice. Each HmuT mutant was mixed with 2 mL of cold 2-butanone and cold 1 M HCl was used to drop the pH to around 2.0. The solution was vortexed and sat on ice for 30 min to allow separation. The organic heme/butanone (top) layer was discarded. The aqueous (lower) layer was placed into a 13,000 MWCO dialysis bag and dialyzed against 20 mM Tris-Cl, pH 7.0 for 6 h at 4˚C and then again overnight. The concentration of apo-Y235A and apo-M292A were determined using the ExPASy ε_{280} = 14,440 $M^{-1}cm^{-1}$ and 15,930 $M^{-1}cm^{-1}$, respectively.

4.1.4 HmuT Y235A and M292A heme reconstitution

Reconstitution was monitored using UV-visible absorption spectroscopy. Hemin solutions were prepared fresh by dissolving 1 mg of hemin in 5 mL of dimethyl sulfoxide (DMSO, EMD Chemicals) to prevent aggregation. Hemin concentration was spectroscopically determined using the extinction coefficient of 188 $mM^{-1}cm^{-1}$ at 404 nm *(4)*. The stock hemin solution was then titrated in 1 μL aliquots to the apoprotein (~5 μM) while the solution slowly stirred. The solution stirred for 30 min in between each addition of heme. Once a 2:1 ratio of the Soret band to the 280 band was reached, the sample was stored overnight at 4˚C. The reconstituted HmuT mutant was checked spectrally for heme aggregation the next day. Reconstituted Y235A and M292A were then dialyzed into the appropriate buffer. Samples which have not been reconstituted are referred to as “as-isolated” samples.

4.1.5 Electrospray ionization (ESI) mass spectrometry of HmuT mutants

Samples (50 μM) of H136A and reconstituted M292A were concentrated into Nanopure water using a Millipore YM-3 centrifugal filtration unit (30,000 MWCO) following the manufacturer's protocol. Y235A, Y272A, R237A, and as-isolated M292A (50 μM) were concentrated into 50 mM ammonium acetate, pH 6.8, using an Amicon centrifugal filtration unit (30,000 MWCO) following the manufacturer's protocol. The samples were then dialyzed for five days in 50 mM ammonium acetate, pH 6.8, to remove residual salts. Fresh buffer was used every 24 h.

ESI spectra were obtained using a Waters Micromass Q-TOF Micro mass spectrometer in the positive mode. Samples were prepared with either 50:50 acetonitirile to water and 0.1% formic acid or 10% methanol when indicated. Deconvolution of the charged states were performed using the MaxEnt program with the MassLynx™ software. Peaks were rounded to the nearest Dalton.

4.1.6 pH titrations of as-isolated and reconstituted HmuT Y235A

Samples of either as-isolated or reconstituted Y235A (5 μM) were monitored using UV-visible absorption spectroscopy from pH 4 – 9.5 and 7 – 11, respectively, in a series of pH titrations. For as-isolated Y235A, two titrations were performed; one from pH 4 – 7 and 6 – 9.5. The reconstituted Y235A was titrated from pH 7 – 11. Aliquots of 1 M NaOH were used to adjust the pH in all titrations with the exception of the as-isolated Y235A pH 4 – 7 titration in which aliquots of 1M HCl were used to adjust pH. The pH was adjusted between scans after a constant spectrum was obtained with an absorbance change of less than 0.002 at the Soret. All data were fit to either a one or two pK_a model with global fitting analysis software using Equations 1 or 2, respectively:

$$Abs_{obs} = \frac{Abs_A \times 10^{(\mathrm{pH} - \mathrm{p}K_a)} + Abs_B}{1 + 10^{(\mathrm{pH} - \mathrm{p}K_a)}} \quad [1]$$

$$Abs_{obs} = \frac{Abs_A + Abs_B \times 10^{(\mathrm{pH} - \mathrm{p}K_{a1})} + Abs_C \times 10^{((2 \times pH) - pK_{a1} - pK_{a2}))}}{1 + 10^{(\mathrm{pH} - \mathrm{p}K_a)} + 10^{((2 \times pH) - pK_{a1} - pK_{a2}))}} \quad [2]$$

4.1.7 Chemical unfolding studies of HmuT

Chemical denaturation of WT HmuT (5 µM) was performed using guanidinium hydrochloride (GdnCl) and monitored at 406 nm via NanoDrop UV-visible absorption spectroscopy to approximate the $D_{1/2}$. A series of WT HmuT samples at various GdnCl concentrations were incubated at room temperature overnight in 50 mM Tris-Cl, pH 7.0. A stock solution of 8.0 M GdnCl was prepared in 50 mM Tris-Cl, pH 7.0 and refractive index was used to verify the concentration of the stock *(5)*. The desired GdnCl concentration was achieved by varying the amount of buffer in the sample.

The unfolding curve was analyzed using a two-state unfolding model, Equation 3 (*2*):

$$y = [(A_F + m_F[D]) + (A_U + m_U[D])\exp[m([D]-[D]_{1/2})/RT])]/1 + \exp[m([D]-[D]_{1/2})/RT] \quad [3]$$

where y is the absorbance at any point along the fitted denaturation curve, y_F is the absorbance of the folded state, y_U is the absorbance of the unfolded state, m is the slope at the midpoint, and also the dependence of the free energy of unfolding on the denaturant concentration, m_F is the slope of the folded state, m_U is the slope of the unfolded state, [D] is the concentration of GdnCl, $[D]_{1/2}$ is the concentration of GdnCl at the midpoint of the unfolding curve, R is the gas constant, and T is the temperature (Kelvin).

In a separate set of experiments, solutions of 5 μM WT, Y235A, and H136A in 50 mM Tris-Cl, pH 7.0 were monitored via UV-visible absorption spectroscopy at the Soret as a function of time for 24 h at the estimated $D_{1/2}$ concentrations. The data were fit to a first-order reaction using Equation 4:

$$Abs_{obs} = A \exp(-k_U t) + b \quad [4]$$

where Abs_{obs} is the observed change in absorbance, A is the amplitude of the change corresponding to unfolding, k_U is the rate constant of the unfolding, b is the offset, and t is time.

4.2 Results

4.2.1 Circular dichroism spectroscopy of HmuT and mutants

CD studies were performed on WT, Y272A, Y349A, and Y349F HmuT. Each sample varied in heme loading as detailed in the experimental. All spectra indicated the presence of α-helical content, with varied positions of the maxima and minima around 190, 208, and 222 nm (Figure 4.1). Analysis of the CD data using DichroWeb showed WT HmuT to have 91% α-helical content, 8% turns, and 1% unordered. Each mutation, with the exception of Y272A, resulted in a decrease in α-helical content of the protein with Y349F having the largest reduction in α-helicity (Table EBIII75).

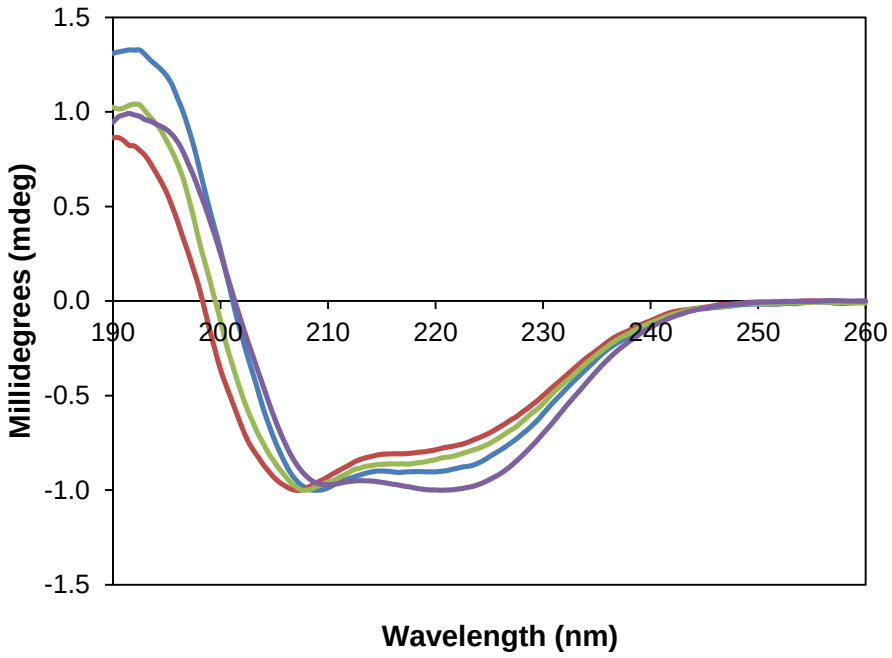

Figure 4.1 CD spectra of WT HmuT (purple), Y272A (blue), Y349A (red) and Y349F (green). Samples were measured in 10 mM potassium phosphate, pH 7.0.

Table 4.1 DichroWeb CD estimated secondary structural deconvolution of HmuT and mutants.

Protein	α-Helix (%)	Turns (%)	Unordered (%)
WT	91	8	1
Y272A	91	5	4
Y349A	78	13	9
Y349F	45	28	27

4.2.2 Reconstitution of Y235A and M292A

Y235A was reconstituted in order to increase heme loading and reduce fluorescent signal due to the presence of apoprotein before use in resonance Raman experiments. As-isolated Y235A heme loading varied with each expression. The sample used for reconstitution was ~20% heme loaded based on the Soret:280 nm ratio. Reconstituted Y235A was 100% heme loaded after titration with heme. Normalized UV-visible absorption spectral overlay (Figure 4.2)

of the as-isolated compared to the reconstituted sample showed minimal changes in regards to band positions. Reconstituted Y235A gave a broader Soret compared to the as-isolated protein.

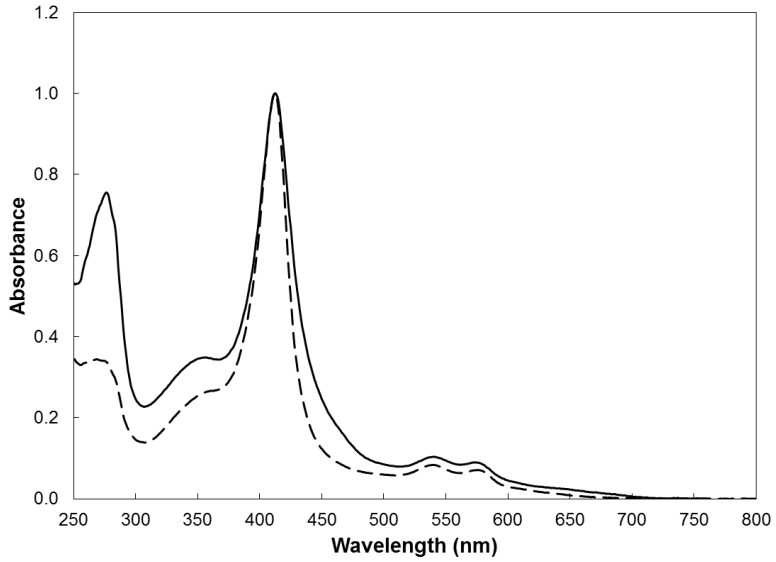

Figure 4.2 Normalized UV-visible absorption spectra of as-isolated Y235A (solid line) and reconstituted Y235A (dashed line). Both samples are in 50 mM Tris-Cl, pH 7.0.

The same experiment was performed on HmuT M292A to reduce fluorescent signal due to a mixture of heme and protoporphyrin potentially bound to the protein which can cause noise in resonance Raman experiments. M292A is ~90% heme loaded prior to reconstitution. Figure 4.3 normalized spectral overlay of the two samples showed relevant bands to be in the same position before and after reconstitution. Reconstituted M292A had a slight shoulder next to the Soret compared to the as-isolated sample.

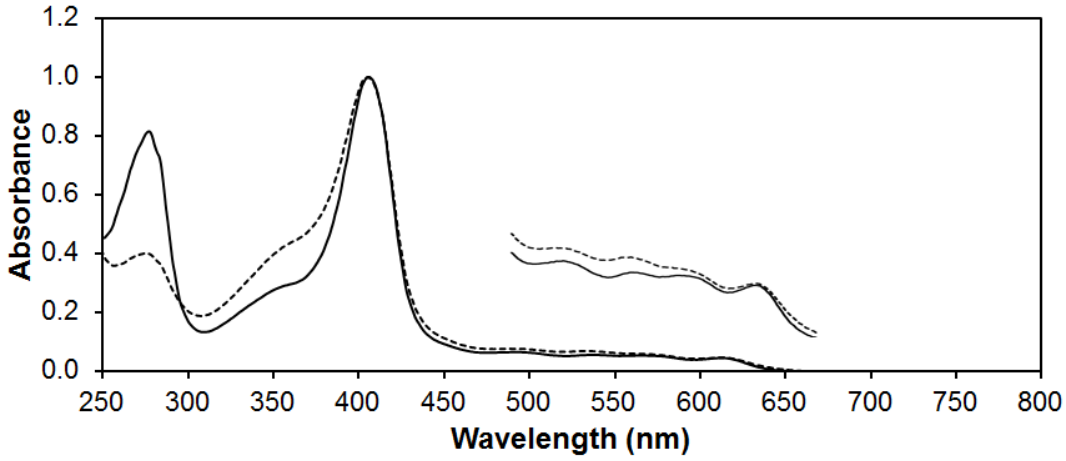

Figure 4.3 Normalized UV-visible absorption spectra of as-isolated M292A (solid line) and reconstituted M292A (dashed line). Both samples are in 50 mM Tris-Cl, pH 7.0.

4.2.3 Electrospray ionization (ESI) mass spectrometry of HmuT mutants

Samples of H136A, Y235A, R237A, Y272A, and both as-isolated and reconstituted M292A were analyzed using ESI-MS. H136A and reconstituted M292A were incubated with either a 50:50 mixture of acetonitrile/0.1% formic acid or 10% methanol. Both conditions are used to increase signal to noise during MS data collection *(6, 7)*. It should be noted that the addition of formic acid reduces the sample pH below 2 and therefore can lead to heme loss and the detection of only apoprotein. Y235A, R237A, Y272A, and as-isolated M292A were prepared in 50 mM ammonium acetate at neutral pH.

The electrospray mass spectrum of H136A in acetonitrile and formic acid (Figure 4.4) showed a clean peak at 36,129 Da (the expected molecular weight of the apoprotein is 36,129 Da). The apoprotein is expected due to the addition of formic acid to the sample. The spectral envelope gave clear peaks from charges +18 to +41 with the highest peak having a charge of +30.

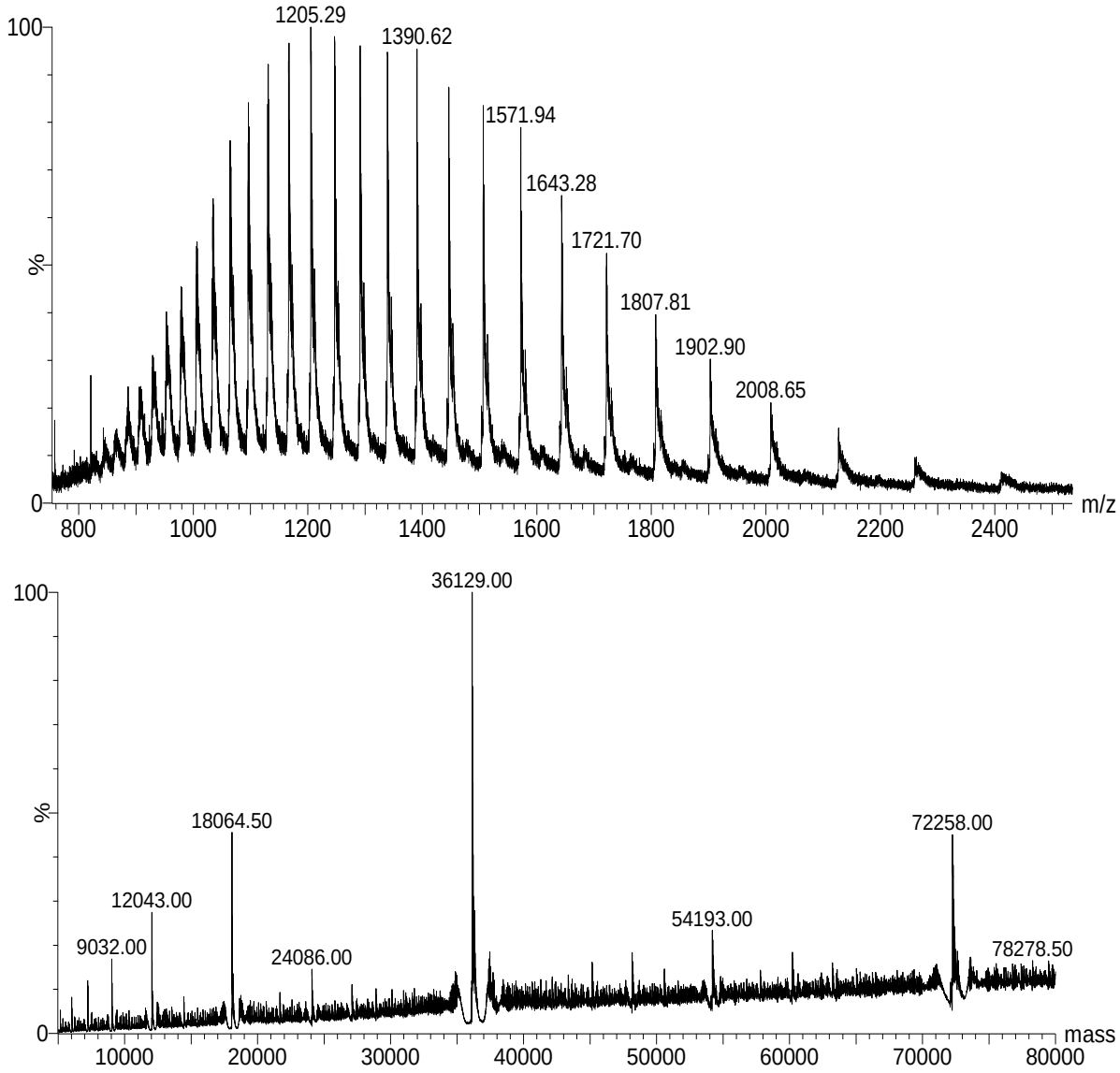

Figure 4.4 Electrospray ionization mass spectrum in the positive mode of purified HmuT H136A. Protein was exposed to 0.1% formic acid to give the apoprotein. The top panel shows the spectral envelope. The bottom panel shows the deconvoluted region. The predicted mass of the apoprotein is 36,129 Da. The experimental mass is 36,129 Da and is consistent with the expected mass of the apoprotein.

The Y235A deconvoluted electrospray mass spectrum (Figure 4.5) showed a peak at 36,104 Da (the expected molecular weight of the apoprotein is 36,103 Da). Charge states for the protein ranged from +13 to +40, with two distinct charged envelopes.

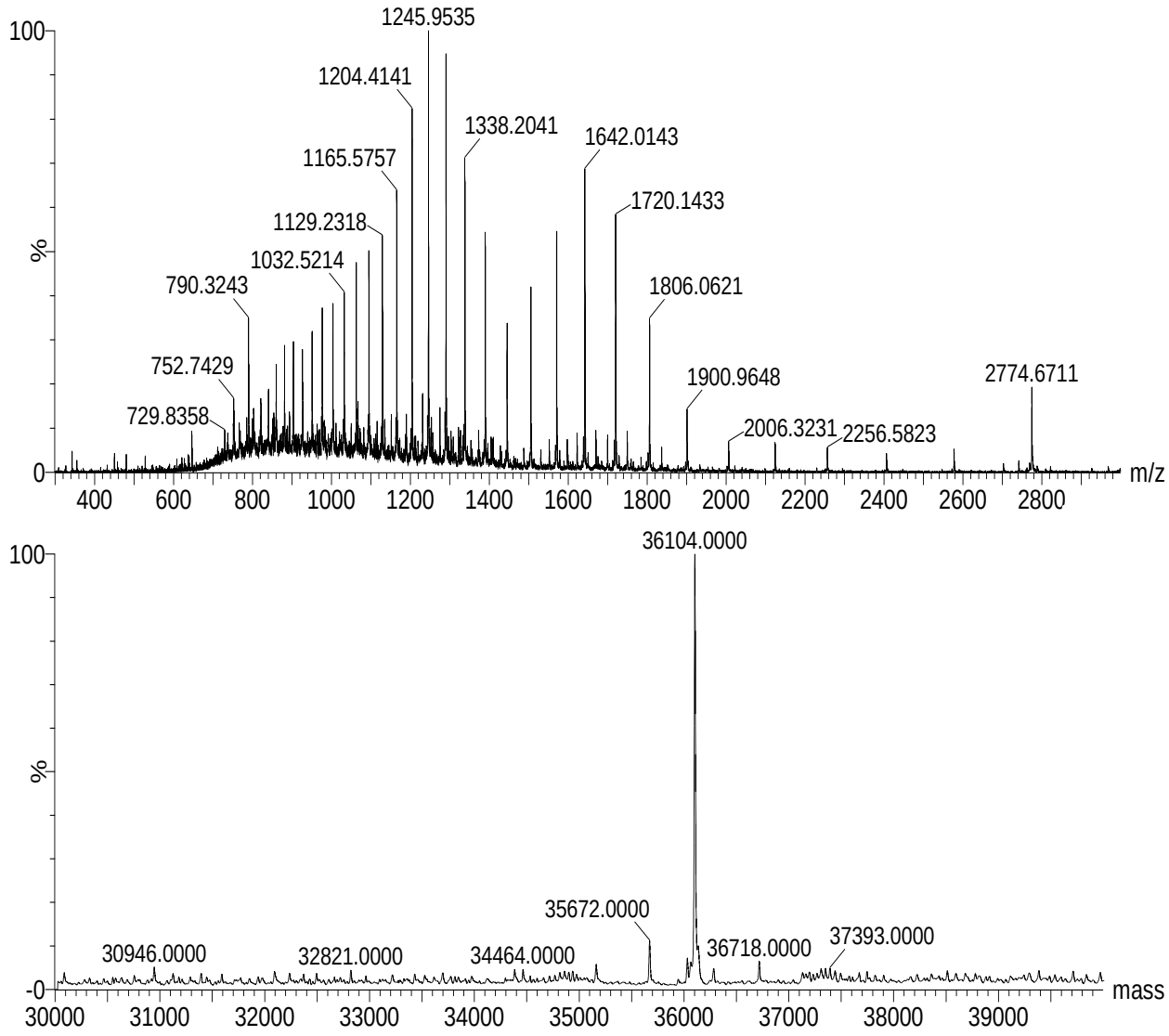

Figure 4.5 Electrospray ionization mass spectrum in the positive mode of purified HmuT Y235A. Bottom panel: The deconvoluted region shows HmuT Y235A at 36,104 Da. The predicted mass of the apoprotein is 36,103 Da.

The electrospray mass spectrum of as-isolated M292A (Figure 4.6) showed a clean peak representing the apoprotein at 36,268 Da (the expected molecular weight of the apoprotein is 36,265 Da). Another peak representing the holoprotein is seen at 36,886 Da (the expected molecular weight of the holoprotein is 36,881 Da). The charged envelope window consisted of two envelopes ranging from +12 to +23 with charges centered at +13 and +22.

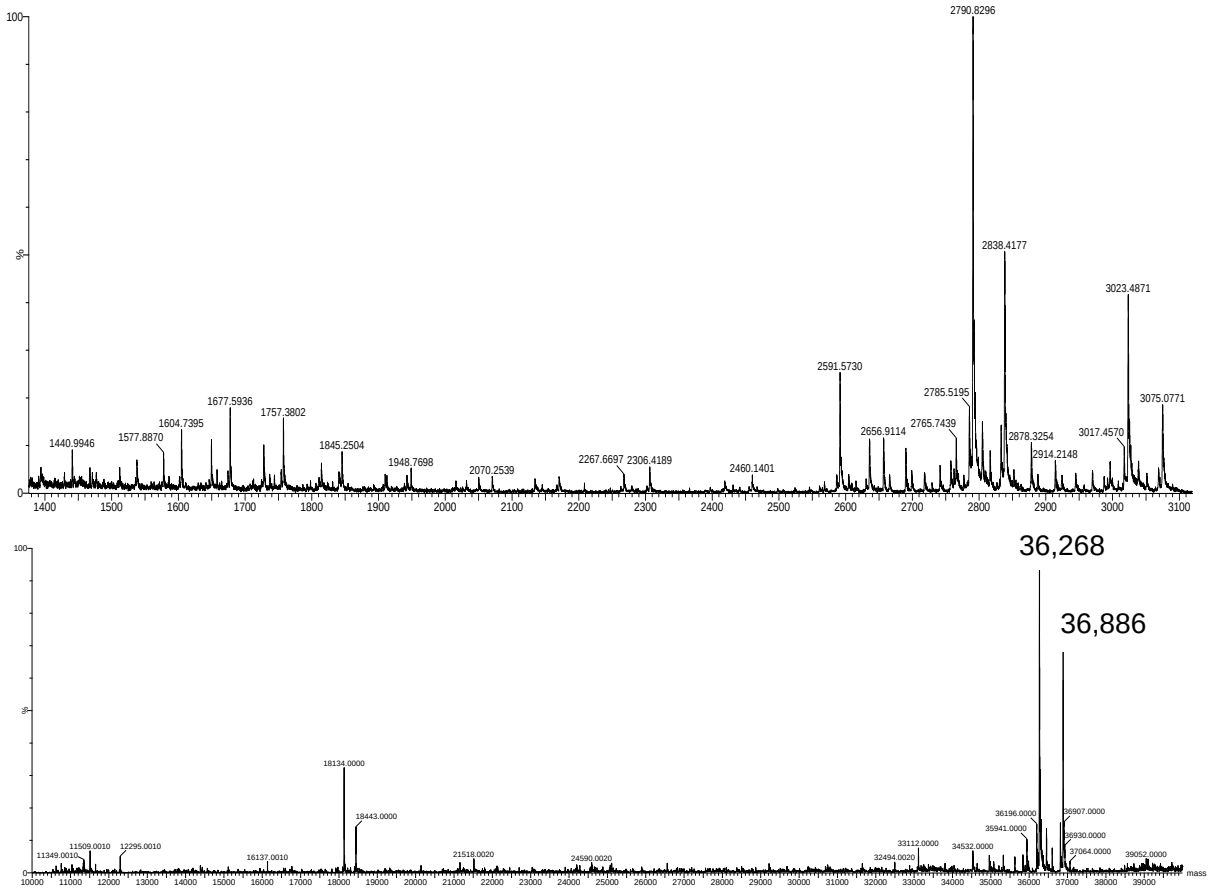

Figure 4.6 Electrospray ionization mass spectrum in the positive mode of as-isolated HmuT M292A. Bottom panel: The deconvoluted region shows HmuT M292A at 36,268 Da and 36,886 Da, indicative of apo- and holoprotein, respectively. The predicted mass of the apoprotein is 36,265 Da and 36,881 Da for the holoprotein. Samples were prepared in 50 mM ammonium acetate at neutral pH.

ESI of reconstituted M292A also showed a mixture of apoprotein and holoprotein based on the two distinct spectral envelopes (Figure 4.7). The positions for apo- and holo-reconstituted M292A differed from that of the as-isolated sample. A peak at 36,185 Da (the expected molecular weight of the apoprotein is 36,265 Da) was seen for the apoprotein and a peak at 36,785 Da (the expected molecular weight of the holoprotein is 36,881 Da) was observed for the holoprotein (Figure 4.7, bottom panel). The charged envelope ranged from +15 to +30 and was centered at +23.

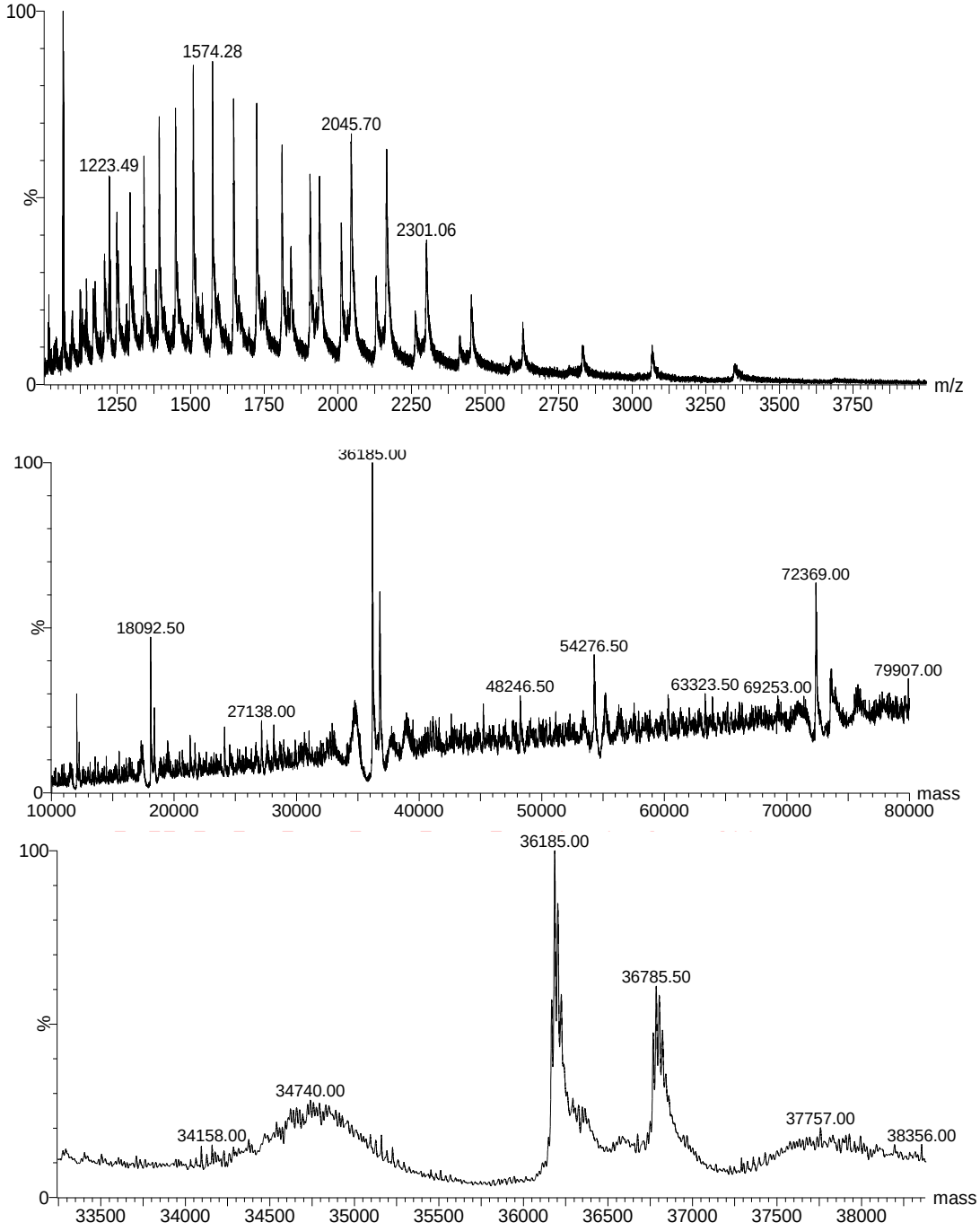

Figure 4.7 Electrospray ionization mass spectrum in the positive mode of reconstituted HmuT M292A. Middle and bottom panels: The deconvoluted region shows HmuT M292A at 36,185 Da and 36,785 Da, indicative of apo- and holoprotein, respectively. The predicted mass of the apoprotein is 36,265 Da and 36,881 Da for the holoprotein. Samples were prepared in Nanopure water.

HmuT Y272A ESI gave two peaks representing the holo and apo forms of the protein (Figure 4.8). The predominant peak representing the holoprotein was at 36,719 Da (expected molecular weight of the holoprotein is 36,719 Da). The minor peak at 36,104 Da was the apoprotein (expected molecular weight of the holoprotein is 36,103 Da). The charged envelope ranged from +19 to +40 and is centered at +30. A smaller envelope was also observed around +13.

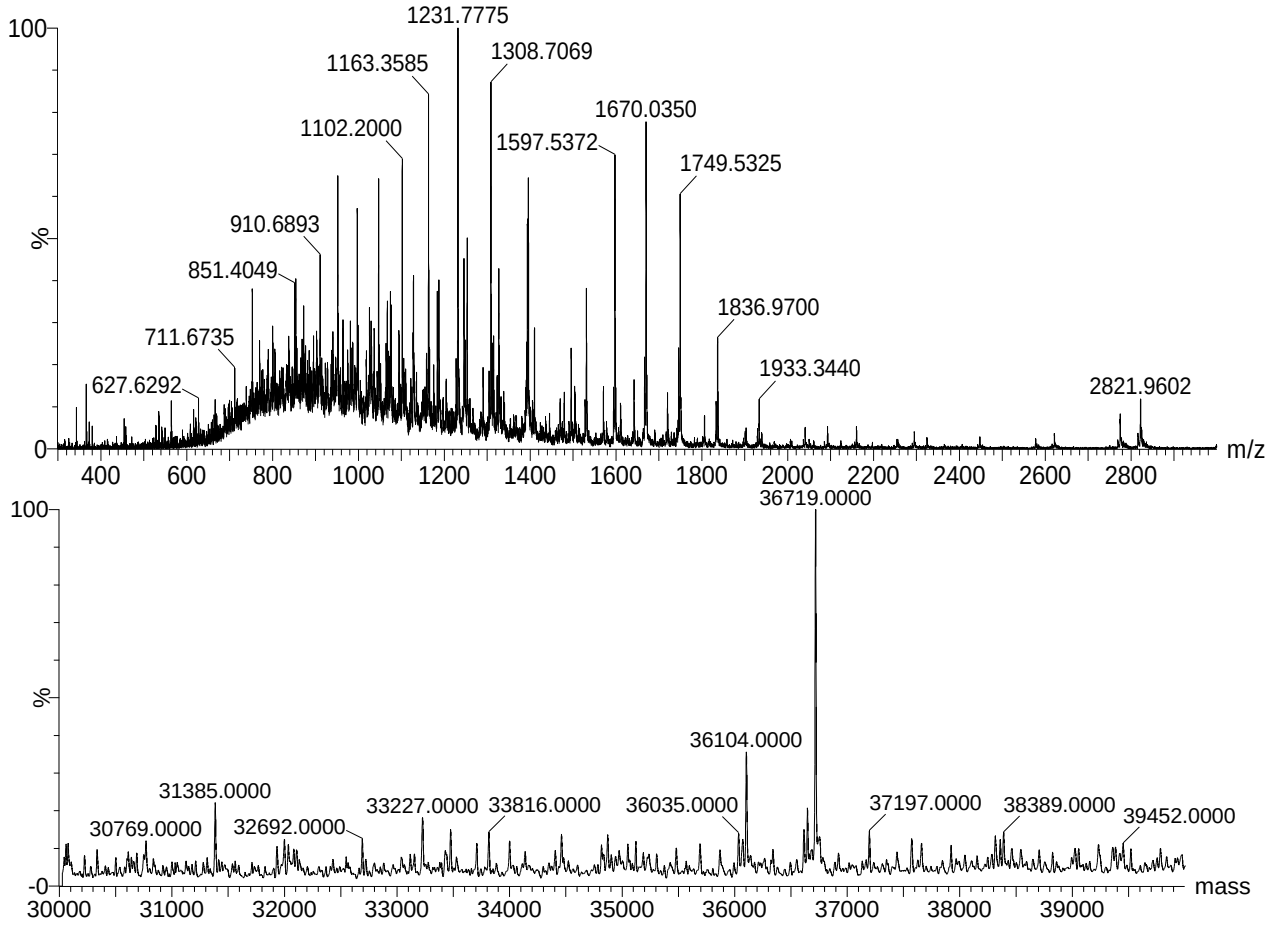

Figure 4.8 Electrospray ionization mass spectrum in the positive mode of purified HmuT Y272A. Bottom panel: The deconvoluted region shows HmuT Y272A at both 36,104 Da and 36,719 Da, indicative of a mixture of apo- and holoprotein, respectively. The predicted mass of the apoprotein is 36,103 Da and 36,719 Da. The sample was prepared in 50 mM ammonium acetate at neutral pH.

The ESI mass spectrum for R237A gave two clean peaks at 36,242 Da and 36,860 Da indicative of apo and holoproteins, respectively (Figure 4.9). The expected molecular weight of the apoprotein was 36,240 Da and the holoprotein is 36,856 Da. Two charged envelopes were observed ranging from +24 to +20 and from +14 to +11 with the latter being the predominant envelope based on peak intensity.

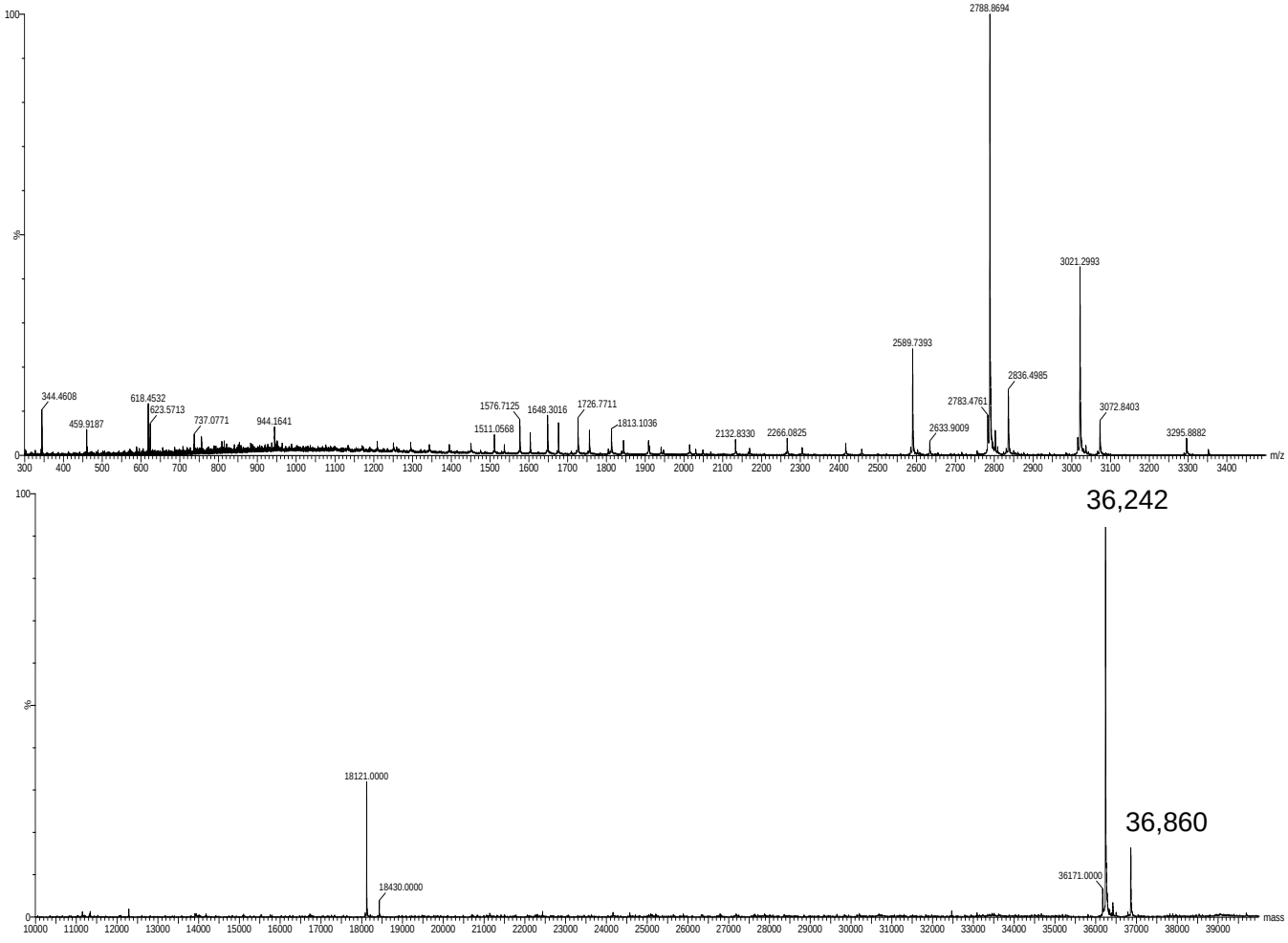

Figure 4.9 Electrospray ionization mass spectrum in the positive mode of purified HmuT R237A. Bottom panel: The deconvoluted region shows HmuT R237A at both 36,242 Da and 36,860 Da, indicative of a mixture of apo- and holoprotein, respectively. The predicted mass of the apoprotein is 36,240 Da and 36,856 Da. The sample was prepared in 50 mM ammonium acetate at neutral pH.

4.2.4 pH titrations of as-isolated and reconstituted HmuT Y235A

Previous work from our group showed as-isolated HmuT Y235A to be sensitive to pH, while WT HmuT is not affected by pH *(1)*. To probe the pH effect on Y235A, UV-visible absorption titrations were performed on both as-isolated and reconstituted Y235A.

As-isolated Y235A was titrated with HCl over a pH range of 4 – 7. Only data from pH 5 – 7 were used to determine the pK_a due to protein precipitation around pH 4.8; the pI of Y235A is at 4.7. The data were fit to a one-state pK_a equation and gave a pK_a of 6.3 ± 0.1 (Figure 4.10).

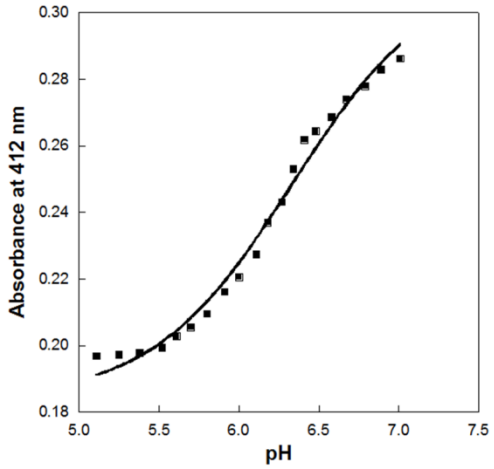

Figure 4.10 pH titration fit of as-isolated Y235A from pH 4 – 7. The data were fit using a one-state pKa equation. The pKa is 6.3 ± 0.1.

A second titration from pH 7 – 9.5 was also performed. UV spectral data indicate heme loss as shown by the increase in the 280 and 380 nm bands and a slight decrease in the Soret absorbance (Figure 4.11). The data were not fit.

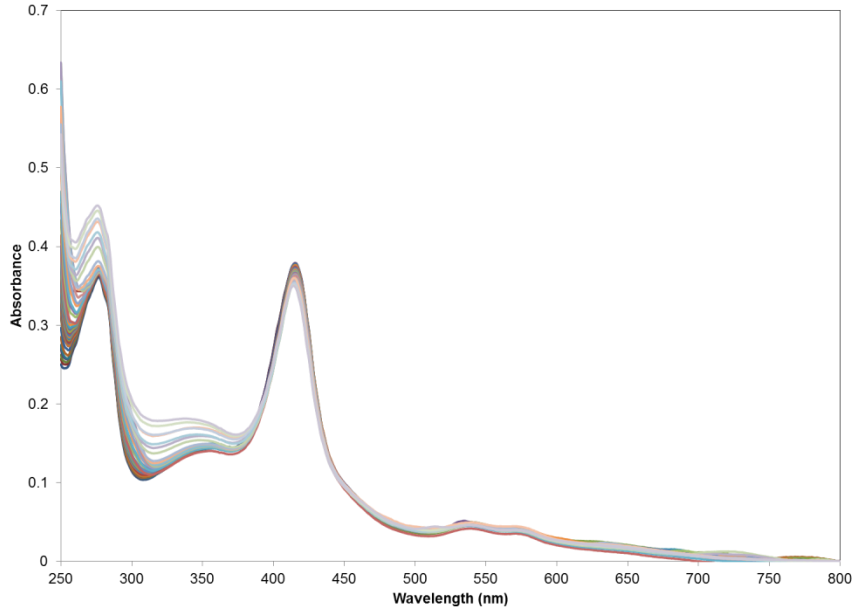

Figure 4.11 UV absorbance spectra of as-isolated HmuT Y235A pH titration from pH 7 – 9.5. Minimal change at the Soret and increase in the 280 and 380 nm bands indicate heme loss from the protein. The data were not fit.

pH effects of reconstituted Y235A were also investigated from pH 7 – 11 (Figure 4.12). As the absorbance of the heme at 412 nm went down, the absorbance at 380 nm increased, indicative of heme loss from the protein. The data were followed at 412 nm and fit to a two-state pK_a equation with an appearance of a two-state pK_a transition and were fitted to give a pK_{a1} = 7.8 ± 0.1 and a pK_{a2} = 10.6 ± 0.1.

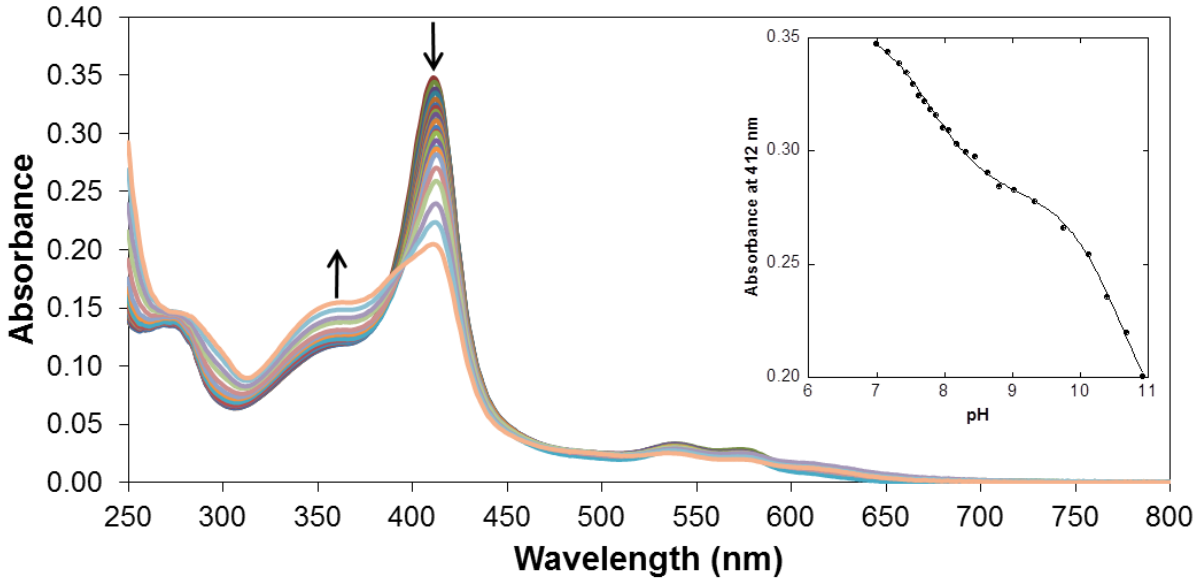

Figure 4.12 UV-visible absorption pH titration of reconstituted Y235A from pH 7 – 11 (accounted for dilution). Arrows indicate the change in absorbance as the pH was increased. Inset: The data were fit best to a two-state pK_a model. The pK_a's are 7.8 ± 0.1 and 10.6 ± 0.1.

4.2.5 Chemical unfolding studies of HmuT

WT HmuT was incubated in a series of GdnCl concentrations to determine the approximate $D_{1/2}$ of the protein. The change in absorbance was followed at 406 nm and fit to a two-state protein denaturation model with a $D_{1/2}$ of 2.0 ± 0.1 M (Figure 4.13).

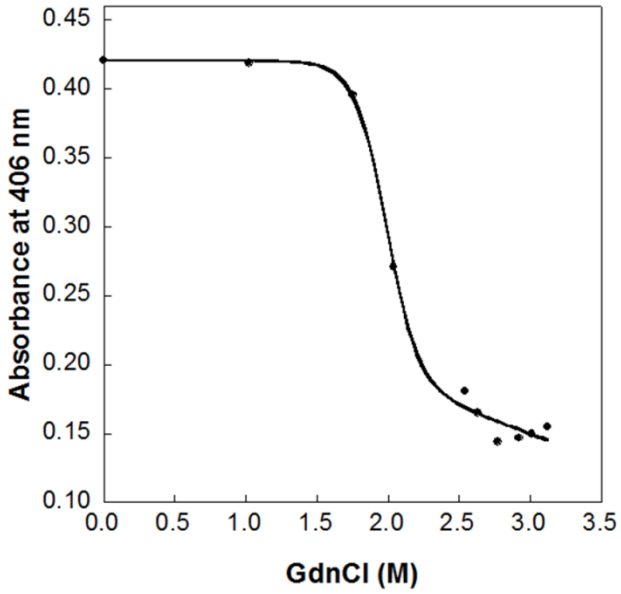

Figure 4.13 WT HmuT GdnCl denaturation curve fit to a two-state protein unfolding model. Samples were in 50 mM Tris-Cl, pH 7.0. The D1/2 is 2.0 ± 0.1 M.

Based on the $D_{1/2}$ study, WT HmuT was incubated in 2.0 M GdnCl and monitored at 406 nm via UV-visible absorption spectroscopy for 24 h. Change in absorbance at the Soret ceased after 10 h. The unfolding curve was fit to a first-order reaction which gave an unfolding rate of 0.011 ± 0.001 min^{-1} (Figure 4.14). Fitting to a two sequential rate constant equation gave unreasonable extinction coefficients.

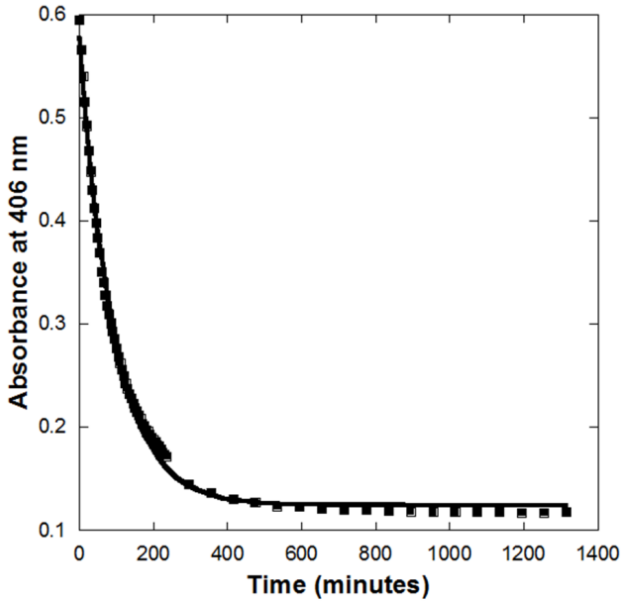

Figure 4.14 Time-scale unfolding curve for WT HmuT in 2.0 M GdnCl for 24 h. The data were fit to a first-order reaction scheme giving an unfolding fast phase rate of 0.011± 0.001 min^{-1}. The sample was in 50 mM Tris-Cl, pH 7.0.

Both H136A and Y235A HmuT were also incubated at 1.0 M and 1.5 M GdnCl (estimated $D_{1/2}$ concentrations), respectively, and followed at the Soret over time. After 10 h, H136A was still unfolding while Y235A was completely unfolded. The data sets were fit to a first-order unfolding reaction with H136A unfolding at 0.004 ± 0.001 min^{-1} and Y235A unfolding at 0.007 ± 0.001 min^{-1} (Figures 4.15 and 4.16, respectively).

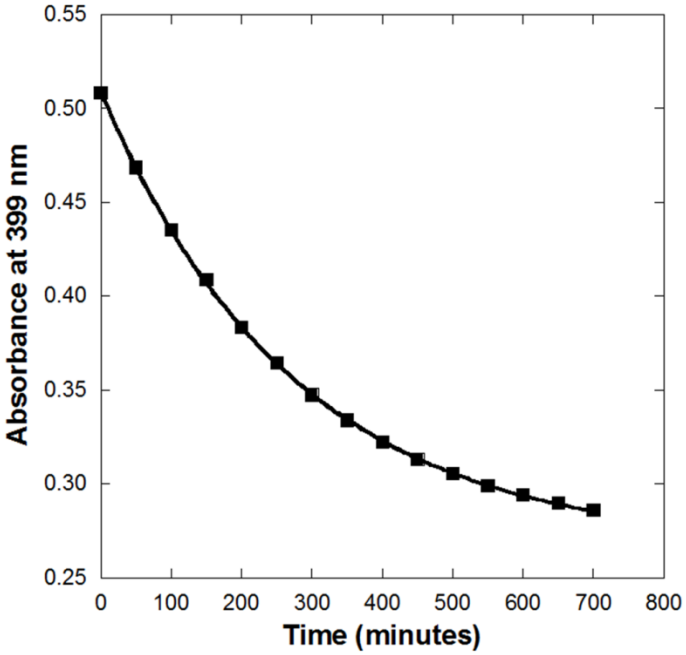

Figure 4.15 Time-scale unfolding curve for H136A HmuT in 1.5 M GdnCl. The data were fit to a first-order unfolding reaction scheme giving an unfolding rate of 0.004 ± 0.001 min^{-1}. The sample was in 50 mM Tris-Cl, pH 7.0.

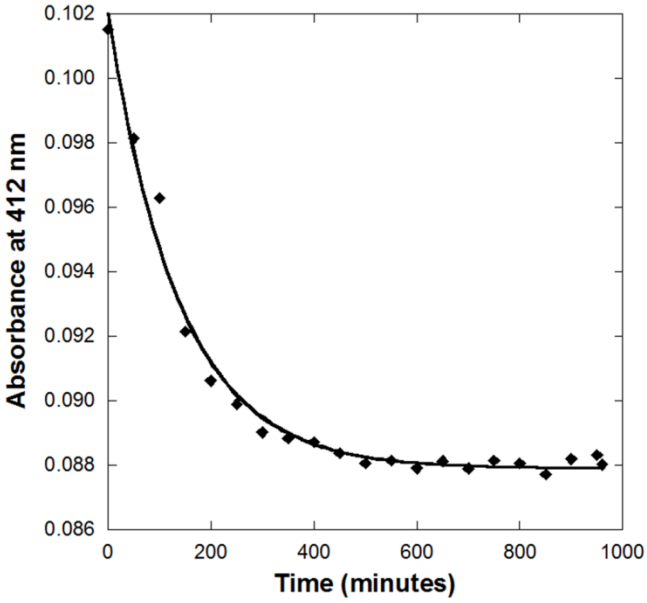

Figure 4.16 Time-scale unfolding curve for Y235A HmuT in 1.0 M GdnCl. The data were fit to a first-order unfolding reaction scheme giving an unfolding rate of 0.007 ± 0.001 min^{-1}. The sample was in 50 mM Tris-Cl, pH 7.0.

4.3 Discussion

4.3.1 Circular dichroism of HmuT and mutants

A series of tyrosine mutants were created to investigate the potential roles these residues may contribute to HmuT heme binding (see Chapter 3). Firstly, Y272 was mutated to an alanine to assess if this residue was acting as a hydrogen-bonding partner to the axial Y235. Y272A exhibited similar heme loading as the WT, but gave an altered α,β-region compared to the WT. A sequence alignment of HmuT with a protein homolog of known structure, *Y. pestis* HmuT, shows *Yp*HmuT to have an Arg residue in the same position as Y272 *(8)*. This arginine (R199) has been shown to form a van der Waals interaction with the heme propionate. In addition, Y200 in *Yp*HmuT forms a hydrogen-bond with the other heme propionate. Based on this comparison, it could be the case that *Cd*HmuT Y272 is participating in one of these types of interactions.

Secondly, Y349A and Y349F mutants were constructed due to conservation across many *Corynebacterium* species although homology modeling predicted this residue to not be in proximity of the heme binding pocket. Both Y349 mutants gave similar UV-spectral signatures compared to the WT, but were much less heme loaded than the WT protein (< 20%). Therefore, CD spectroscopy was utilized to investigate protein secondary structural changes due to amino acid mutation.

The CD spectral bands around 190, 210, and 222 nm in Figure EBIII35 were indicative of α-helical content in WT HmuT and mutants *(9)*. Changes in relative intensities at these wavelengths differed upon mutation. For example, Y349A exhibited the most change in secondary structural content with the least pronounced 222 nm band among all of the samples.

Similarly, the 210 nm band shifted to about 208 nm and increased in intensity compared to the WT.

Y349A is minimally heme loaded and a large presence of apoprotein could be the result of the observed spectral shift. Shifts in CD spectra due to secondary structural alteration as a result of heme removal (or minimal heme loading) have been seen in other heme proteins. The data are limited and the change in the intensities of the 210 nm versus 222 nm bands in regards to heme loss varies. For example, holo- and apo-cytochrome b_{562} from *E. coli* gave similar CD intensities at both 210 and 222 nm *(10)*. *Serratia marcescens* HasA CD spectra showed a more pronounced 222 nm, compared to the 210 nm, for both holo and apo forms of the protein *(11)*. Alternatively, both *S. pyogenes* SiaA and FixLH from *Bradyrhizobium japonicum* had a more pronounced 210 nm band for the apoprotein compared to the holoprotein *(12, 13)*, as seen in all of the HmuT mutants in Figure EBIII75. It should also be noted that CD experiments were carried out on samples which varied in relative amounts of heme-loading. If minimal heme-loading results in alteration of CD spectra, it is not surprising that Y349A and Y349F experience the most spectral change in comparison to the WT as they are the least heme-loaded of all the samples.

CD data were deconvoluted using DichroWeb to estimate the relative amounts of α-helical content, although these results have not always been reliable in our hands *(2)*. The data were analyzed using both the CONTIN and SELCON3 analysis programs, both using two reference protein sets. Percentage estimations for secondary structural content were obtained by an average of the two analysis programs. Comparison of the estimations in Table EBIII75 to the CD spectra indicated discrepancies between the deconvolution and the raw data. For example, Y349A is predicted to have 78% α-helical content while Y349F is predicted to have 45%, yet the

CD data for Y349A is the least similar to WT, which is predicted to have 91% α-helical content. Additionally, Y272A is predicted to have the same amount of α-helical content as the WT, yet the CD spectra are different between the two samples.

4.3.2 ESI-MS of HmuT mutants

In all cases except for H136A and Y235A, the ESI-MS of HmuT mutants detected both the presence of apo and holoproteins. H136A did not give holoprotein as formic acid was used to increase the signal to noise and resulted in solely apoprotein detection. Y235A under all conditions, either water or acetic acid, resulted in the detection of apoprotein as the heme loading of this protein is minimal and removal of the heme axial ligand diminishes the ability of the protein to bind heme effectively (see Chapter 3).

For all samples in which both apo and holoproteins were detected, two charged envelopes were also observed in the lower m/z region. It has been shown that charged envelopes can vary based on the extent of protein folding *(14)*. Generally, charged envelopes with smaller charge distributions are indicative of a more folded protein while larger charge distributions can be a result of a partially unfolded protein. Heme removal alters the secondary structural content of proteins and has been shown to also alter protein conformation and fold *(15)*. HmuT and mutants are all mixtures of apo and holoprotein which could lead to multiple charged envelopes which vary in the extent of distribution. For example, R237A in Figure 4.9 shows two envelopes at +24 to +20 and from +14 to +11, with the first being attributed to the apoprotein and the latter to the holoprotein.

Mass spectrometry was also performed on both as-isolated and reconstituted M292A. Both samples indicated the presence of apo and holoprotein, but different masses for each protein species in the sample were obtained. For example, the as-isolated apo-M292A gives a

mass at 36,268 Da (the correct mass for the protein), while the reconstituted apo-M292A gives a mass at 36,185 Da; a difference of 83 Da between the two apo-M292A samples. A comparison of Figure 4.6 and Figure 4.7 showed a difference in spectral quality. Figure 4.7 was a noisy spectrum as indicated by the increasing baseline in the second panel of the figure. Additionally, in the expanded region of Figure 4.7, multiple peaks are observed around 36,185 Da, rather than one single peak. This could be due to the fact that the reconstituted sample data were prepared in only water and not much care was taken into removing residual salts which could affect spectral signal to noise. Alternatively, the as-isolated sample was prepared by dialysis in a series of fresh ammonium acetate solutions over a week-long period and resulted in the proper mass expected for apo-M292A with minimal signal to noise issues.

4.3.3 Protein reconstitution and heme loading

Our group has previously shown the potential disadvantages in utilizing a reconstitution method as a means of increasing protein heme loading (Chapter 3). Although as-isolated and reconstituted samples may appear similar in the UV spectra, as seen for Y235A and M292A HmuT (Figures 4.2 and 4.3), the samples can have different spectral signatures in resonance Raman spectroscopy. This could indicate the reconstituted heme is bound to the pocket in a different orientation than seen in the as-isolated protein. Differences in heme orientations, either in the as-isolated or reconstituted form, have previously been seen in other *b*-type heme proteins, including by our group [Chapter 3 and *(13)*]. As a result of this finding, all published works were performed on as-isolated proteins, unless otherwise noted.

The method in which to prepare proteins for reconstitution requires a large reduction in pH and the addition of an organic solvent to effectively unfold the protein and remove heme from the pocket. Some hemoproteins are able to withstand this technique, as seen for HmuT and

mutants, while other proteins precipitate out of solution, such as *S. pyogenes* SiaA (see Chapter 6). As-isolated Y235A is only about ~20% heme loaded and reconstitution resulted in a fully heme-loaded protein with minimal spectral changes between the two samples (Figure 4.2). M292A did not respond as well to reconstitution as indicated by differences in as-isolated versus reconstituted UV spectra and the large shoulder at 380 nm for the reconstituted sample (Figure 4.3).

Alternative methods to increase heme loading of proteins involve supplementing expression media such as adding the heme precursor δ-aminolevulinic acid (ALA) to promote the production of holoprotein *(16, 17)*. ALA synthesis is the first committed step in heme synthesis *(18)*. Glycine and succinyl CoA condense to form ALA with CO_2 and CoA released as byproducts. Some protocols suggest adding ferrous ammonium sulfate, in addition to ALA *(16)*. Previous attempts to make this work in our systems showed no appreciable difference between proteins exposed to ALA compared to those which were not.

4.3.4 pH titrations of as-isolated and reconstituted Y235A

Both as-isolated and reconstituted Y235A were monitored with UV-visible absorption spectroscopy as a function of pH. Previous studies on as-isolated WT HmuT showed no spectral changes over a pH range of 6 – 11 *(1)*. MCD studies of as-isolated Y235A at acidic and basic pH environments were indicative of water binding *trans* to the axial histidine. A comparison of pH titrations between the as-isolated and reconstituted Y235A samples gave different results and further indicated reconstitution alters heme orientation or binding in the pocket in some fashion.

Titration of the as-isolated Y235A from pH 4 – 7 gave a pK_a of 6.3 ± 0.1 (Figure 4.10). To our knowledge, this is the lowest known pK_a for a heme protein with a bound water *trans* to a histidine (see Chapter 2). Additional studies indicated an arginine in the pocket (R237) which

could be acting as a hydrogen-bonding partner to the axial tyrosine *(1)*. This low pK_a value would ensure R237 is able to H-bond with the hydroxide in the Y235A form of HmuT. As-isolated Y235A was also monitored over a pH range of 7 – 9.5. Minimal changes were seen at the Soret and the data were not fit as the protein started to precipitate out of solution.

A similar titration was performed on reconstituted Y235A, but from pH 7 – 11. The data were fit and gave two pK_a values at 7.8 ± 0.1 and 10.6 ± 0.1. Unlike the as-isolated Y235A, the reconstituted Y235A did not precipitate out of solution as the pH was increased above a pH of 9.5.

Previous resonance Raman pH studies on both as-isolated and reconstituted Y235A indicated at high pH the protein is a mixture of high-spin and low-spin and at low pH is all converted to high-spin *(1)*. At pH 7 the protein is a partial mixture of high-spin and low-spin heme, indicated by the ratio of the ν_3 high-spin peak at 1473 cm^{-1} to the low-spin peak 1501 cm^{-1}. As the pH increases to 10, the low-spin ν_3 marker at 1501 cm^{-1} continues to increase. The first pK_a around 7.8 in reconstituted Y235A could be due to this shift in spin-states. This UV spectral shift between pH 7 and 10 was observed in both the Rodgers and Dixon labs.

The second pK_a at 10.6 could be due to the deprotonation of R237 which is proposed to H-bond to the axial Y235 ligand and is H-bonded to water in the Y235A mutant. Removal of this H-bonding partner could result in a destabilization of the heme and may be why heme loss is observed in the UV as this transition occurs. The titration could not be completed because the pH electrode utilized was not equipped to go above pH 11.

4.3.5 Chemical unfolding studies of HmuT

A GdnCl unfolding titration of WT HmuT indicated the protein to have a $D_{1/2}$ of ≈ 2 M. As there are only few points along the curve, the titration would need to be repeated. Chemical

unfolding $D_{1/2}$ studies of other *b*-type heme proteins are limited. The hemophore HasA from *S. marcescens* unfolds at 2.7 ± 0.2 M GdnCl *(19)* and also utilizes a His/Tyr heme binding motif. Rat microsomal outer membrane cytochrome b_5 and *S. pyogenes* SiaA are His/Met heme proteins which unfold at 2.6 ± 0.3 M GdnCl *(20)* and 3.1 ± 0.1 M *(13)*, respectively. Cytochrome b_{562} from *E. coli*, also His/Met, unfolds at 2.2 ± 0.2 M GdnCl *(21)*. These comparisons put HmuT in line with other *b*-type heme proteins in regards to protein unfolding and indicate heme axial ligation does not necessarily dictate the ease of protein unfolding.

Kinetic unfolding data of WT HmuT was fit to a first-order reaction giving a half-life of about one hour. Attempts to fit the data to a biphasic first-order reaction and the sum of two-term exponential functions were unsuccessful. Kinetic unfolding studies of *b*-type heme proteins are also limited. In the case of *S. pyogenes* SiaA, our group showed this protein slowly unfolded in two phases attributed to differences in heme orientation in the pocket *(13)*. The half-lives of the fast and slow phases ranged from 1 – 3 and 8 – 53 h, respectively. This type of unfolding has also been seen in other proteins such as horse heart myoglobin and cytochrome b_5 although these proteins unfolded with half-lives of seconds and less than five minutes for the fast and slow phases, respectively *(22, 23)*. Cytochrome b_{562} from *E. coli* also unfolded with one phase, with the unfolding completed in seconds *(24)*. In contrast, horseradish peroxidase and soybean peroxidase unfold with one phase, but the unfolding is very slow *(25)*.

Removal of either HmuT axial ligand altered the half-lives of HmuT unfolding. HmuT H136A and Y235A gave half-lives of 3 h and 1.6 h, respectively. The half-life of unfolding for the WT was 1 h which is less than the axial ligand mutants. One explanation is that the $D_{1/2}$ values of H136A and Y235A were not accurately determined since the GdnCl concentrations used for the mutant unfolding experiments were approximations. In order to have a complete

story on the effects which heme axial ligand removal has on HmuT unfolding, it would be best to have multiple unfolding profiles for the WT, H136A, and Y235A at different GdnCl concentrations (above and below the $D_{1/2}$). Those rates could then be plotted and extrapolated back to 0 M GdnCl.

4.4 References

[1] Draganova, E. B., Akbas, N., Adrian, S. A., Lukat-Rodgers, G. S., Collins, D. P., Dawson, J. H., Allen, C. E., Schmitt, M. P., Rodgers, K. R., and Dixon, D. W. (2015) Heme binding by *Corynebacterium diphtheriae* HmuT: Function and heme environment. *Biochemistry 54*, 6598-6609.

[2] Whitmore, L., and Wallace, B. A. (2004) DICHROWEB, an online server for protein secondary structure analyses from circular dichroism spectroscopic data. *Nucleic Acids Res. 32*, W668-W673.

[3] Teale, F. W. (1959) Cleavage of the heme protein by acid methyl ethyl ketone. *Biochim. Biophys. Acta 35*, 543.

[4] Collier, G. S., Pratt, J. M., De Wet, C. R., and Tshabalala, C. F. (1979) Studies on haemin in dimethyl sulphoxide/water mixtures. *Biochem. J 179*, 281-289.

[5] Pace, C. N., and Scholtz, J. M. (1997) Measuring the conformational stability of a protein, In *Protein Structure: A Practical Approach* (Creighton, T., Ed.) 2nd ed., pp 299-321, Oxford University Press, Oxford.

[6] Wu, Z., Gao, W., Phelps, M. A., Wu, D., Miller, D. D., and Dalton, J. T. (2004) Favorable effects of weak acids on negative-ion electrospray ionization mass spectrometry. *Anal. Chem. 76*, 839-847.

[7] Mawhinney, D. B., Stanelle, R. D., Hamelin, E. I., and Kobelski, R. J. (2007) Enhancing the response of alkyl methylphosphonic acids in negative electrospray ionization liquid chromatography tandem mass spectrometry by post-column addition of organic solvents. *J. Am. Soc. Mass Spectrom. 18*, 1821-1826.

[8] Mattle, D., Zeltina, A., Woo, J. S., Goetz, B. A., and Locher, K. P. (2010) Two stacked heme molecules in the binding pocket of the periplasmic heme-binding protein HmuT from *Yersinia pestis*. *J. Mol. Biol. 404*, 220-231.

[9] Kelly, S. M., Jess, T. J., and Price, N. C. (2005) How to study proteins by circular dichroism. *Biochimica et Biophysica Acta-Proteins and Proteomics 1751*, 119-139.

[10] Feng, Y. Q., and Sligar, S. G. (1991) Effect of heme binding on the structure and stability of *Escherichia coli* apocytochrome b_{562}. *Biochemistry 30,* 10150-10155.

[11] Izadi, N., Henry, Y., Haladjian, J., Goldberg, M. E., Wandersman, C., Delepierre, M., and Lecroisey, A. (1997) Purification and characterization of an extracellular heme-binding protein, HasA, involved in heme iron acquisition. *Biochemistry 36,* 7050-7057.

[12] Landfried, D. A., Vuletich, D. A., Pond, M. P., and Lecomte, J. T. J. (2007) Structural and thermodynamic consequences of *b* heme binding for monomeric apoglobins and other apoproteins. *Gene 398,* 12-28.

[13] Akbas, N., Draganova, E. B., Block, D. R., Sook, B. R., Chan, Y. F., Zhuo, J., Eichenbaum, Z., Rodgers, K. R., and Dixon, D. W. (2015) Heme-bound SiaA from *Streptococcus pyogenes*: Effects of mutations and oxidation state on protein stability. *J. Inorg. Biochem.*

[14] Tiedemann, M. T., and Stillman, M. J. (2012) Heme binding to the IsdE(M78A; H229A) double mutant: Challenging unidirectional heme transfer in the iron-regulated surface determinant protein heme transfer pathway of *Staphylococcus aureus*. *J. Biol. Inorg. Chem. 17,* 995-1007.

[15] Smith, L. J., Kahraman, A., and Thornton, J. M. (2010) Heme proteins - Diversity in structural characteristics, function, and folding. *Proteins: Struct. Funct. Bioinform. 78,* 2349-2368.

[16] Graves, P. E., Henderson, D. P., Horstman, M. J., Solomon, B. J., and Olson, J. S. (2008) Enhancing stability and expression of recombinant human hemoglobin in *E-coli*: Progress in the development of a recombinant HBOC source. *Biochim. Biophys. Acta 1784,* 1471-1479.

[17] Sudhamsu, J., Kabir, M., Airola, M. V., Patel, B. A., Yeh, S. R., Rousseau, D. L., and Crane, B. R. (2010) Co-expression of ferrochelatase allows for complete heme incorporation into recombinant proteins produced in *E. coli*. *Protein Expr. Purif. 73,* 78-82.

[18] Heinemann, I. U., Jahn, M., and Jahn, D. (2008) The biochemistry of heme biosynthesis. *Arch. Biochem. Biophys. 474,* 238-251.

[19] Wolff, N., Sapriel, G., Bodenreider, C., Chaffotte, A., and Delepelaire, P. (2003) Antifolding activity of the SecB chaperone is essential for secretion of HasA, a quickly folding ABC pathway substrate. *J. Biol. Chem. 278,* 38247-38253.

[20] Arnesano, F., Banci, L., Bertini, I., Faraone-Mennella, J., Rosato, A., Barker, P. D., and Fersht, A. R. (1999) The solution structure of oxidized *Escherichia coli* cytochrome *b*(562). *Biochemistry 38*, 8657-8670.

[21] Arnesano, F., Banci, L., Bertini, I., Ciofi-Baffoni, S., Woodyear, T. D., Johnson, C. M., and Barker, P. D. (2000) Structural consequences of *b*- to *c*-type heme conversion in oxidized *Escherichia coli* cytochrome b_{562}. *Biochemistry 39*, 1499-1514.

[22] Moczygemba, C., Guidry, J., and Wittung-Stafshede, P. (2000) Heme orientation affects holo-myoglobin folding and unfolding kinetics. *FEBS Lett. 470*, 203-206.

[23] Manyusa, S., Mortuza, G., and Whitford, D. (1999) Analysis of folding and unfolding reactions of cytochrome *b*(5). *Biochemistry 38*, 14352-14362.

[24] Garcia, P., Bruix, M., Rico, M., Ciofi-Baffoni, S., Banci, L., Shastry, M. C. R., Roder, H., Woodyear, T. D., Johnson, C. M., Fersht, A. R., and Barker, P. D. (2005) Effects of heme on the structure of the denatured state and folding kinetics of cytochrome b_{562}. *J. Mol. Biol 346*, 331-344.

[25] Kamal, J., and Behere, D. V. (2008) Kinetic stabilities of soybean and horseradish peroxidases. *Biochem. Eng. J. 38*, 110-114.

[26] Culbertson, D. S., and Olson, J. S. (2010) Role of heme in the unfolding and assembly of myoglobin. *Biochemistry 49*, 6052-6063.

5 HEME-BOUND SIAA FROM *STREPTOCOCCUS PYOGENES*: EFFECTS OF MUTATIONS AND OXIDATION STATE ON PROTEIN STABILITY

This chapter is verbatim in press for a special issue in Akbas, N., Draganova, E. B., Block, D. R., Sook, B. R., Chan, Y. F., Zhuo, J., Eichenbaum, Z., Rodgers, K. R., and Dixon, D. W. (2015), *Journal of Inorganic Biochemistry*, http://dx.doi.org/10.1016/j.jinorgbio.2015.10.016. The expression, purification, circular dichroism studies and chemical unfolding experiments were performed by E. B. Draganova at Georgia State University.

5.1 Abstract

The protein SiaA (HtsA) is part of a heme uptake pathway in *Streptococcus pyogenes*. In this report, we present the heme binding of the alanine mutants of the axial histidine (H229A) and methionine (M79A) ligands, as well as a lysine (K61A) and cysteine (C58A) located near the heme propionates (based on homology modeling) and a control mutant (C47A). pH titrations gave pK_a values ranging from 9.0 to 9.5, close to the value of 9.7 for WT SiaA. Resonance Raman spectra of the mutants suggested that the ferric heme environment may be distinct from the wild-type; spectra of the ferrous states were similar. The midpoint reduction potential of the K61A mutant was determined by spectroelectrochemical titration to be 61 ± 3 mV vs. SHE, similar to the wild-type protein (68 ± 3 mV). The addition of guanidine hydrochloride showed two processes for protein denaturation, consistent with heme loss from protein forms differing by the orientation of the heme in the binding pocket (the half-life for the slower process was one to three days). The ease of protein unfolding was related to the strength of interaction of the residues with the heme. We hypothesize that kinetically facile but only partial unfolding, followed by a very slow approach to the completely unfolded state, may be a fundamental attribute of heme trafficking proteins. Small motions to release/transfer the heme accompanied by resistance to extensive unfolding may preserve the three dimensional form of the protein for further uptake and release.

5.2 Introduction

Iron is a key nutrient for many bacteria [1]. Iron(III), however, has very low aqueous solubility [2,3], making strategies that do not involve direct uptake of uncomplexed iron imperative. In the human body, about 95% of the iron occurs in the heme cofactor [4,5], which

serves as a significant source of iron for bacterial pathogens. The most common protein source of heme iron in human bacterial infections is methemoglobin [6].

Heme uptake is often key in the virulence of pathogenic bacteria [7]. Gram-positive and Gram-negative bacteria have evolved similar strategies for acquiring heme [1,8-17]. All pathways studied to date involve a series of proteins that transfer the heme from the exterior milieu into the cell interior. Recent reviews have focused on the structures of heme transport proteins [5,18,19] and pathways in specific bacteria including *Bacillus anthracis* [20] and *Staphylococcus aureus* [21-24].

A large number of bacteria have been studied to determine their method of obtaining heme; some acquire heme from their environment, others have a biosynthetic pathway to produce the heme, and some use both approaches [25]. Using bioinformatics techniques, Cavallaro et al. found that approximately 5% of the species rely only on heme uptake, 30% use biosynthesis only, 50% use both pathways, and 15% use neither. Those which use only heme uptake are of particular interest because absent a biosynthetic pathway, they may be susceptible to iron starvation via interruptions in external heme uptake. Interference with heme uptake might reduce the virulence of infections with these organisms. Cavallaro et al. have noted that heme uptake seems to be related to pathogenicity in Gram-positive bacteria, with approximately 80% of bacteria that acquire heme being pathogenic [25].

Streptococcus pyogenes is one of the few species of bacteria that can only obtain heme from its environment. *S. pyogenes*, also known as Group A streptococcus (GAS), is a pathogenic Gram-positive bacterium that causes a variety of infections [26,27]. Iron is an essential nutrient for *S. pyogenes* and a number of heme-containing sources can support *in vitro* growth of this organism, including hemoglobin, the haptoglobin-hemoglobin complex, myoglobin, heme-

albumin, and catalase [28]. The ability to obtain iron has been shown to affect the virulence of this pathogen as observed in mutants of *S. pyogenes* which are defective in heme uptake [29]; mutations resulted in attenuated virulence in animal models. *S. pyogenes* is increasingly resistant to macrolide antibiotics [30-33], potentially posing significant risks for infected populations.

In *S. pyogenes*, one pathway for heme import employs a dedicated ATP binding cassette (Figure 5.1). This cassette has been termed the streptococcal iron acquisition or SiaABC system [34] and is also known as HtsABC (heme transport system) [35].

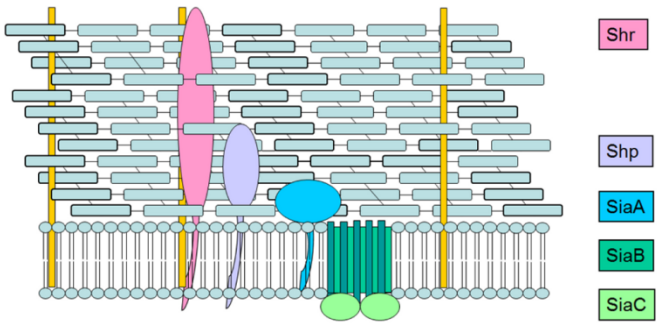

Figure 5.1 Overview of the S. pyogenes Sia/Hts heme uptake pathway.

In this ABC transporter, SiaA is the membrane-anchored heme binding protein that acquires heme and transfers it to SiaB which in turn carries the heme across the lipid bilayer. In this process, energy is provided from ATP hydrolysis by SiaC, which is located on the inner side of the membrane. The SiaABC heme transport system is part of a conserved ten-gene cluster [34]. The two genes upstream express Shr [34,36] and Shp [37,38]. Shr receives heme from hemoglobin [39,40] and transfers it to Shp [36]. Shp, which has two axial methionine ligands [37], transfers heme to SiaA [41] with rate constants that are similar in the oxidized and reduced forms [42-44]. Our previous biophysical studies on wild-type (WT) SiaA showed the heme was six-coordinate (6c) and low-spin (LS) in both the ferric and ferrous oxidation states of the protein with methionine and histidine as the axial ligands [45]; further spectroscopic analyses have

confirmed these findings [46]. Homology modeling (Figure 5.2), with IsdE from *Staphylococcus aureus* [48] as the closest homologous protein, indicated that the specific axial ligand residues were likely to be M79 and H229; site-directed mutagenesis studies have verified this [46,47].

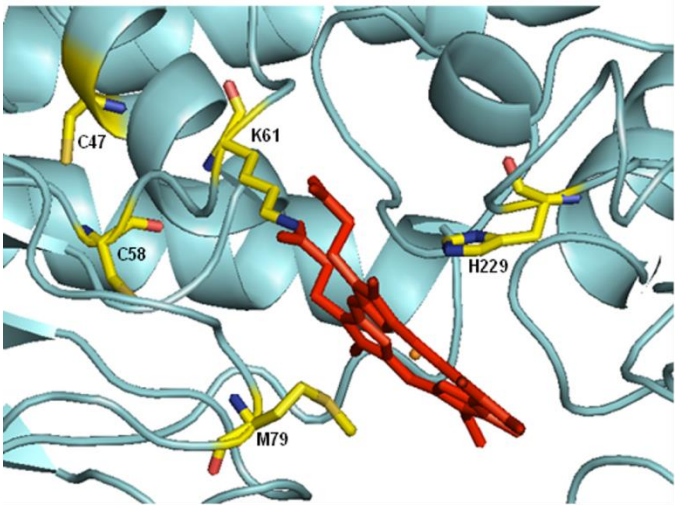

Figure 5.2 Homology model of SiaA. Shown are the locations of C47, C58, K61, M79, and H229.

Elucidation of the factors controlling heme binding and release steps along heme acquisition pathways are benefiting from biophysical studies of the proteins. The main controlling factors emerging from this work are the nature of the axial ligand(s), electrostatic interactions between the protein and the heme, through its propionates and the iron center, and hydrophobic interactions between the protein and the porphyrin face [5,49-53]. Herein, we describe the factors affecting the stabilities of heme-bound states of SiaA and selected mutants. We report results on two new mutants, C58A and K61A, as well as a control mutant, C47A, predicted to be at some distance from the heme. Homology modeling suggests that C58 is near the heme propionates and K61 is close to the propionate that extends from the heme binding pocket. In addition, we expand on recent studies of M79A and H229A [46,47]. The reduction potentials of the mutants of SiaA have been determined by spectroelectrochemical titration and

compared with that of WT SiaA. Structural aspects of the heme pocket, states of the bound heme, and heme protein interactions have been probed by resonance Raman (rR) spectroscopy [16,54-56].

Unfolding studies, using guanidine hydrochloride (GdnHCl) as a denaturant, have been used here to probe the influence of residues near the heme on the relative stabilities of the heme-bound states of WT SiaA and its aforementioned mutants. Unfolding studies of heme protein mutants have been used to gain information on the contributions of specific residues to heme binding in other *b*-type heme proteins. For example, the roles of various residues in myoglobin were probed by unfolding specific mutants [57]. Similar studies have also been performed on cytochrome b_{562} [58,59] and cytochrome b_5 [60,61]. These types of studies provide insight into the overall stability of the protein in which specific heme pocket residues, predicted to interact with the heme, are probed. In the case of heme binding and transport proteins, we anticipate that disrupting these interactions by unfolding can lead to a better understanding of the important residues involved in the heme uptake and release mechanism of the protein.

5.3 Experimental

5.3.1 Homology modeling

The homology model of SiaA was built by using I-TASSER, a secondary structure prediction program [62]. IsdE from *Staphylococcus aureus* [48] was the closest homologous protein (PSI-BLAST results for SiaA show 45% identity to IsdE with 69% positives); the root mean square difference (RMSD) between the model and IsdE was 1.35 Å. The model was visualized using PyMOL [63].

5.3.2 Materials

E. coli strain Top10 competent cells, ShuAf, ShuAr primers and Top10/pSiaA-His cells were made as described previously [45]. The QuikChange II Site-Directed Mutagenesis Kit was from Stratagene (La Jolla, CA). The Plasmid Mini Kit, Taq PCR Master Mix Kit, and QIAquick® Gel Extraction Kit were from QIAGEN (Valencia, CA). Oligonucleotides for site-directed mutagenesis were synthesized by Invitrogen (Carlsbad, CA). L-arabinose was manufactured by Acros Organic (Gell, Belgium).

5.3.3 Preparation of plasmids

Site-directed mutagenesis was used to construct recombinant SiaA proteins with C47A, C58A, K61A, M79A or H229A amino acid substitutions. A QuikChange II kit was used to prepare the mutants essentially according to the manufacturer's instructions using the pSiaA-His plasmid as a template [34]. The forward and reverse primers (underlined letters indicate the mismatches) for each mutant are shown in Table 1. The constructed plasmids were introduced into *E. coli* Top10 competent cells by chemical transformation and clones were selected on Luria-Bertani (LB) plates containing 100 µg/mL ampicillin. The resulting plasmids express the corresponding SiaA mutant as an N-terminal fusion to His-Xpress epitope from the arabinose-regulated promoter, P_{BAD} as described previously [34]. Taq PCR Master Mix Kit was used to amplify SiaA DNA segments, and the sequence of the wild type and mutant proteins was determined by Applied Biosystems model ABI 377 DNA sequencer at the DNA Core Facility at Georgia State University. Sequencing confirmed the presence of the mutant gene in the correct orientation in each of the plasmids.

Table 5.1 Forward and reverse primers for the mutants in this work.

C47Af	5'-CCACTTCGGTTGCTGTGGTTGATATCGCTGACCGTTTAAATTTA-3'
C47Ar	5'-TAAATTTAAACGGTCAGCGATATCAACCACAGCAACCGAAGTGG-3'
C58Af	5'-TTTAGACCTCGTTGGGGTTGCTGATAGTAAA TTATATACCCTTCC-3'
C58Ar	5'-GGAAGGGTATATAATTTACTATCAGC AACCCCAACGAGGTCTAAA-3'
H229Af	5'-CTTGATTTTACGAACAGCTGCTGCCATTCCAGACAAGG-3'
H229Ar	5'-CCTTGTCTGGAATGGCAGCAGCTGTTCGTAAAATCA AG-3'
M79Af	5'-GCGTGTGGGTTTACCCGCCAATCCTGATATAGAGTTGATTG-3'
M79Ar	5'-CAATCA ACTCTATATCAGGATTGGCGGGTA AACCCACACGC-3'
K61Af	5'-CCTCGTTGGGGTTTGTGATAGTGCATTATATACCCTTCCTAAACGC-3'
K61Ar	5'-GCGTTTAGGAAGGGTATATAATGCACTATCACAAACCCCAACGAGG-3'

5.3.4 Expression and purification of mutants

The proteins were expressed and purified from the appropriate plasmids as previously described [45] with small modifications. A representative description is given for the C58A mutant. C58A expression was induced with 0.02% arabinose for 4 h. The cell pellet was ruptured with two cycles of French press in 45 mL of buffer containing 20 mM Tris-HCl (pH 8.0), 100 mM NaCl, 0.1% Triton X-100, 10% v/v glycerol, and four tablets of protease inhibitor (Roche Complete Mini, EDTA-free). The solution was centrifuged for 20 min at 8,000 *g*, and the supernatant was syringe-filtered with a 0.45 μm filter (surfactant-free cellulose acetate membrane, Nalgene). All of the following purification steps were conducted at 4 °C using a GE Healthcare ÄKTA fast protein liquid chromatography instrument (FPLC, Amersham BioSciences), and all buffer solutions were pH 7.4 unless specified otherwise. The sample was loaded onto a GE Healthcare HisTrap™ HP column (5 mL, Amersham BioSciences) equilibrated with binding buffer (20 mM sodium phosphate, 500 mM NaCl, and 20 mM imidazole).

Unbound material was washed out with 5 column volumes (CV) of binding buffer. C58A was eluted with buffer containing 20 mM sodium phosphate, 500 mM NaCl, and 500 mM imidazole via a 20 CV linear gradient. The purities of the fractions were evaluated using sodium dodecyl sulfate polyacrylamide gel electrophoresis. Fractions containing the individual SiaA mutants were combined, and imidazole and salts were removed by centrifugal filtration (Amicon Ultra-15, 5 kDa molecular weight cut-off, Millipore) using a buffer of 50 mM Tris-HCl, pH 7.0. The protocols for the other mutants were similar with the exceptions that M79A was purified using a HiTrap Q column (GE Healthcare) equilibrated with a buffer of 20 mM Tris-HCl and 10% v/v glycerol (designated as Buffer A). Unbound material was washed out with 8 CV of Buffer A. M79A was eluted with 10 CV of Buffer A containing 1 M NaCl via a linear gradient (0 – 100% NaCl).

5.3.5 Heme loading

Purified SiaA and mutants were a mixture of holo and apo forms. The holo protein was isolated in the ferric state. The extinction coefficients and heme loading of SiaA mutants were measured using the pyridine hemochrome assay [64]. The extinction coefficients are as follows: C47A ε_{414} = 145.3 $mM^{-1}\,cm^{-1}$; K61A ε_{406} = 135.9 $mM^{-1}\,cm^{-1}$. Total protein concentration was determined using the Bradford assay (Thermo Fisher Scientific, Inc.) with bovine serum albumin as a standard. The WT extinction coefficient was previously reported [35,46]. M79A and H229A were also previously reported [46,65].

5.3.6 SiaA heme extraction and refolding

Apo-SiaA was prepared using the Teale method [66]. A solution of SiaA (10 μM) in PBS buffer, pH 7.4, was reduced to pH 2 in a drop-wise fashion using 3 M HCl. The acidic SiaA

solution was mixed with cold 2-butanone and placed on ice for 15 min. The heme layer was discarded.

To aid in protein refolding, urea was added to the apoprotein solution to give a final concentration of 8 M urea [67]. The solution sat at room temperature for 2 h. The apo-SiaA solution was dialyzed at 4 ˚C against 4 M urea (in PBS) for 24 h, against 2 M urea (in PBS) for 2 h, and against 10 mM potassium phosphate, pH 7.0, for 24 h. The apoprotein solution was centrifuged at 4 ˚C for 15 min at 5,000 *g* to remove any precipitate. The concentration of apo-SiaA was determined using the ExPASy ε_{280} = 37,360 $M^{-1}cm^{-1}$ [68].

5.3.7 UV-visible absorption spectroscopy

UV–visible absorption spectra were recorded on a Varian 50 Bio spectrophotometer with a thermostated cell compartment. A TC125 temperature control unit (Quantum Northwest, Spokane, WA) was used to set the temperature of the cuvette compartment to 25 ˚C. Quartz black-masked Suprasil cuvettes (Spectrocell, Inc.) with a 1 cm path length were used.

5.3.8 Circular dichroism spectroscopy

Circular dichroism (CD) spectra were recorded using a Jasco J-810 Spectropolarimeter. Quartz Suprasil cuvettes (Fisherbrand, Inc.) with a 1 mm path length were used. Holo-SiaA (10 μM) and apo-SiaA (10 μM) were recorded in 10 mM potassium phosphate buffer, pH 7.0 in a spectral window of 190 to 260 nm. The final scan represents an average of ten scans.

5.3.9 Resonance Raman spectroscopy

Resonance Raman spectra were recorded at ambient temperature using a 0.67-m spectrograph equipped with a 2400 g/mm holographic grating and a LN_2 cooled CCD detector. Spectra were excited with 413.1 nm emission from a Kr^+ laser or 441.6 nm emission from a HeCd laser. The beam was focused to a line at the sample and scattered light was collected in

the 135˚ backscattering geometry using *f*1 optics and a holographic notch filter to remove Rayleigh scattered light. Samples were contained in 5 mm NMR tubes and spun at ~20 Hz to minimize the risk of laser-induced damage to the samples. Sample integrity after laser irradiation during the rR experiment was verified by comparing UV-visible absorption absorbance spectra with those recorded before laser exposure. Spectra were calibrated against the Raman shifts of pure toluene and CH_2Br_2 and are reproducible to one wavenumber or less.

5.3.10 Denaturation studies

The following proteins were monitored with UV-visible absorption spectroscopy at the indicated wavelengths and concentrations upon the addition of GdnHCl: C47A (414 nm, 7 µM), C58A (409 nm, 7 µM), K61A (412 nm, 4 µM), M79A (402 nm, 9 µM), and H229A (403 nm, 7 µM). The refractive index of GdnHCl was used to verify the concentration of the stock GdnHCl solutions (50 mM Tris-Cl, pH 7.0) [69]. GdnHCl was titrated into each protein until the unfolding reached equilibrium which was considered to have been established when the absorbance did not change by more than 0.002 from the previous measurement.

The unfolding curves were analyzed using Equation 1 [69]:

$$y = [(A_F + m_F[D]) + (A_U + m_U[D])\exp[m([D]-[D]_{1/2})/RT])]/1 + \exp[m([D]-[D]_{1/2})/RT] \quad [1]$$

where y is the absorbance at any point along the fitted denaturation curve, A_F is the absorbance of the folded state, A_U is the absorbance of the unfolded state, m is the slope at the midpoint, and also the dependence of the free energy of unfolding on the denaturant concentration, m_F is the slope of the folded state, m_U is the slope of the unfolded state, [D] is the concentration of

GdnHCl, $[D]_{1/2}$ is the concentration of GdnHCl at the midpoint of the unfolding curve, R is the gas constant, and T is the temperature (Kelvin).

In another set of experiments, samples of WT SiaA (5 μM) in 50 mM Tris-Cl, pH 7.0 were incubated for 29 h at room temperature in various concentrations of GdnHCl (5.93 M stock solution). Each sample was monitored by UV-visible absorption spectroscopy before loading onto a washed PD-10 desalting column (GE Healthcare). The column was equilibrated with 25 mL of 50 mM Tris-Cl, pH 7.0. Each SiaA sample (2.5 mL) was allowed to enter the column bed before eluting with 3.5 mL of 50 mM Tris-Cl, pH 7.0. Fractions of 500 μL were collected. The protein eluted in the third fraction. The Soret:280 nm ratios of the desalted protein samples were fit to an unfolding curve. Control experiments were also run on horse heart myoglobin (Sigma-Aldrich).

5.3.11 Studies of unfolding rates

Solutions (5 μM) in 50 mM Tris-Cl, pH 7.0 of WT, C47A, C58A, and K61A were monitored by optical absorbance at the Soret as a function of time for 24 h at the pre-determined $D_{1/2}$ concentrations. The unfolding was fit to the sum of two exponential processes using Equation 2:

$$A_t = A_f \exp^{-k_f t} + A_s \exp^{-k_s t} \qquad [2]$$

where A_t is the total absorbance of the solution, A_f is the relative absorbance of the fast phase, k_f is the rate of the unfolding for the fast phase, A_s is the relative absorbance of the slow phase, k_s is the rate of the unfolding for the slow phase, and t is time. Attempts to fit the data to a model with an intermediate were not successful.

5.3.12 Spectrophotometric pH titrations

The pH titrations were performed by the addition of 1.0 M NaOH aliquots to the protein solutions (5 μM). A buffer of CAPS (20 mM), CHES (20 mM), and Tris-Cl (20 mM) was utilized throughout the titration. Changes in absorbance in the Soret region were analyzed with Kaleidagraph using Equation 3 [70]:

$$A_{obs} = (A_A \cdot 10^{(pKa - pH)} + A_B)/[1 + 10^{(pKa - pH)}] \quad [3]$$

where A_{obs} is the experimental absorbance observed, A_A is the absorbance of the acidic form, and A_B is the absorbance of the basic form.

5.3.13 Reduction potential determination

Midpoint potentials were determined by spectroelectrochemical titration of the protein in a homemade cell using a Pt working electrode, a Ag|AgCl reference electrode, and a standard pH meter in its mV mode. The absorbance contributions of all non-heme chromophores had been subtracted from each spectrum for the following experiments. The cell was loaded with ~6 mL of solution at holoprotein concentrations such that absorbance at the Soret maximum was between 0.2 and 0.6. The solution was exhaustively equilibrated under an atmosphere of H_2O-saturated N_2 and the absorbance spectrum of the ferric protein was recorded. The heme was then completely reduced by anaerobic addition of 20 mM aqueous $S_2O_4^{2-}$ and the absorbance spectrum of the ferrous heme was recorded. Electron transfer dye cocktail was added to the protein solution to reach a final concentration of 10 μM in each dye. The resulting solution was titrated with $S_2O_4^{2-}$ until the UV-visible absorption spectrum of the heme no longer changed and the dyes were completely reduced. Cell potential was monitored using a strip chart recorder to

make it easily apparent when equilibrium had been established, at which point the absorbance spectrum was recorded between 350 and 800 nm. The reduced solution was then titrated by anaerobic additions of 40 mM $[Fe(CN)_6]^{3-}$ to oxidize the dyes and heme. Cell potentials and spectra were recorded after each titrant addition and equilibration. Finally, the solution was titrated again with 20 mM $S_2O_4^{2-}$. After the second cathodic titration, the reference electrode was calibrated against the quinhydrone half cell so that cell potentials could be corrected to the SHE reference. Absorbance at the Soret maximum for the ferrous heme was plotted vs. cell potential and fit to the Nernstian relationship in Equation 4 for both the cathodic and anodic titrations. The resulting midpoint potentials were within 10 mV of one another.

$$A_{434} = [A_\infty + A_0 \exp([E - E_m]/0.0257\ V)]/1 + \exp([E - E_m]/0.0257\ V) \quad [4]$$

5.4 Results

5.4.1 Spectroscopic studies

WT SiaA and the C47A, C58A, and K61A mutants were purified as red colored proteins (Figure 5.3). The Soret band of the WT SiaA was observed at 413 nm, consistent with previous reports [41,45]. UV-visible absorption absorbance spectra of the C47A and K61A mutants were very similar. The Soret maximum of the C58A mutant occurred at 409 nm. All three mutants and WT SiaA showed α- and β-bands near 532 and 567 nm.

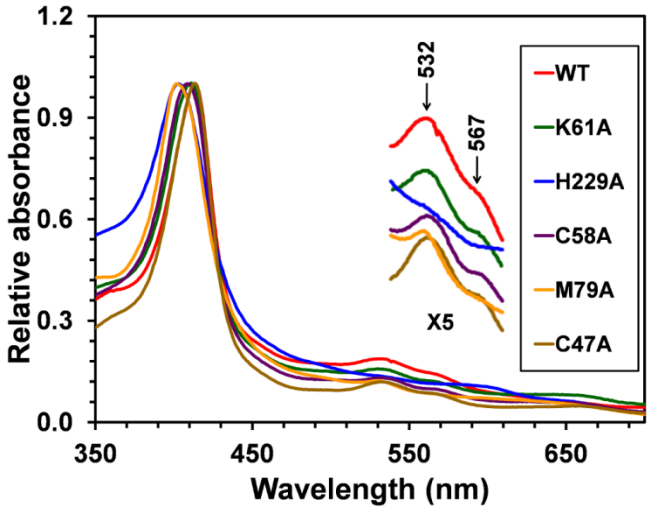

Figure 5.3 UV-visible absorption spectra of the Fe(III) forms of C47A, C58A, K61A, M79A, H229A and WT SiaA normalized at the Soret. The solutions were in 50 mM Tris-Cl, pH 7.0.

In contrast to these three mutants, the purified mutants having axial ligand mutations (M79A and H229A) were pale yellow in color, suggesting low heme loading. Additionally, M79A and H229A had much larger spectral shifts than the other mutants, with Soret bands at 402 and 403 nm, respectively, similar to those reported in the literature [47].

CD spectroscopy was used to probe the overall fold of holo-SiaA versus apo-SiaA (Figure 5.4). Both proteins contained bands around 190, 210, and 222 nm, indicative of α-helical content. The band at 210 nm was more pronounced for the apoprotein compared to the holoprotein. This indicates that the overall fold of the protein is altered upon heme removal from the protein [47].

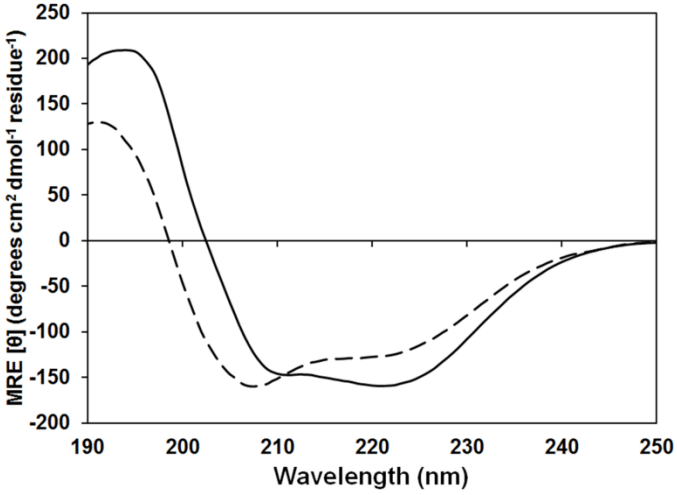

Figure 5.4 CD spectra of holo-SiaA (solid line) and apo-SiaA (dashed). The spectra were recorded in 10 mM potassium phosphate, pH 7.0.

5.4.2 Guanidine-induced denaturation of WT SiaA and mutants

Preliminary studies indicated that unfolding of SiaA was very slow. Therefore, unfolding was followed as a function of time for WT, C47A, C58A, and K61A. Fast and slow unfolding phases were observed for all four proteins. Figure 5.5 shows the data for WT at the GdnHCl midpoint concentration; plots of the data for the mutants are in the Supplemental Information (Figures S1 – S3). For WT, fitting the data to the sum of two exponential processes gave the rate of the fast process (15%) as 0.32 ± 0.02 h^{-1} and the rate of the slower process (85%) as 0.026 ± 0.001 h^{-1}. The percentages of the faster process ranged from 10 – 30% (Table 5.2). Faster rate constants for the first phase correlated with smaller abundance of this fast phase and slower rate constants for the second phase. C58A showed the largest difference between the two phases, with half-times of 1.5 h for the fast phase (12%) and 46 h for the slow phase (88%).

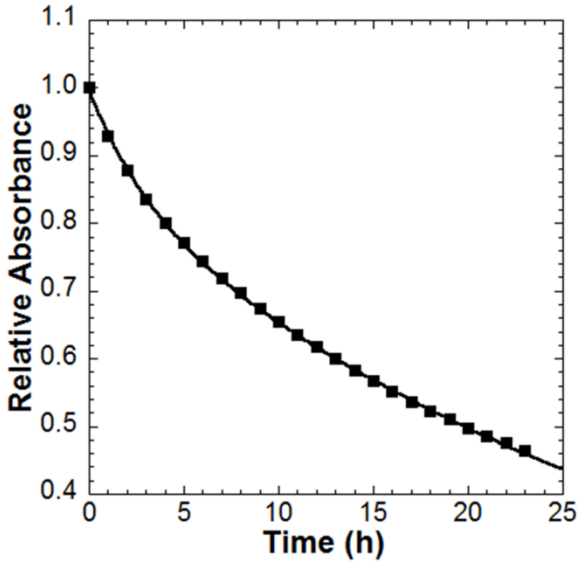

Figure 5.5 Time-scale unfolding of WT SiaA at the D1/2 (3.1 M GdnHCl). Data were taken in 50 mM Tris-Cl, pH 7.0. The data were fit using the sum of two exponential processes.

Table 5.2 $D_{1/2}$ unfolding rate constants and relative abundances for SiaA and mutants.

Protein	k_{fast} (h^{-1})	Abundance of the Fast Phase (%)	k_{slow} (h^{-1})	Abundance of the Slow Phase (%)	$D_{1/2}$ (M)
WT	0.32 ± 0.02	15	0.026 ± 0.001	85	3.1
C47A	0.24 ± 0.02	30	0.033 ± 0.001	70	2.9
C58A	0.46 ± 0.02	12	0.010 ± 0.001	88	2.4
K61A	0.41 ± 0.04	11	0.012 ± 0.001	89	2.5

In the measurements of $D_{1/2}$, waiting the times necessary to reach equilibrium resulted in anomalies due to changes in protein concentration. Therefore, a single cuvette titration technique was utilized [71-75] in which increasing concentrations of GdnHCl were added to a single cuvette. This technique can give the approximate relative ease of denaturation in a series. Fitting the C58A data to a two-state model gave a midpoint denaturant concentration of 2.4 ± 0.1 M GdnHCl. The C47A, K61A and M79A proteins were also investigated with the same

technique and gave $D_{1/2}$ values of 2.9 ± 0.1 M, 2.5 ± 0.1 M, and 1.5 ± 0.1 M, respectively (Figure 5.6). WT SiaA had a $D_{1/2}$ of 3.1 ± 0.1 M as previously reported [45].

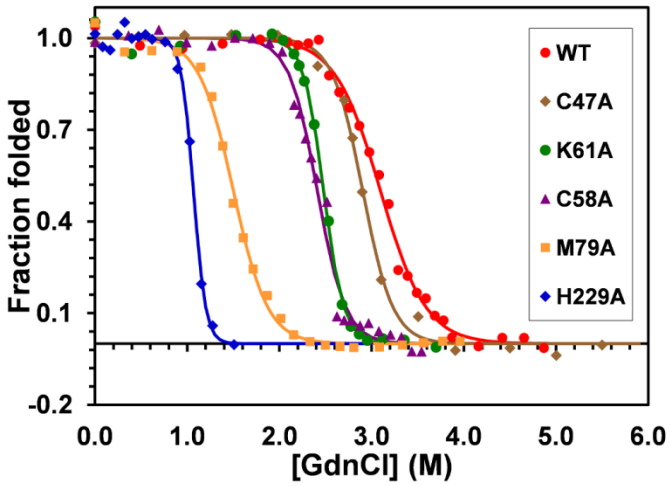

Figure 5.6 Fraction of folded WT SiaA and mutants as a function of the concentration of GdnHCl. Data from the titrations were fit via nonlinear least squares to a two state unfolding model. Protein samples were in 50 mM Tris-Cl, pH 7.0.

The H229A mutant spectrum did not show clear α,β-bands during the titration. For this protein, equilibrium was reached in less than 20 min after each GdnHCl addition. This was a substantially shorter amount of time than that required for WT SiaA to reach equilibrium (which in the transition region was well over one hour). This is consistent with weak binding of the heme to the protein. The Soret absorbance decreased and shifted toward the red as guanidine was added up to 1.5 M GdnHCl. Fitting the data from 0 to 1.5 M GdnHCl gave a $D_{1/2}$ of approximately 1.1 M.

The unfolding of WT SiaA was also investigated by incubating samples with various concentrations of GdnHCl and then passing the solution through a desalting column to remove loosely-bound heme (Figure S4) [73]. Fitting to a two-state model gave a $D_{1/2}$ of 2.6 ± 0.1 M, somewhat lower than the 3.1 ± 0.1 M in the experiment above, consistent with this not being an equilibrium measurement.

It should be noted that unfolding of WT SiaA and mutants was performed on samples that contained both holo and apo forms of the protein. Freshly prepared apo-SiaA largely precipitated by 24 h after isolation. Thus, it was presumably decreasing in concentration over the long time of the unfolding experiments. However, the effects of protein concentration on unfolding are often small and depend on the exact mechanism of the unfolding process [76].

5.4.3 Spectrophotometric pH titrations

For the three mutants not involving the heme ligands (C47A, C58A, and K61A), titrations with aliquots of 1 M NaOH gave a Soret absorbance that decreased as the pH increased (representative data from C47A are shown in Figure 5.7). The transitions were isosbestic for pH < 11. The absorbance at 280 nm also increased above pH 11. This is consistent with high pH leading to unfolding of the protein which in turn results in exposure and deprotonation of some of the 14 tyrosines in the sequence (the extinction coefficient of tyrosinate (2500 M^{-1} cm^{-1} at 295 nm) is higher than that of tyrosine (1400 M^{-1} cm^{-1} at 275 – 280 nm) [77]). Data from pH 7 to approximately pH 10.9 were fit using a two state model to give pK_a values of 9.22 ± 0.03, 9.04 ± 0.03 and 9.45 ± 0.05 for C47A, C58A, and K61A, respectively. The pK_a of WT SiaA is 9.7 ± 0.1 [45].

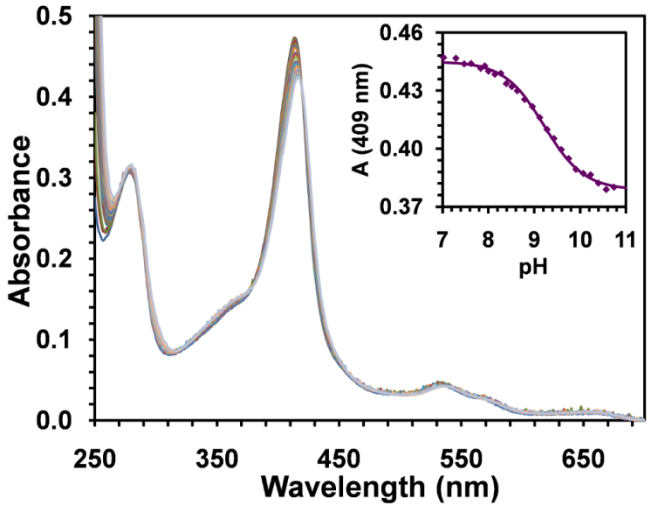

Figure 5.7 Spectrophotometric pH titration of C47A, titrated with 1.0 M NaOH, in a buffer of 20 mM each CAPS, CHES and Tris-Cl. UV-visible absorption spectra are shown from pH 7.0 to 10.7. The inset shows the nonlinear least squares fit of the data at 409 nm to a single pKa; the value was 9.22 ± 0.03.

5.4.4 Resonance Raman spectra of ferric and ferrous SiaA mutants

The spectra of ferrous and ferric C58A SiaA are shown in Figure S5 in the Supplementary Material. In contrast to WT SiaA [45], this mutant is susceptible to photo-induced reduction during spectral acquisition. Consequently, the spectra were recorded with low laser power (3.7 mW), and exhibit only a modest signal-to-noise ratio. The spectra are characteristic of hexacoordinate, low-spin (6cLS) hemes and reminiscent of those previously reported for WT SiaA. Thus the spectral signatures for ferric and ferrous C58A SiaA are consistent with the heme conformations and axial ligand set being the same as those for the WT protein. However, the shifted Soret maximum (6 nm to the blue of the WT SiaA) as well as the photolability of the ferric state suggest that its heme environment may be distinct from WT SiaA. By contrast, the spectral signatures and behaviors of the ferrous proteins are rather similar.

Because the K61A SiaA was not photolabile, it was possible to record higher quality rR spectra, as shown in Figure 5.8. Like the WT protein, it also exhibits rR fingerprints

characteristic of 6cLS ferric and ferrous heme proteins. In fact, the rR spectra of WT SiaA and K61A SiaA are nearly identical for both the ferric and ferrous forms. Although homology modeling suggests that K61 is able to interact with one of the heme propionate groups in the WT protein, the loss of that interaction is not apparent in the rR spectra of K61A SiaA. Specifically, comparison of the WT and K61A rR spectra reveal that the propionate bending bands are virtually identical in the ferric and ferrous forms. Thus, loss of the electrostatic interaction between K61 and the heme periphery does not drive significant changes in propionate conformation. This result is consistent with the insensitivity of the reduction potential (§ 3.5) to the mutation of K61.

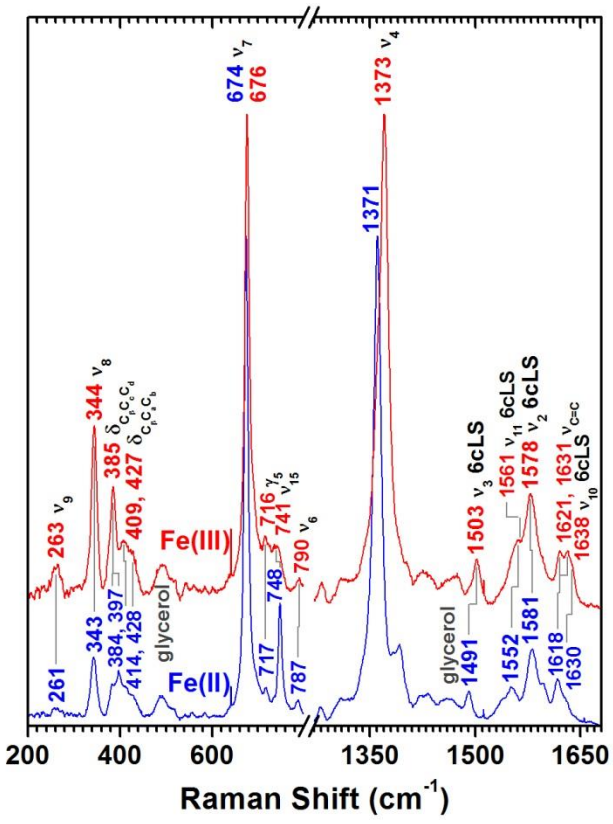

Figure 5.8 Soret-excited rR spectra of ferric (top) and ferrous (bottom) K61A SiaA. The in-plane porphyrin stretching (high frequency) and low frequency regions are shown. Samples were 250 μM in holo-SiaA and in 20 mM Tris-Cl at pH 8.0. Ferrous K61A SiaA was generated by anaerobic introduction of a 15-fold molar excess of buffered dithionite to the ferric protein. Complete reduction was verified by UV-visible absorption absorbance spectroscopy.

5.4.5 Spectroelectrochemical titrations

In previous work on WT SiaA, we reported an irreversible midpoint potential that lies between 64 and 83 mV vs SHE [45]. Reanalysis of those data revealed more than one Fe(III)|Fe(II) couple, as shown in Figure S6. After oxidation with $[Fe(CN)_6]^{3-}$, the reductive titration with $S_2O_4^{2-}$ showed a single midpoint potential of 68 ± 3 mV vs SHE. Following complete reduction with $S_2O_4^{2-}$, the reverse (oxidative) titration with $[Fe(CN)_6]^{3-}$ revealed two potentials, one at 15 ± 5 mV, accounting for ~60% of the heme, and the other at 72 ± 10 mV, accounting for ~40% (see Figure S6 for further details). The 68 and 72 mV potentials are indistinguishable with these uncertainties. This finding is consistent with heme oxidation triggering a redox-coupled change in structure or conformation that (a) changes the Fe(III)|Fe(II) potential and (b) is kinetically sluggish to reverse, even after reoxidation of the heme.

Spectroelectrochemical titration of K61A revealed a reversible potential of 61 ± 3 mV. Absorbance spectra and the absorbance at the ferrous Soret maximum are shown in Figure 5.9. The forward and reverse titrations are superimposable and well modeled by the Nernstian expression shown in Equation 4. Consistent with the rR spectra of WT and K61A, these reduction potentials indicate that the replacement of K61 (which homology modeling suggests is near a heme propionate) with the small hydrophobic methyl group of alanine has only a small effect on the relative stabilities of the oxidized and reduced heme states. Even though the change in reduction potential in response to the loss of the positive charge from K61 is only −7 mV, it is in the direction consistent with stabilization of the ferric heme, which is expected upon loss of the cationic side chain from K61.

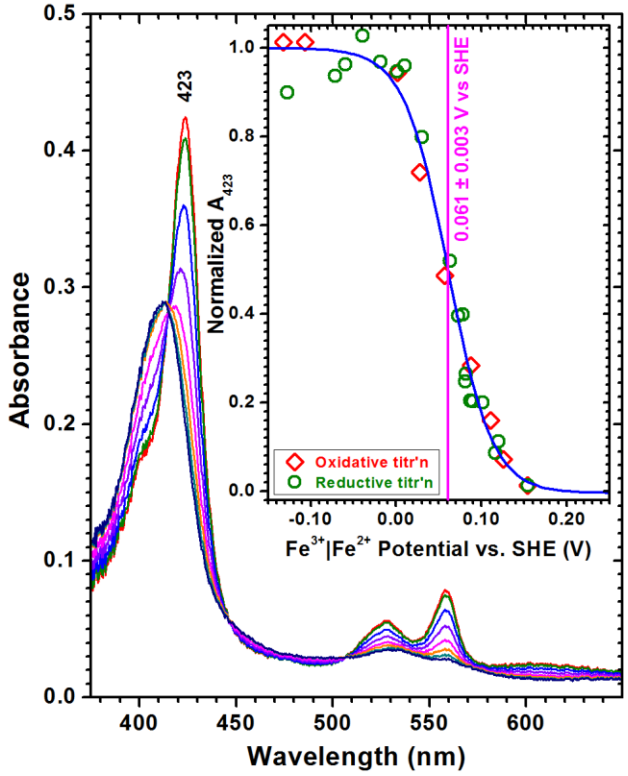

Figure 5.9 UV-visible absorption absorbance spectra of K61A SiaA during the course of the spectroelectrochemical titration with dithionite. Spectral contributions from the dyes, ferricyanide, ferrocyanide and dithionite ions have been subtracted from each spectrum to show the clean isosbestic behavior of the system. The inset shows absorbance at the Soret maximum for ferrous K61A SiaA (423 nm) as a function of cell potential (vs SHE reference). The oxidative and reductive titration curves are superimposable and fitting to a single Nernstian wave (Equation 4) yielded a midpoint potential of 61 ± 3 mV vs SHE. Titrations were carried out in 50 mM Tris/Tris-Cl at pH 8.0, 100 mM NaCl.

In contrast, the reduction of the C58A mutant was < 0 V vs. SHE, significantly more negative than that of the WT protein and irreversible (Figure S7). Although the irreversibility of the reduction precluded reliable determination of its potential, its negative potential indicates that replacement of cysteine 58 with alanine changes the heme pocket so as to destabilize the ferrous state and/or stabilize the ferric state relative to the WT protein. Given that the spectroscopic behavior of the ferric protein is distinct from that of WT SiaA, it is concluded that the negative reduction potential is likely attributable to destabilization of the ferric heme in C58A SiaA.

5.5 Discussion

5.5.1 Guanidinium-induced unfolding

WT SiaA in the ferric form undergoes guanidinium-induced unfolding with a $D_{1/2}$ of 3.1 M [45]. To probe specific heme-protein interactions and their influence on heme binding, we looked at the unfolding of five mutants: C47A, C58A, K61A, M79A, and H229A. Because homology modeling predicts C47 to be distant from the heme, the C47A mutation was studied as a control. The $D_{1/2}$ value of C47A was 2.9 M, similar to the WT $D_{1/2}$ at 3.1 M.

The K61A mutant was chosen because homology modeling showed the residue to be at the entrance to the pocket on the side of M79, close to the propionic acid that is less buried in the protein. K61 is in a similar position to K62 in IsdE (Figure S8), for which the crystal structure is known [48]. In the IsdE structure, K62 hydrogen bonds to a water molecule, which in turn hydrogen bonds to both propionates. K62 in IsdE is also involved in a complex network of non-bonded interactions wherein K62 forms a salt bridge with E265, which in turn hydrogen bonds to H229 via water. E265 also hydrogen bonds directly with Y61 (which corresponds to Y63 in SiaA). Y61 hydrogen bonds to one of the heme propionates, as does the adjacent S60 (conserved in the SiaA model). In view of this complex hydrogen bonding network, it was expected that mutation of the K61 in SiaA would change the stability of the holoprotein. Indeed this was observed, with the K61A mutant ($D_{1/2}$ of 2.5 M) being less stable than the WT protein ($D_{1/2}$ of 3.1 M). The reduction in stability may also be due to loss of a salt bridge between the positively charged lysine and the negatively charged heme propionate. Heme propionates often form salt bridges with nearby cationic residues, with the most prevalent amino acid being arginine; lysine and histidine are common as well [5,49-53,78]. We note, however, that the resonance Raman data indicate that mutation of K61 to alanine in this protein does not induce measurable changes

in the propionate vibrational signatures, although it does affect the overall stability of the holoprotein.

Homology modeling also suggested that C58A is near the heme propionates on the methionine side of the heme. Although there is no expected electrostatic interaction between C58 and the heme, loss of this residue clearly lowers the thermodynamic cost of unfolding this protein. Cysteine 58 is near the H-bonding network involving S60, described above. It is also near a second hydrogen bonding network involving S40, S271 and a water molecule (T40, T271 and H_2O in IsdE). In IsdE, the water molecule in this network hydrogen bonds to one of the heme propionates [48]. Mutation of the cysteine to alanine in SiaA results in a decrease in the $D_{1/2}$ value to 2.4 M, consistent with disruption of these hydrogen-bonding patterns.

The two axial ligand mutants (M79A and H229A) released heme more easily than the other three mutants. The M79A protein was expected to be significantly less stable than WT, because the presumed contribution of the $Fe{-}S_{Met79}$ bond to the stability of the protein fold is eliminated in this mutant. Consistent with this reasoning, the midpoint of the transition occurred at 1.5 M GdnHCl, indicating the importance of this iron-ligand bond in stabilizing the holo-SiaA fold. Spectroscopy has indicated that the M79A is hexacoordinate, presumably with a water molecule replacing the methionine [46]. Finally, the H229A mutant had the lowest $D_{1/2}$ of approximately 1.1 M, consistent with the expected importance of the H229-heme interaction (the heme is pentacoordinate in this mutant [46]). This order of unfolding is consistent with previous studies using other techniques; Ran et al. found that the extent of heme transfer from holo-SiaA to an apo-myoglobin mutant was H229A > M79A > WT [46]. The acid-induced unfolding showed the same pattern. H229A and M79A both showed single kinetic processes with the former faster than the latter. These were both faster than the WT protein (considering the slower

step of the two step process was for the WT) [47]. Equilibrium dialysis and inductively coupled plasma mass spectrometry (ICP-MS) experiments indicate that the relative order of heme affinity is WT > M79A > H229A [47]; Ran et al. have concluded that all three of these proteins have binding constants of > 10^{12} M^{-1} [46,65].

Heme protein unfolding of *b*-type heme proteins can have intermediates in which the heme is bound to a partially unfolded structure. For example, in an early study, it was postulated that ferric hemoglobin unfolds in a way that allows the heme to be released while the protein is unfolding [79]. In contrast, it was proposed that carboxyhemoglobin unfolds completely while the heme moiety stays bound at the active site until its release [79]. Data for horse heart myoglobin unfolding as a function of GdnHCl concentration were interpreted as an initial unfolding ($D_{1/2}$ = 1.5 M) followed by loss of heme only at high concentrations of denaturant (> 5 M) [73]. Sperm whale myoglobin unfolding has been fit to a model involving native, intermediate, and unfolded states as well as their hemin-bound counterparts [57,76].

5.5.2 The time-scale of protein unfolding

The kinetic data for WT SiaA and its mutants were well fit by a two-term exponential function with the majority of the protein (~60 – 90%) unfolding with the slower rate constant. This two-phase process may reflect forms of the protein with two different orientations of the heme in the pocket related by a 180˚ rotation around the α,δ-*meso* axis [80]. The fast and slow phases had half-lives of 2 – 3 and 70 – 90 h, respectively. Although there are extensive studies of guanidinium denaturation of heme proteins, kinetic studies are more limited. For example, bovine microsomal cytochrome b_5 has major and minor heme-bound forms that occur in an 8:1 ratio, as shown by NMR [81,82]. Unfolding of this protein had a fast and slow phase, interpreted as arising from the two forms of the protein with different heme orientations, with a half-time of

~ 30 sec for the first process and a second process that was 3 – 4 times slower at the $D_{1/2}$ of 3 M GdnHCl [60,83]. Horse heart myoglobin shows a similar pattern, with a the first process (20%) having a half-time of seconds and the second process (80%) ~10 times slower at the $D_{1/2}$ of 1.6 M GdnHCl [73]. Circular dichroism studies on the horse heart protein were in line with this ratio of isomers. Sperm whale myoglobin has a heme isomer ratio of 15:1 [84], and thus unfolding would not be expected to show two isomers. Olson and co-workers have looked at the unfolding process in detail and proposed a kinetic scheme with one form of the protein, but with one or more intermediates in the unfolding pathway [57,76,85]. Horseradish peroxidase (HRP) exists almost exclusively as a single isomer [80]. HRP has a $t_{1/2}$ of 520 sec at 6.0 M GdnHCl (pH 7) [86,87]; the apparent $D_{1/2}$ is 5.5 M. Soybean peroxidase unfolds approximately 200 – 300-fold more slowly than horseradish peroxidase [87]. The rates for bovine microsomal cytochrome b_5 and horse heart myoglobin differed approximately by a factor of ten. WT SiaA and C47A are similar. These results are consistent with the two unfolding phases of SiaA being attributable to the two heme orientations. The amplitude ratios of the faster and slower processes for SiaA are in the order of C58 > K61 > WT > C47, with the values of 46 > 34 > 12 > 7.3, respectively. Mutations near the propionates of the heme edge (C58A and K61A) gave the largest ratios and largest percentages of the slow phase.

For SiaA and its mutants, we have observed that the unfolding steps are sensitive to mutations in the heme pocket, where bonded and non-bonded interactions must be made and broken in the course of fairly rapid heme transfer reactions. However, overall unfolding rates as probed by GdnHCl denaturation are very slow, with half-lives for the slower process of one to three days at the $D_{1/2}$. This slow intrinsic heme loss may protect the organism from the deleterious effects of free heme. Heme transfer would be accomplished only by direct transfer to

a partner protein, along a facile heme release coordinate for which the kinetic barrier is relatively low. This would allow a change of conformation sufficient to release the heme without the risk of the protein proceeding along a steep, cooperative unfolding pathway that could leave it extensively unfolded and perhaps dysfunctional.

5.5.3 Spectrophotometric pH titrations

When titrated with base, all of the mutants gave spectra that were isosbestic from pH 7 to ~10.9. The data from each mutant were fit with a two state model to give pK_a values for C47A, C58A, and K61A of 9.22 ± 0.03, 9.04 ± 0.03, and 9.45 ± 0.05, respectively. These are all somewhat lower than the pK_a of WT SiaA (9.7 ± 0.1). We have proposed [45] that this pK_a is due to deprotonation of the axial histidine, which falls in the range of 8 – 11 for heme proteins [88-94].

The largest effect is seen for the C58A mutant. As described above, homology modeling indicates that C58 is near the heme propionates; mutation of this residue to alanine reduces the pK_a by approximately 0.7 units from the WT protein. In IsdE, the corresponding residue is a proline [48]. This P58 is near P77, which is adjacent to the axial methionine. P80 is also very near the axial methionine (PMEP). SiaA has homologous prolines in the sequence near the axial methionine (PMNP). These clusters of prolines may result in rigidity of the protein structure near the heme. This rigidity may allow significant change in the pK_a of the protein upon replacement of C58 with alanine. Even mutation of cysteine 47 has a significant effect on the pK_a, indicating that long range effects of slight changes in protein structure are being transmitted to the heme binding site.

K61 in SiaA aligns with K62 in IsdE. In IsdE, K62 is part of a complex network of hydrogen bonds involving the axial histidine, Y61, E265, two water molecules, and both heme

propionates [48]. The reduction in pK_a for the K61A mutant may have to do with changes in the hydrogen bonding network arising from the substitution.

5.5.4 The effect of redox state

For heme protein unfolding that is reversible, a thermodynamic cycle can be constructed from reduction potentials of the free heme and holoprotein, and the free energies of folding of the two oxidation states [95-97]. This cycle is illustrated for SiaA in Figure 5.10. The difference in the free energies of folding of SiaA around the ferric and ferrous hemes ($\Delta\Delta G_{fld}^{(III-II)}$) is given simply as the difference in the free energies of heme reduction in the unfolded protein and in the native holoprotein, as shown in Equation 5. In this work, chemically induced unfolding was not reversible, as shown experimentally. However, the reduction potentials can still be used to estimate the difference in folding free energies of oxidized and reduced SiaA. Reduction potentials of the holoprotein that are similar to that of free heme give systems in which the energy costs of unfolding of the two oxidation states are similar. For WT SiaA, the reduction potential is 68 ± 3 mV. Taken together with the −60 mV reduction potential of free heme [98], the thermodynamic cycle indicates that the folding of SiaA around the ferrous heme is more strongly driven than folding around hemin, albeit by only ~12.4 kJ·mol^{-1} for the WT; the corresponding driving force for the K61A mutant is similar at 11.7 kJ·mol^{-1}.

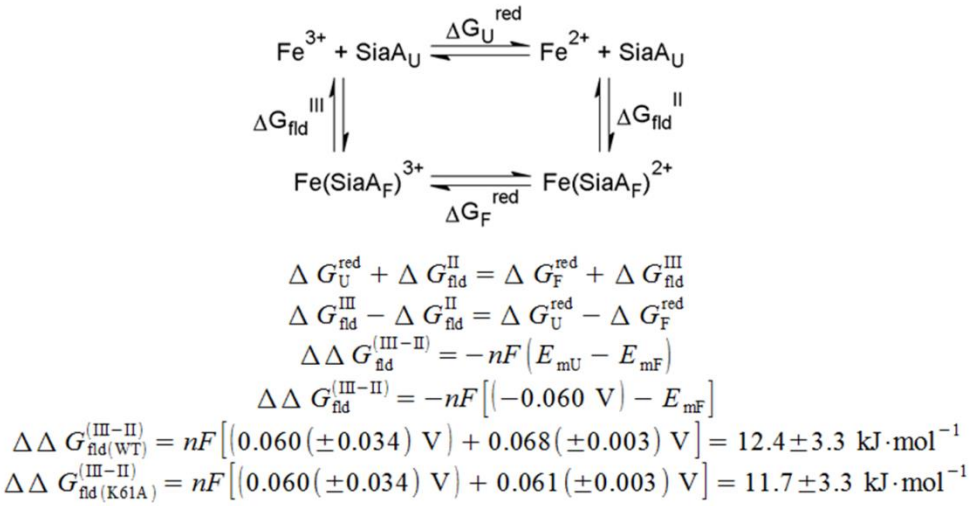

Figure 5.10. Thermodynamic cycle of heme binding in SiaA.

The heme donor to SiaA *in vivo* is Shp [34,35,41]. It is not yet known in which oxidation state the heme is transferred. Our electrochemical data indicates that the two oxidation states are similar with respect to the free energy of unfolding. Nygaard et al. have looked at the transfer of both heme and hemin from Shp to SiaA [42]. They fit the kinetics to a model involving an equilibrium for complexation of the two proteins, followed by intracomplex transfer of the iron porphyrinate from Shp to SiaA. The reported dissociation constants for ferrous and ferric Shp with apo-SiaA are 120 ± 18 μM and 48 ± 7 μM, respectively. Thus, the two oxidation states of Shp differed only by a factor of 2.5 in their binding affinity for apo-SiaA. The heme transfer rate constants within the Shp:SiaA complex were calculated to be 28 ± 6 s^{-1} and 43 ± 3 s^{-1}, respectively. Thus, this model indicates that the ferric and ferrous hemes are transferred within their respective complexes with similar rate constants. This kinetic result is consistent with our thermodynamic electrochemical data, indicating that both oxidation states of the heme should be released with comparable thermodynamic and kinetic ease.

5.6 Conclusions

SiaA is part of a pathway that facilitates heme acquisition by *S. pyogenes*. Guanidinium-induced denaturation showed that, as expected, the axial ligands (M79 and H229) play significant roles in the stability of the holo-SiaA fold. Other residues near the heme, specifically C58 and K61, which are near the propionic acids, are also important in stabilizing the protein fold. Guanidinium-induced denaturation occurred from two forms of the protein, with the slower process having a half-time of one to three days. The very slow unfolding may indicate that heme transfer proteins can unfold sufficiently to release heme, but are resistant to further unfolding that might result in conformations that could not easily bind heme for further heme transfer reaction cycles. Spectrophotometric pH titration studies gave pK_a values ranging from 9.0 to 9.5 for the mutants studied; these may be due to deprotonation of the axial histidine. Spectroelectro-chemical titrations showed that the midpoint reduction potential of the K61A SiaA was 61 ± 3 mV, similar to the 68 ± 3 mV potential of WT SiaA. The midpoint potential differs from that of free heme by 125 mV, indicating that the reduced protein is only ~12 kJ/mole more difficult to unfold than the oxidized protein. These results, together with kinetic data from the literature, reveal that the thermodynamic stabilities of the surface-bound heme acquisition protein SiaA are balanced so as to be nearly insensitive to the oxidation state of the heme. This result is consistent with the system having the flexibility to acquire heme in both its ferrous and ferric oxidation states.

5.7 Acknowledgments

We thank Brian Basden, Giselle Delgado, Armrita Nargund, and P.N. Nguyen for assistance with the experiments. We thank Dr. Kara Bren for useful discussions. We also thank the Georgia State University Molecular Basis of Disease Fellowship program for financially

supporting E. B. Draganova. This work was supported by National Institutes of Health Grants AI057877 (ZE) and AI072719−02 (KRR), and the Research Corporation (DWD).

5.8 References

[1] V.Braun, K.Hantke, Curr. Opin. Chem. Biol. 15 (2011) 328 - 334. Recent insights into iron import by bacteria.

[2] J.R.Chipperfield, C.Ratledge, Biometals 13 (2000) 165 - 168. Salicylic acid is not a bacterial siderophore: A theoretical study.

[3] A.L.Crumbliss, J.M.Harrington, Advances in Inorganic Chemistry, Vol 61: Metal Ion Controlled Reactivity 61 (2009) 179 - 250. Iron sequestration by small molecules: Thermodynamic and kinetic studies of natural siderophores and synthetic model compounds.

[4] A.Wilks, K.A.Burkhard, Nat. Prod. Reports 24 (2007) 511 - 522. Heme and virulence: How bacterial pathogens regulate, transport and utilize heme.

[5] Y.Tong, M.Guo, Arch. Biochem. Biophys. 481 (2009) 1 - 15. Bacterial heme-transport proteins and their heme-coordination modes.

[6] H.Contreras, N.Chim, A.Credali, C.W.Goulding, Curr. Opin. Chem. Biol. 19 (2014) 34 - 41. Heme uptake in bacterial pathogens.

[7] L.L.Anzaldi, E.P.Skaar, Infect. Immun. 78 (2010) 4977 - 4989. Overcoming the heme paradox: Heme toxicity and tolerance in bacterial pathogens.

[8] J.A.Mayfield, C.A.Dehner, J.L.Dubois, Curr. Opin. Chem. Biol. 15 (2011) 260 - 266. Recent advances in bacterial heme protein biochemistry.

[9] A.Wilks, K.D.Barker, Mechanisms of heme uptake and utilization in bacterial pathogens, in K.M.Kadish, K.M.Smith, R.Guilard (Eds.), Handbook of Porphyrin Science with Applications to Chemistry, Physics, Materials Science, Engineering, Biology and Medicine, Vol 15: Biochemistry of Tetrapyrroles, World Scientific, Hacksensack, NJ, 2011, pp. 357-398.

[10] C.L.Nobles, A.W.Maresso, Metallomics 3 (2011) 788 - 796. The theft of host heme by Gram-positive pathogenic bacteria.

[11] A.Gruss, E.Borezée-Durant, D.Lechardeur, Environmental heme utilization by heme-auxotrophic bacteria, in R.K.Poole (Ed.), Advances in Bacterial Respiratory Physiology, Academic Press, London, England, 61 edn, 2012, pp. 69-124.

[12] A.D.Smith, A.Wilks, Curr. Top. Membr. 69 (2012) 359 - 392. Extracellular heme uptake and the challenges of bacterial cell membranes.

[13] D.R.Benson, M.Rivera, Met. Ions Life Sci. 12 (2013) 279 - 332. Heme uptake and metabolism in bacteria.

[14] L.J.Runyen-Janecky, Front. Cell Infect. Microbio. 3 (2013) 55 Role and regulation of heme on acquisition in gram-negative pathogens.

[15] A.J.Farrand, E.P.Skaar, Heme and infectious diseases, in G.C.Ferreira, K.M.Kadish, K.M.Smith, R.Guilard (Eds.), Handbook of Porphyrin Science with Applications to Chemistry, Physics, Materials Science, Engineering, Biology and Medicine, Vol 26: Heme Biochemistry, World Scientific, Hackensack, NJ, 26 edn, 2014, pp. 317-377.

[16] K.R.Rodgers, G.S.Lukat-Rodgers, Handbook of Porphyrin Science with Applications to Chemistry, Physics, Materials Science, Engineering, Biology and Medicine, Vol. 30: Heme Proteins, Part II 30 (2014) 249 - 309. Biophysical perspectives on the acquisition, transport, and trafficking of heme in bacteria.

[17] A.Wilks, M.J.O'Neill, Extracellular heme uptake and metabolism in bacterial pathogenesis, in G.C.Ferreira, K.M.Kadish, K.M.Smith, R.Guilard (Eds.), Handbook of Porphyrin Science with Applications to Chemistry, Physics, Materials Science, Engineering, Biology and Medicine, Vol 26: Heme Biochemistry, World Scientific, Hackensack, NJ, 2014, pp. 267-315.

[18] K.D.Krewulak, H.J.Vogel, Biochim. Biophys. Acta 1778 (2008) 1781 - 1804. Structural biology of bacterial iron uptake.

[19] B.C.Chu, H.J.Vogel, Biol. Chem. 392 (2011) 39 - 52. A structural and functional analysis of type III periplasmic and substrate binding proteins: Their role in bacterial siderophore and heme transport.

[20] E.S.Honsa, A.W.Maresso, Biometals 24 (2011) 533 - 545. Mechanisms of iron import in anthrax.

[21] J.C.Grigg, G.Ukpabi, C.F.M.Gaudin, M.E.P.Murphy, J. Inorg. Biochem. 104 (2010) 341 - 348. Structural biology of heme binding in the *Staphylococcus aureus* Isd system.

[22] N.D.Hammer, E.P.Skaar, Annu. Rev. Microbiol. 65 (2011) 129 - 147. Molecular mechanisms of *Staphylococcus aureus* iron acquisition.

[23] K.P.Haley, E.P.Skaar, Microbes Infect. 14 (2012) 217 - 227. A battle for iron: Host sequestration and *Staphylococcus aureus* acquisition.

[24] M.T.Tiedemann, D.E.Heinrichs, M.J.Stillman, J. Am. Chem. Soc. 134 (2012) 16578 - 16585. Multiprotein heme shuttle pathway in *Staphylococcus aureus*: Iron-regulated surface determinant cog-wheel kinetics.

[25] G.Cavallaro, L.Decaria, A.Rosato, J. Proteome Res. 7 (2008) 4946 - 4954. Genome-based analysis of heme biosynthesis and uptake in prokaryotic systems.

[26] M.W.Cunningham, Adv. Exp. Med. Biol. 609 (2008) 29 - 42. Pathogenesis of group A streptococcal infections and their sequelae.

[27] Z.Eichenbaum, Virulence 3 (2012) 553 - 555. The streptococcal hemoprotein receptor. A moonlighting protein or a virulence factor?

[28] Z.Eichenbaum, E.Muller, S.A.Morse, J.R.Scott, Infect. Immun. 64 (1996) 5428 - 5429. Acquisition of iron from host proteins by the group A *Streptococcus*.

[29] M.Fisher, Y.S.Huang, X.R.Li, K.S.Mciver, C.Toukoki, Z.Eichenbaum, Infect. Immun. 76 (2008) 5006 - 5015. Shr is a broad-spectrum surface receptor that contributes to adherence and virulence in Group A Streptococcus.

[30] R.Gattringer, R.Sauermann, H.Lagler, K.Stich, A.Buxbaum, W.Graninger, A.Georgopoulos, Int. J. Antimicrob. Agents 24 (2004) 290 - 293. Antimicrobial susceptibility and macrolide resistance genes in *Streptococcus pyogenes* collected in Austria and Hungary.

[31] K.Szczypa, E.Sadowy, R.Izdebski, W.Hryniewicz, J. Antimicrob. Chemother. 54 (2004) 828 - 831. A rapid increase in macrolide resistance in *Streptococcus pyogenes* isolated in Poland during 1996-2002.

[32] D.E.Bessen, Inf. Genetics Evol. 9 (2009) 581 - 593. Population biology of the human restricted pathogen, *Streptococcus pyogenes*.

[33] A.Villaseñor-Sierra, E.Katahira, A.N.Jaramillo-Valdivia, M.D.Barajas-García, A.Bryant, R.Morfin-Otero, F.Márquez-Díaz, J.C.Tinoco, J.Sanchez-Corona, D.L.Stevens, Int. J. Infect. Dis. 16 (2012) E178 - E181. Phenotypes and genotypes of erythromycin-resistant *Streptococcus pyogenes* strains isolated from invasive and non-invasive infections from Mexico and the USA during 1999-2010.

[34] C.S.Bates, G.E.Montañez, C.R.Woods, R.M.Vincent, Z.Eichenbaum, Infect. Immun. 71 (2003) 1042 - 1055. Identification and characterization of a *Streptococcus pyogenes* operon involved in binding of hemoproteins and acquisition of iron.

[35] B.F.Lei, M.Y.Liu, C.I.Prater, S.V.Kala, F.R.Deleo, J.M.Musser, Infect. Immun. 71 (2003) 5962 - 5969. Identification and characterization of HtsA, a second heme-binding protein made by *Streptococcus pyogenes*.

[36] H.Zhu, M.Y.Liu, B.F.Lei, BMC Microbio. 8 (2008) 15 The surface protein Shr of *Streptococcus pyogenes* binds heme and transfers it to the streptococcal heme-binding protein Shp.

[37] R.Aranda, C.E.Worley, M.Liu, E.Bitto, M.S.Cates, J.S.Olson, B.F.Lei, G.N.Phillips, J. Mol. Biol. 374 (2007) 374 - 383. Bis-methionyl coordination in the crystal structure of the heme-binding domain of the streptococcal cell surface protein Shp.

[38] B.Lei, L.M.Smoot, H.M.Menning, J.M.Voyich, S.V.Kala, F.R.Deleo, S.D.Reid,

J.M.Musser, Infect. Immun. 70 (2002) 4494 - 4500. Identification and characterization of a novel heme-associated cell surface protein made by *Streptococcus pyogenes*.

[39] M.Ouattara, E.B.Cunha, X.Li, Y.S.Huang, D.W.Dixon, Z.Eichenbaum, Mol. Microbiol. 78 (2010) 739 - 756. Shr of Group A streptococcus is a new type of composite NEAT protein involved in sequestering haem from methaemoglobin.

[40] M.Ouattara, A.Pennati, D.J.Devlin, Y.S.Huang, G.Gadda, Z.Eichenbaum, Arch. Biochem. Biophys. 538 (2013) 71 - 79. Kinetics of heme transfer by the Shr NEAT domains of Group A Streptococcus.

[41] M.Y.Liu, B.F.Lei, Infect. Immun. 73 (2005) 5086 - 5092. Heme transfer from streptococcal cell surface protein Shp to HtsA of transporter HtsABC.

[42] T.K.Nygaard, G.C.Blouin, M.Y.Liu, M.Fukumura, J.S.Olson, M.Fabian, D.M.Dooley, B.F.Lei, J. Biol. Chem. 281 (2006) 20761 - 20771. The mechanism of direct heme transfer from the streptococcal cell surface protein Shp to HtsA of the HtsABC transporter.

[43] T.S.Hanks, M.Y.Liu, M.J.McClure, M.Fukumura, A.Duffy, B.F.Lei, Infect. Immun. 74 (2006) 5132 - 5139. Differential regulation of iron- and manganese-specific MtsABC and heme-specific HtsABC transporters by the metalloregulator MtsR of group A Streptococcus.

[44] Y.C.Ran, H.Zhu, M.Y.Liu, M.Fabian, J.S.Olson, R.I.Aranda, G.N.Phillips, D.M.Dooley, B.Lei, J. Biol. Chem. 282 (2007) 31380 - 31388. Bis-methionine ligation to heme iron in the streptococcal cell surface protein Shp facilitates rapid hemin transfer to HtsA of the HtsABC transporter.

[45] B.R.Sook, D.R.Block, S.Sumithran, G.E.Montañez, K.R.Rodgers, J.H.Dawson, Z.Eichenbaum, D.W.Dixon, Biochemistry 47 (2008) 2678 - 2688. Characterization of SiaA, a streptococcal heme-binding protein associated with a heme ABC transport system.

[46] Y.C.Ran, M.Y.Liu, H.Zhu, T.K.Nygaard, D.E.Brown, M.Fabian, D.M.Dooley, B.F.Lei, Biochemistry 49 (2010) 2834 - 2842. Spectroscopic identification of heme axial ligands in HtsA that are involved in heme acquisition by *Streptococcus pyogenes*.

[47] X.Sun, R.Ge, D.Zhang, H.Sun, Q.Y.He, J. Biol. Inorg. Chem. 15 (2010) 1265 - 1273. Iron-containing lipoprotein SiaA in SiaABC, the primary heme transporter of *Streptococcus pyogenes*.

[48] J.C.Grigg, C.L.Vermeiren, D.E.Heinrichs, M.E.Murphy, J. Biol. Chem. 282 (2007) 28815 - 28822. Heme coordination by *Staphylococcus aureus* IsdE.

[49] S.Schneider, J.Marles-Wright, K.H.Sharp, M.Paoli, Nat. Prod. Reports 24 (2007) 621 - 630. Diversity and conservation of interactions for binding heme in *b*-type heme proteins.

[50] C.Fufezan, J.Zhang, M.R.Gunner, Proteins Str. Funct. Bioinf. 73 (2008) 690 - 704. Ligand preference and orientation in *b*- and *c*-type heme-binding proteins.

[51] Z.Zheng, A.R.Gunner, Proteins Str. Funct. Bioinf. 75 (2008) 719 - 734. Analysis of the electrochemistry of hemes with E(m)s spanning 800 mV.

[52] L.J.Smith, A.Kahraman, J.M.Thornton, Proteins Str. Funct. Bioinf. 78 (2010) 2349 - 2368. Heme proteins-Diversity in structural characteristics, function, and folding.

[53] T.Li, H.L.Bonkovsky, J.T.Guo, BMC Struct. Biol. 11 (2011) Structural analysis of heme proteins: Implications for design and prediction.

[54] A.Desbois, Biochimie 76 (1994) 693 - 707. Resonance Raman spectroscopy of *c*-type cytochromes.

[55] J.R.Kincaid, Methods Enzymol. 246 (1995) 460 - 501. Structure and dynamics of transient species using time-resolved resonance Raman spectroscopy.

[56] G.Smulevich, A.Feis, B.D.Howes, A.Ivancich, Handbook of Porphyrin Science with Applications to Chemistry, Physics, Materials Science, Engineering, Biology and Medicine, Vol 6: Nmr and Epr Techniques 6 (2010) 367 - 453. Structure-Function Relationships Among Heme Peroxidases: New Insights from Electronic Absorption, Resonance Raman and Multifrequency Electron Paramagnetic Resonance Spectroscopies.

[57] D.S.Culbertson, J.S.Olson, Biochemistry 49 (2010) 6052 - 6063. Role of heme in the unfolding and assembly of myoglobin.

[58] P.Garcia, M.Bruix, M.Rico, S.Ciofi-Baffoni, L.Banci, M.C.R.Shastry, H.Roder, T.D.Woodyear, C.M.Johnson, A.R.Fersht, P.D.Barker, J. Mol. Biol. 346 (2005) 331 - 344. Effects of heme on the structure of the denatured state and folding kinetics of cytochrome b_{562}.

[59] S.Hay, T.Wydrzynski, Biochemistry 44 (2005) 431 - 439. Conversion of the *Escherichia coli* cytochrome *b*(562) to an archetype cytochrome *b*: A mutant with bis-histidine ligation of heme iron.

[60] S.Manyusa, G.Mortuza, D.Whitford, Biochemistry 38 (1999) 14352 - 14362. Analysis of folding and unfolding reactions of cytochrome *b*(5).

[61] A.B.Cowley, A.Altuve, O.Kuchment, S.Terzyan, X.Zhang, M.Rivera, D.R.Benson, Biochemistry 41 (2002) 11566 - 11581. Toward engineering the stability and hemin-binding properties of microsomal cytochromes b(5) into rat outer mitochondrial membrane cytochrome b(5): Examining the influence of residues 25 and 71.

[62] J.Y.Yang, R.X.Yan, A.Roy, D.Xu, J.Poisson, Y.Zhang, Nature Methods 12 (2015) 7 - 8. The I-TASSER Suite: protein structure and function prediction.

[63] W.L.DeLano, http://www. pymol. org (2015) The PyMOL Molecular Graphics System, Version 1.7.4 Schrödinger, LLC.

[64] E.A.Berry, B.L.Trumpower, Anal. Biochem. 161 (1987) 1 - 15. Simultaneous determination of hemes *a*, *b*, and *c* from pyridine hemochrome spectra.

[65] Y.C.Ran, G.R.Malmirchegini, R.T.Clubb, B.F.Lei, Biochemistry 52 (2013) 6537 - 6547. Axial ligand replacement mechanism in heme transfer from streptococcal heme-binding protein Shp to HtsA of the HtsABC transporter.

[66] F.W.Teale, Biochim. Biophys. Acta 35 (1959) 543 Cleavage of the heme protein by acid methyl ethyl ketone.

[67] H.Yamaguchi, M.Miyazaki, Biomolecules 4 (2014) 235 - 251. Refolding techniques for recovering biologically active recombinant proteins from inclusion bodies.

[68] E.Gasteiger, C.Hoogland, A.Gattiker, S.Duvaud, M.R.Wilkins, R.D.Appel, A.Bairoch, Protein identification and analysis tools on the ExPASy server, in J.M.Walker (Ed.), The Proteomics Protocols Handbook, Humana Press, Totowa, N.J, 2005, pp. 571-607.

[69] C.N.Pace, J.M.Scholtz, Measuring the conformational stability of a protein, in T.Creighton (Ed.), Protein Structure: A Practical Approach, Oxford University Press, Oxford, 2nd edn, 1997, pp. 299-321.

[70] T.L.Ying, F.F.Zhong, J.Xie, Y.J.Feng, Z.H.Wang, Z.X.Huang, X.S.Tan, J. Bioenerg. Biomembr. 41 (2009) 251 - 257. Evolutionary alkaline transition in human cytochrome *c*.

[71] F.Arnesano, L.Banci, I.Bertini, D.Koulougliotis, Biochemistry 37 (1998) 17082 - 17092. Solution structure of oxidized rat microsomal cytochrome *b*(5) in the presence of 2 M guanidinium chloride: Monitoring the early steps in protein unfolding.

[72] P.Wittung-Stafshede, Protein Sci. 8 (1999) 1523 - 1529. Equilibrium unfolding of a small low-potential cytochrome, cytochrome c_{553} from *Desulfovibrio vulgaris*.

[73] C.Moczygemba, J.Guidry, P.Wittung-Stafshede, FEBS Lett. 470 (2000) 203 - 206. Heme orientation affects holo-myoglobin folding and unfolding kinetics.

[74] N.H.Andersen, A.Nørgaard, T.J.Jensen, J.Ulstrup, J. Inorg. Biochem. 88 (2002) 316 - 327. Sequential unfolding of the two-domain protein *Pseudomonas stutzeri* cytochrome *c*(4).

[75] R.Roncone, E.Monzani, S.Labo, A.M.Sanangelantoni, L.Casella, J. Biol. Inorg. Chem. 10 (2005) 11 - 24. Catalytic activity, stability, unfolding, and degradation pathways of engineered and reconstituted myoglobins.

[76] D.S.Culbertson, J.S.Olson, Folding and stability of myoglobins and hemoglobins, in C.M.Gomes, P.Wittung-Stafshede (Eds.), Protein Folding and Metal Ions: Mechanisms,

Biology and Disease, CRC Press, Boca Raton, FL, 2011, pp. 97-122.

[77] W.M.Atkins, R.W.Wang, A.W.Bird, D.J.Newton, A.Y.H.Lu, J. Biol. Chem. 268 (1993) 19188 - 19191. The catalytic mechanism of glutathione-S-transferase (GST) - Spectroscopic determination of the p*K*(a) of Tyr-9 in rat alpha-1-1 GST.

[78] V.Guallar, B.Olsen, J. Inorg. Biochem. 100 (2006) 755 - 760. The role of the heme propionates in heme biochemistry.

[79] J.W.Allis, J.Steinhar, Biochemistry 9 (1970) 2286 - 2293. Acid denaturation of carbonylhemoglobin - Protein unfolding without heme detachment.

[80] K.M.Kadish, K.M.Smith, R.Guilard, The Porphyrin Handbook, Academic Press, San Diego, 2000.

[81] S.N.McLachlan, G.N.La Mar, P.D.Burns, K.M.Smith, K.C.Langry, Biochim. Biophys. Acta 874 (1986) 274 - 284. ^{1}H-NMR assignments and the dynamics of interconversion of the isomeric forms of cytochrome b_5 in solution.

[82] T.C.Pochapsky, S.G.Sligar, S.J.McLachlan, G.N.La Mar, J. Am. Chem. Soc. 112 (1990) 5258 - 5263. Relationship between heme binding site structure and heme orientations of two ferrocytochrome b_5s. A study in prosthetic group recognition.

[83] S.Manyusa, D.Whitford, Biochemistry 38 (1999) 9533 - 9540. Defining folding and unfolding reactions of apocytochrome *b*(5) using equilibrium and kinetic fluorescence measurements.

[84] G.N.La Mar, N.L.Davis, D.W.Parish, K.M.Smith, J. Mol. Biol. 168 (1983) 887 - 896. Heme orientational disorder in reconstituted and native sperm whale myoglobin. Proton nuclear magnetic resonance characterizations by heme methyl deuterium labeling in the met-cyano protein.

[85] M.S.Hargrove, J.S.Olson, Biochemistry 35 (1996) 11310 - 11318. The stability of holomyoglobin is determined by heme affinity.

[86] G.Tsaprailis, D.W.S.Chan, A.M.English, Biochemistry 37 (1998) 2004 - 2016. Conformational states in denaturants of cytochrome *c* and horseradish peroxidases examined by fluorescence and circular dichroism.

[87] J.K.A.Kamal, D.V.Behere, Biochem. Eng. J. 38 (2008) 110 - 114. Kinetic stabilities of soybean and horseradish peroxidases.

[88] P.M.A.Gadsby, A.J.Thomson, FEBS Lett. 150 (1982) 59 - 63. Identification of the imidazolate anion as a ligand in metmyoglobin by near infrared magnetic circular dichroism spectroscopy.

[89] G.R.Moore, R.J.P.Williams, J.Peterson, A.J.Thomson, F.S.Mathews, Biochim. Biophys. Acta 829 (1985) 83 - 96. A spectroscopic investigation of the structure and redox

properties of *Escherichia coli* cytochrome b_{562}.

[90] G.N.La Mar, J.T.Jackson, L.B.Dugad, M.A.Cusanovich, R.G.Bartsch, J. Biol. Chem. 265 (1990) 16173 - 16180. Proton NMR study of the comparative electronic/magnetic properties and dynamics of the acid <--> alkaline transition in a series of ferricytochromes *c′*.

[91] L.Banci, I.Bertini, P.Turano, M.V.Oliver, Eur. J. Biochem. 204 (1992) 107 - 112. NOE and two-dimensional correlated ^{1}H-NMR spectroscopy of cytochrome *c′* from *Chromatium vinosum*.

[92] L.M.Saraiva, G.Denariaz, M.-Y.Liu, W.J.Payne, J.Legall, I.Moura, Eur. J. Biochem. 204 (1992) 1131 - 1139. NMR and EPR studies on a monoheme cytochrome c_{550} isolated from *Bacillus halodenitrificans*.

[93] R.Bogumil, R.Maurus, D.P.Hildebrand, G.D.Brayer, A.G.Mauk, Biochemistry 34 (1995) 10483 - 10490. Origin of the pH-dependent spectroscopic properties of pentacoordinate metmyoglobin variants.

[94] F.Arnesano, L.Banci, I.Bertini, S.Ciofi-Baffoni, T.D.Woodyear, C.M.Johnson, P.D.Barker, Biochemistry 39 (2000) 1499 - 1514. Structural consequences of *b*- to *c*-type heme conversion in oxidized *Escherichia coli* cytochrome b_{562}.

[95] J.Bixler, G.Bakker, G.McLendon, J. Am. Chem. Soc. 114 (1992) 6938 - 6939. Electrochemical probes of protein folding.

[96] J.R.Telford, P.Wittung-Stafshede, H.B.Gray, J.R.Winkler, Acc. Chem. Res. 31 (1998) 755 - 763. Protein folding triggered by electron transfer.

[97] C.J.Reedy, B.R.Gibney, Chem. Rev. 104 (2004) 617 - 649. Heme protein assemblies.

[98] C.J.Reedy, M.L.Kennedy, B.R.Gibney, Chem. Commun. (2003) 570 - 571. Thermodynamic characterization of ferric and ferrous haem binding to a designed four-a-helix protein.

5.9 Supplemental Information

5.9.1 Supplemental Figures

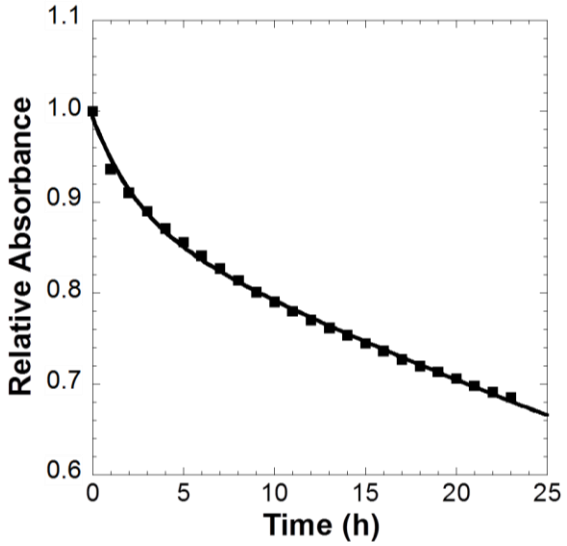

Figure 5.11 S1 Unfolding of K61A SiaA at the $D_{1/2}$ (2.5 M GdnCl). The protein was unfolded in 50 mM Tris-Cl, pH 7.0. The data were fit using the sum of a two exponential processes.

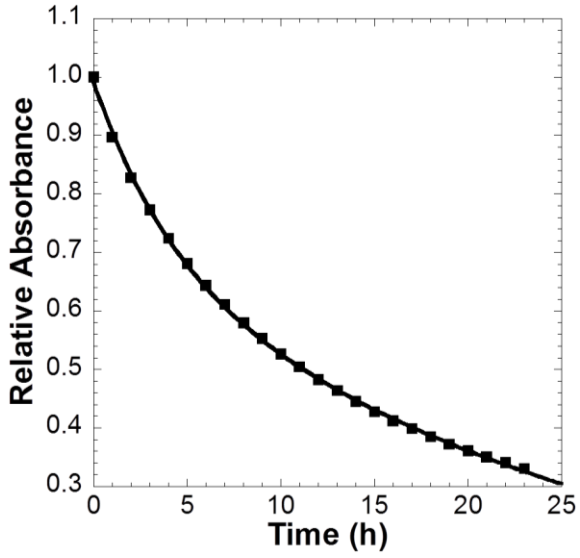

Figure 5.12 S2 Unfolding of C47A SiaA at the D1/2 (2.95 M GdnCl). The protein was unfolded in 50 mM Tris-Cl, pH 7.0. The data were fit using the sum of a two exponential processes.

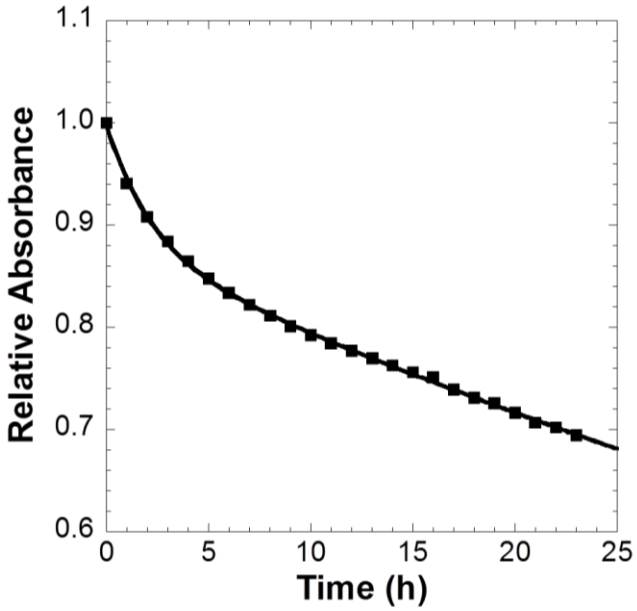

Figure 5.13 S3 Unfolding of C58A SiaA at the D1/2 (2.42 M GdnCl). The protein was unfolded in 50 mM Tris-Cl, pH 7.0. The data were fit using the sum of a two exponential processes.

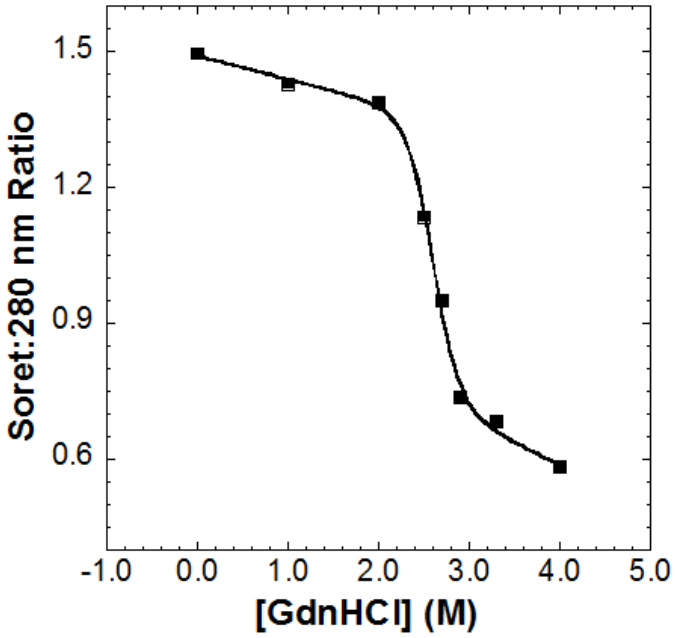

Figure 5.14 S4 GdnHCl unfolding of WT SiaA using a desalting column. The protein was unfolded in 50 mM Tris-Cl, pH 7.0. The data were fit using a two-state model and gave a D1/2 of 2.6 ± 0.1 M.

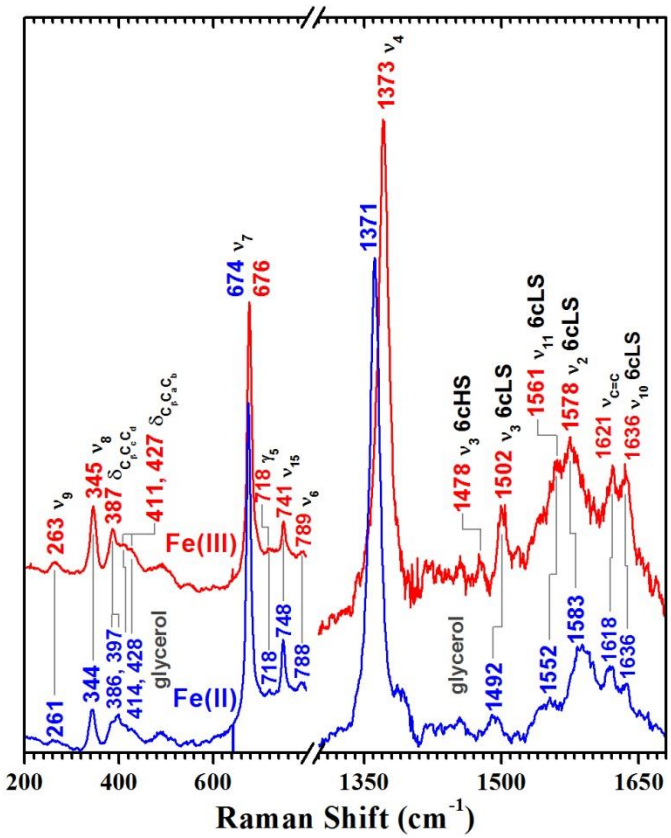

Figure 5.15 S5 Soret-excited rR spectra of ferric (top) and ferrous (bottom) C58A SiaA. The high frequency (in-plane porphyrin stretching) and low frequency regions are shown. Samples were 50 μM in holo-SiaA and 10 mM in Tris-HCl at pH 8.0. Ferrous C58A SiaA was generated by anaerobic introduction of a 10-fold molar excess of buffered dithionite to the ferric protein. Complete reduction was verified by UV-visible absorption absorbance spectroscopy.

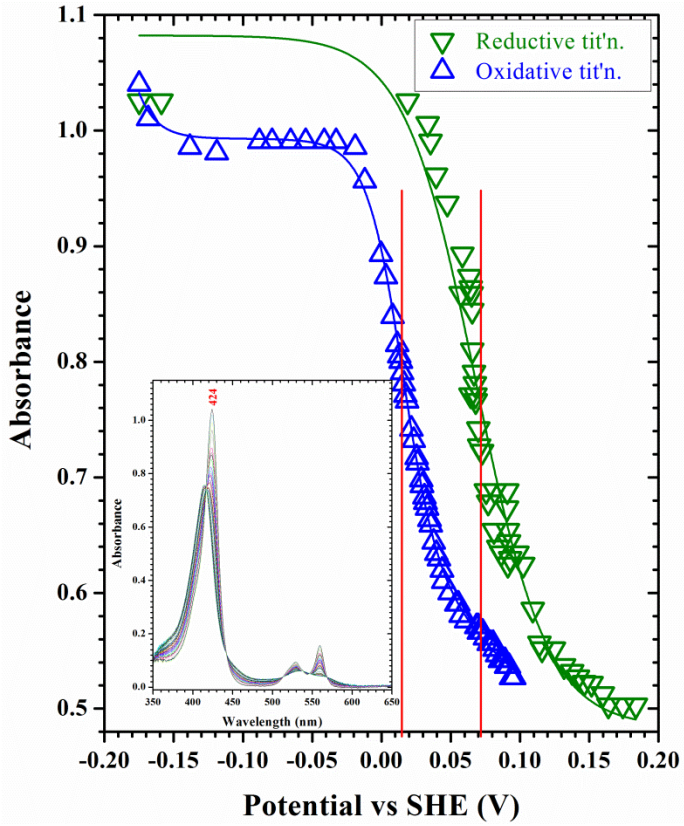

Figure 5.16 S6 Spectroelectrochemical titrations of WT SiaA. Normalized absorbance at the Soret maximum for ferrous WT SiaA (424 nm) is plotted versus cell potential (vs SHE), revealing electrochemical irreversibility of the Fe(III)|Fe(II) couple. The oxidative titration curve (Δ, blue) was best modeled by three Nernstian waves. Midpoint heme potentials at 15 and 72 mV are shown by vertical red lines. The 72 mV potential is somewhat uncertain in the oxidative curve due to the truncation of its small amplitude wave at ~100 mV. A third, very negative, potential resulted from the fitting in order to account for absorbance changes at the lowest cell potentials. This may be due to dithionite absorbance in this potential range. The reductive titration curve (Λ, green) was well modeled by a single Nernstian wave having a midpoint potential of 68 mV. The 68 and 72 mV potentials are taken to represent the same reversible Fe(III)|Fe(II) couple, which accounts for only ~40% of the heme during the titrimetric reoxidation. This behavior suggests that, following reduction and equilibration in the reducing solution, WT SiaA adopts a structure or conformation having a lowered potential of 15 mV. The small fraction of the heme having the higher potential upon reoxidation suggests the reduced conformer is kinetically slow to revert back to that of the ferric protein before reduction. Titrations were carried out in 50 mM Tris at pH 8.0, 100 mM NaCl.

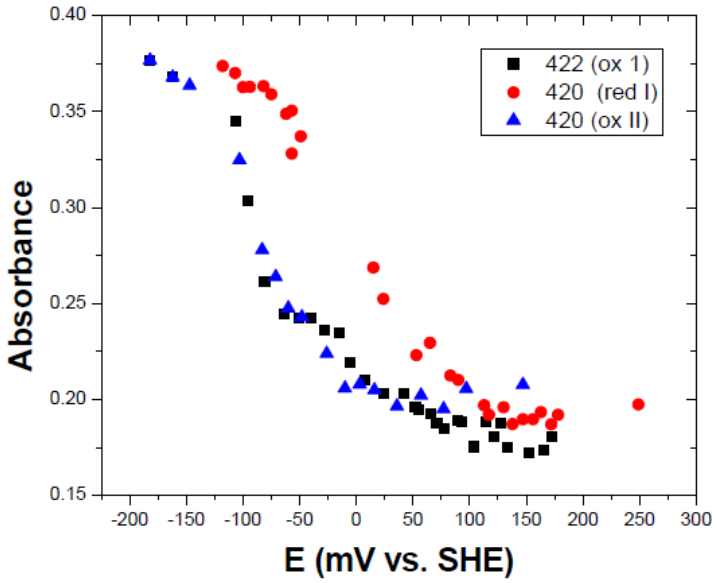

Figure 5.17 S7 Spectroelectrochemical titration of C58A. A solution of 2 μM SiaA C58A was initially reduced, oxidatively titrated with ferricyanide to yield a midpoint potential of -96 ±15 mV, reductively titrated with dithionite to yield a midpoint potential from global analysis of 1±8 mV, and oxidatively titrated with ferricyanide to yield a midpoint potential from global analysis of -120±1 mV. Titration curves at the indicated wavelengths are shown below for each titration. This suggests that the redox behavior for the protein is irreversible (similar to WT), and the oxidative potential is reproducible.

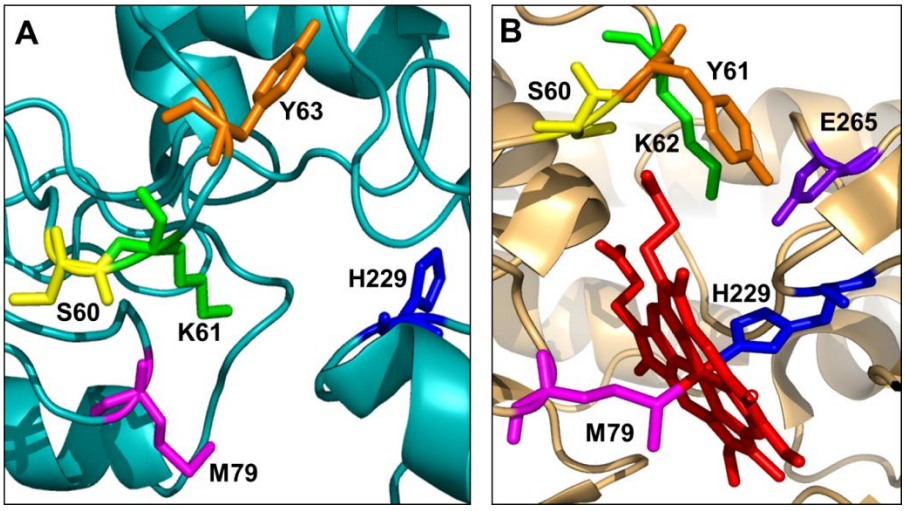

Figure 5.18 S8 Comparison of the A) S. pyogenes SiaA and B) S. aureus IsdE heme binding sites. Images are displayed using PyMOL. The structure of IsdE was downloaded from the Protein Data Bank (PDB ID: 2Q8Q).

6 ADDITIONAL STUDIES ON THE CHARACTERIZATION OF *S. PYOGENES* SIAA

Chapter 1 gave a detailed overview of heme uptake in some of the most commonly studied pathogenic bacteria. Chapter 5 was published work by our group which expanded on initial studies of the Sia heme uptake pathway involving work on WT SiaA and a series of mutants. This chapter gives additional experimental data and literature discussions related to our previously published work on SiaA. All of the experiments in this chapter were performed at Georgia State University.

6.1 Experimental

6.1.1 Expression and purification of SiaA and mutants

Expression and purification of WT, M79A, H229A, K61A, C58A, and C47A were previously described (Chapter 5). Purity of the samples was evaluated by SDS-PAGE electrophoresis and performed as previously described in Chapter 5. Extinction coefficients and heme loading were also calculated as previously described in Chapter 5.

6.1.2 Heme extraction and refolding of SiaA

Apo-SiaA was prepared using the Teale method (*1*). A solution of SiaA (2 mL) in PBS buffer, pH 7.4, was reduced to pH 2 in a drop-wise fashion using 3 M HCl. The acidic SiaA solution was mixed with cold 2-butanone for 30 s and placed on ice for 15 min. The heme layer was discarded.

To aid in protein refolding, urea was added to the apoprotein solution to a final concentration of 8 M urea (*2*). The solution sat at room temperature for 2 h. The apo-SiaA solution was dialyzed at 4˚C against 4 M urea (in PBS) for 24 h, against 2 M urea (in PBS) for 2 h, and against 10 mM KH_2PO_4, pH 7.0, for 24 h. The apoprotein solution was centrifuged at 4˚C

for 15 min at 5,000 *g* to remove any precipitate. The concentration of apo-SiaA was determined using the ExPASy $\varepsilon_{280} = 37{,}360\ M^{-1}cm^{-1}$ (*3*).

6.1.3 Optical spectroscopy

Samples of holo- and apo-SiaA were analyzed by UV-visible absorption spectroscopy using a Varian 50 Bio spectrophotometer in 1 cm quartz cuvettes at room temperature. Circular dichroism (CD) spectra were recorded using a Jasco J-810 Spectropolarimeter using quartz Suprasil cuvettes (Fisherbrand, Inc.) with a 1 mm path length. Holo- and apo-SiaA (10 μM) were recorded in 10 mM KH_2PO_4 buffer at pH 7.0 (adjusted with KOH) in a spectral window of 190 to 260 nm. The final spectrum represents an average of 10 scans.

6.1.4 Stability of holo-SiaA and apo-SiaA

Holo-SiaA (5 μM) in 50 mM Tris-Cl, pH 7.0, sat covered in a 1 cm cuvette at room temperature. A UV-visible absorption scan was taken every 48 h to monitor protein degradation for a total of 228 h. Apo-SiaA (10 μM) in 10 mM KH_2PO_4, pH 7.0, sat at room temperature in an Eppendorf tube for three days. A CD spectrum was taken every 24 h to monitor protein degradation.

6.1.5 Denaturation of apo-SiaA via guanidinium hydrochloride

A series of apo-SiaA samples (10 μM) were incubated in 10 mM KH_2PO_4, pH 7.0, and GdnCl. A stock solution of 7.83 M GdnCl in 10 mM KH_2PO_4, pH 7.0 buffer was prepared (*4*). The desired GdnCl concentration was achieved by varying the amount of buffer in the sample. All total sample volumes were 300 μL with a final concentration of 8 μM protein. The samples were incubated at room temperature overnight. CD spectra were recorded for each sample.

6.1.6 Denaturation of apo-SiaA via urea

A series of apo-SiaA samples (10 μM) were incubated in 10 mM KH_2PO_4, pH 7.0, and urea. A stock solution of 5.83 M urea in 10 mM KH_2PO_4, pH 7.0 was prepared (*4*). The desired urea concentration was achieved by varying the amount of buffer in the sample. All total sample volumes were 300 μL with a final concentration of 2.0 μM protein for the small-scale titration and 5.0 μM protein for the large-scale titration. The samples incubated at room temperature overnight. CD spectra were recorded for each sample. The raw data (millidegrees) at 222 nm were converted to molar ellipticity and plotted as a function of urea concentration.

6.1.7 Electrospray ionization (ESI) mass spectrometry

Samples of C47A (50 μM) and K61A (30 μM) were concentrated into 50 mM ammonium acetate, pH 6.8, using an Amicon centrifugal filtration unit (30,000 MWCO) following the manufacturer's protocol. Each sample was then dialyzed for five days in 50 mM ammonium acetate, pH 6.8, to remove residual salts.

ESI spectra were obtained using a Waters Micromass Q-TOF Micro mass spectrometer in the positive mode. Samples were prepared with 50:50 acetonitirile to water and 0.1% formic acid. Deconvolution of the charged state was performed using the MaxEnt program with the MassLynx™ software. Peaks were rounded to the nearest Dalton.

6.1.8 Myoglobin and SiaA unfolding and desalting

Samples of equine skeletal muscle myoglobin (2.65 μM) (Sigma-Aldrich) [extinction coefficient $\varepsilon_{410} = 188{,}000\ M^{-1}\ cm^{-1}$ (*5*)] in 50 mM Tris-Cl, pH 7.0 were incubated for 20 min at room temperature in solutions of 1.0, 1.5, 2.0, and 2.5 M GdnCl (5.93 M stock solution). Each sample was monitored by UV-visible absorption spectroscopy before loading onto a washed PD-10 desalting column (GE Healthcare). The column was equilibrated with 25 mL of 50 mM Tris-

Cl, pH 7.0. Each myoglobin sample (2.5 mL) was allowed to enter the column bed before eluting with 3.5 mL of 50 mM Tris-Cl, pH 7.0. Fractions of 500 µL were collected. The protein eluted in the third fraction. The Soret:280 nm ratios of the desalted myoglobin samples were fit to an unfolding curve in KaleidaGraph using Equation 1:

$$y = [(A_F + m_F[D]) + (A_U + m_U[D])\exp[m([D]-[D]_{1/2})/RT])]/1 + \exp[m([D]-[D]_{1/2})/RT] \quad [1]$$

where y is the absorbance at any point along the fitted denaturation curve, A_F is the absorbance of the folded state, A_U is the absorbance of the unfolded state, m is the slope at the midpoint, and also the dependence of the free energy of unfolding on the denaturant concentration, m_F is the slope of the folded state, m_U is the slope of the unfolded state, [D] is the concentration of GdnHCl, $[D]_{1/2}$ is the concentration of GdnHCl at the midpoint of the unfolding curve, R is the gas constant, and T is the temperature (Kelvin).

The same experiment was repeated using 5 µM SiaA, as described above. The samples incubated for 29 h and the data were fit using Equation 1.

6.2 Results

6.2.1 Heme extraction and refolding of SiaA

Removal of heme from holo-SiaA using the Teale method resulted in 60% recovery of the SiaA protein with a final concentration of 12 µM. The absorbance spectrum of apo-SiaA is shown in Figure 6.1. Initial protocols used to remove the heme resulted in precipitation of the protein during the refolding process. Dialysis using urea during refolding diminished protein denaturation. However, apo-SiaA samples slowly precipitated out of solution over an approximately 24 h time period at 4˚C.

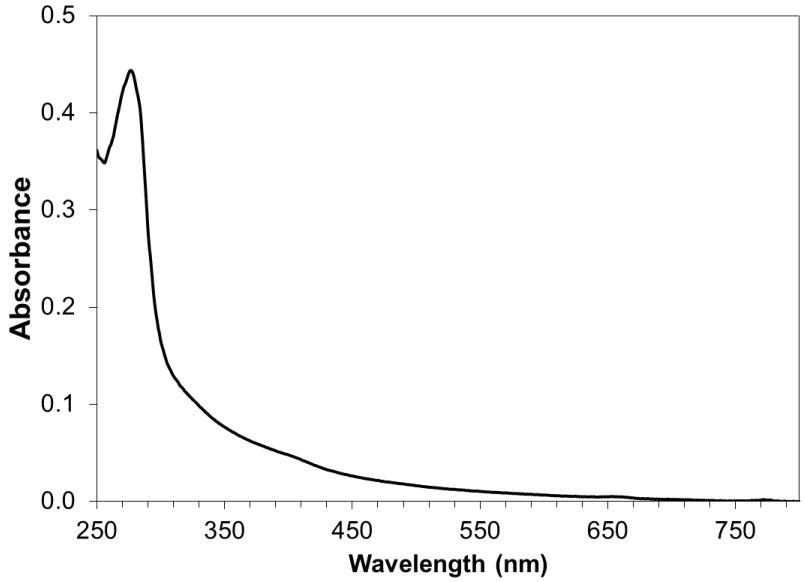

Figure 6.1 UV-visible absorption absorbance spectrum of apo-SiaA in PBS buffer, pH 7.4. The apoprotein is represented by the peak maxima at 280 nm. The final apo-SiaA concentration is 12 μM.

6.2.2 Circular dichroism spectroscopy of holo- and apo-SiaA

A comparison of normalized holo- and apo-SiaA CD spectra is shown in Figure 6.2. Both proteins contain bands around 190, 210, and 222 nm, indicative of α-helical content. The band at 210 nm is more pronounced for the apoprotein compared to the holoprotein. This would indicate that the overall fold of the protein is altered upon heme removal from the protein.

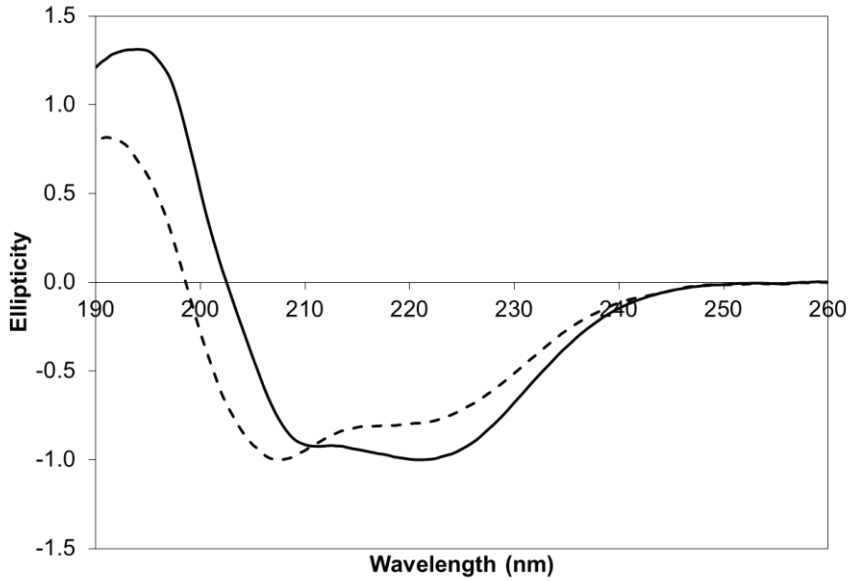

Figure 6.2 Normalized circular dichroism spectra of holo-SiaA (solid line) and apo-SiaA (dashed line). Samples (10 μM) were recorded in 10 mM phosphate buffer, pH 7.0.

6.2.3 Stability studies of holo- and apo-SiaA

Holo- and apo-SiaA were allowed to sit at room temperature for twelve and three days, respectively. Holo-SiaA was monitored every 48 h using UV-visible absorption spectroscopy while apo-SiaA was monitored every 24 h using CD spectroscopy. Holo-SiaA showed a slow increase of the 280 nm band over the twelve day time period (Figure 6.3). Apo-SiaA slowly precipitated out of solution (Figure 6.4). The normalized apo-SiaA spectra of each time point showed the protein to have the same secondary structure over the three days (Figure 6.5).

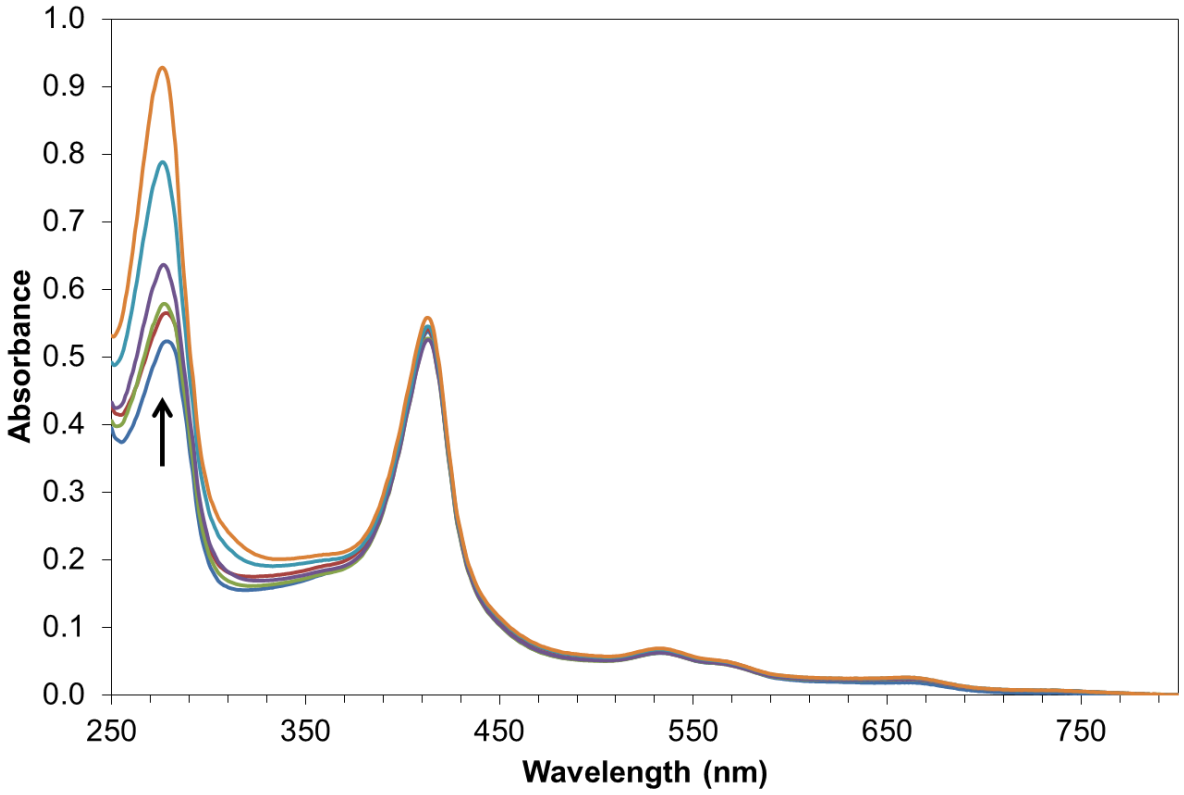

Figure 6.3 UV-visible absorption spectra of WT SiaA at 48 h time intervals (total time 228 h). The protein solution sat covered at room temperature in 50 mM Tris-Cl, pH 7.0 between readings. Protein degradation is shown by the increase in the 280 nm band over time indicated by the arrow.

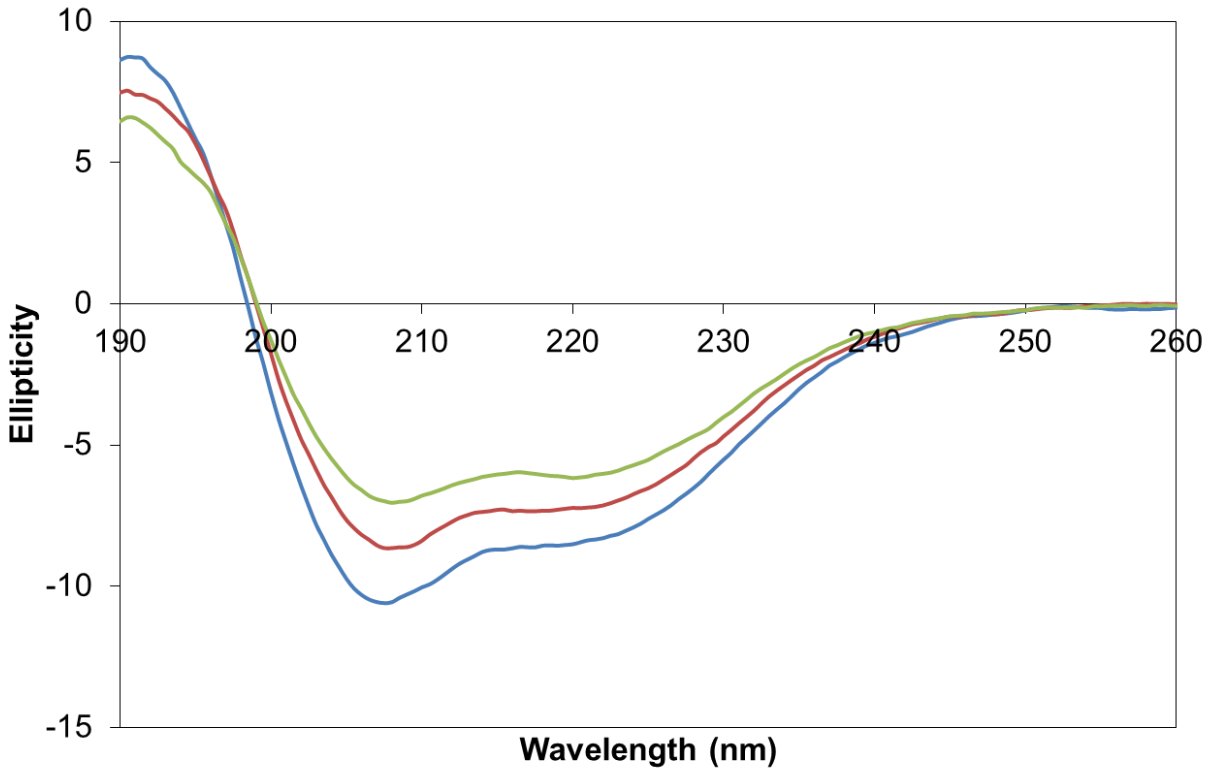

Figure 6.4 Circular dichroism spectra of apo-SiaA over a 72 h period. The protein solution sat covered in a cuvette at room temperature. A scan was taken every 24 h to monitor changes. The sample was in 10 mM potassium phosphate, pH 7.0. The scans are as follows: 24 h (blue), 48 h (red), and 72 h (green).

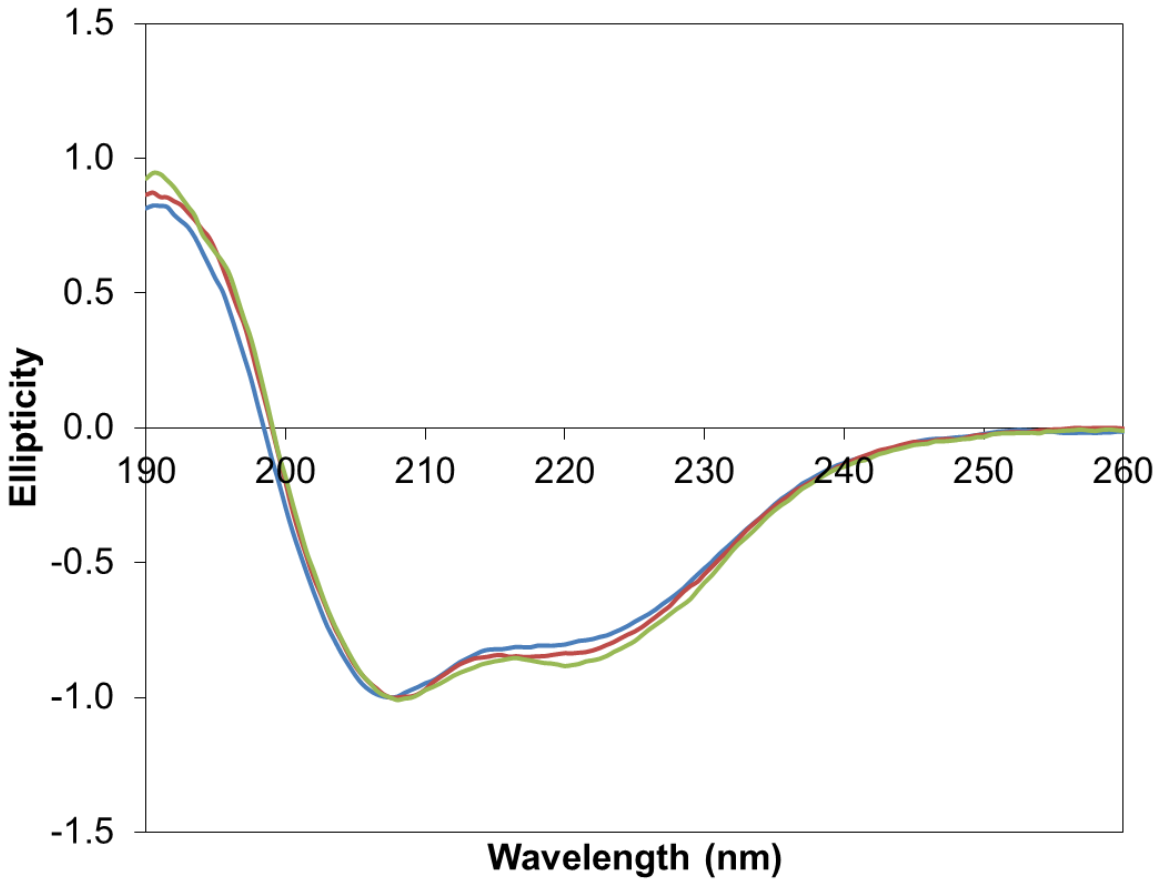

Figure 6.5 Normalized circular dichroism spectra of apo-SiaA from the previous figure. Spectra are normalized at 208 nm.

6.2.4 Denaturation of apo-SiaA

Holo-SiaA unfolds very slowly with a midpoint GdnCl concentration of 3.1 M (*6*). In an initial small-scale titration, freshly prepared apo-SiaA samples were incubated for 2 h with GdnCl at varying concentrations to determine an approximate $D_{1/2}$. The protein appeared to unfold between 0 and 1.5 M GdnCl (Figure 6.6). To ensure the samples incubated long enough, spectra were recorded again after 16 h; unfolding was complete after 2 h (Figure 6.7).

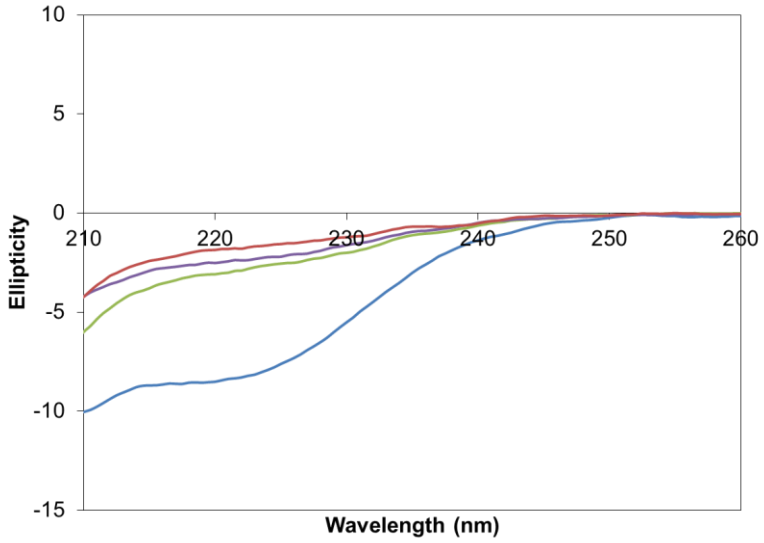

Figure 6.6 Circular dichroism spectra of apo-SiaA samples at different GdnCl concentrations for D1/2 determination. Samples are as follows: 0 M GdnCl (blue), 0.5 M GdnCl (purple), 1.0 M GdnCl (green), and 1.5 M GdnCl (red). Spectra were recorded in 10 mM potassium phosphate, pH 7.0. All of the samples were incubated at room temperature for 16 h.

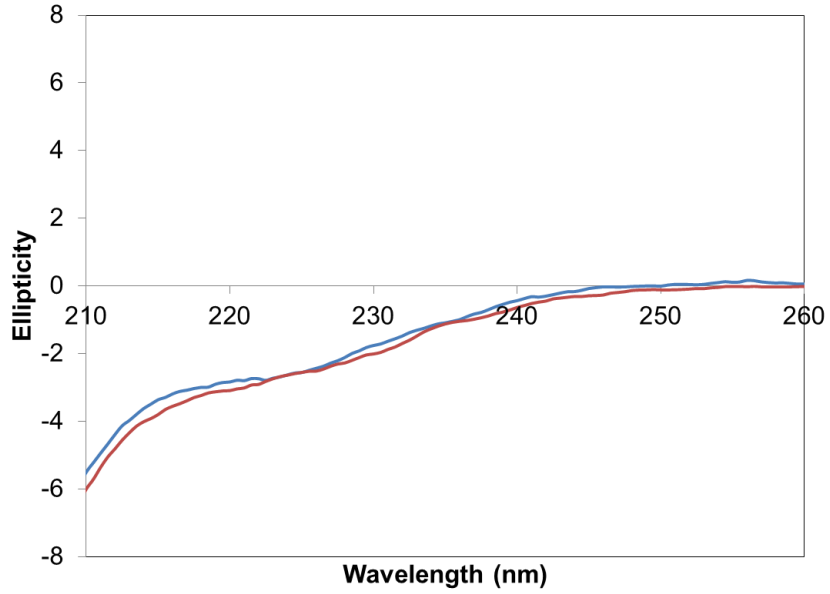

Figure 6.7 Circular dichroism spectra of apo-SiaA (8 μM) incubated for 2 h (blue) and for 16 h (red) with 1.0 M GdnCl. Samples were recorded in 10 mM potassium phosphate, pH 7.0 and incubated at room temperature.

Incubation of the same apo-SiaA stock used for the small-scale experiment (but after sitting at 4˚C for 24 h) with GdnCl was used to complete a full titration. The data showed the protein had started to precipitate out of solution. To confirm this, spectra comparing apo-SiaA at 0.5 M GdnCl from the small-scale titration were compared to the large-scale titration apo-SiaA at 0.5 M GdnCl (Figure 6.8). The decreases in negative intensity indicate protein precipitation.

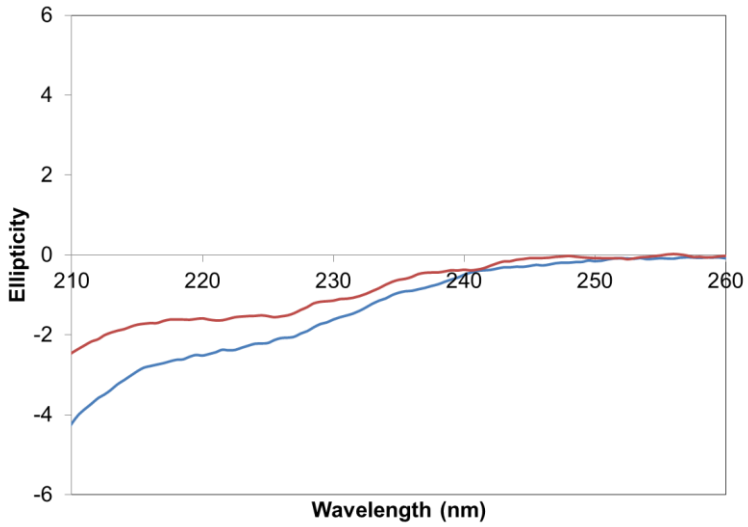

Figure 6.8 Circular dichroism spectra of 8 μM apo-SiaA in 0.5 M GdnCl after incubation at room temperature for 16 h. Guanidinium was added either directly after preparation (blue) (from Figure 6.7) or after standing at 4 °C for 24 h (red).

GdnCl is a strong denaturant and may unfold the protein too readily; it is common to investigate the unfolding of apo heme proteins with urea which is a milder denaturant (*2*). Freshly prepared apo-SiaA was used within the first 24 h after completion of the refolding process to diminish the amount of precipitation in the sample. An initial small-scale titration (using very little protein) was performed to determine an approximate midpoint value (Figure 6.9). The results indicated apo-SiaA to have a $D_{1/2}$ ~ 1.5 M. A complete titration of apo-SiaA with urea (Figure 6.10) gave a shallow unfolding curve (Figure 6.11). The apparent $D_{1/2}$ is ~ 1.4 to 1.7 M.

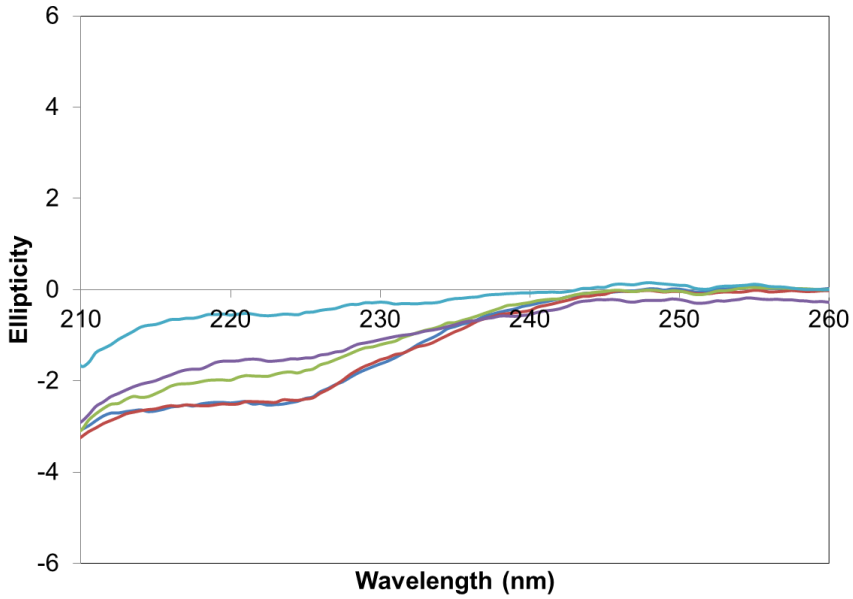

Figure 6.9 Circular dichroism spectra of an initial urea unfolding titration with apo-SiaA (2.0 μM). Samples were scanned in 10 mM potassium phosphate, pH 7.0. Urea concentrations were from 0 to 2.8 M as follows: 0 M (dark blue), 0.75 M (red), 1.49 M (green), 2.2 M (purple), and 2.8 M (light blue). The samples incubated for 2 h at room temperature.

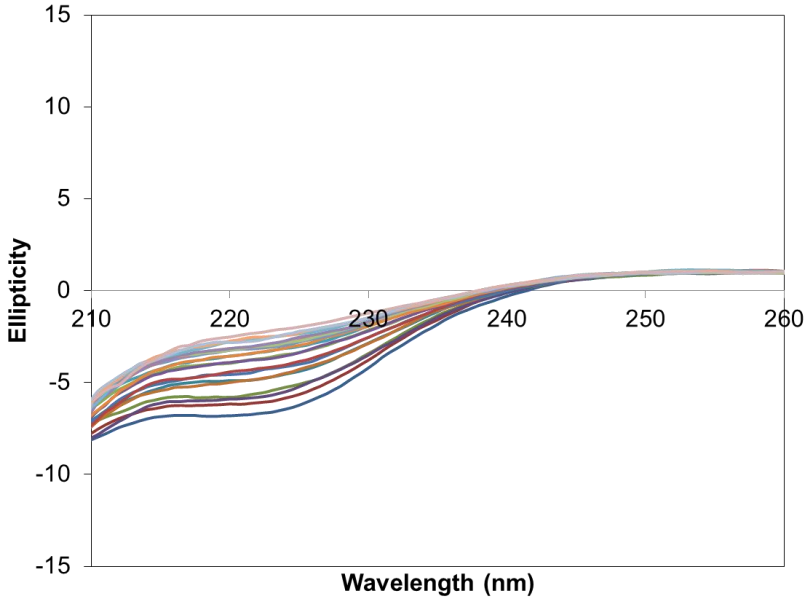

Figure 6.10 Circular dichroism spectra of a urea-induced apo-SiaA (5.1 μM) unfolding titration. Samples were made in 0 to 3 M urea. Samples were recorded in 10 mM potassium phosphate, pH 7.0 and incubated at room temperature for 16 h.

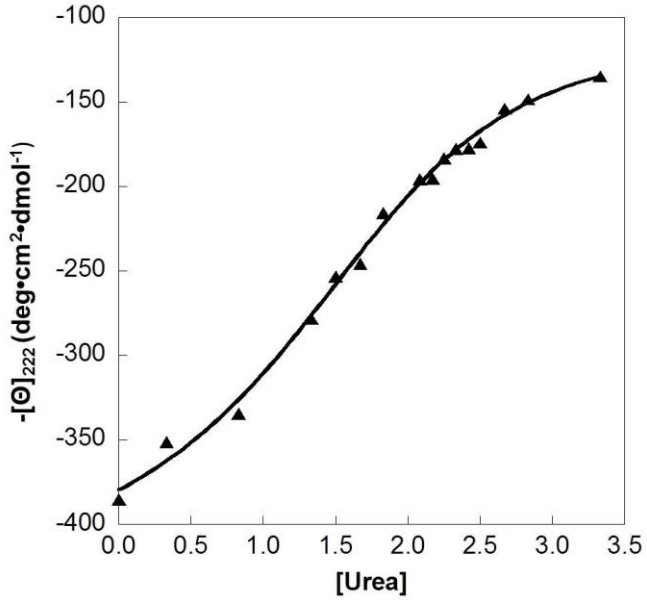

Figure 6.11 Circular dichroism molar ellipticity at 222 nm versus urea concentration. The full spectra are given in the previous figure. The data were fit to the unfolding equation given in the Experimental. The apparent $D_{1/2}$ is between 1.5 and 1.7 M urea.

6.2.5 Myoglobin and SiaA unfolding and desalting

A solution of myoglobin was divided into aliquots to which different concentrations of GdnCl were added. These solutions were passed through a desalting column to remove any heme not tightly bound to the protein. The Soret:280 nm ratios of the eluents were plotted against GdnCl concentration to obtain an unfolding curve with a $D_{1/2}$ of 1.9 ± 0.6 M. The guanidinium-induced $D_{1/2}$ for this myoglobin assessed via UV/visible spectroscopy was 1.38 ± 0.02 M (data not shown).

The same experiment was also performed using holo-SiaA which has a reported $D_{1/2}$ value of 3.1 M (*6*). The $D_{1/2}$ value assessed via the desalting technique was 2.59 ± 0.05 M.

6.2.6 ESI mass spectrometry

Mass spectrometry data were obtained for C47A and K61A. The deconvoluted spectrum of C47A gave an observed mass of 36,062 Da. The expected mass of the holo-protein is 36,071 Da (Figure 6.12). C47A gave charge state window from +12 to +21.

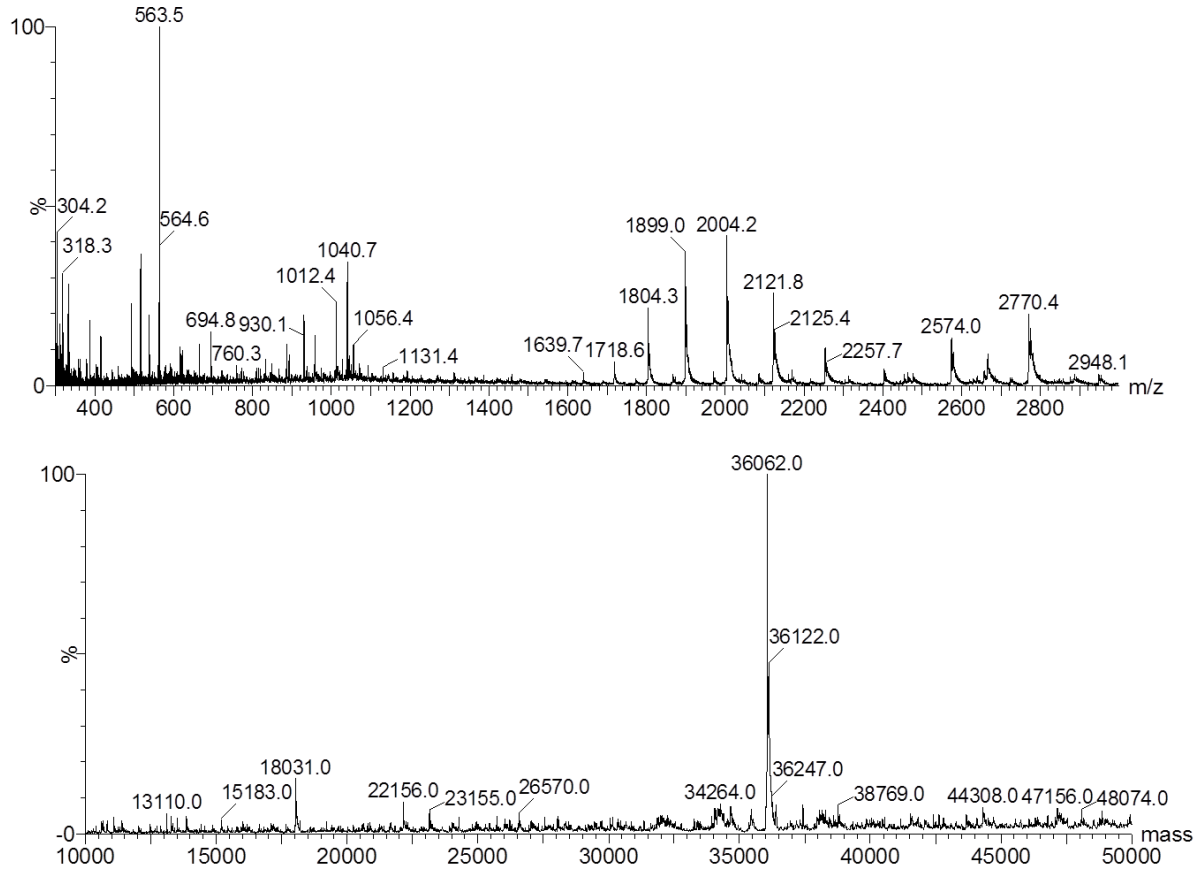

Figure 6.12 Electrospray mass spectrum of SiaA C47A. The sample was prepared in 50:50 acetonitrile:ammonium acetate and 0.1% formic acid. Top panel: charge distribution spectrum. Bottom panel: The SiaA C47A peak is seen at 36,062 Da. The expected peak is 36,071 Da.

The deconvoluted spectrum of K61A gave an observed mass of 36,037 Da. The expected mass of the holo-protein is 36,046 Da (Figure 6.13). K61A also gave a charge state window range of +13 to +20, similar to C47A.

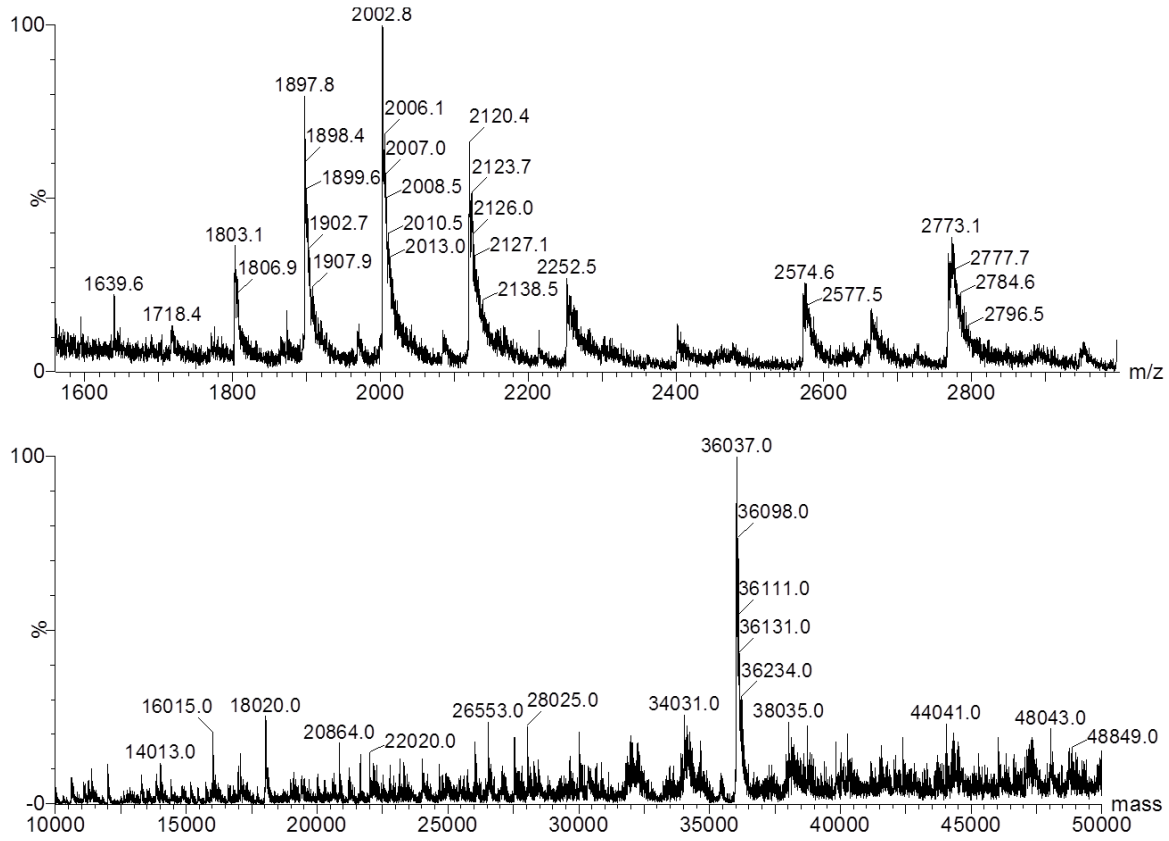

Figure 6.13 Electrospray mass spectrum of SiaA K61A. The sample was prepared in 50:50 acetonitrile:ammonium acetate and 0.1% formic acid. Top panel: charge distribution spectrum. Bottom panel: The SiaA C47A peak is seen at 36,037 Da. The expected peak is 36,046 Da.

6.3 Discussion

6.3.1 Heme extraction and refolding of SiaA

SiaA was very sensitive to the extraction and refolding process. Heme extraction requires the use of a strong acid to successfully remove the heme from the active site by reducing the pH of the environment and therefore eliminating interactions between the heme moiety and the protein (*1*). Butanone (methyl ethyl ketone) is used to separate the heme from the aqueous protein layer and to ensure the free heme stays in solution after separation. The exposure of proteins to acidic environments and organic chemicals such as butanone can damage the protein during the extraction process.

Initial attempts to prepare apo-SiaA involved extracting the heme and then allowing the protein to dialyze first in sodium bicarbonate and then by the buffer of choice. Using this protocol, apo-SiaA precipitated out of solution once the heme was removed and did not go back into solution.

Protein precipitation during the refolding process results from the presence of protein aggregates and other inactive forms of proteins in solution (*2*). It has been shown that using urea (or any other denaturant) during the refolding process allows the protein to properly fold and diminish or prevent precipitation (*7*). The refolding of apo-SiaA using urea proved to be successful, although not all of the protein stayed in solution. Protein precipitation upon heme removal has been seen in other systems. For example, cytochrome c_{551} from *Pseudomonas aeruginosa* precipitates out of solution during refolding after heme extraction (*8*). The same result was also seen in cytochrome P450 from rat liver microsomes (RLM) (*9*).

6.3.2 Circular dichroism spectroscopy of holo- and apo-SiaA

Circular dichroism comparison of holo- vs. apo-SiaA showed different protein conformations between the two forms of the protein (Figure 6.2). Both apo- and holo-SiaA gave bands around 190, 210, and 222 nm, indicative of α-helical structure. This is consistent with the I-TASSER homology modeling predictions discussed above. Holo-SiaA gave two negative bands at 210 and 222 nm, with the 222 nm band a more negative minima than the 210 nm band. Apo-SiaA also has two negative bands at 208 and 222 nm with the most negative minima at 208 nm, rather than at 222 nm as seen with holo-SiaA. There is also a positive peak at 192 nm compared to holo-SiaA which has a more intense positive peak at 195 nm and is indicative of increased α-helical content.

An increase in α-helical content upon the binding of heme has also been seen in other systems. Apo-cytochrome b_{562} from *Escherichia coli* was shown by circular dichroism to also go under a conformational change once heme is bound (*10*). CD data were interpreted using CONTIN and showed that apo-cytochrome b_{562} has ~60% helicity while the holoprotein has ~80%. For sperm whale myoglobin, an increase is seen in helicity from 60% for apo-myoglobin compared to 71% for holo-myoglobin (*11*). This trend is also seen in RLM cytochrome P450 in which the apoprotein loses α-helical content upon heme removal (*9*). In contrast, previous studies on SiaA were interpreted as indicating significantly more helical structure in the apoprotein (*12*). Additionally, proteins involved in heme transfer are more open in the apo form, as shown by crystallography (*13*). This is expected, as they must fluctuate between an open and closed form during the heme binding and release processes.

6.3.3 Denaturation and stability studies of Holo- and apo-SiaA

Using circular dichroism, it was confirmed that apo-SiaA slowly precipitates out of solution over time. Figure 6.4 shows apo-SiaA to precipitate out by about 20% every 24 h at room temperature. Although the protein is precipitating, Figure 6.5 shows the protein is not changing in overall conformation over time.

The precipitation of apo-SiaA was also seen during denaturation studies with GdnCl. Initial GdnCl unfolding experiments were performed using apo-SiaA prepared on the same day as incubation of the samples for the titration. The full-scale titration was performed two days later using the same stock solution made for the small-scale titration. Therefore, samples from either titration, at the same GdnCl concentration, should give the same CD spectra. Figure 6.6 shows that the samples do not give the same spectra. Since the signal intensity is decreased for the large-scale titration, it appears that the stock solution had begun to precipitate out of solution.

Overall, it may be the case that apo-SiaA cannot be stored for long periods of time and must be freshly prepared for each experiment.

The stability of the holo-SiaA was investigated, as shown in Figure 6.3, with UV-visible absorption spectroscopy. Over a period of twelve days, heme continued to stay bound to the protein, as indicated by the position and shape of the Soret and the presence of well-defined α,β-bands. The appearance of free heme can be monitored spectrally by the appearance of a shoulder around 380 nm and the loss of defined bands in the α,β-region. These features were not observed for holo-SiaA, indicating heme is still bound at the active site after twelve days. However, the absorbance at the 280 nm band continuously increased over time. This could possibly be insoluble apo-SiaA slowly going into solution. In the case of apo-SiaA, protein samples were kept in buffers of low ionic strength for CD purposes. Holo-SiaA is purified and stored in buffers with much higher ionic strengths. Holo-SiaA may be purified with partial amounts of insoluble apo-SiaA that go into solution over time.

Preliminary studies showed GdnCl to be too strong of a denaturant and completely unfolded the protein, even at concentrations less than 0.1 M. Alternatively, urea was used to study the unfolding of apo-SiaA. A small-scale unfolding titration on freshly prepared apo-SiaA indicated the $D_{1/2}$ was between 1.4 - 1.7 M. A full-scale unfolding titration was then performed on the same stock of apo-SiaA prepared the same day as the titration to diminish the chances of precipitation. The unfolding curve (Figure 6.11) shows a shallow curve with an apparent $D_{1/2}$ range of 1.5 - 1.7 M. The errors in the fit indicate that this is not a good fit for the data. This is expected if the protein is slowly precipitating out of solution.

The $D_{1/2}$ for apo-SiaA in urea is considerably less than the $D_{1/2}$ for holo-SiaA of 3.1 M in GdnCl. Urea is not as strong of a denaturing agent as GdnCl and has been used to unfold apo-

hemoproteins, which tend to be easier to unfold when the heme is not bound to the protein (*14*). There are a few examples of unfolding studies comparing apo vs. holo heme proteins (Table 6.1). Apo-SiaA unfolding is most similar to cytochrome c_{551} from *P. aeruginosa* (not shown in Table) which becomes unstable in the apo-form and unfolds around the same midpoint as apo-SiaA (1.6 M in urea) (*8*). In all of the studies, the apoprotein was easier to unfold than the holoprotein, as seen for SiaA.

Rates of holo vs. apoprotein unfolding are known in a few instances; as expected, the apoprotein unfolds much faster than the holoprotein. For example, apo-horseradish peroxidase and apo-soybean peroxidase unfold rapidly while their holo counterparts unfold slowly (*15*). Apo-Mc cyt b_5 unfolds much faster than holo-Mc cyt b_5, with rates of ~0.2 s^{-1} and ~ 4.5 x 10^{-6} s^{-1}, respectively (*16*). For SiaA, the apoprotein unfolds completely in ~2 h while the holoprotein has a half-life ~24 h (this work).

6.3.4 $D_{1/2}$ determination of myoglobin and holo-SiaA desalting

It has been shown that heme protein unfolding and heme release can occur in different ways. For example, ferric hemoglobin unfolds in a way that allows the heme to leave the active site while the protein is unfolding (*17*). In this case, protein unfolding leads to heme release. Carboxyhemoglobin unfolds completely while the heme moiety stays bound at the active site before release (*17*). Myoglobin unfolding is shown to fit to a six-state model, indicative of a more complicated unfolding process with heme-bound intermediates (*18*).

To investigate protein heme retention upon unfolding, the protein with various concentration of denaturant was run through a desalting column, which is expected to remove

Table 6.1 Comparison of D1/2 values of b-type holo- and apo-hemoproteins.

Protein	Source of Protein	Method	Conditions	GdnCl $D_{1/2}$ (M)		Urea $D_{1/2}$ (M)	
				Holo	Apo	Holo	Apo
Cytochrome b_{562}	*E. coli*	Absorbance	pH 5.0, 20 ˚C	2.15 ± 0.2 (*19*)	--	--	--
		Absorbance	pH 7.0	1.8 (*20*)	--	--	--
		CD	pH 7.0, 22 ˚C	--	--	~ 4.9 (*10*)	~ 2.3 (*10*)
OM Cytochrome b_5	Rat microsomal	NMR	pD 7.0, in D_2O	2.6 ± 0.3 (*21*)	--	--	--
		Absorbance	pH 7.0, 25 ˚C	3.64 ± 0.1 (*22*)	--	--	--
		Fluorescence		3.51 ± 0.1 (*22*)	1.2 ± 0.2 (*22*)	--	--
MC Cytochrome b_5	Bovine microsomal	Absorbance	pH 7.0, 25 ˚C	3.05 ± 0.1 (*22*)	--	--	--
		Fluorescence		2.99 ± 0.1 (*22*)	1.6 (*22*)	--	--
FixLH	*B. japonicum*	CD	pH ~ 8.8, 20 ˚C	--	--	4.2 ± 0.3 (*23*)	Not reported
Myoglobin	Sperm whale	Absorbance	pH 8.0	2 (*24*)	--	--	--
		CD		--	~ 1.6 (*24*)	--	--
	Equine Skeletal Muscle	UV/DSTD	pH 6.6, 25 ˚C	1.8 (*14;25*)	--	3.9 (*25*)	--
			pH 5.7, 25 ˚C	--	--	6.6 (*14*)	--
			pH 7.0, 25 ˚C	2.44 (*14;26*)	--	--	--
			pH 7.0, 20 ˚C	1.5 (*14;27*)	--	--	--
			pH 7.2, 20 ˚C	1.7 (*14*)	--	7.6 (*14*)	--
SiaA	*S. pyogenes*	Absorbance	pH 7.0, 22 ˚C	3.1 (*6*)	--	--	--
		CD		--	--	--	~ 1.5-1.7 (this work)

unbound heme. When the experiment was performed on myoglobin, a $D_{1/2}$ of 1.9 M was obtained. This is very similar to values in the literature, which range between 1.5 M (*27*) and 1.8 M (*25*). However, these results were very different than observed previously by Moczygemba et al., who observed that the heme remained bound up to 5 M GdnCl, indicating that the heme stays bound to both the partially unfolded and fully unfolded protein (*27*). The difference in these experiments may indicate a significant role of the experimental conditions and type of resin in this type of experiment.

A control experiment using partially denatured myoglobin and the desalting column were performed. The unfolding of myoglobin in the literature has been extensively characterized and various $D_{1/2}$ values have been reported between 1.5 M (*27*) and 1.8 M (*25*). These values are less than the $D_{1/2}$ for myoglobin (1.9 M) which has been passed through a desalting column. This would indicate that heme stays bound to the protein as it unfolds which is in correlation with previous studies of myoglobin unfolding described above. Heme binds very tightly to myoglobin. Therefore, it is not unexpected that the heme will stay bound to the protein, even once the protein has been partially unfolded.

In comparison, SiaA shows a lower $D_{1/2}$ measured using the desalting column compared to that measured via optical spectroscopy. The apparent decrease in the $D_{1/2}$ is consistent with the unfolding process priming the release of the heme molecule. Unfolding may act as a trigger for the protein to pass the heme off to the next acceptor in the pathway, in preparation for loading of another heme molecule.

6.3.5 ESI mass spectrometry

Mass spectrometry of C47A gives two charge state envelopes in the charge state window; one from +12 to +14 and the other from +15 to +21. The deconvoluted region gives a mass of

36,062 Da which corresponds to the mass of the expected holoprotein (36,071 Da). Only the holoprotein is detected by the spectrometer indicating the two charge envelopes are both forms of holo-C47A SiaA.

A similar result is obtained in the mass spectrum for K61A. The charge state window shows two envelopes: +13 to +14 and +16 to +20 with maxima at +13 and +18, respectively. The deconvoluted region gives a mass of 36,037 Da which corresponds to the mass of the expected holoprotein (36,046 Da). Only the holoprotein is detected by the spectrometer indicating the two charge envelopes are both forms of holo-K61A SiaA.

Multiple charge state envelopes representing the same form of the protein have also been seen in myoglobin (*28*). Fully folded holo-Mb exhibits a small charge envelope from +10 to +7, centered at +9. As acetic acid is added to the protein, the pH decreases and the Mb begins to unfold. This results in an expanded charge envelope with multiple peaks representing partially unfolded holo-Mb. As the protein completely unfolds, heme leaves the protein, the number of peaks in the charge window increases, and the entire charge envelope shifts to lower m/z ratios representing the unfolded apo-Mb.

It could be the case for both C47A and K61A that the spectra represent a mixture of folded holoprotein and partially unfolded holoprotein. Acetonitrile and 0.1% formic acid were added to the samples to enhance signal to noise and to reduce the pH to ensure protonation, respectively. Addition of the organic solvent and exposure to low pH could have induced the alternative fold of the protein and led to different protonation states of the protein samples.

6.4 References

1. Teale, F. W. (1959) Cleavage of the heme protein by acid methyl ethyl ketone. *Biochim. Biophys. Acta 35*, 543.

2. Yamaguchi, H. and Miyazaki, M. (2014) Refolding techniques for recovering biologically active recombinant proteins from inclusion bodies. *Biomolecules 4*, 235-251.

3. Gasteiger, E., Hoogland, C., Gattiker, A., Duvaud, S., Wilkins, M. R., Appel, R. D., and Bairoch, A. (2005) Protein identification and analysis tools on the ExPASy server, in *The Proteomics Protocols Handbook* (Walker, J. M., Ed.) pp 571-607, Humana Press, Totowa, N.J.

4. Castellino, F. J. and Barker, R. (1968) Denaturing effectiveness of guanidinium carbamoylguanidinium and guanylguanidinium salts. *Biochemistry 7*, 4135-4138.

5. Antonini, E. and Brunori, M. (1971) *Hemoglobin and Myoglobin in their Reactions with Ligands* North-Holland Publishing Company, Amsterdam.

6. Sook, B. R., Block, D. R., Sumithran, S., Montañez, G. E., Rodgers, K. R., Dawson, J. H., Eichenbaum, Z., and Dixon, D. W. (2008) Characterization of SiaA, a streptococcal heme-binding protein associated with a heme ABC transport system. *Biochemistry 47*, 2678-2688.

7. Tsumoto, K., Ejima, D., Kumagai, I., and Arakawa, T. (2003) Practical considerations in refolding proteins from inclusion bodies. *Protein Expr. Purif. 28*, 1-8.

8. Borgia, A., Gianni, S., Brunori, M., and Travaglini-Allocatelli, C. (2008) Fast folding kinetics and stabilization of apo-cytochrome c. *FEBS Lett. 582*, 1003-1007.

9. Yu, X. C., Shen, S., and Strobel, H. W. (1995) Denaturation of cytochrome P450 2B1 by guanidine hydrochloride and urea: Evidence for a metastable intermediate state of the active site. *Biochemistry 34*, 5511-5517.

10. Feng, Y. Q. and Sligar, S. G. (1991) Effect of heme binding on the structure and stability of *Escherichia coli* apocytochrome b_{562}. *Biochemistry 30*, 10150-10155.

11. Harrison, S. C. and Blout, E. R. (1965) Reversible conformational changes of myoglobin and apomyoglobin. *J. Biol. Chem. 240*, 299-&.

12. Sun, X., Ge, R., Zhang, D., Sun, H., and He, Q. Y. (2010) Iron-containing lipoprotein SiaA in SiaABC, the primary heme transporter of *Streptococcus pyogenes*. *J. Biol. Inorg. Chem. 15*, 1265-1273.

13. Smith, L. J., Kahraman, A., and Thornton, J. M. (2010) Heme proteins-Diversity in structural characteristics, function, and folding. *Proteins Str. Funct. Bioinf. 78*, 2349-2368.

14. Bramanti, E., Allegrini, C., Onor, M., Raspi, G., Skogerboe, K. J., and Synovec, R. E. (2006) Flow injection analysis with diode array absorbance detection and dynamic surface tension detection for studying denaturation and surface activity of globular proteins. *Anal. Biochem. 351*, 100-113.

15. Kamal, J. K. A. and Behere, D. V. (2008) Kinetic stabilities of soybean and horseradish peroxidases. *Biochem. Eng. J. 38*, 110-114.

16. Manyusa, S., Mortuza, G., and Whitford, D. (1999) Analysis of folding and unfolding reactions of cytochrome *b*(5). *Biochemistry 38*, 14352-14362.

17. Allis, J. W. and Steinhar, J. (1970) Acid denaturation of carbonylhemoglobin - Protein unfolding without heme detachment. *Biochemistry 9*, 2286-2293.

18. Culbertson, D. S. and Olson, J. S. (2010) Role of Heme in the Unfolding and Assembly of Myoglobin. *Biochemistry 49*, 6052-6063.

19. Arnesano, F., Banci, L., Bertini, I., Koulougliotis, D., and Monti, A. (2000) Monitoring mobility in the early steps of unfolding: The case of oxidized cytochrome *b*(5) in the presence of 2 M guanidinium chloride. *Biochemistry 39*, 7117-7130.

20. Wittung-Stafshede, P., Lee, J. C., Winkler, J. R., and Gray, H. B. (1999) Cytochrome b_{562} folding triggered by electron transfer: Approaching the speed limit for formation of a four-helix-bundle protein. *Proc. Natl. Acad. Sci. USA 96*, 6587-6590.

21. Arnesano, F., Banci, L., Bertini, I., and Koulougliotis, D. (1998) Solution structure of oxidized rat microsomal cytochrome *b*(5) in the presence of 2 M guanidinium chloride: Monitoring the early steps in protein unfolding. *Biochemistry 37*, 17082-17092.

22. Silchenko, S., Sippel, M. L., Kuchment, O., Benson, D. R., Mauk, A. G., Altuve, A., and Rivera, M. (2000) Hemin is kinetically trapped in cytochrome *b*(5) from rat outer mitochondrial membrane. *Biochem. Biophys. Res. Commun. 273*, 467-472.

23. Landfried, D. A., Vuletich, D. A., Pond, M. P., and Lecomte, J. T. J. (2007) Structural and thermodynamic consequences of *b* heme binding for monomeric apoglobins and other apoproteins. *Gene 398*, 12-28.

24. Hargrove, M. S. and Olson, J. S. (1996) The stability of holomyoglobin is determined by heme affinity. *Biochemistry 35*, 11310-11318.

25. Ahmad, F. and Bigelow, C. C. (1982) Estimation of the free energy of stabilization of ribonuclease A, lysozyme, alpha-lactalbumin, and myoglobin. *J. Biol. Chem. 257*, 12935-12938.

26. Saito, Y. and Wada, A. (1983) Comparative-Study of GuHCl Denaturation of Globular-Proteins .2. A Phenomenological Classification of Denaturation Profiles of 17 Proteins. *Biopolymers 22*, 2123-2132.

27. Moczygemba, C., Guidry, J., and Wittung-Stafshede, P. (2000) Heme orientation affects holo-myoglobin folding and unfolding kinetics. *FEBS Lett. 470*, 203-206.

28. Sogbein, O. O., Simmons, D. A., and Konermann, L. (2000) Effects of pH on the kinetic reaction mechanism of myoglobin unfolding studied by time-resolved electrospray ionization mass spectrometry. *J. Amer. Soc. Mass. Spectrom. 11*, 312-319.

7 THE FIRST HEME-BINDING NEAT DOMAIN OF SHR IN *STREPTOCOCCUS PYOGENES*

This chapter is intended for publication and is verbatim of the manuscript in progress. The expression, purification, UV-visible absorption spectroscopy, and thermal unfolding were performed by E. B. Draganova at Georgia State University.

7.1 Abstract

The hemoprotein receptor Shr, of the *Streptococcus pyogenes* Sia heme uptake pathway, contains two heme-binding NEAT domains. Herein, we report the biophysical characteristics of the NEAT domain closest to the N-terminus (Shr-N1). A combination of UV-visible absorption, magnetic circular dichroism, and resonance Raman spectroscopies reveal Shr-N1 to have a bismethionine heme axial ligation set. pH titrations show Shr-N1 to be sensitive to pH with a predominantly six-coordinate low-spin species in acidic environments and five-coordinate high-spin species in alkaline conditions. Spectroelectrochemical titrations of Shr-N1 give 260 ± 9 mV (reductive) and 230 ± 26 mV (oxidative) vs. SHE. Stability of this domain towards heme release is analyzed via guanidinium and thermal denaturation studies of oxidized and reduced Shr-N1. Overall, sequence alignment, homology modeling, and spectral signatures are consistent with two axial methionines as the heme ligands of this novel heme binding NEAT domain.

7.2 Introduction

Many bacterial pathogens require iron for survival and virulence *(1-3)*. In the human host, iron is commonly found in the form of heme (protoporphyrin IX) and bound to proteins

such as hemoglobin *(3)*. Therefore, bacteria have evoked various strategies to obtain needed iron through the use of heme. Bacteria can acquire heme through biosynthesis, uptake pathways, or utilize both strategies *(4-6)*.

Pathogens which rely on heme uptake utilize multiple cellular surface proteins to bind and transfer heme to be brought into the cell from the extracellular space *(3, 7-13)*. In Gram-positive bacteria *(14)*, studies have focused particularly on *Corynebacterium diphtheriae (15, 16)*, *Staphylococcus aureus (17-20)*, *Bacillus anthracis (21)* and *Streptococcus pyogenes* [Group A Streptococcus (GAS)] *(22-27)*. The latter three species employ near iron transporter (NEAT) domains for heme uptake and transfer *(28-30)*. NEAT domains have conserved secondary structural features including β-strands and a 3_{10} α-helix, preceded by a serine which hydrogen bonds to one of the heme propionates, which assist in the binding of heme *(30)*.

Almost all NEAT domains characterized to date utilize a five coordinate heme binding geometry with an YXXXY pattern arising from the β-8 strand in which the first Tyr serves as an axial ligand and the second is hydrogen bonded to the first. These include *S. aureus* IsdA *(31)*, IsdB-N2 *(32)*, IsdC *(33)*, and IsdH-N3 *(34)* as well as *B. anthracis* IsdX1 and IsdX2-N5 *(30, 35, 36)*. In addition, the NEAT protein BslK from *B. anthracis* has the YXXXY motif according to sequence alignment studies *(37)*.

Proteins utilizing this motif, but with slight variations in the heme axial ligands, include IsdB-N2 with a six coordinate Met/Tyr heme center under some conditions *(32)* and IsdA with a tyrosine ligand in the ferric state and a histidine ligand in the ferrous state *(38, 39)*. Recently, the second NEAT domain from the proposed hemophore Hbp2 of *Listeria monocytogenes* (Hbp2-N2) has been described *(40)*. The axial tyrosine of Hbp2-N2 differs from other known NEAT domains in that it is located in the β-7 strand, rather than the β-8 strand. This NEAT domain also

lacks the second tyrosine in the conserved YXXXY motif, which is replaced with an alanine. HalA from *B. anthracis* also lacks the second tyrosine, using a YXXXF motif instead *(41)*. Honsa and coworkers have proposed, based on sequence analysis, that additional heme binding motifs will be discovered in the NEAT family *(30)*.

S. pyogenes is a hemolytic bacterium with a heme uptake pathway that employs NEAT domains. *S. pyogenes* causes a wide variety of invasive and non-invasive infections including necrotizing fasciitis, pharyngitis, and toxic shock syndrome *(25, 42)*. This pathogen is found increasingly resistant to macrolide antibiotics *(43, 44)*, potentially posing significant risks for infected populations. *S. pyogenes* requires iron to survive and can only obtain heme from the environment *(5, 45-47)*. Since *S. pyogenes* is not able to synthesize heme, and the pathogen heme uptake pathway may therefore be a target for inhibition in the development of new therapies.

The Sia heme uptake system in *S. pyogenes* consists of two cell surface heme binding proteins, Shr (streptococcal hemoprotein receptor) *(24, 48)* and Shp (streptococcal cell surface protein) *(49, 50)*, in conjunction with an ABC (ATP-binding cassette) heme transporter comprised of SiaA (HtsA, the periplasmic binding protein) *(23, 51-54)*, SiaB (the permease), and SiaC (the ATPase). Shr can acquire heme from hemoglobin *(24)* and transfer the heme to Shp *(26, 48)*; Shp donates heme to SiaA *(22, 55-57)*. The heme is then brought into the intracellular space by the SiaBC proteins.

Shr is a large protein of 1,275 amino acids that has been shown to span the cell wall and be exposed to the extracellular environment *(58)*. Shr has two NEAT domains, Shr-NEAT1 (Shr-N1) and Shr-NEAT2 (Shr-N2), both of which can bind heme *(24)*. The two Shr NEAT domains are separated by an EF-hand motif and a leucine rich repeat region. Shr has a signal

region in the N-terminus and two domains of unknown function (DUF1533) preceding the first NEAT domain. The C-terminus of the protein has a hydrophobic segment with a positively charged tail; presumably to anchor the protein to the cytoplasmic membrane. Null *shr* mutants displayed attenuated virulence in both zebrafish *(47)* and murine models of skin and systemic infection *(59)*, indicating the possible role of this protein in pathogenicity.

Sequence alignment of Shr-N1 showed only one tyrosine in the predicted heme binding region. This corresponded to the first tyrosine of the YXXXY pattern as seen in other characterized NEAT domains, with threonine in the position of the second tyrosine. Thus, in comparison to the classical heme binding NEAT domains, Shr-N1 may have a novel set of ligands binding the heme. Sequence alignment and homology modeling indicated the likelihood that a methionine (M22) is the N-terminal axial ligand. There are four potential heme binding amino acids on the opposite side of the proposed heme binding pocket: M107, H116, Y117, and K119.

Herein we report the biophysical characterization of the heme binding of Shr-N1. This extends work from our laboratories showing that a protein fragment containing the N-terminal domain plus the first NEAT domain is sufficient to sequester heme directly from methemoglobin *(24)*. We have characterized the Shr-N1 domain in terms of UV-visible absorption, magnetic circular, and resonance Raman spectroscopies, as well as reduction potential; these lead to the conclusion that Shr-N1 has a bismethionine ligand set, novel ligands for a NEAT domain. The presumed role of Shr-N1 *in vivo* is to take heme from hemoglobin and transfer it to the next heme binding domain in the heme uptake pathway. In this regard, we report thermal and guanidinium denaturation of the oxidized and reduced Shr-N1 to assess stability of this domain towards heme release.

7.3 Materials and Methods

7.3.1 Homology modeling and molecular dynamics

A homology model of Shr-N1 (Figure 7.2) was built using I-TASSER *(60)*. IsdX2-N5 from *B. anthracis* was the closest protein with an identity percentage of 24%; the root mean square difference (RMSD) between the model and IsdX2-N5 was 1.38 Å. The model was visualized using PyMOL *(61)*.

Dynamic simulations using *S. aureus* IsdC as a model used an explicit TIP3P *(62)* water cubic box in the Amber 8 program *(63)*. The all-atom parm99SB force field parameters *(64)* and the heme all-atom force field parameters *(65)* were used. During the simulation, a 50 ps minimization step with an integration time step of 0.001 ps followed by two steps with an integration time step of 0.002 ps at 300 K (a 50 ps MD step and a 50 ps equilibration step) were used to minimize and equilibrate the system in a NTP ensemble to a pressure of 1 bar (1 bar = 100 kPa) and a temperature of 300 K. This was followed by a 15 ns dynamic simulation step at 300 K with an integration time step of 0.002 ps. Structures were visualized in PyMOL *(61)* and VMD *(66)*.

7.3.2 Construction, expression and purification of Shr-N1 and Shr-N1 K119A

The recombinant Shr-N1 protein expressed from plasmid pEB11 was previously described *(24)*. Site-directed mutagenesis was used to construct a recombinant Shr-N1 mutant with K119A amino acid substitution (Shr-N1-K119A). The mutant was constructed using a QuickChange Lightning Site-Directed Mutagenesis Kit (Agilent Technologies) according to the manufacturer's instructions. DNA amplification was performed with the mutation-containing primers ZE641 (5' GATTTAAACCACTATGACGCATACACCAAACTTGACATG 3') and ZE642 (5' CATGTCAAGTTTGGTGTATGCGTCATAGTGGTTTAAATC 3') using plasmid

pEB11 as a template, generating plasmid pCN2. The proteins were expressed in *E. coli* XL1 blue strains grown in a Luria-Bertani (LB) medium containing 100 µg/mL ampicillin. Inoculation was done with an overnight pre-culture and cells were grown at 30 °C. When the OD_{600} of the culture reached 0.5 – 0.6, protein expression was induced by adding anhydrotetracycline (AHT) to a final concentration of 200 ng/mL. The culture was incubated overnight at 27 °C. Cells were harvested by centrifugation at 8000 *g* and 4 °C. The cell pellet was resuspended in extract solution (20 mM Tris-HCl, 100 mM NaCl, Triton X-100 0.1%). Protease inhibitor (Roche Complete Mini, EDTA-free) cocktail was added to the cell suspension (1 tablet per liter of culture). The cells were lysed by French press (SIM AMINCO). The cell lysate was centrifuged at 8000 *g* and 4 °C.

All of the following purification steps were conducted at 4 °C using fast protein liquid chromatography and all buffer solutions were pH 8.0 unless specified otherwise. The protein supernatant was loaded onto a Strep-Tactin Superflow column (5 mL, IBA BioTAGnology), washed with 15 column volumes of buffer A (100 mM Tris-HCl, 150 mM NaCl, pH 8.0) and eluted with 10 column volumes of buffer B (100 mM Tris-HCl, 150 mM NaCl, 2.5 mM *d*-desthiobiotin, pH 8.0) via a linear gradient. Protein fractions were collected and analyzed for purity using sodium dodecyl sulfate polyacrylamide gel electrophoresis. Minor differences in the optical spectra were observed as a function of the buffer type. The Shr-N1 protein has been isolated in the ferric state and in some instances isolated as a mixture of ferric and ferrous states.

Native-PAGE gel electrophoresis and size exclusion chromatography (Sephacryl S-200, GE Healthcare) were used to determine protein oligomerization state. Shr-N1 was passed through a column with 50 mM sodium phosphate and150 mM NaCl at pH 7.0. Fractions that

contained protein were also analyzed using Native-PAGE and UV-visible absorption spectroscopy.

7.3.3 Magnetic circular dichroism spectroscopy

Magnetic circular dichroism (MCD) spectra were measured with a magnetic field strength of 1.41 T by using a JASCO J815 spectrophotometer. The instrument was equipped with a JASCO MCD-1B electromagnet and interfaced with a Silicon Solutions PC through a JASCO IF-815-2 interface unit. Data acquisition and manipulation using Cary or Jasco software has been previously described *(67)*. To ensure homogeneity of ferric oxidation for the proteins, ferricyanide was used to fully oxidize the heme center, followed by desalting chromatography. The resulting spectra were compared to data from other heme-containing proteins with known active site structures and optical spectra. All spectral measurements for all proteins were carried out with a 0.2 cm quartz cuvette at 4 °C in 50 mM sodium phosphate. Complete reduction of the heme iron was accomplished by adding a few microliters of concentrated sodium dithionite solution (25 mg/mL of H_2O) with a microliter syringe. Ferrous−CO adducts were prepared by bubbling CO gas into the ferrous protein samples. UV−visible absorption spectra were recorded with a Cary 400 spectrophotometer interfaced to a PC, before and after the MCD measurements to verify sample integrity.

7.3.4 Resonance Raman spectroscopy

Resonance Raman (rR) spectra were collected using excitation at 413.1 nm from a krypton ion laser whose power was adjusted to 2 – 5 mW at the sample. The spectra of the proteins were recorded following oxidation with ferricyanide and buffer exchange by centrifugal concentration and dilution to remove excess oxidant and glycerol. The pH was adjusted by

diluting a concentrated stock solution of protein into 20 mM MES, 20 mM TAPS, and 20 mM CAPS adjusted to the specified pH.

7.3.5 Spectrophotometric pH titrations

Shr-N1was diluted into buffers containing 20 mM MES, 20 mM TAPS, and 20 mM CAPS adjusted to pH 6.5. The sample was titrated to pH 9.5 using 0.5 M NaOH. In a separate titration, the sample was titrated from pH 9.5 to 13 using 0.5 M NaOH. The data were analyzed by global analysis.

7.3.6 Electrochemistry

Shr-N1was diluted to 10 μM with 50 mM Tris-HCl, pH 8 and 100 mM NaCl. A mediator solution was prepared by dissolving phenazine methosulfate, 2,6-dimethyl benzoquinone, 2-methyl-1,4-benzoquinone, 1,2-napthoquinone-4-sulfonate, and quinhydrone in DMSO for a final concentration of 10 mM for each dye. The final concentration of the mediator was 10 μM in the sample cuvette and covered the potential range of 80 – 280 mV. The titrations were carried out under a nitrogen atmosphere using 0.05 M dithionite as the reductant and 0.02 M ferricyanide as the oxidant. The Ag/AgCl reference 216 electrode was calibrated using buffered quinhydrone at pH 7 (E_m = 292 mV vs. NHE) *(68)*. The UV-visible absorption absorbance spectra were recorded at each experimental potential after equilibrium had been established, as judged by the cell having reached a constant potential.

The samples were initially treated with enough dithionite to completely reduce the heme. The solution was then titrated with ferricyanide to follow the heme oxidation spectroelectro-chemically. The reverse, reductive titration was then carried out by stepwise addition of dithionite. The data were subsequently analyzed by global analysis and fit to a single potential model, as the mediator dyes contribute minimally to the overall absorbance changes observed.

7.3.7 Guanidinium hydrochloride (GdnHCl) denaturation studies

Protein unfolding experiments were performed using GdnHCl as the denaturant, according to the standard protocols *(69)*. The unfolding process was followed by UV-visible absorption spectroscopy in 50 mM Tris-HCl, pH 7.0 (Varian 50 Bio spectrophotometer, 1.5 mL quartz Supracil cuvettes (Spectracell) with 1 cm path lengths), following changes at the Soret, using the single cell technique *(70-73)*. The GdnHCl stock solution concentration was 8.32 M (50 mM Tris-HCl, pH 7.0) measured by refractive index *(69)*. Data were analyzed using Equation 1 describing a two-state process *(69)*:

$$y = [(Abs_F + m_F[D]) + (Abs_U + m_U \exp[m([D]-[D]_{1/2})/RT])]/1 + \exp[m([D]-[D]_{1/2})/RT] \quad [1]$$

where y is the absorbance at any point along the fitted denaturation curve, Abs_F is the absorbance of the folded state, Abs_U is the absorbance of the unfolded state, m is the slope at the midpoint, and also the dependence of the free energy of unfolding on the denaturant concentration, m_F is the slope of the folded state, m_U is the slope of the unfolded state, [D] is the concentration of GdnHCl, $[D]_{1/2}$ is the concentration of GdnHCl at the midpoint of the unfolding curve, R is the gas constant, and T is the temperature (Kelvin).

7.3.8 Thermal denaturation studies

Thermal denaturation of Shr-N1 was carried out with a UV-visible absorption spectrophotometer (Cary 50 Bio) equipped with a temperature control (TC 125, Quantum Northwest). Quartz Supracil cuvettes (Spectracell) with 1 cm path lengths were used. The protein (~5 μM) was unfolded in sodium phosphate (50 mM, pH 7.5) and the spectrum (250 – 800 nm) was recorded every 2 °C from 20 °C to 60 °C after the sample was equilibrated for each

temperature. The samples were cooled to room temperature and observed via UV-visible absorption spectroscopy for refolding. In both the ferric and ferrous proteins, the protein was prone to precipitation above 60 °C. The data were fit to a two-state unfolding model in Equation 2 *(74)*:

$$Y_{abs} = \{(Y_F + m_F T) + (Y_U + m_U T) \exp[\Delta H_m/R(1/T_m - 1/T)]\}/\{1 + \exp(\Delta H_m/R(1/T_m - 1/T)]\} \quad [2]$$

where the ΔH_m is the enthalpy of unfolding, T_m is the temperature at which the protein is half unfolded and the remaining variables are as described above. The extent of protein unfolding is presented as the fraction of folded protein.

7.4 Results

7.4.1 Sequence alignment and homology modeling

Figure 7.1 shows the ClustalW *(75)* alignment of Shr-N1 with the following homologous NEAT proteins: *S. pyogenes* Shr-NEAT2 (Shr-N2) and Shp, *S. aureus* IsdA, IsdB-N2, IsdC, and IsdH-N3, *B. anthracis* IsdX1 and IsdX2-N5, and *L. monocytogenes* Hbp2-N2. The alignment shows significant differences in the conservation of amino acids and motifs utilized in heme binding. First, Shr-N1 does not contain the YXXXY heme binding motif as seen in the Isd and IsdX systems, rather it is an YXXXT sequence. Second, the SXXXXY/SXXXXF 3_{10} helix motif, conserved in the Isd, IsdX and Hbp2 proteins, is not complete, i.e., the Shr-N1 has an alanine rather than an aromatic acid at the end of this sequence. In addition, Shr-N1 does not have a tyrosine that corresponds to the β-7 axial tyrosine in *L. monocytogenes* Hbp2-N2. All of these differences imply that the axial ligands in Shr-N1 are different than those in previously described NEAT domains.

Figure 7.1 Alignment of the amino acid sequence of Shr-N1 with homologous proteins (selected portions shown). The proposed Shr-N1 ligand positions (M22 and M107) are indicated by the red triangles. The conserved Isd YXXXY heme binding motif is shown by the blue box. The conserved 3_{10} helix SXXXXY motif is shown by the green box. The orange box shows the position of the β7 axial tyrosine from L. monocytogenes Hbp2-N2.

Figure 7.2 shows an I-TASSER model of the protein. The heme cavity is taken to be in the lower right corner of the structure as drawn. Logical axial ligands are M22 on the N-terminal side of the protein and one of M107, Y117, H116, or K119 on the C-terminal side. Structurally, the model predicted Shr-N1 to have a β-strand secondary structure. A small α-helix is also observed, with M22 extending from the helix, and the other potential heme binding residues are positioned on an unstructured loop opposite M22.

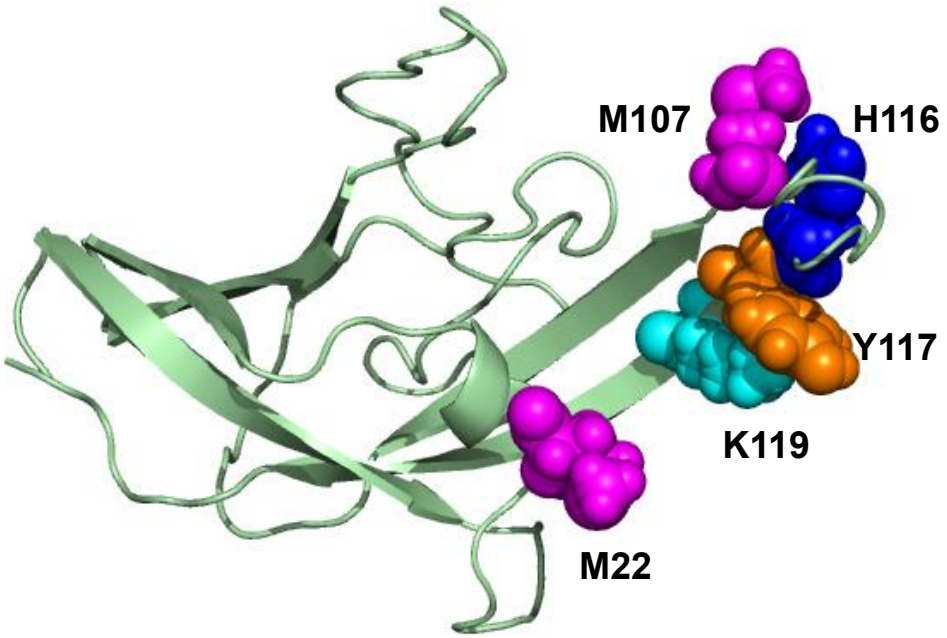

Figure 7.2 I-TASSER homology model of Shr-N1. Shown in magenta are the two proposed heme axial ligands, M22 and M107. Nearby residues H116, Y117, and K119 are also shown in blue, orange, and cyan, respectively.

7.4.2 Molecular dynamics

Molecular dynamics were performed on a homology model of Shr-N1 (Figure 7.3). In the resulting structure, four residues were close enough to bind to the putative heme: M22, M107, Y117 and K119. In the final third of the simulation, M22 was consistently within 5 – 8 Å of the heme. M107 also spent substantial time near the heme iron on the opposite side. Both Y117 and K119 also spent part of this time near the heme. Thus, the molecular dynamics are consistent with M22 and M107 as potential axial ligands, but do not rule out Y117 or K119 in the relatively unstructured portions of the three dimensional structure as axial ligands.

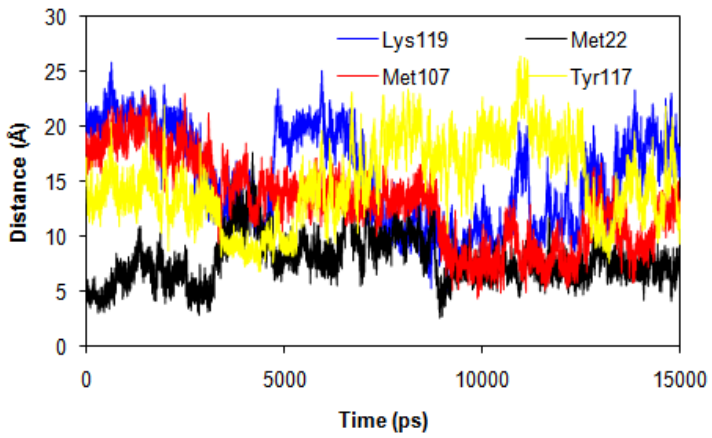

Figure 7.3 The distance in Shr-N1 between the side chains of potential heme binding amino acids and the heme iron center over time.

7.4.3 Oligomerization of Shr-N1

Size exclusion chromatography was utilized to determine the oligomerization state of Shr-N1 (Figure 7.4). The elution in Figure 7.4A showed three major bands, two smaller peaks at approximately 36 (F1) and 40 mL (F2) and a large peak at 48 mL (F3). Each fraction was analyzed via UV-visible absorption spectroscopy (Figure 7.4B). Fraction 1 showed very little holoprotein; Fractions 2 and 3 were similar and exhibited significantly more heme loading. An SDS-PAGE of each fraction showed a band of approximately 58 kDa (Figure 7.4C) indicating each fraction was Shr-N1 (expected molecular weight of 58,944 Da). Native PAGE showed fractions 1 and 2 had a large concentration of multimeric species as seen by the multiple bands on the gel (Figure 7.4D). Fraction 3 (the largest SEC elution peak) gave a single band consistent with the dimeric form of the protein (~120 kDa). The elution volume was also consistent with a dimer.

Additional size exclusion chromatography experiments were performed on protein samples with very little protein concentration (maximum peak absorbance at 280 nm of < 0.01).

No significant peaks eluting later than the dimer were observed, indicating the protein is found in dimers or higher multimers even in dilute solutions (data not shown). Overall, these results indicate Shr-N1 exists predominantly as a mixture of dimer and multimer in solution.

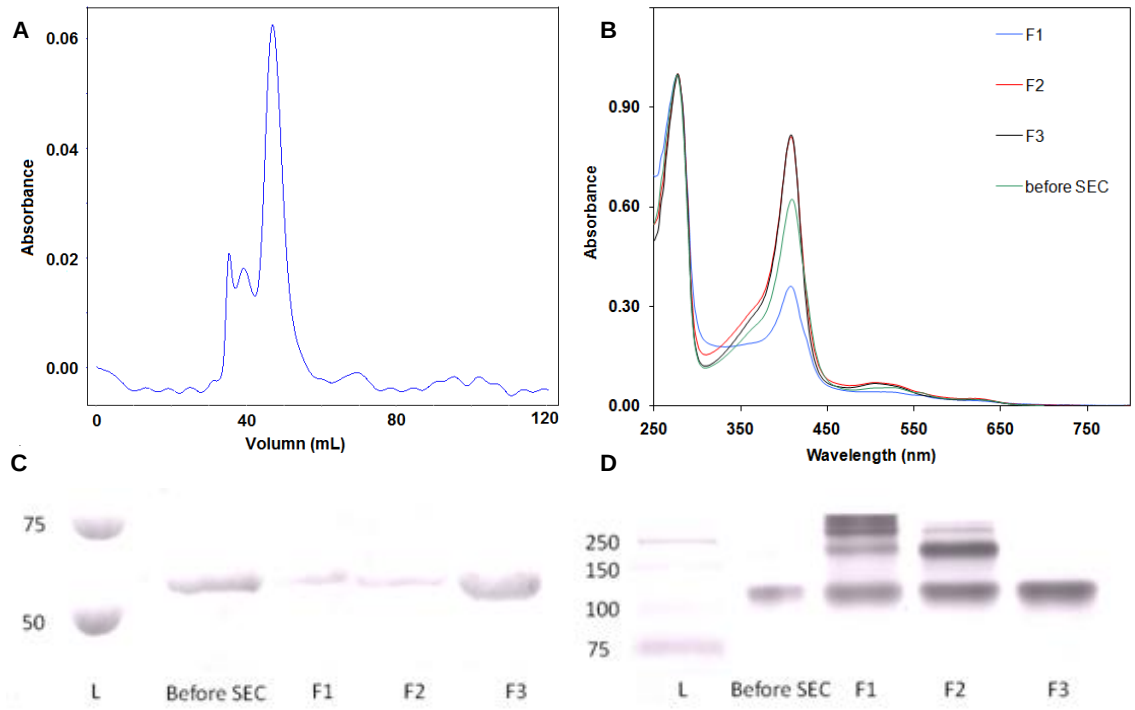

Figure 7.4 Size exclusion chromatography of Shr-N1.(A) The elution trace monitored at 280 nm. Three major fractions were observed and collected as F1, F2 and F3. (B) UV-visible absorption spectra of the three fractions: F1 (blue), F2 (red), and F3 (black). Shr-ntdN1 before SEC is shown in green. (C) SDS-PAGE of Shr-N1 before SEC and the SEC elution fractions. All bands are around 60 kDa. The molecular weight of Shr-N1 is expected to be 58 kDa. (D) Native-PAGE of the fractions and Shr-N1 before SEC.

7.4.4 Spectroscopic studies of Shr-N1

Fe (III) Shr-N1. UV-visible absorption spectroscopy (Figure 7.5) gave a Soret at 409 nm and four α,β-bands at 506, 540, 585, and 645 nm in 50 mM Tris-HCl, pH 7.0. In 50 mM sodium phosphate, pH 6.5, the Soret is at 412 nm and the α,β-bands are slightly shifted (505, 535, 570, and 640 nm).

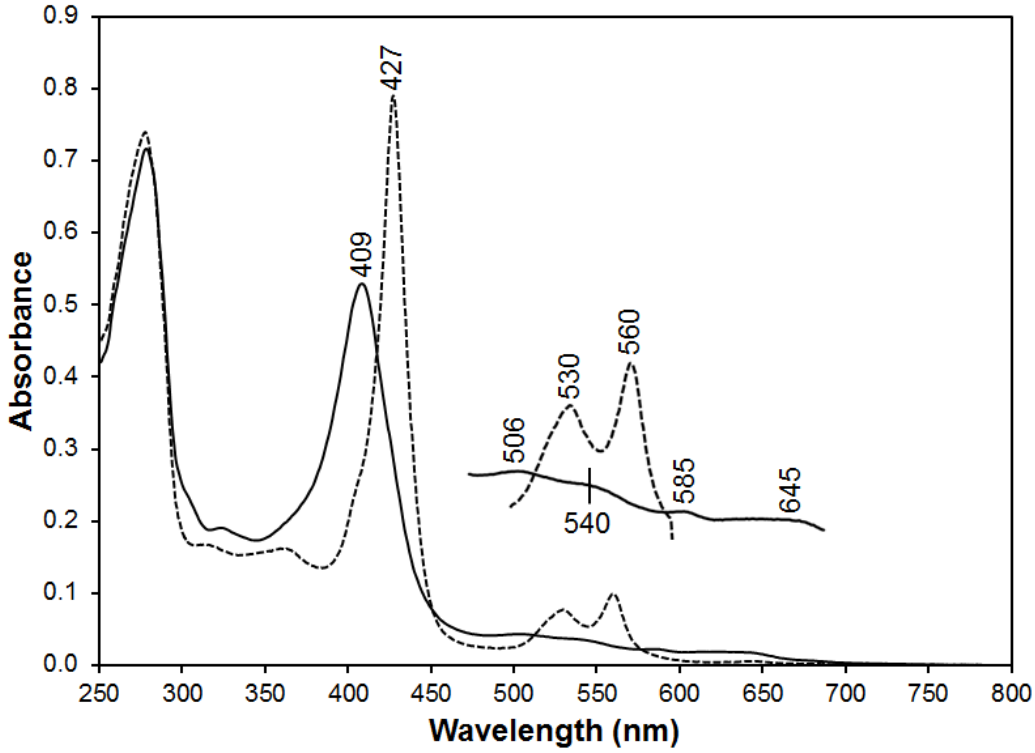

Figure 7.5 UV-visible absorption absorbance spectra of ferric (solid line) and ferrous (dashed) Shr-N1 in 50 mM Tris-HCl, pH 7.0.

MCD spectroscopy was utilized to assist in heme axial ligation determination for Shr-N1. The spectra did not match standard axial ligand sets of His, His/His, His/Met, Tyr, or His/Tyr *(76)*. Ferric Shr-N1 at pH 6.5 was then compared to derivatives of the H93G myoglobin (Mb) cavity mutant ligated by tetrahydrothiophene (THT) (Figure 7.6). H93G Mb can bind to THT using either five-coordinate thioether or a six-coordinate bis-thioether axial ligation *(77)*. The MCD of Shr-N1 at pH 6.5 resembles the six-coordinate low-spin (6cLS) active site environment of the bis-THT H93G Mb, perhaps with some of the heme adopting the mono-THT coordination.

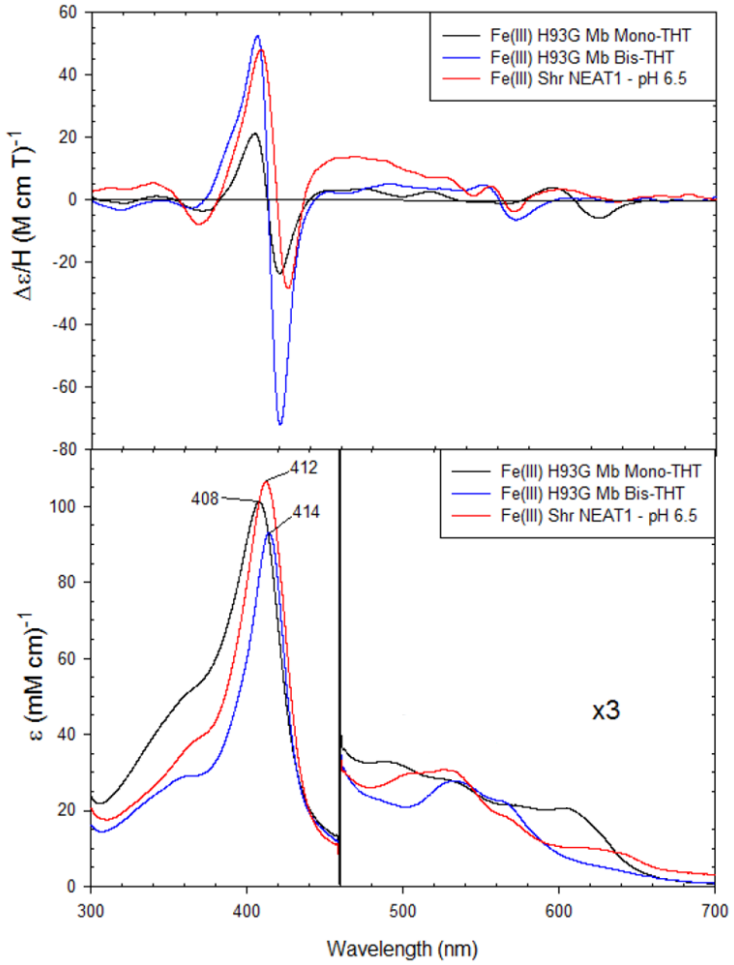

Figure 7.6 MCD and UV-visible absorption spectra of Fe (III) Shr-N1 (red), H93G Mb bis-THT (blue), and H93G Mb mono-THT (black) at pH 6.5.

Resonance Raman spectroscopy provided additional detail into the heme ligation of Shr-N1. The rR spectra of ferric Shr-N1at pH 6.25 is shown in Figure KRxxx. Ferric Shr-N1 gave the following bands: ν_3 at 1500, ν_{11} at 1566, and ν_{10} at 1622 cm^{-1}. These frequencies indicate predominantly 6cLS heme in an acidic environment.

Fe(III) K119A Shr-N1. Homology modeling indicated K119 to be opposite the proposed M22 heme binding ligand. A mutant protein with K119A amino acid substitution gave the same spectral signatures as WT Shr-N1 (Figure 7.11 S1) with a Soret at 409 nm and four bands in the α,β region. This finding ruled out K119 as a potential heme binding ligand.

Fe(II) Shr-N1. Shr-N1 is readily reduced by both dithionite and dithiothreitol to give the ferrous form of the protein with a Soret at 427 nm as well as α,β-bands at 530 and 560 nm (Figure 7.5). The position of the reduced Soret is the same with both reducing agents. A weak optical band at approximately 640 nm was also observed.

In the MCD, the reduced Shr-N1 was compared to the H93G Mb mono-THT and bis-THT model systems spectra at pH 6.5 (Figure 7.12 S2) *(77).* The MCD spectrum for the bis-THT Mb complex is similar to Shr-N1, indicating a bis-Met coordination system for the Fe(II) species. Fe(II) Shr-N1 was also studied at pH 10, but no changes were observed in the spectra as a function of pH (data not shown).

In the Raman spectra, the heme was also shown to be is 6cLS as evidenced by ν_3 at 1493 cm^{-1} (Figure 7.13 S3) (full reduction with dithionite was shown by the position of ν_4 at xxxx). This assignment from the rR data of a 6cLS state for the ferrous protein is consistent with the visible spectrum and MCD of reduced Shr-N1.

Fe(II)-CO Shr-N1. Shr-N1was reduced with dithionite in the presence of CO. The UV-visible absorption and MCD spectra are shown in Figure 7.14 S4. Shr-N1 Fe(II)-CO complexes at both pH 6.5 and 10.0 exhibit the same spectral signatures. Comparison with the ferrous-CO complex of mono-THT H93G Mb indicate a Met-Fe(II)-CO coordination environment. In the MCD, the intensities of the characteristic peaks and the troughs for Shr-N1 are similar to the mono-THT ferrous-CO model system; the only difference is a slight blue-shift (5 nm) for the entire spectrum compared to the mono-THT H93G Mb system. This indicates that upon binding of exogenous CO, Shr-N1loses a methionine ligand and adopts a 5C Met-Fe(II)-CO motif. The resonance Raman spectrum of the Fe(II)-CO protein was also consistent with a 6c LS CO complex.

7.4.5 Shr-N1 pH studies

A spectrophotometric pH titration of ferric Shr-N1from pH 6 to 9.5 is shown in Figure DB9.4. The data were analyzed by global analysis and were fit to a single acid-base equilibrium. Figure DB9.4B shows titration curves at select wavelengths and the fit of the data to this model. The residuals are calculated and shown at the bottom of the figure. The data were fit and gave a pK_a of 8.15 ± 0.06.

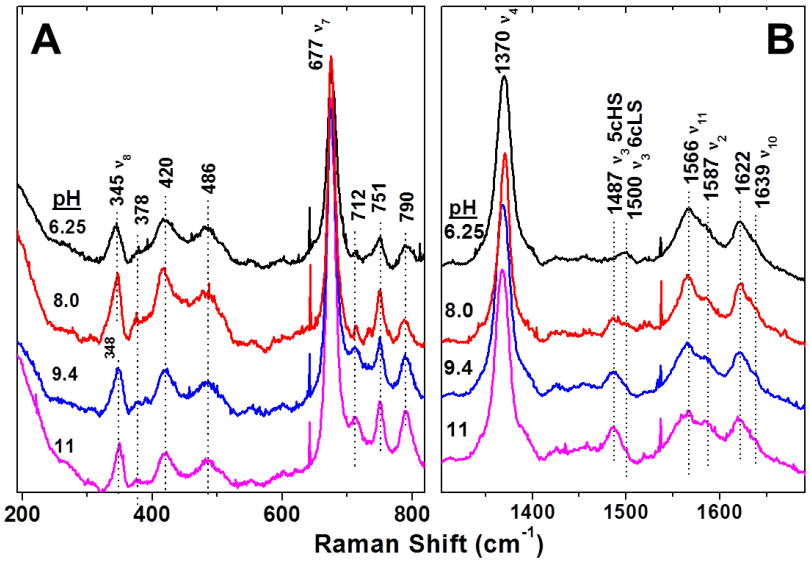

Figure 7.7 Resonance Raman spectra of ferric Shr-N1 as a function of pH. Soret-excited (413.1 nm) spectra were recorded in the (A) low frequency and (B) high frequency regions. Samples are 40 μM and prepared in 20 mM MES, 20 mM TAPS, 20 mM CAPS adjusted to pH 6.25 (black), 8.0 (red), 9.4 (blue), and 11 (pink). The 6cLS and 5cHS bands are labeled accordingly.

The rR spectra of ferric Shr-N1 over the pH range from 6.25 to 11 are shown in Figure 7.7. Figure 7.7A shows the low frequency region, where no pH dependent changes are observed. Figure 7.7B shows the high frequency region where porphyrin core size marker bands are observed. At pH 6.25 the heme is primarily 6c and LS (ν_3 at 1500 cm^{-1}). As the pH increases,

the intensity of the ν_3 corresponding to 6cLS heme decreases, while that due to five-coordinate high-spin (5cHS) heme (1487 cm^{-1}) increases. Thus, the Raman data are consistent with the UV-visible absorption spectroscopic data.

MCD was also used to study Fe(III) Shr-N1 at pH 10 (Figure S DC6.3). In the bottom UV-visible absorption panel, a peak is displayed at 605 nm which is due to the presence of a HS species, as seen in the rR data. The MCD spectral comparison to the same Mb derivatives as described above showed Shr-N1 to be similar to the five-coordinate, mono-THT model. These results, along with UV-visible absorption and rR data, indicate Shr-N1 has a 6cLS bis-Met heme ligation motif at pH 6.5, but loses a methionine as the pH is increased above 10 and to give a 5cHS mono-Met coordination.

7.4.6 Electrochemistry

Figure 7.8 shows the oxidative titration of ferrous Shr-N1with arrows indicating the direction of change in absorbance. The sample was subsequently titrated reductively with dithionite (data not shown). Both sets of data were analyzed by global analysis to yield midpoint potentials of 260 ± 9 mV (reductive vs. SHE) and 230 ± 26 mV (oxidative vs. SHE). Figure 7.8B shows the titration curves constructed from normalized absorbance at the wavelength for maximum Soret absorbance for the reduced heme as a function of potential. The solid line represents the best fit of the data to a single potential model.

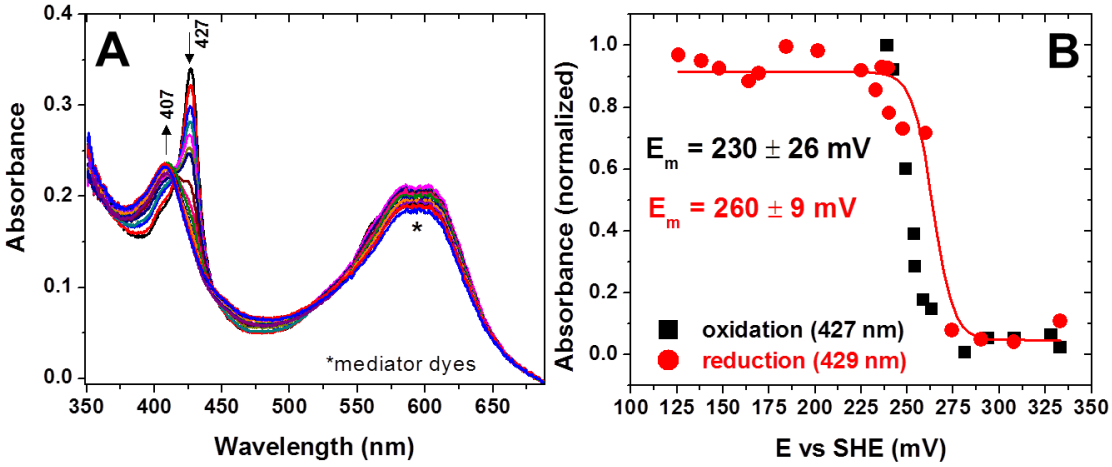

*Figure 7.8 Spectrophotometric redox titration of Shr-N1. (A) Oxidative titration of ferrous Shr-N1 with ferricyanide. The arrows indicate the direction of absorbance change. The * indicates where the mediator dyes have absorbance. (B) Titration curves form global analysis of the oxidative (▪) and reductive titrations (●) at 427 and 429 nm, respectively. The midpoint potential is reversible with an oxidative E_m = 230 ± 26 mV and reductive E_m = 260 ± 9 mV.*

7.4.7 Unfolding studies of Shr-N1

Ferric Shr-N1 was treated with GdnHCl to evaluate the denaturant-induced unfolding of the protein. The data fit well to a standard two state transition model (Figure 7.9) with a midpoint of the transition at 0.90 ± 0.01 M GdnHCl. The unfolding of the ferrous Shr-N1 gave a $D_{1/2}$ value of 1.10 ± 0.01 M. Thus, the ferrous protein is only slightly more stable to chemical denaturation than the ferric protein.

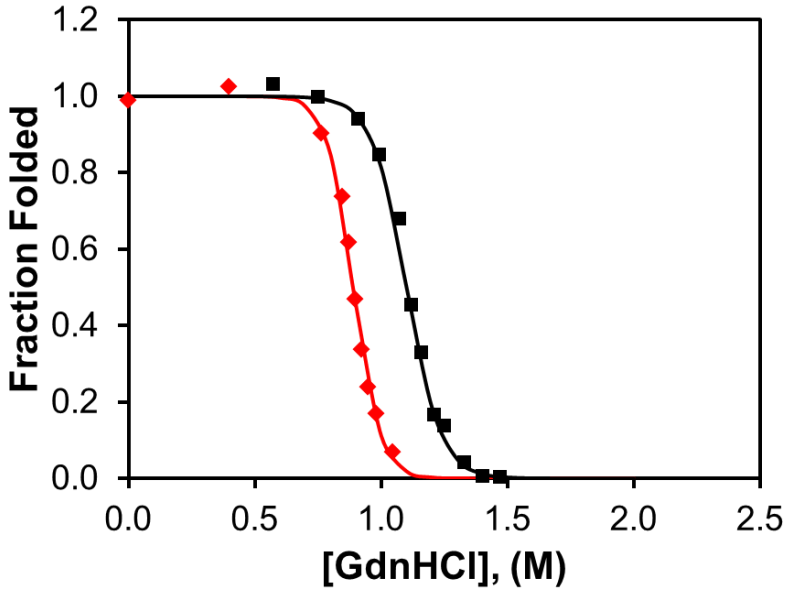

Figure 7.9 Fraction of folded ferric (diamonds) and ferrous (circles) Shr-N1 as a function of GdnHCl concentration. The absorbance changes were monitored at 411 and 427 nm for the ferric and ferrous data, respectively. Data from the titrations were fit via nonlinear least squares to a two state unfolding model. Protein samples were in 50 mM Tris-HCl, pH 7.0.

Thermal denaturation provides another method of assessing the ease of heme loss due to protein unfolding. The normalized thermal denaturation curve as a function of folded protein for ferric Shr-N1 is shown in Figure 7.10. The data were fit to a two state unfolding process, giving a T_m value of 47.0 ± 0.1 °C. The sample could be recooled beneath 60 °C; spectral analysis indicated only approximately 75% refolding. Thus, thermal unfolding for this protein is not a completely reversible process.

Unfolding data for the ferrous form of the protein are shown in Figure 7.10. Fitting the denaturation as a two state process gave a T_m of approximately 55 °C. The sample precipitated above this temperature. As with chemical denaturation, the reduced protein appears to be slightly more stable toward unfolding than the oxidized protein.

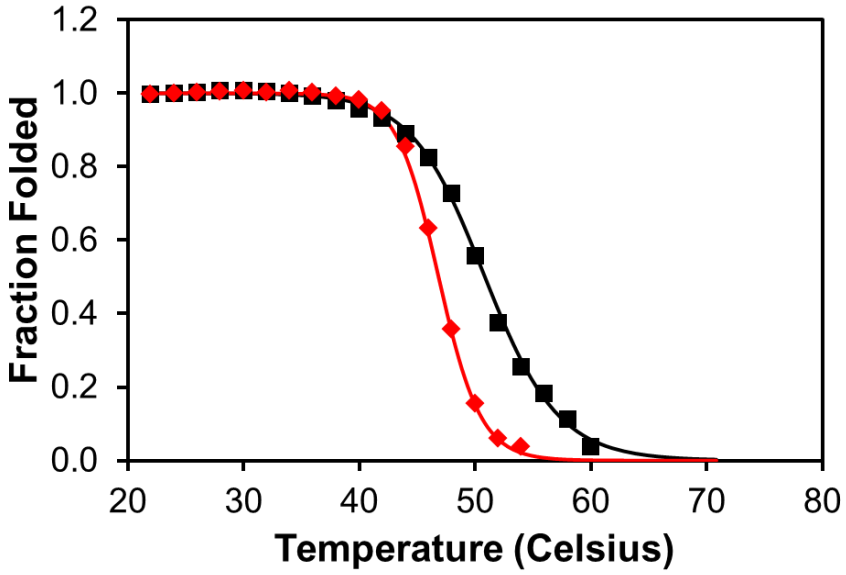

Figure 7.10 Normalized fraction folded of ferric Shr-N1 (diamond) and ferrous Shr-N1 (square) as a function of temperature followed by UV-visible absorption absorbance. Data from the unfolding were fit via nonlinear least squares to a two state unfolding model. Protein samples were in 50 mM potassium phosphate, pH 7.5. In both the ferric and ferrous, proteins were prone to denaturation after 60 °C.

7.5 Discussion

7.5.1 Heme ligation

Heme binds to proteins via linkages between the iron center and the atoms from adjacent amino acid side chains *(78)*. Common axial ligands are His, Met, Cys, and Tyr, with others employed in selected instances (e.g., Asn, Gln, Lys, and the N-terminal amine). All canonical NEAT proteins reported to date have axial tyrosine ligands *(30)*. Our data, however, are not consistent with an axial tyrosine ligand, but rather ligation by two methionine residues. Aranda et al. predicted Shp, the protein that receives heme from Shr-N1, is related to NEAT proteins *(50)*. Shp is a bismethionine protein. Although Shr-N1 and Shp have only 19% amino acid sequence identity *(75)*, bioinformatics analysis by Honsa et al. *(30)* indicated that these two proteins may be considered as distantly related to the canonical NEAT proteins.

At physiological pH, ferric Shr-N1 has bands at 412, 500 and 533 nm, consistent with the presence of both LS and HS hemes. The spectrum is similar to that of known bismethionine proteins including *E. coli (79)* and *Pseudomonas aeruginosa (80)* bacterioferritin; *S. pyogenes* Shp *(56)*; and the H102M and R98C/H102M variants of cytochrome b_{562} (in which a methionine replaces the axial histidine to give a possible bismethionine ligand set) *(80)* (Table 7.1). Titration of the model system H93GMb with high concentrations of THT and cooling to 4 ^{o}C allowed characterization of a ferric (bis-THT) H93GMb six-coordinate LS structure *(79)*. In each of these cases, the Q-band to the blue was significantly larger of the two (Table 7.1).

The Raman spectra were also consistent with a mixture of 5c HS and 6c LS species. The bismethionine heme center has been characterized by resonance Raman spectroscopy for the oxidized state of bacterioferritin from *A. vinelandii (81)* and for the N-acetylmethionine complexes of both ferrous and ferric microperoxidase *(82)*.

The most widely studied bis-methionine protein is bacterioferritin, in which the heme is bound to two axial methionine residues from different subunits *(83, 84)*. This protein can adopt various conformations with somewhat different biophysical characteristics. For example, *Desulfovibrio desulfuricans* bacterioferritin has both HS and LS forms, depending on the buffer *(85)*. Additionally, *E. coli* covR98C/H102M bacterioferritin can exist as a mixture of LS and HS in solution *(80)*.

In the MCD, for both Shr-N1 and bis-THT H93G Mb, the major trough in the visible region is located at 570-575 nm, while the mono-THT model trough is substantially red-shifted and at 627 nm. Overall, the ferric Shr-N1 MCD spectra are similar to both mono-THT and bis-THT H93G with the bis-thioether a somewhat better fit. This is consistent with a mixture of the five-coordinate and six-coordinate methionine species observed in the Raman spectra. The

Table 7.1 Optical absorption bands for proteins with one and two methionine ligands. Bands with the symbol "≈"were approximated from published spectra. The relative intensities (compared to the ≈ 530 nm band) for the ferric Q-bands are given.

Protein [Fe(III)]	**Organism**	**Soret**	**α,β-Region (≈ 530 nm intensity = 1.0)**				**Reference**
Bacterioferritin	*E. coli*	418	--	531	570	--	*(86)*
	P. aeruginosa	417	--	527	562 (0.7)	--	*(86)*
	A. vinelandii						
Shp	*S. pyogenes*	420	≈ 510 (0.7)	≈ 530	≈ 560 (0.6)	≈ 630 (0.1)	*(56)*
Shp M66A		406	≈ 490 (1.2)	≈ 530	--	≈ 605 (0.9)	
Shp M153A		402	≈ 485	--	--	≈ 600	
H102M cytochrome b_{562}	*E. coli*	404	495 (1.2)	530	--	610 (0.9)	*(80)*
R98C/H102M cytochrome b_{562} (acidic)	*E. coli*	418	--	528	≈ 555 (0.7)	--	*(80)*
R98C/H102M cytochrome b_{562} (basic)		401	≈ 486 (1.2)	≈ 530	≈ 555 (0.8)	604 (0.9)	
H93GMb bisTHT	Sperm whale	415	--	535	562 (0.8)	--	*(79)*
H93GMb monoTHT		408	500 (1.2)	532	565 (0.7)	603 (0.7)	
ShrN1 (acidic)	*S. pyogenes*	412	505 (0.9)	535	570 (0.6)	640 (0.3)	This work
ShrN1 (basic)		408	490 (1.4)	535	--	605 (1.1)	
Protein [Fe(II)]	**Organism**	**Soret**	**α,β-Region**				**Reference**
Bacterioferritin	*Pseudomonas aeruginosa*	420	519		554		*(86)*
Shp	*S. pyogenes*	428	≈ 528		≈ 561		*(56)*
ShrN1 (acidic)	*S. pyogenes*	427	530		560		This work
H102M cytochrome b_{562}	*E. coli*	430	530		561.5		*(80)*
R98C/H102M cytochrome b_{562}	*E. coli*	426	528		557		*(80)*
H93GMb bisTHT	Sperm whale	427	528		558		*(79)*

MCD of ferric H102M cytochrome b_{562} (also a mixture of 5-coordinate and 6-coordinate species) is similar to both ferric Shr-N1 and bis-THT H93G Mb *(80)*. Ferric Shr-N1 coverts to a HS species with a pK_a of 8.15. The R98C/H102M variant of cytochrome b_{562} is similar, converting

to a HS species as the pH is raised (pK_a of 7.1) *(80)*. The ferric Shr-N1 species formed at high pH is presumably the five-coordinate mono-methionine heme.

The spectrum of ferrous Shr-N1 (427, 530 and 560 nm) is consistent with those of other ferrous bismethionine hemes (Table 7.1). Specifically, the spectrum of Shr-N1 is almost identical in wavelength and relative Q-band intensity to those of Shp (428, 528 and 561 nm) *(56)*, *P. aeruginosa* bacterioferritin (420, 519 and 554 nm) *(86)*, H102M cytochrome b_{562} (430, 530 and 561.5 nm) *(80)* and the ferrous bis-THT H93G Mb complex (427, 529, and 558 nm, fully formed at -40 ^{o}C in 60% vol/vol ethylene glycol but with little apparent temperature dependence of the spectrum) *(77)*. In the MCD, the spectrum of the mono-THT H93G Mb was not in agreement with that of Shr-N1, indicating that both methionines bind in the ferrous state in the protein.

The ferrous-CO Shr-N1 complex was also investigated. UV studies in acidic and basic pH gave the same spectral profile. The spectrum of the ferrous Shr-N1 carbon monoxide complex (421, 539 and 568 nm) is also consistent with that of the H93G Mb THT/CO complex (432, 541 and 572 nm). In the MCD, comparison with the CO adduct of mono-THT H93G Mb gave similar intensities of characteristic peaks and the troughs between the two proteins. These results indicated upon reduction of the heme iron and addition of exogenous CO, Shr-N1 loses an axial methionine to form a Met-Fe(II)-CO ligand set.

The probability of M22 and M107 as Shr-N1 axial ligands is enhanced by the alignment of the sequences of the known heme binding NEAT domains: IsdA, IsdB-N2, IsdC, IsdH-N3, Shr-N1 and Shr-N2 along with the heme binding protein Shp. In this alignment, M22 and M107 of Shr-N1 are at the sequence positions, respectively, of the axial ligands of Shp: M66 and M153 *(50)*. The molecular dynamics simulations are also consistent with this conclusion.

7.5.2 Electrochemistry

Shr-N1 has midpoint potentials of 260 ± 9 mV (reductive) and 230 ± 26 mV (oxidative) vs. SHE. Tyrosine-ligated hemes have negative reduction potentials, because the axial tyrosinate stabilizes the ferric form of the protein. Thus, the reduction potential of Shr-N1 rules out tyrosine as a potential heme axial ligand. In contrast, hemes with two axial methionines show a very wide range of reduction potentials. The reduction potential of the bis-methionine H102M mutant of cytochrome b_{562} was +440 mV at pH 4.8, with reduction coupled to coordination-state changes *(80)*. The reduction potential for *D. desulfuricans* bacterioferritin was +140 mV and independent of whether the protein was in the HS (50 mM phosphate buffer) or LS (300 mM phosphate buffer) forms *(85)*. The *D. desulfuricans* protein has iron uroporphyrin, rather than iron protoporphyrin, as the prosthetic group, though it has been proposed that the effect of this change on the reduction potential is minor *(85)*. In contrast to the *D. desulfuricans* protein, the reduction potentials of *Azotobacter vinelandii* bacterioferritin were -225 and -475 mV for the apo and iron loaded forms, respectively *(87)*, while bacterioferritin from *Rhodopseudomonas sphaeroides* had a reduction potential of -204 mV *(88)*. Thus, the reduction potential of SHR-N1 is consistent with a bismethionine axial ligand set, although the range of known reduction potentials for the members of this class is very wide.

7.5.3 Oligomerization

For Shr-N1, protein oligomerization and heme loading were related, with the more aggregated form showing less heme loading. The relationship between these two observations is not clear. There are examples of proteins involved in heme transfer that bind heme at sites other than the primary binding site. For example, ChaN from *Campylobacter jejuni* has two cofacial hemes bound between the two monomers of a ChaN dimer *(89)*. The x-ray structure of Shp

shows a dimer; each of the two monomers binds a heme and two additional hemes are found at the interface between the two monomers *(50)*. Of most direct relevance, Watanabe et al. have found that IsdHN3 binds with multiple hemes in two configurations. They also found that excess heme promoted that multimerization of the NEAT domains. Our work and that of Watanabe et al. indicated that multimerization and heme binding seem to be associated processes for NEAT domains, although the details may vary depending on the exact system *(34)*.

7.5.4 Unfolding Studies of Shr-N1

Shr-N1 can obtain heme from hemoglobin *(24)*. Presumably it then transfers the heme to Shp, unless it is exposed to an abundance of heme; under such conditions, it has been proposed that the heme can be transferred from Shr-N1 to Shr-N2 for storage until needed by the cell *(26)*. It is of interest to determine how easily the protein releases heme to gain a better understanding of the overall heme protein to heme protein transfer process.

Denaturation with guanidinium hydrochloride is widely used to probe the stability of heme proteins *(90, 91)*. The ferric Shr-N1 $D_{1/2}$ of 0.90 ± 0.01 M can be compared with other *b*-type heme proteins ($D_{1/2}$) including the hexacoordinated proteins cytochrome b_{562} (1.5 – 1.8 M) *(92, 93)*; OM cytochrome b_5 (2.6 – 3.6 M) *(70, 94)*; HasA (2.7 M) *(95)*; MC cytochrome b_5 (3.1 M) *(96)*; SiaA (3.1 M) *(23)* and the pentacoordinated proteins horse heart myoglobin (1.6 -1.8 M) *(97, 98)* and sperm whale myoglobin (2 – 2.5 M) *(97-99)*. Shr-N1 unfolds the most easily of all of these examples; of note also is the steepness of the unfolding transition (*m*-value of approximately 10). This high *m*-value presumably is observed because Shr-N1 is found as dimers and multimers in solution; the *m*-values generally increase with the number of hydrophobic interactions disrupted in the denaturation *(100, 101)*. The irreversible nature of the

denaturation, and the existence of multimers, precluded calculations of the thermodynamics of unfolding *(69)*.

The unfolding of the ferrous Shr-N1 gave a $D_{1/2}$ value of 1.10 ± 0.01 M. Thus, the ferrous protein is only slightly more stable to chemical denaturation than the ferric protein. Other *b*-type hexacoordinate proteins have greater $D_{1/2}^{red}$ - $D_{1/2}^{ox}$ differences, e.g., cytochrome b_{562} has a $D_{1/2}^{red}$ - $D_{1/2}^{ox}$ difference of ~ 4.2 M *(93)* while SiaA has a difference value of 1.9 M *(23)*.

In thermal unfolding studies, T_m values for the ferrous and ferric protein Shr-N1are essentially the same. We are aware of a few other heme proteins for which thermal denaturation has been measured in both the ferrous and ferric forms. Four of these are cytochrome *c* derivatives (His-Met axial ligands), with T_m^{red} - T_m^{ox} of almost 30 °C *(102-104)*. Cytochrome b_{562}, a *b*-type heme protein with His-Met ligands, has a T_m^{red} - T_m^{ox} value of 15 °C *(105)*. For hemopexin, a *b*-type heme protein with two histidine ligands, the reduced protein unfolds more easily than the oxidized, but by a relatively small margin of about 3 °C (ferric of 64.6 °C and ferrous of 61.4 °C) *(106)*. The similarity of the T_m values of the two oxidation states is consistent with the similarity of the $D_{1/2}$ values in the unfolding induced by guanidinium.

7.5.5 Role of methionine in heme binding

A possible reason for bismethionine ligation of Shr-N1 is to allow uptake of not only ferric, but also ferrous, heme. In general, thioethers bind ferrous heme more tightly than ferric heme. Early model studies with methionine derivatives showed significantly more binding of the ligand to the ferrous than to the ferric heme *(107, 108)*. The difference in the affinity of methionine for the heme as a function of oxidation state has been used to study protein folding *(109)*. In protein models for bismethionine ligation, the H102M mutant of cytochrome b_{562} has

bisMet ligation in the reduced state. In the oxidized state, both methionines are bound at neutral pH, but addition of base results in only one of the methionines being coordinated to the heme in the ferric state *(80, 110)*. Ferrous H93G Mb forms a monoTHT complex with a K_d value of 10 μM; a second THT binds with a K_d value of 66 mM at 4°C *(77)*. The ferric protein forms a monoTHT with a K_d value of 2.1 mM at 4°C; preparation of the bisTHT complex required 90 mM THT at 4°C *(79)*. It should be noted that although a number of lines of experimental evidence indicate that thioethers bind Fe(II) more tightly than Fe(III), the crystal structures of Fe(II) and Fe(III) iron porphyrins bisligated with tetrahydrothiophene and pentamethylene sulfide show essentially no difference in the iron-sulfur bond distances as a function of oxidation state *(111)*.

Heme transfer studies in the Sia/Hts pathway also indicate that both oxidation states of the heme can be transported *(22, 26, 48, 56, 57, 112)*. It has been shown that Shr-N1 can bind heme from methemoglobin *(24)*. Heme transfer from ferric Shr-N1 to apo-Shp had both a fast and a slow phase with rates of 2.50 ± 0.04 s^{-1} μM^{-1} and 0.017 ± 0.004 s^{-1} μM^{-1}, respectively. Transfer of ferric heme gave ferrous Shp, apparently arising from autoreduction of this protein *(26)*. The transfer process from Shp to SiaA was fit with initial formation of a complex, followed by heme transfer. The dissociation constants of ferric and ferrous Shp to apo-SiaA, 48 ± 7 μM and 120 ± 18 μM, respectively, indicated that complex formation had little dependence on the oxidation state of the heme *(22)*. Similar rate constants of Shp to SiaA heme transfer were reported: 43 ± 3 s^{-1} for ferric heme and 28 ± 6 s^{-1} for ferrous heme. Transfer of either Fe(II) or Fe(III) heme from Shp resulted in ferric heme in SiaA, apparently due to spontaneous autooxidation *(22)*. These kinetic results and observations demonstrate the versatility of this

heme uptake pathway to allow the binding of not only ferric heme, but also ferrous heme, and may be conducive of a method of survival which ensures the cell has heme availability.

7.6 References

[1] Anzaldi, L. L., and Skaar, E. P. (2010) Overcoming the heme paradox: Heme toxicity and tolerance in bacterial pathogens. *Infect. Immun. 78*, 4977-4989.

[2] Braun, V., and Hantke, K. (2011) Recent insights into iron import by bacteria. *Curr. Opin. Chem. Biol. 15*, 328-334.

[3] Benson, D. R., and Rivera, M. (2013) Heme uptake and metabolism in bacteria. *Met. Ions Life Sci 12*, 279-332.

[4] Cescau, S., Cwerman, H., Létoffé, S., Delepelaire, P., Wandersman, C., and Biville, F. (2007) Heme acquisition by hemophores. *BioMetals 20*, 603-613.

[5] Cavallaro, G., Decaria, L., and Rosato, A. (2008) Genome-based analysis of heme biosynthesis and uptake in prokaryotic systems. *J. Proteome Res. 7*, 4946-4954.

[6] Tong, Y., and Guo, M. (2009) Bacterial heme-transport proteins and their heme-coordination modes. *Arch. Biochem. Biophys. 481*, 1-15.

[7] Mayfield, J. A., Dehner, C. A., and DuBois, J. L. (2011) Recent advances in bacterial heme protein biochemistry. *Curr. Opin. Chem. Biol. 15*, 260-266.

[8] Wilks, A., and Barker, K. D. (2011) Mechanisms of heme uptake and utilization in bacterial pathogens, In *Handbook of Porphyrin Science with Applications to Chemistry, Physics, Materials Science, Engineering, Biology and Medicine, Vol 15: Biochemistry of Tetrapyrroles* (Kadish, K. M., Smith, K. M., and Guilard, R., Eds.), pp 357-398, World Scientific, Hacksensack, NJ.

[9] Gruss, A., Borezée-Durant, E., and Lechardeur, D. (2012) Environmental heme utilization by heme-auxotrophic bacteria, In *Advances in Bacterial Respiratory Physiology* (Poole, R. K., Ed.) 61 ed., pp 69-124, Academic Press, London, England.

[10] Smith, A. D., and Wilks, A. (2012) Extracellular heme uptake and the challenges of bacterial cell membranes. *Curr. Top. Membr. 69*, 359-392.

[11] Farrand, A. J., and Skaar, E. P. (2014) Heme and infectious diseases, In *Handbook of Porphyrin Science with Applications to Chemistry, Physics, Materials Science, Engineering, Biology and Medicine, Vol 26: Heme Biochemistry* (Ferreira, G. C., Kadish, K. M., Smith, K. M., and Guilard, R., Eds.) 26 ed., pp 317-377, World Scientific, Hackensack, NJ.

[12] Rodgers, K. R., and Lukat-Rodgers, G. S. (2014) Biophysical perspectives on the acquisition, transport, and trafficking of heme in bacteria. *Handbook of Porphyrin Science with Applications to Chemistry, Physics, Materials Science, Engineering, Biology and Medicine, Vol. 30: Heme Proteins, Part II 30*, 249-309.

[13] Wilks, A., and O'Neill, M. J. (2014) Extracellular heme uptake and metabolism in bacterial pathogenesis, In *Handbook of Porphyrin Science with Applications to Chemistry, Physics, Materials Science, Engineering, Biology and Medicine, Vol 26: Heme Biochemistry* (Ferreira, G. C., Kadish, K. M., Smith, K. M., and Guilard, R., Eds.), pp 267-315, World Scientific, Hackensack, NJ.

[14] Nobles, C. L., and Maresso, A. W. (2011) The theft of host heme by Gram-positive pathogenic bacteria. *Metallomics 3*, 788-796.

[15] Schmitt, M. P. (2014) Iron acquisition and iron-dependent gene expression in *Corynebacterium diphtheriae*, In *Corynebacterium diphtheriae and Related Toxigenic Species: Genomics, Pathogenicity and Applications* (Burkovski, A., Ed.), pp 95-121.

[16] Draganova, E. B., Akbas, N., Adrian, S. A., Lukat-Rodgers, G. S., Collins, D. P., Dawson, J. H., Allen, C. E., Schmitt, M. P., Rodgers, K. R., and Dixon, D. W. (2015) Heme binding by *Corynebacterium diphtheriae* HmuT: Function and heme environment. *Biochemistry 54*, 6598-6609.

[17] Grigg, J. C., Ukpabi, G., Gaudin, C. F., and Murphy, M. E. (2010) Structural biology of heme binding in the *Staphylococcus aureus* Isd system. *J. Inorg. Biochem. 104*, 341-348.

[18] Hammer, N. D., and Skaar, E. P. (2011) Molecular mechanisms of *Staphylococcus aureus* iron acquisition. *Annu. Rev. Microbiol. 65*, 129-147.

[19] Haley, K. P., and Skaar, E. P. (2012) A battle for iron: Host sequestration and *Staphylococcus aureus* acquisition. *Microb. Infect. 14*, 217-227.

[20] Tiedemann, M. T., Pinter, T. B., and Stillman, M. J. (2012) Insight into blocking heme transfer by exploiting molecular interactions in the core Isd heme transporters IsdA-NEAT, IsdC-NEAT, and IsdE of *Staphylococcus aureus*. *Metallomics 4*, 751-760.

[21] Honsa, E. S., and Maresso, A. W. (2011) Mechanisms of iron import in anthrax. *BioMetals 24*, 533-545.

[22] Nygaard, T. K., Blouin, G. C., Liu, M. Y., Fukumura, M., Olson, J. S., Fabian, M., Dooley, D. M., and Lei, B. F. (2006) The mechanism of direct heme transfer from the streptococcal cell surface protein Shp to HtsA of the HtsABC transporter. *J. Biol. Chem. 281*, 20761-20771.

[23] Sook, B. R., Block, D. R., Sumithran, S., Montañez, G. E., Rodgers, K. R., Dawson, J. H., Eichenbaum, Z., and Dixon, D. W. (2008) Characterization of SiaA, a streptococcal heme-binding protein associated with a heme ABC transport system. *Biochemistry 47*, 2678-2688.

[24] Ouattara, M., Cunha, E. B., Li, X., Huang, Y. S., Dixon, D. W., and Eichenbaum, Z. (2010) Shr of Group A streptococcus is a new type of composite NEAT protein involved in sequestering haem from methaemoglobin. *Mol. Microbiol. 78*, 739-756.

[25] Eichenbaum, Z. (2012) The streptococcal hemoprotein receptor. A moonlighting protein or a virulence factor? *Virulence 3*, 553-555.

[26] Ouattara, M., Pennati, A., Devlin, D. J., Huang, Y. S., Gadda, G., and Eichenbaum, Z. (2013) Kinetics of heme transfer by the Shr NEAT domains of Group A Streptococcus. *Arch. Biochem. Biophys. 538*, 71-79.

[27] Akbas, N., Draganova, E. B., Block, D. R., Sook, B. R., Chan, Y. F., Zhuo, J., Eichenbaum, Z., Rodgers, K. R., and Dixon, D. W. (2015) Heme-bound SiaA from *Streptococcus pyogenes*: Effects of mutations and oxidation state on protein stability. *J. Inorg. Biochem.*

[28] Andrade, M. A., Ciccarelli, F. D., Perez-Iratxeta, C., and Bork, P. (2002) NEAT: A domain duplicated in genes near the components of a putative Fe(3+) siderophore transporter from Gram-positive pathogenic bacteria. *Genome Biol. 3*, RESEARCH0047.

[29] Contreras, H., Chim, N., Credali, A., and Goulding, C. W. (2014) Heme uptake in bacterial pathogens. *Curr. Opin. Chem. Biol. 19*, 34-41.

[30] Honsa, E. S., Maresso, A. W., and Highlander, S. K. (2014) Molecular and evolutionary analysis of NEAr-iron Transporter (NEAT) domains. *PLoS One 9*.

[31] Grigg, J. C., Vermeiren, C. L., Heinrichs, D. E., and Murphy, M. E. P. (2007) Haem recognition by a *Staphylococcus aureus* NEAT domain. *Mol. Microbiol. 63*, 139-149.

[32] Gaudin, C. F. M., Grigg, J. C., Arrieta, A. L., and Murphy, M. E. P. (2011) Unique heme-iron coordination by the hemoglobin receptor IsdB of *Staphylococcus aureus*. *Biochemistry 50*, 5443-5452.

[33] Sharp, K. H., Schneider, S., Cockayne, A., and Paoli, M. (2007) Crystal structure of the heme-IsdC complex, the central conduit of the Isd iron/heme uptake system in *Staphylococcus aureus*. *J. Biol. Chem. 282*, 10625-10631.

[34] Watanabe, M., Tanaka, Y., Suenaga, A., Kuroda, M., Yao, M., Watanabe, N., Arisaka, F., Ohta, T., Tanaka, I., and Tsumoto, K. (2008) Structural basis for multimeric heme complexation through a specific protein-heme interaction - The case of the third NEAT domain of IsdH from *Staphylococcus aureus*. *J. Biol. Chem. 283*, 28649-28659.

[35] Ekworomadu, M. T., Poor, C. B., Owens, C. P., Balderas, M. A., Fabian, M., Olson, J. S., Murphy, F., Balkabasi, E., Honsa, E. S., He, C., Goulding, C. W., and Maresso, A. W. (2012) Differential function of Lip residues in the mechanism and biology of an anthrax hemophore. *PLoS Path. 8*.

[36] Honsa, E. S., Owens, C. P., Goulding, C. W., and Maresso, A. W. (2013) The near-iron transporter (NEAT) domains of the anthrax hemophore IsdX2 require a critical glutamine to extract heme from methemoglobin. *J. Biol. Chem. 288*, 8479-8490.

[37] Tarlovsky, Y., Fabian, M., Solomaha, E., Honsa, E., Olson, J. S., and Maresso, A. W. (2010) A *Bacillus anthracis* S-Layer homology protein that binds heme and mediates heme delivery to IsdC. *J. Bacteriol. 192*, 3503-3511.

[38] Vermeiren, C. L., Pluym, M., Mack, J., Heinrichs, D. E., and Stillman, M. J. (2006) Characterization of the heme binding properties of *Staphylococcus aureus* IsdA. *Biochemistry 45*, 12867-12875.

[39] Pluym, M., Muryoi, N., Heinrichs, D. E., and Stillman, M. J. (2008) Heme binding in the NEAT domains of IsdA and IsdC of *Staphylococcus aureus*. *J. Inorg. Biochem. 102*, 480-488.

[40] Malmirchegini, G. R., Sjodt, M., Shnitkind, S., Sawaya, M. R., Rosinski, J., Newton, S. M., Klebba, P. E., and Clubb, R. T. (2014) Novel mechanism of hemin capture by Hbp2, the hemoglobin-binding hemophore from *Listeria monocytogenes*. *J. Biol. Chem. 289*, 34886-34899.

[41] Balderas, M. A., Nobles, C. L., Honsa, E. S., Alicki, E. R., and Maresso, A. W. (2012) Hal is a *Bacillus anthracis* heme acquisition protein. *J. Bacteriol. 194*, 5513-5521.

[42] Cunningham, M. W. (2008) Pathogenesis of group A streptococcal infections and their sequelae. *Adv. Exp. Med. Biol 609*, 29-42.

[43] Ardanuy, C., Domenech, A., Rolo, D., Calatayud, L., Tubau, F., Ayats, J., Martin, R., and Linares, J. (2010) Molecular characterization of macrolide- and multidrug-resistant *Streptococcus pyogenes* isolated from adult patients in Barcelona, Spain (1993-2008). *J. Antimicrob. Chemother. 65*, 634-643.

[44] Walker, M. J., Barnett, T. C., McArthur, J. D., Cole, J. N., Gillen, C. M., Henningham, A., Sriprakash, K. S., Sanderson-Smith, M. L., and Nizet, V. (2014) Disease manifestations and pathogenic mechanisms of group a Streptococcus. *Clin. Microbiol. Rev. 27*, 264-301.

[45] Eichenbaum, Z., Muller, E., Morse, S. A., and Scott, J. R. (1996) Acquisition of iron from host proteins by the group A *Streptococcus*. *Infect. Immun. 64*, 5428-5429.

[46] Eichenbaum, Z., Green, B. D., and Scott, J. R. (1996) Iron starvation causes release from the group A streptococcus of the ADP-ribosylating protein called plasmin receptor or surface glyceraldehyde-3-phosphate-dehydrogenase. *Infect. Immun. 64*, 1956-1960.

[47] Montañez, G. E., Neely, M. N., and Eichenbaum, Z. (2005) The streptococcal iron uptake (Siu) transporter is required for iron uptake and virulence In a zebrafish infection model. *Microbiology-SGM 151*, 3749-3757.

[48] Zhu, H., Liu, M. Y., and Lei, B. F. (2008) The surface protein Shr of *Streptococcus pyogenes* binds heme and transfers it to the streptococcal heme-binding protein Shp. *BMC Microbiol. 8*, 15.

[49] Lei, B., Smoot, L. M., Menning, H. M., Voyich, J. M., Kala, S. V., Deleo, F. R., Reid, S. D., and Musser, J. M. (2002) Identification and characterization of a novel heme-associated cell surface protein made by *Streptococcus pyogenes*. *Infect. Immun. 70*, 4494-4500.

[50] Aranda, R., Worley, C. E., Liu, M., Bitto, E., Cates, M. S., Olson, J. S., Lei, B. F., and Phillips, G. N. (2007) Bis-methionyl coordination in the crystal structure of the heme-binding domain of the streptococcal cell surface protein Shp. *J. Mol. Biol. 374*, 374-383.

[51] Lei, B. F., Liu, M. Y., Prater, C. I., Kala, S. V., Deleo, F. R., and Musser, J. M. (2003) Identification and characterization of HtsA, a second heme-binding protein made by *Streptococcus pyogenes*. *Infect. Immun. 71*, 5962-5969.

[52] Bates, C. S., Montañez, G. E., Woods, C. R., Vincent, R. M., and Eichenbaum, Z. (2003) Identification and characterization of a *Streptococcus pyogenes* operon involved in binding of hemoproteins and acquisition of iron. *Infect. Immun. 71*, 1042-1055.

[53] Sun, X., Ge, R. G., Zhang, D., Sun, H., and He, Q. (2010) Iron-containing lipoprotein SiaA in SiaABC, the primary heme transporter of *Streptococcus pyogenes*. *J. Inorg. Biochem. 15*, 1265-1273.

[54] Ran, Y. C., Liu, M. Y., Zhu, H., Nygaard, T. K., Brown, D. E., Fabian, M., Dooley, D. M., and Lei, B. F. (2010) Spectroscopic identification of heme axial ligands in HtsA that are involved in heme acquisition by *Streptococcus pyogenes*. *Biochemistry 49*, 2834-2842.

[55] Liu, M. Y., and Lei, B. F. (2005) Heme transfer from streptococcal cell surface protein Shp to HtsA of transporter HtsABC. *Infect. Immun. 73*, 5086-5092.

[56] Ran, Y. C., Zhu, H., Liu, M. Y., Fabian, M., Olson, J. S., Aranda, R. I., Phillips, G. N., Dooley, D. M., and Lei, B. (2007) Bis-methionine ligation to heme iron in the streptococcal cell surface protein Shp facilitates rapid hemin transfer to HtsA of the HtsABC transporter. *J. Biol. Chem. 282*, 31380-31388.

[57] Ran, Y. C., Malmirchegini, G. R., Clubb, R. T., and Lei, B. F. (2013) Axial ligand replacement mechanism in heme transfer from streptococcal heme-binding protein Shp to HtsA of the HtsABC transporter. *Biochemistry 52*, 6537-6547.

[58] Fisher, M., Huang, Y. S., Li, X. R., Mciver, K. S., Toukoki, C., and Eichenbaum, Z. (2008) Shr is a broad-spectrum surface receptor that contributes to adherence and virulence in Group A Streptococcus. *Infect. Immun. 76*, 5006-5015.

[59] Dahesh, S., Nizet, V., and Cole, J. N. (2012) Study of streptococcal hemoprotein receptor (Shr) in iron acquisition and virulence of M1T1 group A streptococcus. *Virulence 3*, 566-575.

[60] Yang, J. Y., Yan, R. X., Roy, A., Xu, D., Poisson, J., and Zhang, Y. (2015) The I-TASSER Suite: protein structure and function prediction. *Nat. Methods 12*, 7-8.

[61] DeLano, W., L. (2015) The PyMOL Molecular Graphics System, Version 1.7.4 Schrödinger, LLC. *http://www. pymol. org*.

[62] Jorgensen, W. L., Chandrasekar, J., Madura, J. D., Impey, R. W., and Klein, M. L. (1983) Comparison of simple potential functions for simulating liquid water. *J. Chem. Phys. 79*, 926-935.

[63] Case, D. A., Cheatham, T. E., Darden, T., Gohlke, H., Luo, R., Merz, K. M., Onufriev, A., Simmerling, C., Wang, B., and Woods, R. J. (2005) The Amber biomolecular simulation programs. *J. Comput. Chem. 26*, 1668-1688.

[64] Hornak, V., Abel, R., Okur, A., Strockbine, B., Roitberg, A., and Simmerling, C. (2006) Comparison of multiple Amber force fields and development of improved protein backbone parameters. *Proteins 65*, 712-725.

[65] Giammona, D. A. (1984) *Ph. D. Thesis, University of California at Davis*.

[66] Humphrey, W., Dalke, A., and Schulten, K. (1996) VMD: Visual molecular dynamics. *J. Mol. Graphics 14*, 33-38.

[67] Pond, A. E., Roach, M. P., Thomas, M. R., Boxer, S. G., and Dawson, J. H. (2000) The H93G myoglobin cavity mutant as a versatile template for modeling heme proteins: Ferrous, ferric, and ferryl mixed-ligand complexes with imidazole in the cavity. *Inorg. Chem. 39*, 6061-6066.

[68] Dutton, P. L. (1978) Redox potentiometry: Determination of midpoint potentials of oxidation-reduction components of biological electron-transfer systems. *Methods Enzymol. 54*, 411-435.

[69] Pace, C. N., and Scholtz, J. M. (1997) Measuring the conformational stability of a protein, In *Protein Structure: A Practical Approach* (Creighton, T., Ed.) 2nd ed., pp 299-321, Oxford University Press, Oxford.

[70] Arnesano, F., Banci, L., Bertini, I., and Koulougliotis, D. (1998) Solution structure of oxidized rat microsomal cytochrome *b*(5) in the presence of 2 M guanidinium chloride: Monitoring the early steps in protein unfolding. *Biochemistry 37*, 17082-17092.

[71] Wittung-Stafshede, P. (1999) Equilibrium unfolding of a small low-potential cytochrome, cytochrome c_{553} from *Desulfovibrio vulgaris*. *Protein Sci. 8*, 1523-1529.

[72] Moczygemba, C., Guidry, J., and Wittung-Stafshede, P. (2000) Heme orientation affects holo-myoglobin folding and unfolding kinetics. *FEBS Lett. 470*, 203-206.

[73] Andersen, N. H., Nørgaard, A., Jensen, T. J., and Ulstrup, J. (2002) Sequential unfolding of the two-domain protein *Pseudomonas stutzeri* cytochrome *c*(4). *J. Inorg. Biochem. 88,* 316-327.

[74] Swint, L., and Robertson, A. D. (1993) Thermodynamics of unfolding for turkey ovomucoid third domain: Thermal and chemical denaturation. *Protein Sci. 2*, 2037-2049.

[75] Larkin, M. A., Blackshields, G., Brown, N. P., Chenna, R., McGettigan, P. A., McWilliam, H., Valentin, F., Wallace, I. M., Wilm, A., Lopez, R., Thompson, J. D., Gibson, T. J., and Higgins, D. G. (2007) Clustal W and Clustal X version 2.0. *Bioinformatics 23*, 2947-2948.

[76] Du, J., Sono, M., and Dawson, J. H. (2011) The H93G myoglobin cavity mutant as a versatile scaffold for modeling heme iron coordination structures in protein active sites and their characterization with magnetic circular dichroism spectroscopy. *Coord. Chem. Rev. 255*, 700-716.

[77] Perera, R., Sono, M., Sigman, J. A., Pfister, T. D., Lu, Y., and Dawson, J. H. (2003) Neutral thiol as a proximal ligand to ferrous heme iron: Implications for heme proteins that lose cysteine thiolate ligation on reduction. *Proc. Natl. Acad. Sci. USA 100*, 3641-3646.

[78] Schneider, S., Marles-Wright, J., Sharp, K. H., and Paoli, M. (2007) Diversity and conservation of interactions for binding heme in *b*-type heme proteins. *Nat. Prod. Rep. 24*, 621-630.

[79] Du, J., Sono, M., and Dawson, J. H. (2011) Ferric His93Gly myoglobin cavity mutant and its complexes with thioether and selenolate as heme protein models. *J. Porph. Phthalo. 15*, 29-38.

[80] Barker, P. D., Nerou, E. P., Cheesman, M. R., Thomson, A. J., de Oliveira, P., and Hill, H. A. (1996) Bis-methionine ligation to heme iron in mutants of cytochrome b_{562}. 1. Spectroscopic and electrochemical characterization of the electronic properties. *Biochemistry 35*, 13618-13626.

[81] Watt, G. D., McDonald, J. W., Chiu, C.-H., and Reddy, K. R. N. (1993) Further characterization of the redox and spectroscopic properites of *Azotobacter vinelandii* ferritin. *J. Inorg. Biol. Chem. 51*, 745-758.

[82] Othman, S., and Desbois, A. (1998) Resonance Raman investigation of lysine and N-acetylmethionine complexes of ferric and ferrous microperoxidase - Influences of the axial ligation on the heme *c* structure. *Eur. Biophys. J. Biophys. Lett. 28*, 12-25.

[83] Cheesman, M. R., Thomson, A. J., Greenwood, C., Moore, G. R., and Kadir, F. (1990) Bis-methionine axial ligation of haem in bacterioferritin from *Pseudomonas aeruginosa*. *Nature 346*, 771-773.

[84] George, G. N., Richards, T., Bare, R. E., Gea, Y., Prince, R. C., Stiefel, E. I., and Watt, G. D. (1993) Direct observation of bis-sulfur ligation to the heme of bacterioferritin. *J. Am. Chem. Soc 115,* 7716-7718.

[85] Romão, C. V., Regalla, M., Xavier, A. V., Teixeira, M., Liu, M. Y., and Legall, J. (2000) A bacterioferritin from the strict anaerobe *Desulfovibrio desulfuricans* ATCC 27774. *Biochemistry 39,* 6841-6849.

[86] Cheesman, M. R., Kadir, F. H. A., Albasseet, J., Almassad, F., Farrar, J., Greenwood, C., Thomson, A. J., and Moore, G. R. (1992) EPR and magnetic circular-dichroism spectroscopic characterization of bacterioferritin from *Pseudomonas aeruginosa* and *Azotobacter vinelandii*. *Biochem. J. 286,* 361-367.

[87] Watt, G. D. (1986) Redox properties and Mössbauer spectroscopy of *Azotobacter vinelandii* bacterioferritin. *Biochemistry 25,* 4330-4336.

[88] Meyer, T. E., and Cusanovich, M. A. (1985) Soluble cytochrome composition of the purple phototrophic bacterium, *Rhodopseudomonas sphaeroides* ATCC-17023. *Biochim. Biophys. Acta 807,* 308-319.

[89] Chan, A. C. K., Lelj-Garolla, B., Rosell, F. I., Pedersen, K. A., Mauk, A. G., and Murphy, M. E. P. (2006) Cofacial heme binding is linked to dimerization by a bacterial heme transport protein. *J. Mol. Biol. 362,* 1108-1119.

[90] Wittung-Stafshede, P. (1999) Effect of redox state on unfolding energetics of heme proteins. *Biochim. Biophys. Acta 1432,* 401-405.

[91] Bowler, B. E. (2007) Thermodynamics of protein denatured states. *Mol. Biosyst. 3,* 88-99.

[92] Wittung-Stafshede, P., Gray, H. B., and Winkler, J. R. (1997) Rapid formation of a four-helix bundle. Cytochrome b_{562} folding triggered by electron transfer. *J. Am. Chem. Soc. 119,* 9562-9563.

[93] Wittung-Stafshede, P., Lee, J. C., Winkler, J. R., and Gray, H. B. (1999) Cytochrome b_{562} folding triggered by electron transfer: Approaching the speed limit for formation of a four-helix-bundle protein. *Proc. Natl. Acad. Sci. U. S. A. 96,* 6587-6590.

[94] Silchenko, S., Sippel, M. L., Kuchment, O., Benson, D. R., Mauk, A. G., Altuve, A., and Rivera, M. (2000) Hemin is kinetically trapped in cytochrome *b*(5) from rat outer mitochondrial membrane. *Biochem. Biophys. Res. Commun. 273,* 467-472.

[95] Wolff, N., Sapriel, G., Bodenreider, C., Chaffotte, A., and Delepelaire, P. (2003) Antifolding activity of the SecB chaperone is essential for secretion of HasA, a quickly folding ABC pathway substrate. *J. Biol. Chem. 278,* 38247-38253.

[96] Manyusa, S., Mortuza, G., and Whitford, D. (1999) Analysis of folding and unfolding reactions of cytochrome *b*(5). *Biochemistry 38,* 14352-14362.

[97] Schechter, A. N., and Epstein, C. J. (1968) Spectral studies on the denaturation of myoglobin. *J. Mol. Biol. 35*, 567-589.

[98] Puett, D. (1973) Equilibrium unfolding parameters of horse and sperm whale myoglobin. Effects of guanidine hydrochloride, urea, and acid. *J. Biol. Chem 248*, 4623-4634.

[99] Hargrove, M. S., and Olson, J. S. (1996) The stability of holomyoglobin is determined by heme affinity. *Biochemistry 35*, 11310-11318.

[100] Myers, J. K., Pace, C. N., and Scholtz, J. M. (1995) Denaturant *m* values and heat capacity changes: Relation to changes in accessible surface areas of protein unfolding. *Protein Sci. 4*, 2138-2148.

[101] Thoren, K. L., Connell, K. B., Robinson, T. E., Shellhamer, D. D., Tammaro, M. S., and Gindt, Y. M. (2006) The free energy of dissociation of oligomeric structure in phycocyanin is not linear with denaturant. *Biochemistry 45*, 12050-12059.

[102] Cohen, D. S., and Pielak, G. J. (1995) Entropic stabilization of cytochrome *c* upon reduction. *J. Am. Chem. Soc 117*, 1675-1677.

[103] Lett, C. M., Berghuis, A. M., Frey, H. E., Lepock, J. R., and Guillemette, J. G. (1996) The role of a conserved water molecule in the redox-dependent thermal stability of iso-1-cytochrome *c*. *J. Biol. Chem. 271*, 29088-29093.

[104] Uchiyama, S., Ohshima, A., Nakamura, S., Hasegawa, J., Terui, N., Takayama, S. I. J., Yamamoto, Y., Sambongi, Y., and Kobayashi, Y. (2004) Complete thermal-unfolding profiles of oxidized and reduced cytochromes c. *J. Am. Chem. Soc. 126*, 14684-14685.

[105] Fisher, M. T. (1991) Differences in thermal stability between reduced and oxidized cytochrome b_{562} from *Escherichia coli*. *Biochemistry 30*, 10012-10018.

[106] Rosell, F. I., Mauk, M. R., and Mauk, A. G. (2005) pH- and Metal ion-linked stability of the hemopexin-heme complex. *Biochemistry 44*, 1872-1879.

[107] Harbury, H. A., Cronin, J. R., Fanger, M. W., Hettinger, T. P., Murphy, A. J., Myer, Y. P., and Vinogradov, S. N. (1965) Complex formation between methionine and a heme peptide from cytochrome *c*. *Proc. Natl. Acad. Sci. U. S. A. 54*, 1658-1664.

[108] Warme, P. K., and Hager, L. P. (1970) Heme sulfuric anhydrides. II. Properties of heme models prepared from mesoheme sulfuric anhydrides. *Biochemistry 9*, 1606-1614.

[109] Telford, J. R., Wittung-Stafshede, P., Gray, H. B., and Winkler, J. R. (1998) Protein folding triggered by electron transfer. *Acc. Chem. Res. 31*, 755-763.

[110] Barker, P. D., and Freund, S. M. (1996) Bis-methionine ligation to heme iron in mutants of cytochrome b_{562}. 2. Characterization by NMR of heme-ligand interactions. *Biochemistry 35*, 13627-13635.

[111] Mashiko, T., Reed, C. A., Haller, K. J., Kastner, M. E., and Scheidt, W. R. (1981) Thioether ligation in iron-porphyrin complexes: Models for cytochrome *c*. *J. Am. Chem. Soc. 103*, 5758-5767.

[112] Lu, C. M., Xie, G., Liu, M. Y., Zhu, H., and Lei, B. F. (2012) Direct heme transfer reactions in the group A *Streptococcus* heme acquisition pathway. *PLoS One 7*.

7.7 Supplementary Information

7.7.1 Supplementary Figures

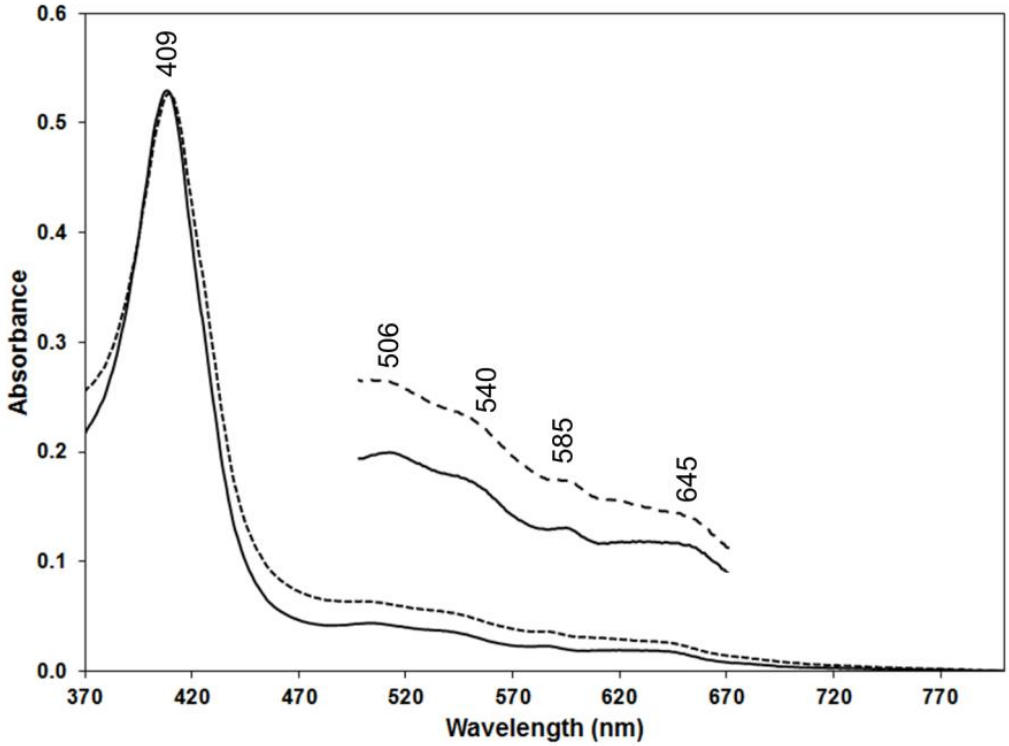

Figure 7.11 S1 UV spectral comparison of Fe(III) WT Shr-N1 (solid line) and Fe(III) K119A Shr-N1 (dashed line). Both samples were recorded in 50 mM Tris-Cl, pH 7.0 and oxidized with potassium ferricyanide.

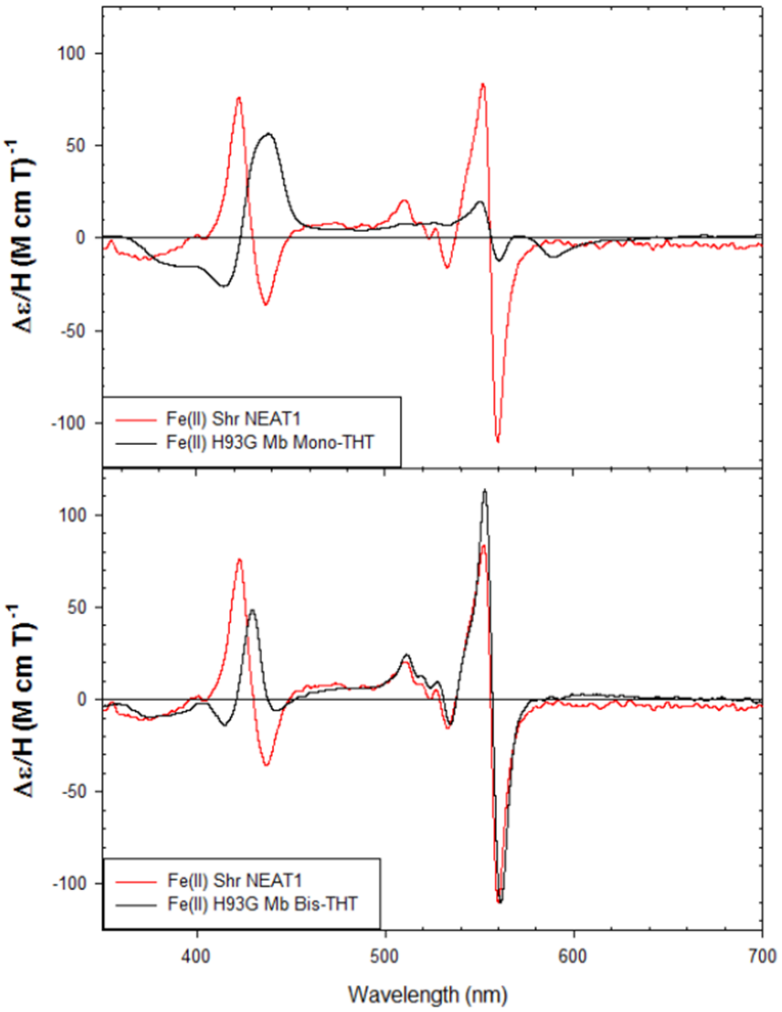

Figure 7.12 S2 Comparison of the MCD spectra for Fe(II) Shr-ntdN1 at pH 6.5 with mono-THT (top panel) and bis-THT H93G Mb (bottom panel). Experiments were completed in 50 mM Tris-Cl buffer at 4˚ C.

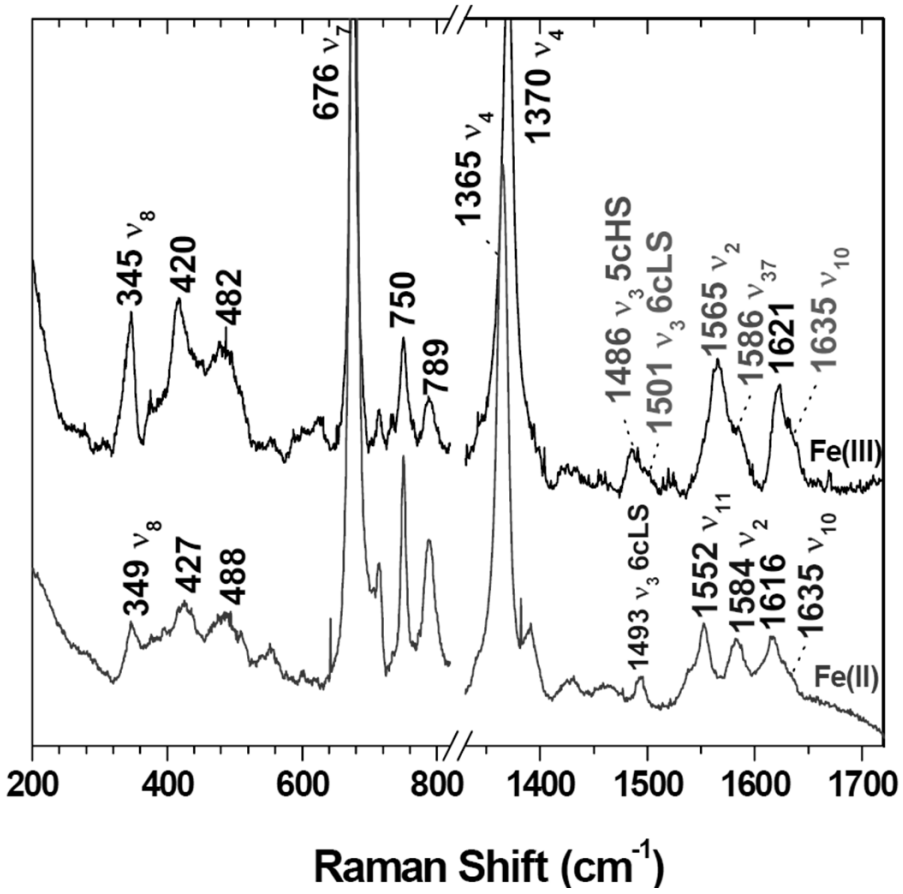

Figure 7.13 S3 Resonance Raman spectra of ferric and ferrous Shr-ntdN1. Soret-excited (413.1 nm) spectra were recoreded for the ferric and ferrous forms. Samples were prepared in 20 mM Tris-Cl, pH 8, 0.1% glycerol. The ferric 6cLS, 5cHS, and ferrous 6cLS marker bands are labeled accordingly.

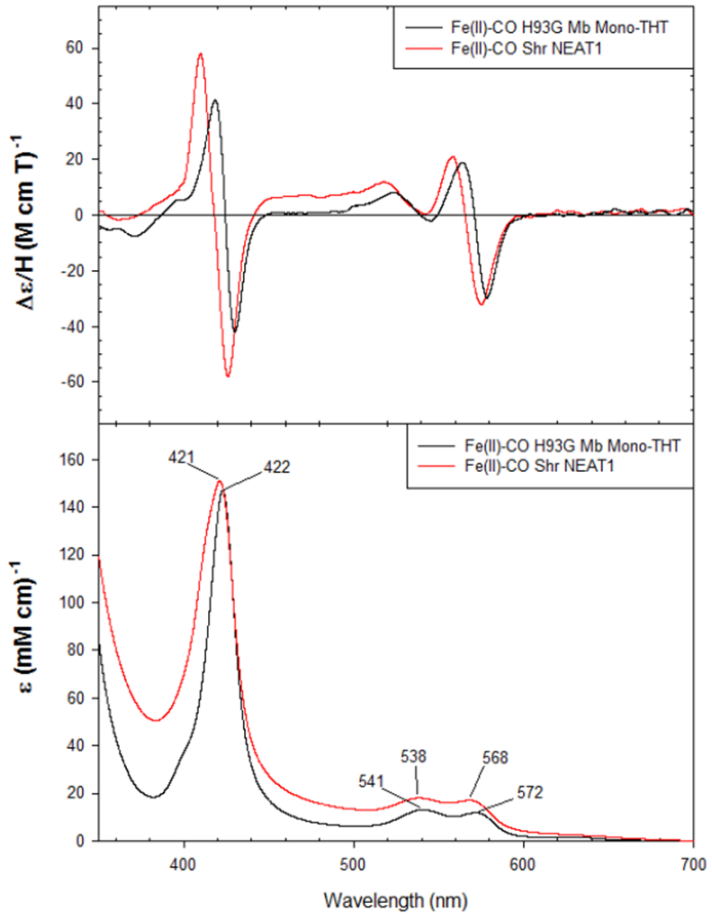

Figure 7.14 S4 Comparison of the MCD and UV-visible spectra for Fe(II)-CO Shr-ntdN1 at pH 6.5 with Fe(II)-CO mono-THT H93G Mb. Experiments were completed in 50 mM Tris-Cl buffer at 4˚ C.

8 THE SECOND HEME-BINDING NEAT DOMAIN OF SHR IN *STREPTOCOCCUS PYOGENES*

This chapter is intended for publication and is verbatim of the manuscript in progress. The site-directed mutagenesis of the lysine mutants, expression, purification, UV-visible absorption spectroscopy, mutant pH titrations, and thermal unfolding were performed by E. B. Draganova at Georgia State University.

8.1 Introduction

Iron is a required metal for many living organisms, including pathogenic bacteria *(1-3)*. In the human body iron is majorly found in the form of heme (protoporphyrin IX) and bound to proteins such as hemoglobin *(2)*. Pathogens have therefore developed different strategies to obtain the necessary iron in the form of heme *(3-6)*. It has been shown that pathogens can synthesize heme, obtain heme from the environment, or evoke both strategies *(7, 8)*.

Numerous studies have been performed on pathogenic bacteria which utilize sophisticated protein machinery to bind and transport heme to the intracellular space *(2, 3, 5, 9-13)*. Specifically, Gram-positive bacterial heme uptake pathway studies have focused on *Corynebacterium diphtheriae (14, 15), Bacillus anthracis (16), Staphylococcus aureus (17, 18),* and *Streptococcus pyogenes* [Group A Streptococcus (GAS)] *(19-22)*. With the exception of *C. diphtheriae*, the heme uptake pathways in *B. anthracis, S. aureus,* and *S. pyogenes* employ the use of near iron transporter (NEAT) domains *(23, 24)*. NEAT domains assist in heme binding and consist of conserved secondary structural features including β-strands and a 3_{10} α-helix *(24)*.

The majority of NEAT domains studied to date have been from the Isd heme uptake systems such as *S. aureus* IsdC *(25)* and IsdH-N3 *(26)* and *B. anthracis* IsdX1 and IsdX2-N5 *(24, 27, 28)*. These NEAT domains bind heme in a five-coordinate fashion utilizing an YXXXY motif in which the first Tyr from the β-8 strand is a heme axial ligand and the second Tyr is hydrogen bonded to the first. Some Isd NEAT domains slightly vary from this canonical heme binding motif. For example, *S. aureus* IsdB-N2 binds heme with a Tyr in the fifth position and sometimes a methionine coordinating the sixth position to form a Met/Tyr ligation *(29)* and IsdA binds tyrosine in the ferric state and histidine in the ferrous state *(30)*. *B. anthracis* HalA utilizes a YXXXF motif, rather than YXXXY *(31)*. The proposed hemophore Hbp2 (Hbp2-N2) from

Listeria monocytogenes differs in that the axial tyrosine extends from the β-7 strand, rather than β-8 *(32)*. Hbp2-N2 does not utilize a hydrogen-bonding tyrosine to the axial tyrosine and instead employs an alanine.

Recently, our group reported a novel type of NEAT domain from *S. pyogenes*, Shr-N1, which utilizes a bis-methionine axial ligation pair (Chapter 7). Shr-N1 lacks the YXXXY motif and is replaced with YXXXT. This domain is sensitive to pH, in that at acidic pH it is six-coordinate low-spin (6cLS) and five-coordinate high-spin (5cHS) in alkaline conditions. This novel NEAT heme ligand set and recent sequence alignment studies by Honsa et al. *(24)* indicate a variety of heme binding motifs may exist among the NEAT family.

S. pyogenes is a Gram-positive pathogen which cannot synthesize heme *(7)* and utilizes a heme uptake pathway containing NEAT domains to obtain heme from the environment *(33-35)*. *S. pyogenes* is the cause of a variety of infections including toxic shock syndrome and necrotizing fasciitis and has shown increasing antibiotic resistance *(19, 36, 37)*. Inhibiting the ability of the pathogen to take heme from the environment by targeting the heme uptake pathway may lead to alternative therapies to combat this pathogen.

The Sia heme uptake system of *S. pyogenes* is made of multiple proteins which bind and transfer heme to the intracellular environment. The first protein in the pathway, Shr (streptococcal hemoprotein receptor), is a cellular surface heme binding protein which can obtain heme from methemoglobin *(21)*. The heme is transferred to a second cellular surface protein, Shp (streptococcal cell surface protein) *(22, 38, 39)* which gives the heme to SiaA (HtsA, the periplasmic binding protein) *(40-42)*. SiaA is part of an ABC (ATP-binding cassette) heme transporter including SiaB (the permease) and SiaC (the ATPase) which brings the heme into the cell *(20, 43-46)*.

Shr contains two NEAT domains, Shr-NEAT1 (Shr-N1) and Shr-NEAT2 (Shr-N2). Previous work by our group showed Shr-N1 to utilize a bis-methionine axial ligation set to coordinate the heme iron. Sequence alignment of Shr-N1 with Shr-N2 indicated Shr-N2 to also potentially employ a bis-methionine axial ligation using a M26 N-terminal ligand and a M136 C-terminal ligand. Heme transfer studies by Ouattara et al. showed Shr-N1 obtains heme from the extracellular space and is able to transfer to either Shr-N2 or to Shp, the next protein in the pathway. Transfer of heme between Shr-N1 and Shr-N2 was shown to be reversible and may indicate Shr-N2 is used as a storage source of heme. Shr-N2 is prone to autoreduction, unlike the sister domain Shr-N1, and could be utilized as a means of ensuring heme remains bound to the protein during storage.

Herein we report the biophysical characterization of *S. pyogenes* Shr-N2, extending previous work from our laboratories. We have shown Shr-N2 to have a bismethionine ligand set using UV-visible absorption, magnetic circular dichroism, and resonance Raman spectroscopies. These data, including determination of the reduction potential, are consistent with a bismethionine ligand pair. In addition, we have probed the role of nearby lysine residues by the creation of alanine mutants (K29A and K57A) in the heme binding pocket in regards to autoreduction of Shr-N2. Protein unfolding studies via guanidinium hydrochloride and temperature of both ferric and ferrous Shr-N2 were also investigated to probe the stability of the domain in regards to heme transfer and release.

8.2 Materials and Methods

8.2.1 Homology modeling

A homology model of Shr-N2 was built using I-TASSER, a secondary structure prediction program *(47)*. The program chooses ten similar programs to create the model. Hbp2-

N2 from *Lysteria monocytogenes* was the closest protein with an identity percentage of 18%. The model was visualized using PyMOL *(48)*.

8.2.2 Construction, expression, and purification of WT Shr-N2 and mutants

The recombinant Shr-N2 protein was cloned as previously described *(21)*. Site-directed mutagenesis was used to construct recombinant Shr-N2 mutants with K29A and K57A amino acid substitutions. 100 ng of each primer containing the targeted base change and 75 ng of plasmid template were used in the mutagenesis reaction. Methylated template DNA was removed via Dpn1 digestions and mutagenized DNA was recovered by transformation into BL21(DE3) competent cells. Base changes were confirmed using sequence analysis. Plasmid pASK-IBA-12 containing the cloned Strep-tag-*neat2* gene was used for the site-directed mutagenesis. The WT protein (*E. coli* XL1 blue strains) and mutants [BL21(DE3) cells] were grown in Luria-Bertani (LB) media containing 100 µg/mL ampicillin. Inoculation was done with an overnight pre-culture and cells were grown at 30 °C. When the OD_{600} of the culture reached 0.5 – 0.6, protein expression was induced by adding anhydrotetracycline (AHT) to a final concentration of 200 ng/mL. The culture was incubated overnight at 27 °C. Cells were harvested by centrifugation at 8000 *g* and 4 °C. The cell pellet was resuspended in extract solution (20 mM Tris-HCl, 100 mM NaCl, Triton X-100 0.1%). Protease inhibitor (Roche Complete Mini, EDTA-free) cocktail was added to the cell suspension (1 tablet per liter of culture). The cells were lysed by French press (SIM AMINCO). The cell lysate was centrifuged at 8000 *g* and 4 °C.

All of the following purification steps were conducted at 4 °C using fast protein liquid chromatography and all buffer solutions were pH 8.0 unless specified otherwise. The protein supernatant was loaded onto a Strep-Tactin Superflow column (5 mL, IBA BioTAGnology),

washed with 15 column volumes of buffer A (100 mM Tris-HCl, 150 mM NaCl, pH 8.0) and eluted with 10 column volumes of buffer B (100 mM Tris-HCl, 150 mM NaCl, 2.5 mM *d*-desthiobiotin, pH 8.0) via a linear gradient. Protein fractions were collected and analyzed for purity using sodium dodecyl sulfate polyacrylamide gel electrophoresis and matrix-assisted laser desorption (MALDI) mass spectrometry. Minor differences in the optical spectra were observed as a function of the buffer type. The Shr-N2 protein is purified as a mixture of ferric and ferrous states.

8.2.3 Magnetic circular dichroism spectroscopy

Magnetic circular dichroism (MCD) spectra were measured with a magnetic field strength of 1.41 T by using a JASCO J815 spectrophotometer. This instrument was equipped with a JASCO MCD-1B electromagnet and interfaced with a Silicon Solutions PC through a JASCO IF-815-2 interface unit. Data acquisition and manipulation using Cary or Jasco software has been previously described *(49)*. To ensure homogeneity of ferric oxidation for the various mutants, ferricyanide was used to fully oxidize the heme center, followed by desalting chromatography. The resulting spectra were compared to data from other heme-containing proteins with known binding site structures and optical spectra. All spectral measurements for all proteins were carried out with a 0.2 cm quartz cuvette at 4 °C in 50 mM phosphate buffer (either pH 6.5 or 10).

8.2.4 Resonance Raman spectroscopy

Resonance Raman (rR) spectra were collected using the 441.6-nm emission line from a HeCd laser or either 406.7 nm or 413.1 nm emission from a Kr^+ laser. The laser power was adjusted to 2 – 5 mW at the sample. Spectra were recorded at ambient temperature using the 135° backscattering geometry with the laser beam focused to a line on a spinning 5 mm NMR

tube. Toluene, DMSO, and CH_2Br_2 were used as external standards for spectral calibration. UV-visible absorption spectra were recorded before and after rR experiments to verify that the samples were not altered by exposure to the laser beam. The ferric spectra of the proteins were recorded following oxidation with ferricyanide and buffer exchange by centrifugal concentration and dilution to remove excess oxidant and glycerol. The pH was adjusted by diluting a concentrated stock solution of protein into 20 mM MES, 20 mM TAPS, and 20 mM CAPS adjusted to the specified pH.

Ferrous Shr-N2 samples (~40 μM) were prepared anaerobically in 5 mm NMR tubes. The protein samples were prepared in 0.1 M Tris-Cl pH 8.2 and equilibrated with water-saturated, O_2-scrubbed N_2 that had been saturated with water. After equilibration under the N_2 atmosphere, an 86-fold excess of aqueous sodium dithionite, buffered at the same pH, was added using a gas-tight 10 μL syringe. Laser power for the ferrous samples ranged from 4 to 8 mW. Ferrous carbonyl adducts (40 to 75 μM) were prepared by reducing the proteins in 0.1 M Tris-Cl pH 8.8 with a 70- to 180-fold excess of buffered sodium dithionite, as described above, except that the reduction was carried out under an atmosphere of natural abundance CO or ^{13}CO (99 atom % ^{13}C) instead of N_2. Laser power for the heme carbonyl samples was held between 2 and 4.5 mW to minimize CO ligand photolysis.

8.2.5 Guanidinium unfolding studies

Protein unfolding experiments were performed using GdnHCl as the denaturant, according to the standard protocols *(50)*. The unfolding process was followed by UV-visible absorption spectroscopy in 50 mM Tris-HCl, pH 7.0 [Varian 50 Bio spectrophotometer, 1.5 mL quartz Supracil cuvettes (Spectracell) with 1 cm path lengths], following the changes at the Soret, using the single cell technique *(51, 52)*. The GdnHCl stock solution concentration was

8.32 M (50 mM Tris-HCl, pH 7.0) measured by refractive index *(50)*. Data were analyzed using the equation describing a two-state process *(50)*:

$$y = [(Abs_F + m_F[D]) + (Abs_U + m_U \exp[m([D]-[D]_{1/2})/RT])]/1 + \exp[m([D]-[D]_{1/2})/RT] \quad [1]$$

where y is the absorbance at any point along the fitted denaturation curve, Abs_F is the absorbance of the folded state, Abs_U is the absorbance of the unfolded state, m is the slope at the midpoint, and also the dependence of the free energy of unfolding on the denaturant concentration, m_F is the slope of the folded state, m_U is the slope of the unfolded state, [D] is the concentration of GdnHCl, $[D]_{1/2}$ is the concentration of GdnHCl at the midpoint of the unfolding curve, R is the gas constant, and T is the temperature (Kelvin).

8.2.6 Thermal unfolding studies

Thermal denaturation of Shr-N2 was carried out with a UV-visible absorption spectrophotometer (Cary 50 Bio) equipped with a temperature control (TC 125, Quantum Northwest). Quartz Supracil cuvettes (Spectracell) with 1 cm path lengths were used. The protein (~5 μM) in sodium phosphate (50 mM, pH 7.5), the spectrum (250 – 800 nm) was recorded every 2 °C from 20 °C to 60 °C after the sample was equilibrated for each temperature. The samples were cooled to room temperature and observed via UV-visible absorption spectroscopy for refolding. In both the ferric and ferrous proteins, the protein was prone to precipitation above 60 °C. The data were fit to a two-state unfolding model *(53)*:

$$Y_{abs} = \{(Y_F + m_F T) + (Y_U + m_U T) \exp[\Delta H_m/R(1/T_m - 1/T)]\}/\{1 + \exp(\Delta H_m/R(1/T_m - 1/T)]\}$$

where the ΔH_m is the enthalpy of unfolding, T_m is the temperature at which the protein is half unfolded and the remaining variables are as described above. The extent of protein unfolding is presented as the fraction of folded protein.

8.2.7 pH titration – autooxidation and autoreduction studies

To analyze the autooxidation and autoreduction of Shr-N2, pH titrations were monitored via UV-visible absorption spectroscopy. All samples were allowed to equilibrate for about 10 min after each addition before a spectrum was obtained. In the first experiment, Shr-N2 was reduced with dithionite followed by removal of the dithionite via ultrafiltration. Aliquots of 1.0 M NaOH were added to Fe(II) Shr-N2 in a buffer of 20 mM each CAPS, MES, and Tris-Cl until the pH was around 10. The sample was then back titrated with 1.0 M HCl to the starting pH and the experiment was performed again using the same sample.

In a second pH study, Shr-N2 in 20 mM each CAPS, MES, and Tris-Cl was treated with small aliquots of 1.0 M HCl or 1.0 M NaOH over a cumulative pH range of 6.5 - 10.5. At each pH point, the solution was held until it reached equilibrium, e.g., until ΔA_{Soret} changed by less than 0.001 over 10 min. UV-visible absorption spectroscopy was used to monitor the protein first in basic pH (10.4), then titrated to an acidic pH (6.6), and finally titrated back to basic pH (10.5). The protein incubated for 24 h at each pH point.

8.2.8 Electrochemistry

Shr-N2was diluted to 10 μM with 50 mM Tris-HCl, pH 8 and 100 mM NaCl. A mediator solution was prepared by dissolving phenazine methosulfate, 2,6-dimethyl benzoquinone, 2-methyl-1,4-benzoquinone, 1,2-napthoquinone-4-sulfonate, and quinhydrone in DMSO for a final concentration of 10 mM for each dye. The final concentration of the mediator was 10 μM in the sample cuvette and covered the potential range of 80 – 280 mV. The titrations

were carried out under a nitrogen atmosphere using 0.05 M dithionite as the reductant and 0.02 M ferricyanide as the oxidant. The Ag/AgCl reference 216 electrode was calibrated using buffered quinhydrone at pH 7 (E_m = 292 mV vs. NHE) *(54)*. The UV-visible absorption absorbance spectra were recorded at each experimental potential after equilibrium had been established, as judged by the cell having reached a constant potential.

The samples were initially treated with enough dithionite to completely reduce the heme. The solution was then titrated with ferricyanide to follow the heme oxidation spectroelectrochemically. The reverse, reductive titration was then carried out by stepwise addition of dithionite. The data were subsequently analyzed by global analysis and fit to a single potential model, as the mediator dyes contribute minimally to the overall absorbance changes observed.

8.3 Results

8.3.1 Sequence alignment and homology modeling

Figure 8.1 shows the Clustal Omega sequence alignment of Shr-N2 with the following homologous proteins: *B. anthracis* IsdX1 and IsdX2-N5, *L. monocytogenes* Hbp2-N2, and *S. aureus* IsdA, IsdB-N2, IsdC, and IsdH-N3. Previous work from our laboratory described the emerging diversity among NEAT proteins with regards to heme binding and secondary structural motifs (Chapter 7). This diversity is also evident in the sequence alignment of Shr-N2. As observed for Shr-N1, Shr-N2 does not contain the heme binding YXXXY motif as seen in the Isd and IsdX systems. The second tyrosine is replaced with a leucine (YXXXL) in Shr-N2. In addition, the conserved SXXXXY/SXXXXF 3_{10} helix motif seen in Hbp2-N2 and the Isd and IsdX systems is also not conserved for Shr-N2. The aromatic residue present at the end of the sequence is alanine in Shr-N2. Furthermore, there is no tyrosine located on the β-7 strand in Shr-

N2 in the position corresponding to the axial ligand in the Hbp2-N2 from *L. monocytogenes*. Together these observations are indicative of Shr-N2 having a unique set of heme axial ligands.

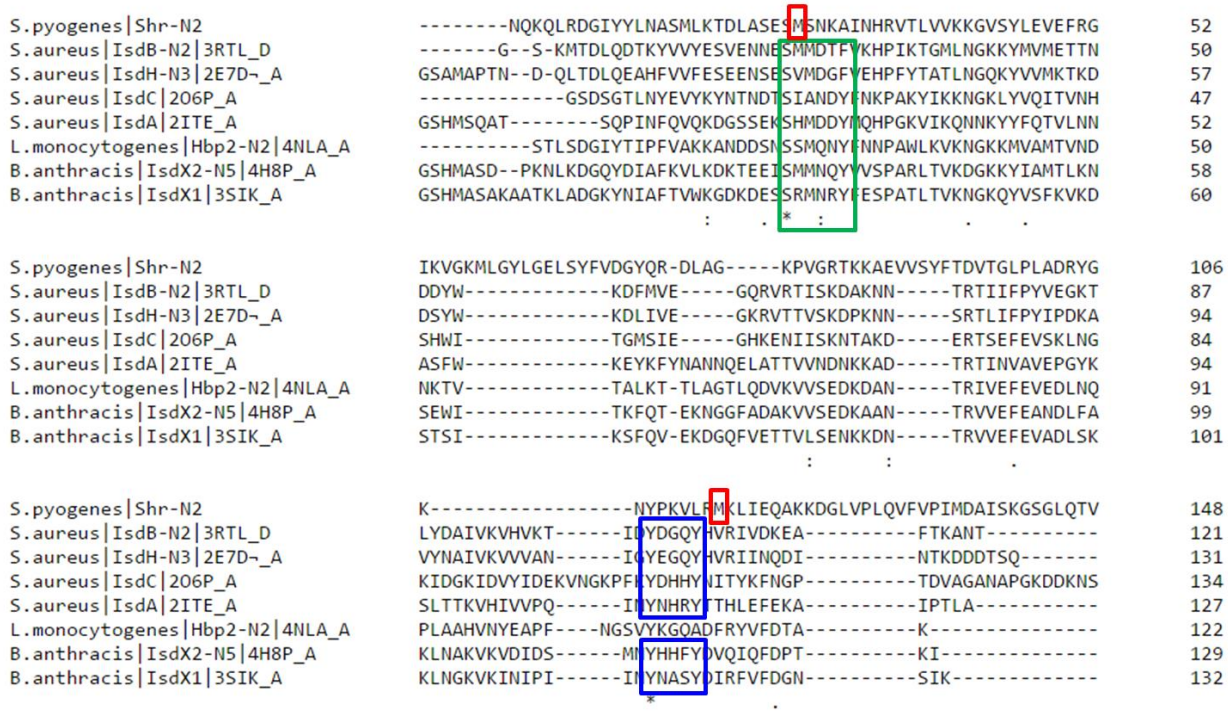

Figure 8.1 Selected alignment of the amino acid sequence of S. pyogenes Shr-N2 with homologous proteins. The proposed Shr-N2 ligand positions M26 and M136 are indicated by the red boxes. The conserved Isd YXXXY heme binding motif is shown by the blue boxes. The conserved 310 helix SXXXXY/F motif is shown by the green box.

Figure 8.2 shows the Clustal Omega sequence alignment of Shr-N2 with *S. pyogenes* Shr-NEAT1 (Shr-N1) and *S. pyogenes* Shp. Both Shr-N1 and Shp have been shown to utilize a bismethionine heme axial ligation *(38)* and (Chapter 7). Alignment reveals the positions of the known heme ligand sets, Shr-N1 (M22 and M107) and Shp (M66 and M153), to be conserved with Shr-N2 M26 and M136.

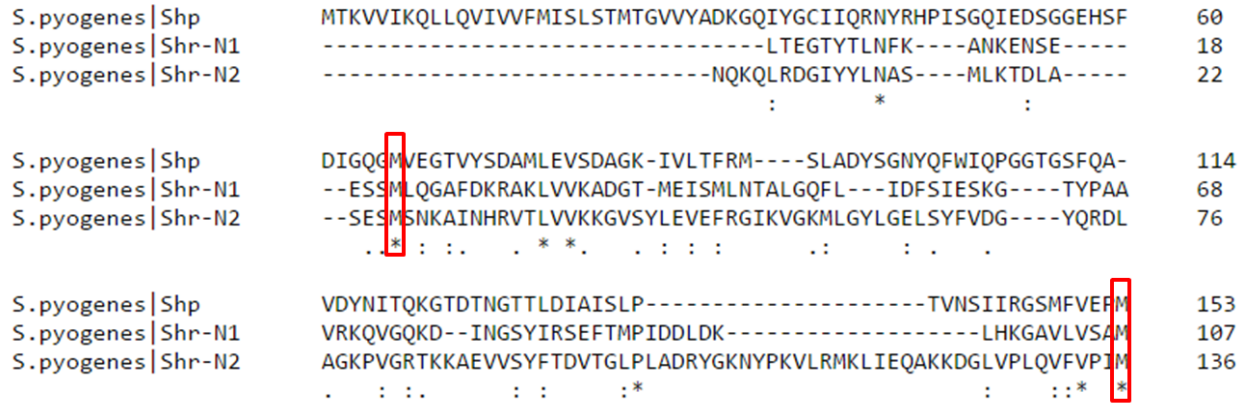

Figure 8.2 Selected alignment of the amino acid sequence of S. pyogenes Shr-N2 with Shr-N1 and Shp. The conserved methionine residues are shown in the red box and are the previously determined heme axial ligands for Shp and Shr-N1 along with the proposed ligands of Shr-N2.

The I-TASSER homology model of Shr-N2 (Figure 8.3) indicated the heme was in an exposed position on the surface of the protein. Based on the sequence alignment and previous work on Shr-N1, it was probable that the heme axial ligands for Shr-N2 were M26 from the N-terminal side and M136 from the C-terminal side of the protein. The model was in agreement with this observation and showed M26 to be located on a small α-helix and the M136 ligand extending from an unstructured loop, opposite to M26.

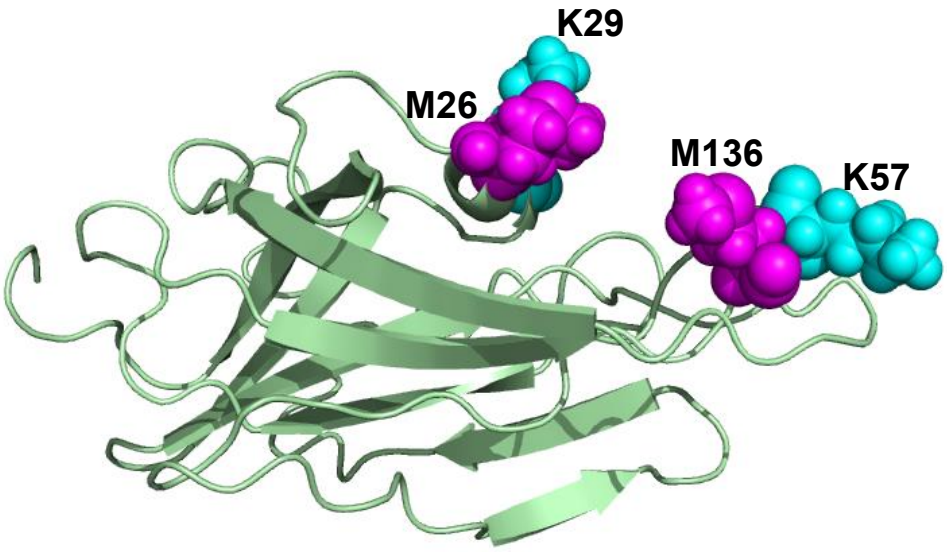

Figure 8.3 I-TASSER homology model of Shr-N2. Shown in magenta are the two proposed heme axial ligands, M26 and M136. Shown in cyan are the predicted lysine residues involved in autoreduction (K29 and K57).

8.3.2 Spectroscopy of Shr-N2

Fe(III) Shr-N2. Shr-N2 is isolated as a mixture of oxidized and reduced species *(21, 39).* The purified protein is easily oxidized with potassium ferricyanide and gives a UV-spectrum with (Figure 8.4) a Soret at 414 nm and α,β-bands at 507, 533, and 562 nm. A weak band is also observed at 645 nm.

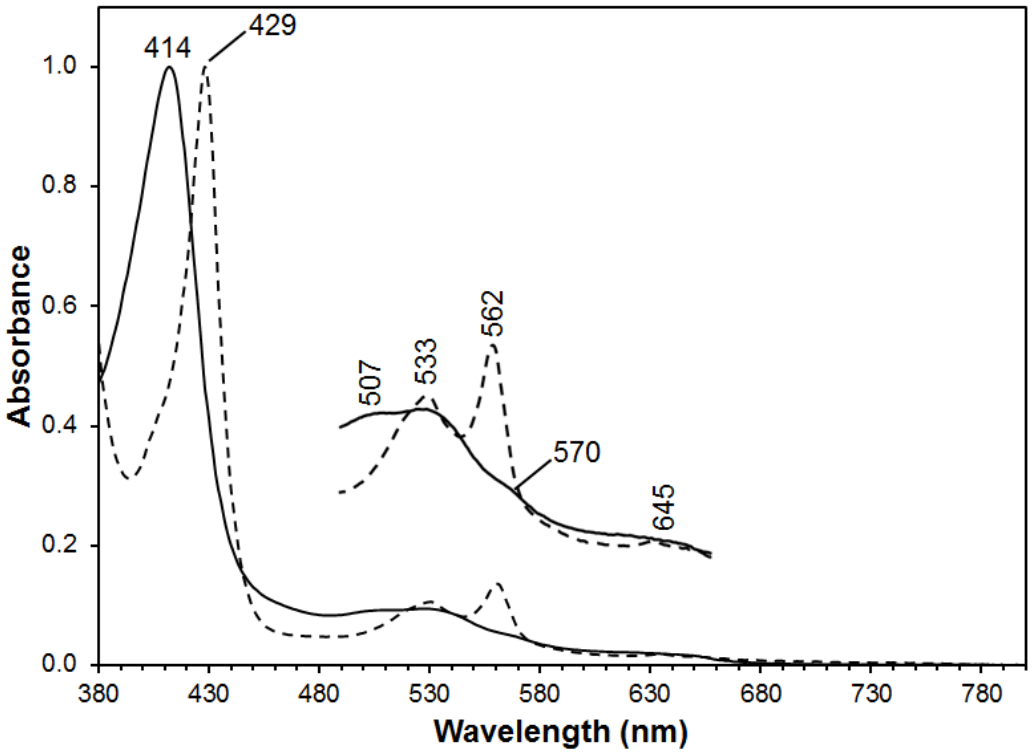

Figure 8.4 UV-visible absorption spectra of oxidized and reduced Shr-N2. Both samples were recorded in 50 mM Tris-Cl, pH 7.0.

MCD spectroscopy was utilized to assist in the determination of the Shr-N2 heme axial ligands. The MCD spectra of Shr-N2 did not match standard axial ligand sets of His, His/His, His/Met, Tyr, or His/Tyr *(55)*. Figure 8.5 compares Fe(III) Shr-N2 at pH 6.5 with both the five- and six- coordinate heme sites of H93G Mb bound with tetrahydrothiophene (THT); H93G Mb can bind to THT using either five-coordinate thioether or a six-coordinate bis-thioether axial ligation *(56)*. The UV and MCD spectra indicate ferric Shr-N2 majorly adopts a bismethionine ligation in the slightly acidic environment. In the MCD, the 551 nm peak and the 575 nm trough are in a similar position to those observed in the H93G bis-THT spectrum; the same peak and trough are red-shifted for the mono-thioether model of H93G. Although the peaks and troughs are in relatively the same position as in the H93G bis-THT spectrum, the intensity of the Shr-N2 575 nm trough is closer to the mono-THT spectrum and indicates there could be a

mixture in solution. Together, the UV and MCD data indicate ferric Shr-N2 is predominantly low-spin (LS) bismethionine at pH 6.5.

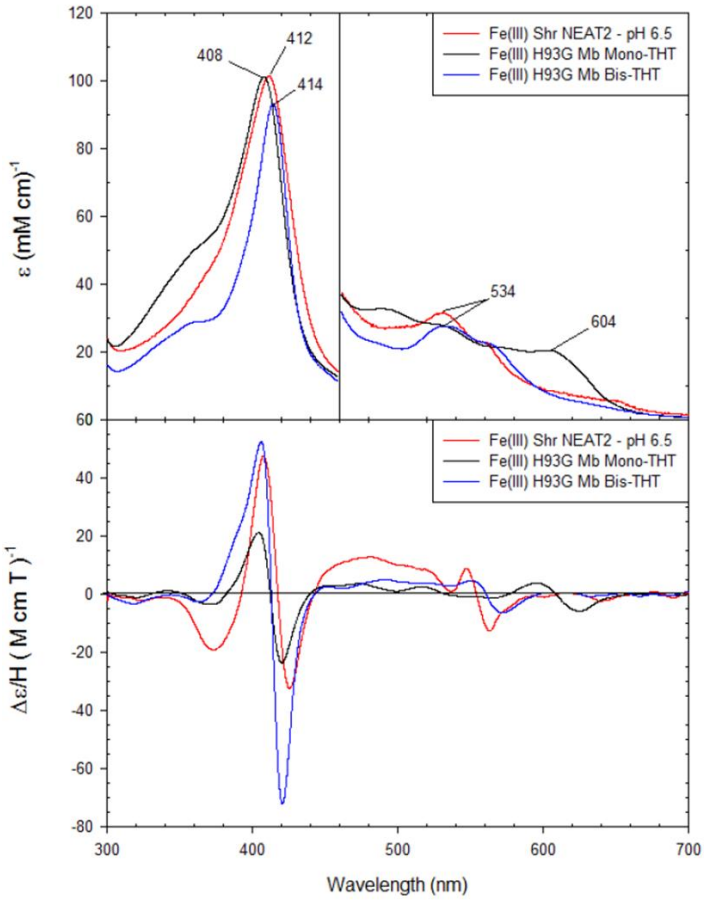

Figure 8.5 The UV-visible absorption and MCD spectra comparison of Fe(III) Shr-N2 with Fe(III) H93G Mb mono-THT and Fe(III) H93G Mb bis-THT. Samples were taken in 50 mM phosphate, pH 6.5.

Ferric Shr-N2 at basic pH was also investigated (Figure 8.6) and gives a different spectrum compared to the acidic form of the protein. Shr-N2 gives a band in the UV at 608 nm which is similar to the HS band marker at 604 nm in the H93G Mb mono-THT model. In the MCD, the visible region peak and trough are located in similar positions to the mono-thioether model. This indicates that basic pH conditions results in Shr-N2 losing an axial methionine and forming a five-coordinate high-spin (5cHS) heme ligation.

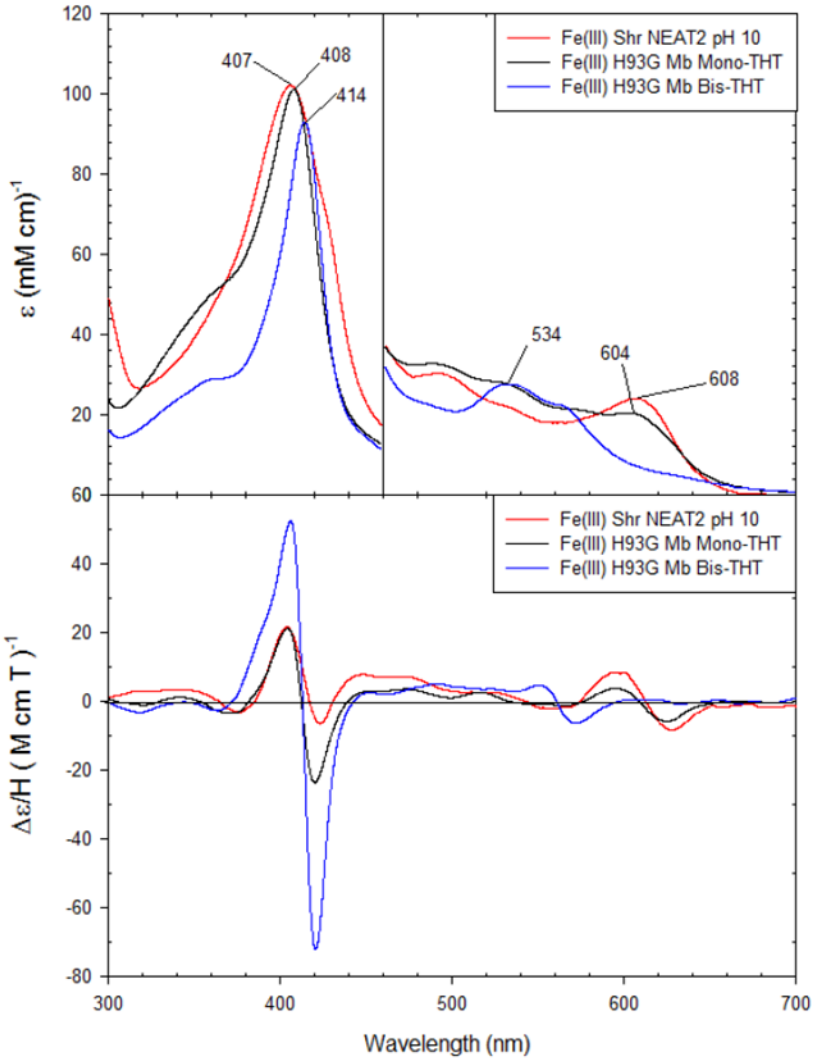

Figure 8.6 The UV-visible absorption and MCD spectra of Fe(III) Shr-N2 with Fe(III) H93G Mb bis-THT and Fe(III) H93G Mb mono-THT at pH 10. Samples were taken in 50 mM phosphate, pH 10.

Resonance Raman spectra of Shr-N2 at pH 8 indicated the protein is a mixture of oxidation states (as seen after purification) if the protein is not treated with an oxidizing agent (Figure 8.7). The as-isolated protein is a mixture of both Fe(III) and Fe(II) 6cLS as indicated by the ν_4 band at 1366 cm^{-1} and the ν_3 band at 1502 cm^{-1}. Upon addition of potassium ferricyanide, predominantly Fe(III) 6cLS is detected (increase in ν_3 band) along with a minor amount of

(FeIII) 5cHS seen at the 1490 cm^{-1} ν_3 band. These results correlate with the change in heme coordination number as a function of pH seen in the MCD.

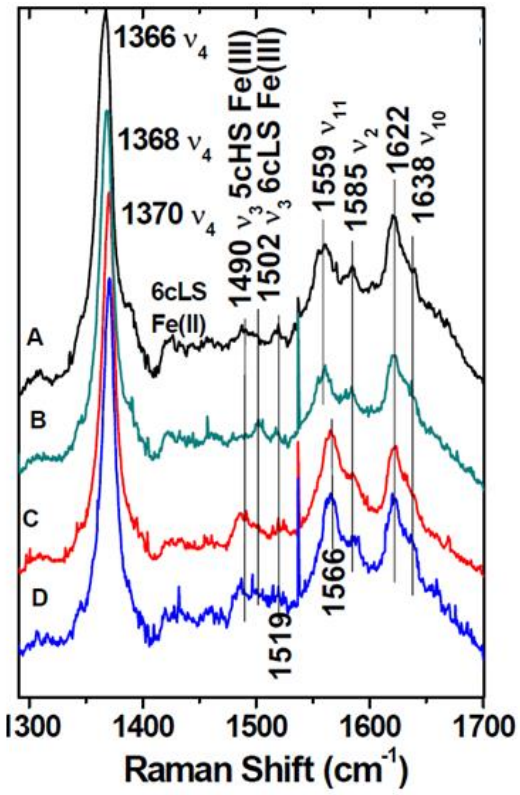

Figure 8.7 Resonance Raman spectral comparison of as-isolated Shr-N2 (black), Fe(III) Shr-N2 (green), purified Shr-N1 (fraction 2, red), and purified Shr-N1 (fraction 3, blue). Samples were prepared in 50 mM Tris-HCl, pH 8.0.

Fe(II) Shr-N2. Shr-N2 can be reduced with either dithiothreitol or sodium dithionite and the UV-spectrum gives a Soret at 429 nm and defined α,β-bands at 533 and 562 nm (Figure 8.4).

The MCD spectrum was compared to Fe(II) bis-THT Mb H93G in Figure 8.8. Fe(II) Shr-N2 does not give a pH dependence as seen in Fe(III) Shr-N2 (data not shown). The MCD shows spectral agreement between Fe(II) Shr-N2 and the model bismethionine system. Therefore, Fe(II) Shr-N2 adopts a 6cLS bismethionine ligation at both pH 6.5 and 10. Similar

results were seen in the rR spectra of Shr-N2 at pH 8 (Figure 8.9). Samples were reduced with excess dithionite and gave a ν_3 band at 1493 cm^{-1}, indicative of 6cLS heme.

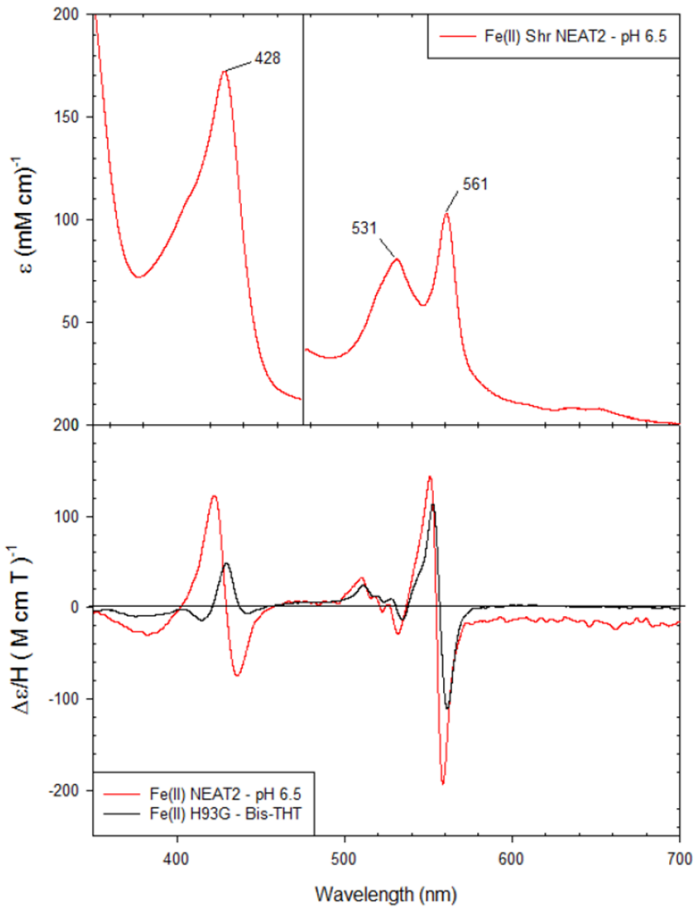

Figure 8.8 The UV-visible absorption and MCD spectra of Fe(II) Shr-N2 with Fe(II) H93G Mb bis-THT. Samples were taken in 50 mM phosphate, pH 6.5.

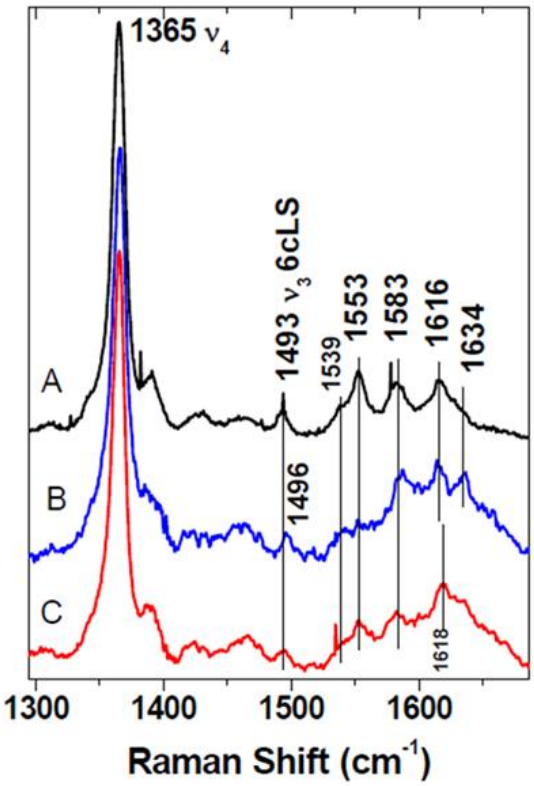

Figure 8.9 Resonance Raman spectral comparison of Fe(II) Shr-N2 (red), Fe(II) Shr-N1 (fraction 2, black), and Fe(II) Shr-N1 (fraction 3, blue). Samples were prepared in 50 mM Tris-HCl, pH 8.0 and reduced with 100-fold excess reducing equivalents of dithionite.

Fe(II)-CO Shr-N2. Reduction of Shr-N2 in the presence of carbon monoxide (CO) resulted in the formation of the Shr-N2 Fe(II)-CO complex. Comparison of the UV-visible absorption and MCD spectra of the Shr-N2 CO adduct with that of Fe(II)-CO H93G Mb mono-THT showed the spectra are very similar in both the UV and the MCD. This indicates that upon the addition of CO, Shr-N2 loses an axial methionine and is replaced with a CO ligand.

8.3.3 Electrochemistry

Spectroelectrochemical titration of Shr-N2 is shown in Figure 8.10 covered the potential range from 50 – 300 mV through two oxidative and reductive cycles. The arrows on the absorbance spectra show the direction of absorbance change as the potential was decreased. The

bottom panel shows the absorbance at the reduced Soret maximum as a function of potential for both cycles. The average oxidative potential is 256 ± 9 mV vs. SHE, and the average reductive potential is 275 ± 10 mV vs. SHE. These data sets agree within error and the potential appears to be irreversible with a difference of ~ 60 mV.

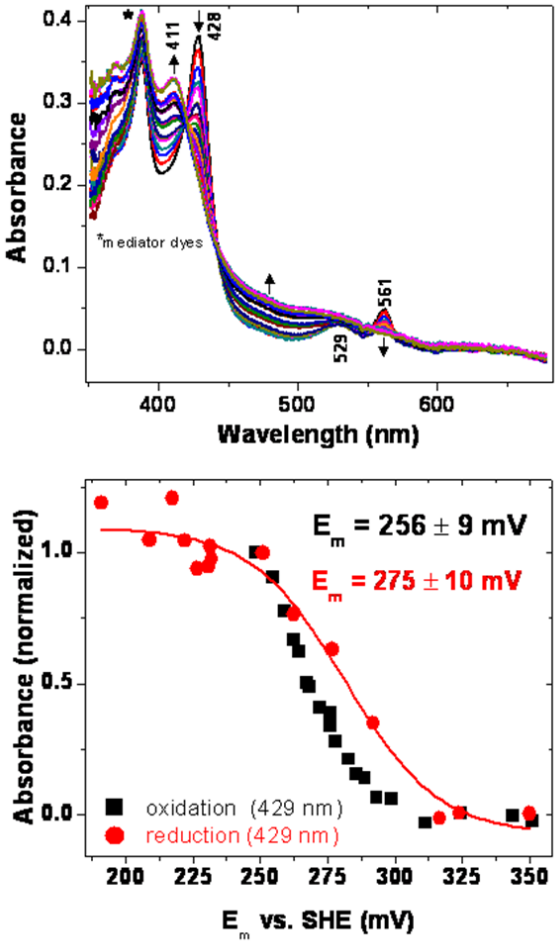

Figure 8.10 Redox potential titration of Shr-N2. A mediator cocktail (10 µL of each dye) that covered the potential range from 50 – 300 mV was titrated to the sample through two oxidative and reductive cycles. This restricted range has the advantage of minimizing absorbance changes due to mediators. The oxidative and reductive titration data sets are shown in the top panel. The bottom panel shows the absorbance at the reduced Soret maximum (428 nm) as a function of potential for both cycles.

8.3.4 pH titration – autooxidation and autoreduction

As-isolated Shr-N2 is a mixture of oxidized and reduced heme and is prone to apparent autoreduction, even in the presence of oxygen *(21)*. To probe this phenomenon, a series of pH titrations were performed. In the first, the fully reduced sample in air was treated with small aliquots of 1 M NaOH (Figure 8.11A). There was essentially no change in the visible spectrum as the pH was increased to 10.4. The sample was then back-titrated to pH 6.2 with 1 M HCl (Figure 8.11B). The protein converted from the reduced species, with a Soret at 428 nm, to the oxidized species, with a Soret at 411 nm. The sample was approximately half oxidized and half reduced. To see if further changes occurred over time, the sample was held at this pH for approximately an hour, and continued to oxidize until it was primarily in the ferric form. The apparent pK_a of the autooxidation was 6.5 – 7.5 as judged by single-wavelength and global fitting (data not shown). During the titration, there was increasing absorbance in the 375 nm region, presumably indicating some protein denaturation and heme loss.

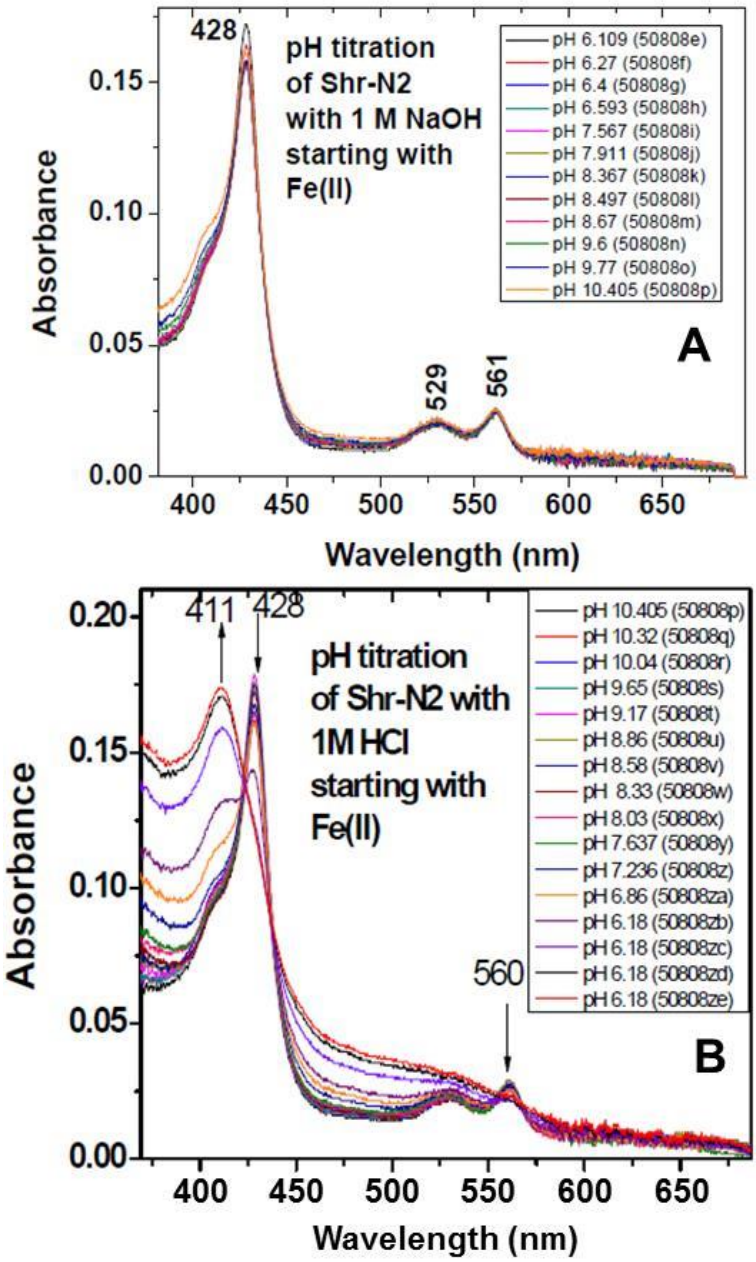

Figure 8.11 pH titrations of Shr-N2. A) NaOH titration of Fe(II) Shr-N2. (B) The second NaOH titration titration.

Another pH titration was performed on Shr-N2 with longer incubation times between changes in pH (Figure 8.12). Shr-N2 at pH 10.4 was approximately 65% in the reduced form at the beginning of the experiment and did not change over 17 h. The pH was adjusted to 6.6, the

reduced Soret began to decrease, and the sample was completely oxidized after 24 h. Figure 8.12B shows that this conversion was not isosbestic. When the pH of this sample was increased to 10.5, only a small amount of protein re-reduced. Overall, the tendency of the protein to autoreduce and autoxidize was variable; experiments to evaluate the effects of EDTA as a metal chelator or glycerol and amine-containing buffers as electron sources gave inconsistent results.

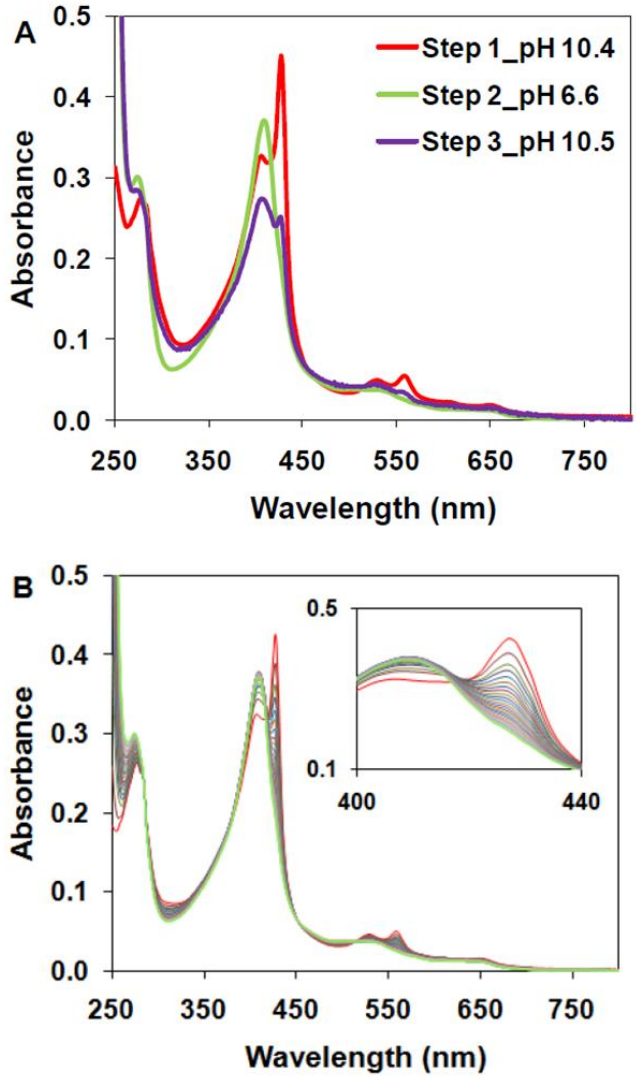

Figure 8.12 pH titration of Shr-N2 in 20 mM each CAPS, MES, and Tris-HCl at 4 oC monitored by UV-visible absorption spectroscopy. (A) After equilibration in each step. (B) Equilibration between step 1 and step 2 in panel A at 1 h intervals.

8.3.5 Guanidinium and thermal unfolding studies

To assess the ease of unfolding of Shr-N2, the protein was treated with increasing concentrations of GdnCl. The data were fit with a standard two state transition model (Figure 8.13). The midpoint of the transition was at 2.2 ± 0.1 M GdnCl for the ferric protein and approximately 2.6 ± 0.5 M GdnCl for the ferrous protein.

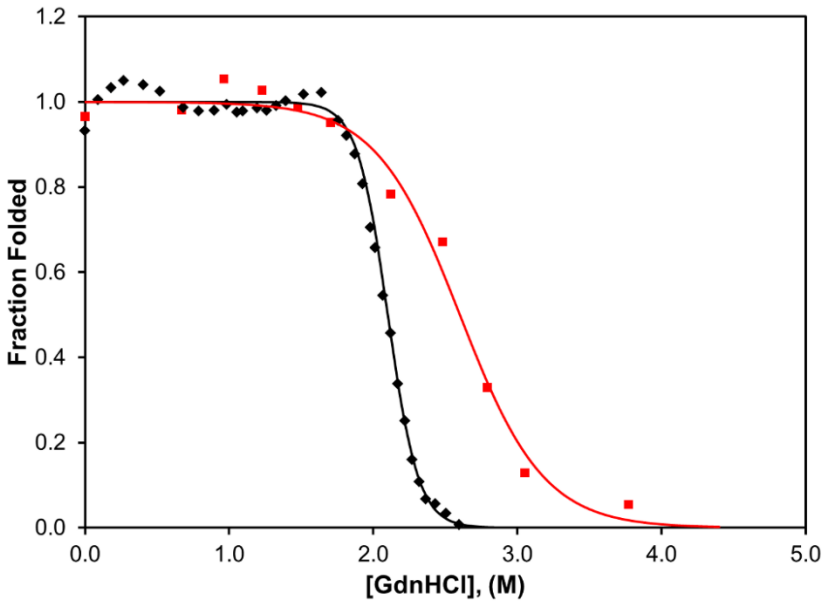

Figure 8.13 GdnCl unfolding of oxidized (black diamonds) and reduced (red squares) Shr-N2 in 50 mM Tris-Cl, pH 7.0.

Thermal unfolding of ferric and ferrous Shr-N2 was also performed to compare the overall protein stability between heme oxidation states (Figure 8.14). Both proteins were unfolded and the data were fit to a two-state transition model. Ferric Shr-N2 gave a T_m of 68.7 ± 0.2 °C compared to a T_m of ≈ 75 °C for ferrous Shr-N2. Ferrous Shr-N2 tends to precipitate out of solution above 80 °C.

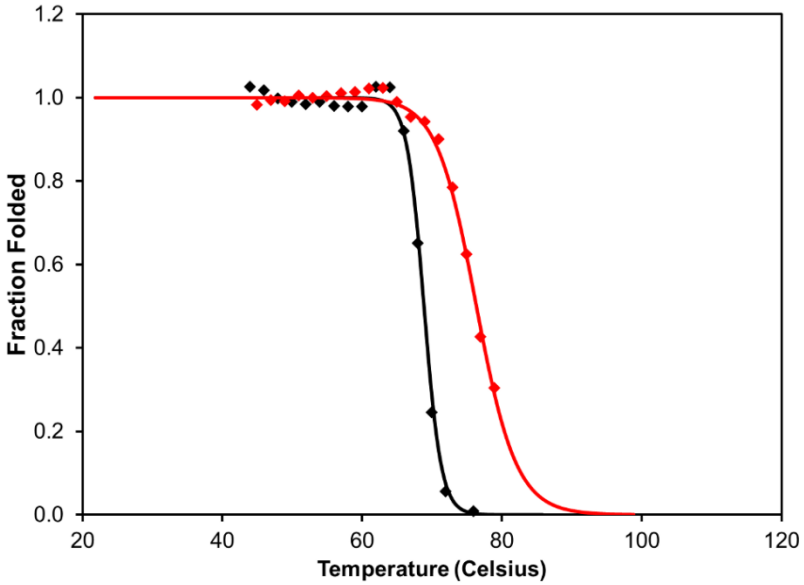

Figure 8.14 Thermal unfolding of oxidized (black squares) and reduced (red diamonds) Shr-N2 in 50 mM potassium phosphate, pH 7.0.

8.4 Discussion

8.4.1 Bismethionine axial ligation

Sequence alignment and homology modeling indicated M26 and M136 to be the potential heme binding residues of Shr-N2. The domain of Shr, Shr-N1, also utilizes a Met/Met heme ligation as previously reported by our group (Chapter 7). Additionally, the observed reduction potential of Shr-N2 ~ +260 mV indicated tyrosine was not an axial ligand. Reduction potentials measured for heme proteins with tyrosine as an axial ligand are very low *(57)*. For example, *S. marcescens* HasA, with a histidine/tyrosine ligand set, has a redox potential of −550 mV *(58)*. Additionally, MCD spectra of Tyr and Met/Tyr models did not match the spectra for Shr-N2 in either the ferric, ferrous, or ferrous-CO states.

The most probable ligand pair candidates were either Met/Met or Lys/Met. Both of these ligand pairs would be consistent with the observed reduction potential of about ~ +260 mV,

leaving reduction potential alone unable to identify the heme ligand pair. Ethylbenzene dehydrogenase from *Aromatoleum aromaticum*, with a Lys/Met axial ligand set, has a reduction potential of +254 mV *(59)*, while the reduction potential of dimethylsulfide dehydrogenase, also thought to have a Lys/Met axial ligand set *(59, 60)*, has a reduction potential of approximately +320 mV *(61) (60)*.

Although K29 and K57 in Shr-N2 are near the heme pocket (and adjacent to the proposed Met axial ligands) according to homology modeling (Figure 8.3), it is possible that these residues are playing a role in stabilization of the bound heme through interactions, such as salt bridges, with the heme propionates. Cationic side chains have showed to play such a role in other heme proteins *(62)*. Lysine could also be present in order to facilitate autoreduction (discussed below). Site-directed mutagenesis ruled out the possibility of a Met/Lys or Lys/Lys heme ligation system in Shr-N2.

UV-visible absorption spectral data comparing Shr-N1 and Shr-N2 showed similarities between ferric species and are almost identical in the ferrous oxidation state. Ferric Shr-N1 gives a Soret at 409 with α,β-bands at 506, 540, 585, and 645 nm, similar to ferric Shr-N2 (414, 507, 533, 570, and 645 nm). Although there are slight differences in optical spectra maxima, there are little known examples of other bismethionine heme systems in which to compare. From the comparisons which can be made, optical data for these proteins and models systems show a wide variety of optical spectra. In addition, sequence alignment indicated a bismethionine pair for Shr-N2 based on known heme ligation for *S. pyogenes* Shr-N1 and Shp which also utilize two methionines for axial ligation. Therefore, the experimental data for Shr-N2 can be interpreted to indicate the protein utilizes a bismethionine axial ligation.

8.4.2 Autoreduction

Shr *(21, 63)* and the Shr-N2 domain *(21)* are isolated as a mixture of oxidized and reduced species. The extent of as-isolated Shr-N2 autoreduction ranged from 20% to 80%. In the presence of 1% EDTA during protein purification, Shr-N2 was also isolated as a mixture of oxidation states. Such findings could indicate metal ions in solution are not serving as the primary source of electrons for the autoreduction phenomenon. No effort was made to exclude oxygen during purification, indicating that autoreduction still occurs in the presence of oxygen.

Changes in pH show Shr-N2 to either readily autoreduce or autooxidize. Upon acid and base titration, the protein goes initially to a mixture of the Fe(II) and Fe(III) forms that are dependent on pH. Attainment of equilibrium at a new pH (as shown by no further changes in the optical spectrum) takes approximately two hours. The apparent pK_a of this process is 6.5 – 7.5. The residue responsible for this pK_a is presumably not the heme propionic acids, as it would be expected that deprotonation to give a propionate would stabilize the ferric form of the protein, and Shr-N2 autoreduces as the pH of the solution increases.

The autoreduction/autooxidation process occurs smoothly through one cycle of pH increase and decrease, and to some extent in a second cycle (Figure YC4.21). The process seems to occur in an amine-containing buffer (e.g., Tris-HCl), but not in phosphate buffer. For the titration in the latter buffer, addition of Tris-HCl two hours after the start of the experiment does not result in autoreduction.

Autoreduction of other heme proteins has been reported. Some of the most studied proteins *(64)* are the cytochromes c_H and c_L from *Methylobacterium extorquens* [originally called *Pseudomonas* AM1 or *Methylobacterium* AM1 *(65)*]. Cytochrome c_L acts as an electron acceptor for methanol dehydrogenase, and transfer electrons to cytochrome c_H *(66)*. Cytochrome

c_H then donates electrons to oxidase. Cytochrome c_L is a protein of 21 kDa with a low isoelectric point (pI) of 4.2 and a reduction potential of +256 mV *(64)*. It has a six-coordinated cysteine-covalently-bonded heme *c* with a histidine as the fifth ligand *(67)*. The sixth ligand is Met109 in solution *(68)* and His112 in the crystal *(67)*, indicating the relatively flexible nature of the heme binding site. Cytochrome c_H is a protein of 11 kDa with a high pI of 8.8 and a reduction potential of +294 mV *(64)*. The heme at the binding site is covalently bonded to a cysteine and six-coordinate with Met and His *(69)*. For these cytochromes, the autoreduction is first-order in 30% glycerol, with a rate constant that increases by approximately a factor of five as the pH of the solution is raised from 9 to 11 *(64)*.

In other studies, cytochrome c_{552} from the Gram-negative bacterium *Pseudomonas alcaliphila* AL15-21^T is isolated in an almost fully reduced state when grown at pH 10 *(70)*. This cytochrome can be reoxidized by potassium ferricyanide, absence the presence of glycerol, and autoreduces at basic pH, but not at neutral pH. The redox potential of the heme in this protein is also sensitive to pH, increasing from +228 mV to +276 mV (E_m values) as the pH is raised from 7.0 to 8.3.

Cytochrome c_6 from *Monoraphidium braunii*, with a pI of 3.6, is also purified predominantly in the reduced state and autoreduces after being oxidized with ferricyanide above pH 8 *(71)*. The reduction potential of this cytochrome is about +358 mV at pH 5.5 – 7, and pH dependent between pH 7 and 9 (decreasing to about +300 mV at pH 9). Cytochrome *f*, a Japanese radish protein, undergoes a slow autoreduction with a midpoint potential of +350 mV *(72)*. Overall, the higher the reduction potential of the heme, the more likely it is to reduce, as expected. Although most reports of autoreduction have not involved formal studies of the

process, it does seem that Shr-N2, with a reduction potential of +260 mV, is at the low end of the proteins that easily autoreduce.

The source of reducing equivalents in the Shr-N2 autoreduction process is not clear. Adventitious metal ions are known to contribute to the autoreduction of cytochrome *c (73)*. Neutral tyrosine radicals might be able to contribute to autoreduction of yeast cytochrome *c (74)*. The observation that the protein is isolated as a mixture of oxidized and reduced protein even in the presence of EDTA argues that metal ions are not the primary source of electrons in the case of Shr-N2.

Shr-N2 has 19 lysines and a pI of 9.74. It is possible that deprotonation of a lysine near the heme allows autoreduction to take place. Such a mechanism was proposed for the cytochrome c_L system *(75)* in which it was hypothesized that increasing the pH resulted in deprotonation of a nearby group, which was then able to transfer an electron to the iron center. In model systems, amines readily reduce iron porphyrins in solution *(76-87)*. It could be that case that K29, K57, or both are contributing to the autoreduction of Shr-N2.

In conjunction with the observation of facile autoreduction of Shr-N2, it is worth noting that the two genes in the *sia* operon after *siaC*, *siaD* and *siaE*, a proposed exporter with significant homology to ABC transporters, in particular, the CydDC exporter system from *E. coli*. CydDC exports cysteine in an ATP-dependent process; it also exports glutathione *(88-90)*. The *cydC* and *cydD* genes are part of an operon containing *cydAB*, which encodes for terminal *bd*-type respiratory oxidases and are required for the assembly of the oxidases. Experimental studies have shown that CydDC controls the redox milieu outside the cell membrane, potentially influencing the formation or reduction of disulfide bonds of the Dsb protein disulfide folding pathway *(90)*. In a study of the *E. coli* system, the periplasm became more oxidizing as Dsb

proteins were removed, indicating that these proteins are part of the redox balance in the periplasmic space *(91)*. Removing DsbC alone increased the reduction potential by about 10 mV.

It could be the case that SiaD and SiaE form a similar exporter system as CysDC in which the reduction potential is controlled by the export of glutathione and cysteine. The redox potential of a cell is approximately -200 to -250 mV *(92)*. The effective redox potential of the environment of Shr-N2, anchored in the cell wall, is unclear. In *E. coli*, the redox potential of the periplasm is about -165 mV *(91)*, significantly higher than that of the cytoplasm. Presumably the cell wall milieu has an even higher redox potential and may be influencing the autoreduction of Shr-N2.

8.4.3 Unfolding studies and oxidation state

Both chemical and thermal unfolding titrations were performed on ferric and ferrous Shr-N2. In both studies, ferrous Shr-N2 was more resistant to unfolding than ferric Shr-N2. Given the reduction potential of free heme is about −60 mV *(93)* and the experimental reduction potential for Shr-N2 of approximately +260 mV, the ferrous state will bind heme approximately five orders of magnitude more tightly than the ferric state. Overall, as the reduction potential of the bound heme increases, the ferric protein loses heme more readily than the ferrous protein. This can be due to a variety of effects: destabilization of the ferric heme only, stabilization of the ferrous heme only, or differential stabilization of the two states such that the binding in the ferric form is disfavored with respect to binding in the ferrous form.

8.4.4 The mechanism of heme uptake

In visualizing the mechanism of heme uptake, it seems most likely that heme enters the pathway in the ferric form. This is consistent with the rapid autooxidation of hemoglobin once it

is released from the cell *(94)*, making ferric hemoglobin (methemoglobin) the most probable source of heme. It is also consistent with experimental studies in which methemoglobin is a source of heme for Shr-N1 and Shr-N2 *(21)*. It was also shown that the full Shr construct accepts heme from methemoglobin *(95)*.

Recent heme transfer studies of either Shr-N1 or Shr-N2 to apo-Shp show Shr-N1 to be the heme donor to Shp in a two-phase process with second-order rates of 2.5 $s^{-1}\mu M^{-1}$ and 0.017 $s^{-1}\mu M^{-1}$ *(22)*. In addition, studies of heme transfer between the two domains were also performed using stopped-flow spectrophotometry. Results showed Shr-N1 rapidly and reversibly transfers heme to Shr-N2. Heme transferred from oxidized Shr-N1 to apo-Shr-N2 showed to be a mixture of oxidized and reduced heme. This indicates the very facile autoreduction of Shr-N2. Shr-N2 autoreduces as the pH is raised and reoxidizes as the pH is lowered. In the absence of added oxidants and reductants, the process takes about two hours. It is possible that both the reduced and oxidized forms of Shr-N2 are important in the heme transfer process. In particular, the next protein in the pathway, Shp, has an active site in which the heme is bound by two methionines *(38, 39, 96)* and has been shown to be able to bind ferrous heme. Methionine ligands are known to bind ferrous heme more tightly than ferric heme *(97-99)*. This was also observed in the guanidinium and thermal unfolding studies of the protein with the ferrous species being more resistant to unfolding in both cases.

As discussed above, the redox potential of the heme bound in Shr-N2 is about +260 mV, which translates to a binding of the ferrous heme that is about six orders of magnitude tighter than the ferric form. The tighter binding of the ferrous form would seem inconsistent with the proposal that the ferrous form is transferred to Shp. However, the strength of binding of the heme and its transfer rate are not necessarily correlated. For example, transfer

of heme from Shp to SiaA has been described as formation of a protein complex followed by heme transfer within the complex *(42)*. Both the equilibria for binding and the rate constants for transfer within the complex are very similar for the ferric and ferrous oxidation states, with values of approximately 100 μM for formation of the complex and 30 – 50 for heme/hemin transfer within the complex. For SiaA, the reduction potential determined via spectro-electrochemistry is about +75 mV (average of oxidative and reductive processes) *(20)*. Taking the SiaA binding constant for hemin as > 10^{12} M^{-1} and the reduction potential for free heme as -75 mV gives a binding constant for ferrous SiaA of 10^{13} M^{-1}.

Outtara et al. proposed that in a plentiful heme environment the heme transferred to Shr-N1 can either transfer directly to Shp or give to Shr-N2 as a means of heme storage. If levels of heme become low, the cell can then transport the stored heme from Shr-N2, to Shr-N1 which delivers the heme to Shp. This idea was based on the kinetic studies discussed above in which Shr-N2 transfers heme to Shp slowly. Shr-N2 autoreduction may be a means in which to store heme for Shr until needed by the cell as reduction of the heme results in a more stable protein as indicated by unfolding studies. The proposed SiaDE exporter may work to control the reduction of Shr-N2 and ultimately assist in the regulation of this pathway.

8.5 References

[1] Braun, V., and Hantke, K. (2011) Recent insights into iron import by bacteria. *Curr. Opin. Chem. Biol. 15*, 328-334.

[2] Benson, D. R., and Rivera, M. (2013) Heme uptake and metabolism in bacteria. *Met. Ions Life Sci 12*, 279-332.

[3] Rodgers, K. R., and Lukat-Rodgers, G. S. (2014) Biophysical perspectives on the acquisition, transport, and trafficking of heme in bacteria. *Handbook of Porphyrin Science with Applications to Chemistry, Physics, Materials Science, Engineering, Biology and Medicine, Vol. 30: Heme Proteins, Part II 30*, 249-309.

[4] Contreras, H., Chim, N., Credali, A., and Goulding, C. W. (2014) Heme uptake in bacterial pathogens. *Curr. Opin. Chem. Biol. 19*, 34-41.

[5] Wilks, A., and O'Neill, M. J. (2014) Extracellular heme uptake and metabolism in bacterial pathogenesis, In *Handbook of Porphyrin Science with Applications to Chemistry, Physics, Materials Science, Engineering, Biology and Medicine, Vol 26: Heme Biochemistry* (Ferreira, G. C., Kadish, K. M., Smith, K. M., and Guilard, R., Eds.), pp 267-315, World Scientific, Hackensack, NJ.

[6] Runyen-Janecky, L. J. (2013) Role and regulation of heme on acquisition in gram-negative pathogens. *Frontiers in Cellular and Infection Microbiology 3*, 55.

[7] Cavallaro, G., Decaria, L., and Rosato, A. (2008) Genome-based analysis of heme biosynthesis and uptake in prokaryotic systems. *J. Proteome Res. 7*, 4946-4954.

[8] Tong, Y., and Guo, M. (2009) Bacterial heme-transport proteins and their heme-coordination modes. *Arch. Biochem. Biophys. 481*, 1-15.

[9] Mayfield, J. A., Dehner, C. A., and DuBois, J. L. (2011) Recent advances in bacterial heme protein biochemistry. *Curr. Opin. Chem. Biol. 15*, 260-266.

[10] Wilks, A., and Barker, K. D. (2011) Mechanisms of heme uptake and utilization in bacterial pathogens, In *Handbook of Porphyrin Science with Applications to Chemistry, Physics, Materials Science, Engineering, Biology and Medicine, Vol 15: Biochemistry of Tetrapyrroles* (Kadish, K. M., Smith, K. M., and Guilard, R., Eds.), pp 357-398, World Scientific, Hacksensack, NJ.

[11] Gruss, A., Borezée-Durant, E., and Lechardeur, D. (2012) Environmental heme utilization by heme-auxotrophic bacteria, In *Advances in Bacterial Respiratory Physiology* (Poole, R. K., Ed.) 61 ed., pp 69-124, Academic Press, London, England.

[12] Smith, A. D., and Wilks, A. (2012) Extracellular heme uptake and the challenges of bacterial cell membranes. *Curr. Top. Membr. 69*, 359-392.

[13] Farrand, A. J., and Skaar, E. P. (2014) Heme and infectious diseases, In *Handbook of Porphyrin Science with Applications to Chemistry, Physics, Materials Science, Engineering, Biology and Medicine, Vol 26: Heme Biochemistry* (Ferreira, G. C., Kadish, K. M., Smith, K. M., and Guilard, R., Eds.) 26 ed., pp 317-377, World Scientific, Hackensack, NJ.

[14] Allen, C. E., and Schmitt, M. P. (2014) Utilization of host iron sources by *Corynebacterium diphtheriae*: Multiple hemoglobin-binding proteins are essential for the use of iron from the hemoglobin/haptoglobin complex. *J. Bacteriol. 195*, 2413-2414.

[15] Draganova, E. B., Akbas, N., Adrian, S. A., Lukat-Rodgers, G. S., Collins, D. P., Dawson, J. H., Allen, C. E., Schmitt, M. P., Rodgers, K. R., and Dixon, D. W. (2015) Heme binding by *Corynebacterium diphtheriae* HmuT: Function and heme environment. *Biochemistry 54*, 6598-6609.

[16] Honsa, E. S., and Maresso, A. W. (2011) Mechanisms of iron import in anthrax. *BioMetals 24*, 533-545.

[17] Hammer, N. D., and Skaar, E. P. (2011) Molecular mechanisms of *Staphylococcus aureus* iron acquisition. *Annu. Rev. Microbiol. 65*, 129-147.

[18] Tiedemann, M. T., Heinrichs, D. E., and Stillman, M. J. (2012) Multiprotein heme shuttle pathway in *Staphylococcus aureus*: Iron-regulated surface determinant cog-wheel kinetics. *J. Am. Chem. Soc. 134*, 16578-16585.

[19] Eichenbaum, Z. (2012) The streptococcal hemoprotein receptor. A moonlighting protein or a virulence factor? *Virulence 3*, 553-555.

[20] Sook, B. R., Block, D. R., Sumithran, S., Montañez, G. E., Rodgers, K. R., Dawson, J. H., Eichenbaum, Z., and Dixon, D. W. (2008) Characterization of SiaA, a streptococcal heme-binding protein associated with a heme ABC transport system. *Biochemistry 47*, 2678-2688.

[21] Ouattara, M., Cunha, E. B., Li, X., Huang, Y. S., Dixon, D. W., and Eichenbaum, Z. (2010) Shr of Group A streptococcus is a new type of composite NEAT protein involved in sequestering haem from methaemoglobin. *Mol. Microbiol. 78*, 739-756.

[22] Ouattara, M., Pennati, A., Devlin, D. J., Huang, Y. S., Gadda, G., and Eichenbaum, Z. (2013) Kinetics of heme transfer by the Shr NEAT domains of Group A Streptococcus. *Arch. Biochem. Biophys. 538*, 71-79.

[23] Andrade, M. A., Ciccarelli, F. D., Perez-Iratxeta, C., and Bork, P. (2002) NEAT: A domain duplicated in genes near the components of a putative Fe(3+) siderophore transporter from Gram-positive pathogenic bacteria. *Genome Biol. 3*, RESEARCH0047.

[24] Honsa, E. S., Maresso, A. W., and Highlander, S. K. (2014) Molecular and evolutionary analysis of NEAr-iron Transporter (NEAT) domains. *PLoS One 9*.

[25] Sharp, K. H., Schneider, S., Cockayne, A., and Paoli, M. (2007) Crystal structure of the heme-IsdC complex, the central conduit of the Isd iron/heme uptake system in *Staphylococcus aureus*. *J. Biol. Chem. 282*, 10625-10631.

[26] Watanabe, M., Tanaka, Y., Suenaga, A., Kuroda, M., Yao, M., Watanabe, N., Arisaka, F., Ohta, T., Tanaka, I., and Tsumoto, K. (2008) Structural basis for multimeric heme complexation through a specific protein-heme interaction - The case of the third NEAT domain of IsdH from *Staphylococcus aureus*. *J. Biol. Chem. 283*, 28649-28659.

[27] Ekworomadu, M. T., Poor, C. B., Owens, C. P., Balderas, M. A., Fabian, M., Olson, J. S., Murphy, F., Balkabasi, E., Honsa, E. S., He, C., Goulding, C. W., and Maresso, A. W. (2012) Differential function of Lip residues in the mechanism and biology of an anthrax hemophore. *PLoS Path. 8*.

[28] Honsa, E. S., Owens, C. P., Goulding, C. W., and Maresso, A. W. (2013) The near-iron transporter (NEAT) domains of the anthrax hemophore IsdX2 require a critical glutamine to extract heme from methemoglobin. *J. Biol. Chem. 288*, 8479-8490.

[29] Gaudin, C. F. M., Grigg, J. C., Arrieta, A. L., and Murphy, M. E. P. (2011) Unique heme-iron coordination by the hemoglobin receptor IsdB of *Staphylococcus aureus*. *Biochemistry 50*, 5443-5452.

[30] Pluym, M., Muryoi, N., Heinrichs, D. E., and Stillman, M. J. (2008) Heme binding in the NEAT domains of IsdA and IsdC of *Staphylococcus aureus*. *J. Inorg. Biochem. 102*, 480-488.

[31] Balderas, M. A., Nobles, C. L., Honsa, E. S., Alicki, E. R., and Maresso, A. W. (2012) Hal is a *Bacillus anthracis* heme acquisition protein. *J. Bacteriol. 194*, 5513-5521.

[32] Malmirchegini, G. R., Sjodt, M., Shnitkind, S., Sawaya, M. R., Rosinski, J., Newton, S. M., Klebba, P. E., and Clubb, R. T. (2014) Novel mechanism of hemin capture by Hbp2, the hemoglobin-binding hemophore from *Listeria monocytogenes*. *J. Biol. Chem. 289*, 34886-34899.

[33] Eichenbaum, Z., Green, B. D., and Scott, J. R. (1996) Iron starvation causes release from the group A streptococcus of the ADP-ribosylating protein called plasmin receptor or surface glyceraldehyde-3-phosphate-dehydrogenase. *Infect. Immun. 64*, 1956-1960.

[34] Eichenbaum, Z., Muller, E., Morse, S. A., and Scott, J. R. (1996) Acquisition of iron from host proteins by the group A *Streptococcus*. *Infect. Immun. 64*, 5428-5429.

[35] Montañez, G. E., Neely, M. N., and Eichenbaum, Z. (2005) The streptococcal iron uptake (Siu) transporter is required for iron uptake and virulence In a zebrafish infection model. *Microbiology-SGM 151*, 3749-3757.

[36] Ardanuy, C., Domenech, A., Rolo, D., Calatayud, L., Tubau, F., Ayats, J., Martin, R., and Linares, J. (2010) Molecular characterization of macrolide- and multidrug-resistant *Streptococcus pyogenes* isolated from adult patients in Barcelona, Spain (1993-2008). *J. Antimicrob. Chemother. 65*, 634-643.

[37] Walker, M. J., Barnett, T. C., McArthur, J. D., Cole, J. N., Gillen, C. M., Henningham, A., Sriprakash, K. S., Sanderson-Smith, M. L., and Nizet, V. (2014) Disease manifestations and pathogenic mechanisms of group a Streptococcus. *Clin. Microbiol. Rev. 27*, 264-301.

[38] Aranda, R., Worley, C. E., Liu, M., Bitto, E., Cates, M. S., Olson, J. S., Lei, B. F., and Phillips, G. N. (2007) Bis-methionyl coordination in the crystal structure of the heme-binding domain of the streptococcal cell surface protein Shp. *J. Mol. Biol. 374*, 374-383.

[39] Zhu, H., Liu, M. Y., and Lei, B. F. (2008) The surface protein Shr of *Streptococcus pyogenes* binds heme and transfers it to the streptococcal heme-binding protein Shp. *BMC Microbiol. 8*, 15.

[40] Lei, J. P., Ju, H. X., and Ikeda, O. (2005) A novel supramolecular assembly film of porphyrin bound DNA: Characterization and catalytic behaviors towards nitric oxide. *Sensors 5*, 171-184.

[41] Nygaard, T. K., Blouin, G. C., Liu, M. Y., Fukumura, M., Olson, J. S., Fabian, M., Dooley, D. M., and Lei, B. F. (2006) The mechanism of direct heme transfer from the streptococcal cell surface protein Shp to HtsA of the HtsABC transporter. *J. Biol. Chem. 281*, 20761-20771.

[42] Ran, Y. C., Malmirchegini, G. R., Clubb, R. T., and Lei, B. F. (2013) Axial ligand replacement mechanism in heme transfer from streptococcal heme-binding protein Shp to HtsA of the HtsABC transporter. *Biochemistry 52*, 6537-6547.

[43] Lei, B. F., Liu, M. Y., Prater, C. I., Kala, S. V., Deleo, F. R., and Musser, J. M. (2003) Identification and characterization of HtsA, a second heme-binding protein made by *Streptococcus pyogenes*. *Infect. Immun. 71*, 5962-5969.

[44] Bates, C. S., Montañez, G. E., Woods, C. R., Vincent, R. M., and Eichenbaum, Z. (2003) Identification and characterization of a *Streptococcus pyogenes* operon involved in binding of hemoproteins and acquisition of iron. *Infect. Immun. 71*, 1042-1055.

[45] Sun, X., Ge, R. G., Zhang, D., Sun, H., and He, Q. (2010) Iron-containing lipoprotein SiaA in SiaABC, the primary heme transporter of *Streptococcus pyogenes*. *J. Inorg. Biochem. 15*, 1265-1273.

[46] Ran, Y. C., Liu, M. Y., Zhu, H., Nygaard, T. K., Brown, D. E., Fabian, M., Dooley, D. M., and Lei, B. F. (2010) Spectroscopic identification of heme axial ligands in HtsA that are involved in heme acquisition by *Streptococcus pyogenes*. *Biochemistry 49*, 2834-2842.

[47] Yang, J. Y., Yan, R. X., Roy, A., Xu, D., Poisson, J., and Zhang, Y. (2015) The I-TASSER Suite: protein structure and function prediction. *Nat. Methods 12*, 7-8.

[48] DeLano, W., L. (2015) The PyMOL Molecular Graphics System, Version 1.7.4 Schrödinger, LLC. *http://www. pymol. org*.

[49] Pond, A. E., Roach, M. P., Thomas, M. R., Boxer, S. G., and Dawson, J. H. (2000) The H93G myoglobin cavity mutant as a versatile template for modeling heme proteins: Ferrous, ferric, and ferryl mixed-ligand complexes with imidazole in the cavity. *Inorg. Chem. 39*, 6061-6066.

[50] Pace, C. N., and Scholtz, J. M. (1997) Measuring the conformational stability of a protein, In *Protein Structure: A Practical Approach* (Creighton, T., Ed.) 2nd ed., pp 299-321, Oxford University Press, Oxford.

[51] Wittung-Stafshede, P. (1999) Equilibrium unfolding of a small low-potential cytochrome, cytochrome c_{553} from *Desulfovibrio vulgaris*. *Protein Sci. 8*, 1523-1529.

[52] Roncone, R., Monzani, E., Labo, S., Sanangelantoni, A. M., and Casella, L. (2005) Catalytic activity, stability, unfolding, and degradation pathways of engineered and reconstituted myoglobins. *J. Biol. Inorg. Chem 10*, 11-24.

[53] Swint, L., and Robertson, A. D. (1993) Thermodynamics of unfolding for turkey ovomucoid third domain: Thermal and chemical denaturation. *Protein Sci. 2*, 2037-2049.

[54] Dutton, P. L. (1978) Redox potentiometry: Determination of midpoint potentials of oxidation-reduction components of biological electron-transfer systems. *Methods Enzymol. 54*, 411-435.

[55] Du, J., Sono, M., and Dawson, J. H. (2011) The H93G myoglobin cavity mutant as a versatile scaffold for modeling heme iron coordination structures in protein active sites and their characterization with magnetic circular dichroism spectroscopy. *Coord. Chem. Rev. 255*, 700-716.

[56] Perera, R., Sono, M., Sigman, J. A., Pfister, T. D., Lu, Y., and Dawson, J. H. (2003) Neutral thiol as a proximal ligand to ferrous heme iron: Implications for heme proteins that lose cysteine thiolate ligation on reduction. *Proc. Natl. Acad. Sci. USA 100*, 3641-3646.

[57] Lukat-Rodgers, G. S., Rodgers, K. R., Caillet-Saguy, C., Izadi-Pruneyre, N., and Lecroisey, A. (2008) Novel heme ligand displacement by CO in the soluble hemophore HasA and its proximal ligand mutants: Implications for heme uptake and release. *Biochemistry 47*, 2087-2098.

[58] Izadi, N., Henry, Y., Haladjian, J., Goldberg, M. E., Wandersman, C., Delepierre, M., and Lecroisey, A. (1997) Purification and characterization of an extracellular heme-binding protein, HasA, involved in heme iron acquisition. *Biochemistry 36*, 7050-7057.

[59] Kloer, D. P., Hagel, C., Heider, J., and Schulz, G. E. (2006) Crystal structure of ethylbenzene dehydrogenase from *Aromatoleum aromaticum*. *Structure 14*, 1377-1388.

[60] Creevey, N. L., McEwan, A. G., Hanson, G. R., and Bernhardt, P. V. (2008) Thermodynamic characterization of the redox centers within dimethylsulfide dehydrogenase. *Biochemistry 47*, 3770-3776.

[61] McDevitt, C. A., Hanson, G. R., Noble, C. J., Cheesman, M. R., and McEwan, A. G. (2002) Characterization of the redox centers in dimethyl sulfide dehydrogenase from *Rhodovulum sulfidophilum*. *Biochemistry 41*, 15234-15244.

[62] Akbas, N., Draganova, E. B., Block, D. R., Sook, B. R., Chan, Y. F., Zhuo, J., Eichenbaum, Z., Rodgers, K. R., and Dixon, D. W. (2015) Heme-bound SiaA from *Streptococcus pyogenes*: Effects of mutations and oxidation state on protein stability. *J. Inorg. Biochem.*

[63] Zhu, H., Xie, G., Liu, M., Olson, J. S., Fabian, M., Dooley, D. M., and Lei, B. (2008) Pathway for heme uptake from human methemoglobin by the iron-regulated surface determinants system of *Staphylococcus aureus*. *J. Biol. Chem. 283*, 18450-18460.

[64] O'Keeffe, D. T., and Anthony, C. (1980) The interaction between methanol dehydrogenase and the autoreducible cytochromes c of the facultative methylotroph *Pseudomonas* AM1. *Biochem. J 190*, 481-484.

[65] Nunn, D. N., and Anthony, C. (1988) The nucleotide sequence and deduced amino acid sequence of the cytochrome cL gene of *Methylobacterium extorquens* AM1, a novel class of c-type cytochrome. *Biochem. J 256*, 673-676.

[66] Anthony, C. (1992) The *c*-type cytochromes of methylotrophic bacteria. *Biochimica et Biophysica Acta-Bioenergetics 1099*, 1-15.

[67] Williams, P., Coates, L., Mohammed, F., Gill, R., Erskine, P., Bourgeois, D., Wood, S. P., Anthony, C., and Cooper, J. B. (2006) The 1.6 Å X-ray structure of the unusual c-type cytochrome, cytochrome c(L), from the methylotrophic bacterium *Methylobacterium extorquens*. *J. Mol. Biol. 357*, 151-162.

[68] Afolabi, P. R., Mohammed, F., Amaratunga, K., Majekodunmi, O., Dales, S. L., Gill, R., Thompson, D., Cooper, J. B., Wood, S. P., Goodwin, P. M., and Anthony, C. (2001) Site-directed mutagenesis and X-ray crystallography of the PQQ-containing quinoprotein methanol dehydrogenase and its electron acceptor, cytochrome c(L). *Biochemistry 40*, 9799-9809.

[69] Read, J., Gill, R., Dales, S. L., Cooper, J. B., Wood, S. P., and Anthony, C. (1999) The molecular structure of an unusual cytochrome c(2) determined at 2.0 Å; the cytochrome c(H) from *Methylobacterium extorquens*. *Protein Sci. 8*, 1232-1240.

[70] Matsuno, T., Morishita, N., Yamazaki, K., Inoue, N., Sato, Y., Ichise, N., Hara, I., Hoshino, T., Matsuyama, H., Yoshimune, K., and Yumoto, I. (2007) Cytochrome c-552 from gram-negative alkaliphilic *Pseudomonas alcaliphila* AL15-21(T) alters the redox properties at high pH. *J. Biosci. Bioeng. 103*, 247-254.

[71] Campos, A. P., Aguiar, A. P., Hervas, M., Regalla, M., Navarro, J. A., Ortega, J. M., Xavier, A. V., De la Rosa, M. A., and Teixeira, M. (1993) Cytochrome c(6) from *Monoraphidium braunii*. A cytochrome with an unusual heme axial coordination. *Eur. J. Biochem 216*, 329-341.

[72] Tanaka, K., Takahashi, M. A., and Asada, K. (1978) Isolation of monomeric cytochrome f from Japanese radish and a mechanism of autoreduction. *jbc 253*, 7397-7403.

[73] Volkov, A. N., Ferrari, D., Worrall, J. A., Bonvin, A. M., and Ubbink, M. (2005) The orientations of cytochrome c in the highly dynamic complex with cytochrome b(5) visualized by NMR and docking using HADDOCK. *Protein Sci. 14*, 799-811.

[74] Moench, S. J., and Satterlee, J. D. (1995) A comparison of spectral and physicochemical properties of yeast iso-1 cytochrome c and Cys 102-modified derivatives of the protein. *J. Protein Chem 14*, 567-582.

[75] Chen, L., Mathews, F. S., Davidson, V. L., Tegoni, M., Rivetti, C., and Rossi, G. L. (1993) Preliminary crystal structure studies of a ternary electron transfer complex between a quinoprotein, a blue copper protein, and a c-type cytochrome. *Protein Sci. 2*, 147-154.

[76] Epstein, L. M., Straub, D. K., and Maricond, C. (1967) Mössbauer spectra of some porphyrin complexes with pyridine, piperidine, and imidazole. *Inorg. Chem. 6*, 1720-&.

[77] Radonovich, L. J., Hoard, J. L., and Bloom, A. (1972) Stereochemistry of low-spin iron porphyrins. 2. Bis(piperidine)-alpha,beta,gamma,delta-tetraphenylporphinatoiron(II). *J. Am. Chem. Soc. 94*, 2073-2078.

[78] Straub, D. K., and Connor, W. M. (1973) Mössbauer spectra of hemichromes and hemochromes derived from alpha beta gamma delta-tetraarylporphins. *Ann. N. Y. Acad. Sci. 206*, 383-396.

[79] Del Gaudio, J., and La Mar, G. N. (1976) Mechanism of autoreduction of ferric porphyrins and activation of coordinated ligands - detection of one-electron oxidized substrates. *J. Am. Chem. Soc. 98*, 3014-3015.

[80] Del Gaudio, J., and La Mar, G. N. (1978) Magnetic resonance investigation of autoreduction of tetraphenylporphinatoiron(iii) chloride in presence of piperidine. *J. Am. Chem. Soc. 100*, 1112-1119.

[81] Connor, W. M., and Straub, D. K. (1979) Mössbauer spectra of substituted pyridine hemes. *Inorg. Chem. 18*, 866-867.

[82] Srivatsa, G. S., and Sawyer, D. T. (1985) Hydroxide-Induced Reduction of (Tetraphenylporphinato)Iron(II) in Pyridine. *Inorg. Chem. 24*, 1732-1734.

[83] Castro, C. E., Jamin, M., Yokoyama, W., and Wade, R. (1986) Ligation and reduction of iron(III) porphyrins by amines - A model for cytochrome P-450 monoamine oxidase. *J. Am. Chem. Soc. 108*, 4179-4187.

[84] Shin, K., Kramer, S. K., and Goff, H. M. (1987) Base-promoted autoreduction of iron(III) porphyrins in dimethylsulfoxide solution - magnetic-resonance spectroscopy of hydroxoiro(II) porphyrin complexes. *Inorg. Chem. 26*, 4103-4106.

[85] Balch, A. L., Noll, B. C., Olmstead, M. M., and Phillips, S. L. (1996) Structural and spectroscopic characterization of iron(III) dioxoporphodimethene complexes and their autoreduction to an iron(II) complex in pyridine. *Inorg. Chem 35*, 6495-6506.

[86] Zhong, X. H., Feng, Y. Y., Huang, J. S., and Shen, P. W. (1996) A new method for preparation of iron(II) porphyrin complex - Isolation and characterization of amine complex of ferrous porphyrin. *Chin. Chem. Lett. 7*, 185-186.

[87] Zhong, X. H., Huang, J. S., Sheng, P. W., and Feng, Y. Y. (1996) A new method of preparation of iron(II) porphyrin complexes - Isolation and characterization of amine complexes of ferrous porphyrin. *Polyhedron 15*, 2677-2679.

References

[1] Braun, V., and Hantke, K. (2011) Recent insights into iron import by bacteria. *Curr. Opin. Chem. Biol. 15*, 328-334.

[2] Benson, D. R., and Rivera, M. (2013) Heme uptake and metabolism in bacteria. *Met. Ions Life Sci 12*, 279-332.

[3] Rodgers, K. R., and Lukat-Rodgers, G. S. (2014) Biophysical perspectives on the acquisition, transport, and trafficking of heme in bacteria. *Handbook of porphyrin science with applications to chemistry, physics, materials science, engineering, biology and medicine, vol. 30: Heme proteins, part II 30*, 249-309.

[4] Contreras, H., Chim, N., Credali, A., and Goulding, C. W. (2014) Heme uptake in bacterial pathogens. *Curr. Opin. Chem. Biol. 19*, 34-41.

[5] Wilks, A., and O'Neill, M. J. (2014) Extracellular heme uptake and metabolism in bacterial pathogenesis, In *Handbook of porphyrin science with applications to chemistry, physics, materials science, engineering, biology and medicine, vol 26: Heme biochemistry* (Ferreira, G. C., Kadish, K. M., Smith, K. M., and Guilard, R., Eds.), pp 267-315, World Scientific, Hackensack, NJ.

[6] Runyen-Janecky, L. J. (2013) Role and regulation of heme on acquisition in gram-negative pathogens. *Front. Cell. Infect. Microbiol. 3*, 55.

[7] Cavallaro, G., Decaria, L., and Rosato, A. (2008) Genome-based analysis of heme biosynthesis and uptake in prokaryotic systems. *J. Proteome Res. 7*, 4946-4954.

[8] Tong, Y., and Guo, M. (2009) Bacterial heme-transport proteins and their heme-coordination modes. *Arch. Biochem. Biophys. 481*, 1-15.

[9] Mayfield, J. A., Dehner, C. A., and DuBois, J. L. (2011) Recent advances in bacterial heme protein biochemistry. *Curr. Opin. Chem. Biol. 15*, 260-266.

[10] Wilks, A., and Barker, K. D. (2011) Mechanisms of heme uptake and utilization in bacterial pathogens, In *Handbook of Porphyrin Science with Applications to Chemistry, Physics, Materials Science, Engineering, Biology and Medicine, Vol 15: Biochemistry of Tetrapyrroles* (Kadish, K. M., Smith, K. M., and Guilard, R., Eds.), pp 357-398, World Scientific, Hacksensack, NJ.

[11] Gruss, A., Borezée-Durant, E., and Lechardeur, D. (2012) Environmental heme utilization by heme-auxotrophic bacteria, In *Advances in Bacterial Respiratory Physiology* (Poole, R. K., Ed.) 61 ed., pp 69-124, Academic Press, London, England.

[12] Smith, A. D., and Wilks, A. (2012) Extracellular heme uptake and the challenges of bacterial cell membranes. *Curr. Top. Membr. 69*, 359-392.

[13] Farrand, A. J., and Skaar, E. P. (2014) Heme and infectious diseases, In *Handbook of porphyrin science with applications to chemistry, physics, materials science, engineering, biology and medicine, vol 26: Heme biochemistry* (Ferreira, G. C., Kadish, K. M., Smith, K. M., and Guilard, R., Eds.) 26 ed., pp 317-377, World Scientific, Hackensack, NJ.

[14] Allen, C. E., and Schmitt, M. P. (2014) Utilization of host iron sources by *Corynebacterium diphtheriae*: Multiple hemoglobin-binding proteins are essential for the use of iron from the hemoglobin/haptoglobin complex. *J. Bacteriol. 195*, 2413-2414.

[15] Draganova, E. B., Akbas, N., Adrian, S. A., Lukat-Rodgers, G. S., Collins, D. P., Dawson, J. H., Allen, C. E., Schmitt, M. P., Rodgers, K. R., and Dixon, D. W. (2015) Heme binding by *Corynebacterium diphtheriae* HmuT: Function and heme environment. *Biochemistry 54*, 6598-6609.

[16] Honsa, E. S., and Maresso, A. W. (2011) Mechanisms of iron import in anthrax. *BioMetals 24*, 533-545.

[17] Hammer, N. D., and Skaar, E. P. (2011) Molecular mechanisms of *Staphylococcus aureus* iron acquisition. *Annu. Rev. Microbiol. 65*, 129-147.

[18] Tiedemann, M. T., Heinrichs, D. E., and Stillman, M. J. (2012) Multiprotein heme shuttle pathway in *Staphylococcus aureus*: Iron-regulated surface determinant cog-wheel kinetics. *J. Am. Chem. Soc. 134*, 16578-16585.

[19] Eichenbaum, Z. (2012) The streptococcal hemoprotein receptor. A moonlighting protein or a virulence factor? *Virulence 3*, 553-555.

[20] Sook, B. R., Block, D. R., Sumithran, S., Montañez, G. E., Rodgers, K. R., Dawson, J. H., Eichenbaum, Z., and Dixon, D. W. (2008) Characterization of SiaA, a streptococcal heme-binding protein associated with a heme ABC transport system. *Biochemistry 47*, 2678-2688.

[21] Ouattara, M., Cunha, E. B., Li, X., Huang, Y. S., Dixon, D. W., and Eichenbaum, Z. (2010) Shr of Group A streptococcus is a new type of composite NEAT protein involved in sequestering haem from methaemoglobin. *Mol. Microbiol. 78*, 739-756.

[22] Ouattara, M., Pennati, A., Devlin, D. J., Huang, Y. S., Gadda, G., and Eichenbaum, Z. (2013) Kinetics of heme transfer by the Shr NEAT domains of Group A Streptococcus. *Arch. Biochem. Biophys. 538*, 71-79.

[23] Andrade, M. A., Ciccarelli, F. D., Perez-Iratxeta, C., and Bork, P. (2002) NEAT: A domain duplicated in genes near the components of a putative Fe(3+) siderophore transporter from Gram-positive pathogenic bacteria. *Genome Biol. 3*, RESEARCH0047.

[24] Honsa, E. S., Maresso, A. W., and Highlander, S. K. (2014) Molecular and evolutionary analysis of NEAr-iron Transporter (NEAT) domains. *PLoS One 9*.

[25] Sharp, K. H., Schneider, S., Cockayne, A., and Paoli, M. (2007) Crystal structure of the heme-IsdC complex, the central conduit of the Isd iron/heme uptake system in *Staphylococcus aureus*. *J. Biol. Chem. 282*, 10625-10631.

[26] Watanabe, M., Tanaka, Y., Suenaga, A., Kuroda, M., Yao, M., Watanabe, N., Arisaka, F., Ohta, T., Tanaka, I., and Tsumoto, K. (2008) Structural basis for multimeric heme complexation through a specific protein-heme interaction - The case of the third NEAT domain of IsdH from *Staphylococcus aureus*. *J. Biol. Chem. 283*, 28649-28659.

[27] Ekworomadu, M. T., Poor, C. B., Owens, C. P., Balderas, M. A., Fabian, M., Olson, J. S., Murphy, F., Balkabasi, E., Honsa, E. S., He, C., Goulding, C. W., and Maresso, A. W. (2012) Differential function of Lip residues in the mechanism and biology of an anthrax hemophore. *PLoS Path. 8*.

[28] Honsa, E. S., Owens, C. P., Goulding, C. W., and Maresso, A. W. (2013) The near-iron transporter (NEAT) domains of the anthrax hemophore IsdX2 require a critical glutamine to extract heme from methemoglobin. *J. Biol. Chem. 288*, 8479-8490.

[29] Gaudin, C. F. M., Grigg, J. C., Arrieta, A. L., and Murphy, M. E. P. (2011) Unique heme-iron coordination by the hemoglobin receptor IsdB of *Staphylococcus aureus*. *Biochemistry 50*, 5443-5452.

[30] Pluym, M., Muryoi, N., Heinrichs, D. E., and Stillman, M. J. (2008) Heme binding in the NEAT domains of IsdA and IsdC of *Staphylococcus aureus*. *J. Inorg. Biochem. 102*, 480-488.

[31] Balderas, M. A., Nobles, C. L., Honsa, E. S., Alicki, E. R., and Maresso, A. W. (2012) Hal is a *Bacillus anthracis* heme acquisition protein. *J. Bacteriol. 194*, 5513-5521.

[32] Malmirchegini, G. R., Sjodt, M., Shnitkind, S., Sawaya, M. R., Rosinski, J., Newton, S. M., Klebba, P. E., and Clubb, R. T. (2014) Novel mechanism of hemin capture by Hbp2, the hemoglobin-binding hemophore from *Listeria monocytogenes*. *J. Biol. Chem. 289*, 34886-34899.

[33] Eichenbaum, Z., Green, B. D., and Scott, J. R. (1996) Iron starvation causes release from the group A streptococcus of the ADP-ribosylating protein called plasmin receptor or surface glyceraldehyde-3-phosphate-dehydrogenase. *Infect. Immun. 64*, 1956-1960.

[34] Eichenbaum, Z., Muller, E., Morse, S. A., and Scott, J. R. (1996) Acquisition of iron from host proteins by the group A *Streptococcus*. *Infect. Immun. 64*, 5428-5429.

[35] Montañez, G. E., Neely, M. N., and Eichenbaum, Z. (2005) The streptococcal iron uptake (Siu) transporter is required for iron uptake and virulence In a zebrafish infection model. *Microbiology-SGM 151*, 3749-3757.

[36] Ardanuy, C., Domenech, A., Rolo, D., Calatayud, L., Tubau, F., Ayats, J., Martin, R., and Linares, J. (2010) Molecular characterization of macrolide- and multidrug-resistant

Streptococcus pyogenes isolated from adult patients in Barcelona, Spain (1993-2008). *J. Antimicrob. Chemother. 65*, 634-643.

[37] Walker, M. J., Barnett, T. C., McArthur, J. D., Cole, J. N., Gillen, C. M., Henningham, A., Sriprakash, K. S., Sanderson-Smith, M. L., and Nizet, V. (2014) Disease manifestations and pathogenic mechanisms of group a Streptococcus. *Clin. Microbiol. Rev. 27*, 264-301.

[38] Aranda, R., Worley, C. E., Liu, M., Bitto, E., Cates, M. S., Olson, J. S., Lei, B. F., and Phillips, G. N. (2007) Bis-methionyl coordination in the crystal structure of the heme-binding domain of the streptococcal cell surface protein Shp. *J. Mol. Biol. 374*, 374-383.

[39] Zhu, H., Liu, M. Y., and Lei, B. F. (2008) The surface protein Shr of *Streptococcus pyogenes* binds heme and transfers it to the streptococcal heme-binding protein Shp. *BMC Microbiol. 8*, 15.

[40] Lei, J. P., Ju, H. X., and Ikeda, O. (2005) A novel supramolecular assembly film of porphyrin bound DNA: Characterization and catalytic behaviors towards nitric oxide. *Sensors 5*, 171-184.

[41] Nygaard, T. K., Blouin, G. C., Liu, M. Y., Fukumura, M., Olson, J. S., Fabian, M., Dooley, D. M., and Lei, B. F. (2006) The mechanism of direct heme transfer from the streptococcal cell surface protein Shp to HtsA of the HtsABC transporter. *J. Biol. Chem. 281*, 20761-20771.

[42] Ran, Y. C., Malmirchegini, G. R., Clubb, R. T., and Lei, B. F. (2013) Axial ligand replacement mechanism in heme transfer from streptococcal heme-binding protein Shp to HtsA of the HtsABC transporter. *Biochemistry 52*, 6537-6547.

[43] Lei, B. F., Liu, M. Y., Prater, C. I., Kala, S. V., Deleo, F. R., and Musser, J. M. (2003) Identification and characterization of HtsA, a second heme-binding protein made by *Streptococcus pyogenes*. *Infect. Immun. 71*, 5962-5969.

[44] Bates, C. S., Montañez, G. E., Woods, C. R., Vincent, R. M., and Eichenbaum, Z. (2003) Identification and characterization of a *Streptococcus pyogenes* operon involved in binding of hemoproteins and acquisition of iron. *Infect. Immun. 71*, 1042-1055.

[45] Sun, X., Ge, R. G., Zhang, D., Sun, H., and He, Q. (2010) Iron-containing lipoprotein SiaA in SiaABC, the primary heme transporter of *Streptococcus pyogenes*. *J. Inorg. Biochem. 15*, 1265-1273.

[46] Ran, Y. C., Liu, M. Y., Zhu, H., Nygaard, T. K., Brown, D. E., Fabian, M., Dooley, D. M., and Lei, B. F. (2010) Spectroscopic identification of heme axial ligands in HtsA that are involved in heme acquisition by *Streptococcus pyogenes*. *Biochemistry 49*, 2834-2842.

[47] Yang, J. Y., Yan, R. X., Roy, A., Xu, D., Poisson, J., and Zhang, Y. (2015) The I-TASSER Suite: protein structure and function prediction. *Nat. Methods 12*, 7-8.

[48] DeLano, W., L. (2015) The PyMOL Molecular Graphics System, Version 1.7.4 Schrödinger, LLC. *http://www. pymol. org*.

[49] Pond, A. E., Roach, M. P., Thomas, M. R., Boxer, S. G., and Dawson, J. H. (2000) The H93G myoglobin cavity mutant as a versatile template for modeling heme proteins: Ferrous, ferric, and ferryl mixed-ligand complexes with imidazole in the cavity. *Inorg. Chem. 39*, 6061-6066.

[50] Pace, C. N., and Scholtz, J. M. (1997) Measuring the conformational stability of a protein, In *Protein Structure: A Practical Approach* (Creighton, T., Ed.) 2nd ed., pp 299-321, Oxford University Press, Oxford.

[51] Wittung-Stafshede, P. (1999) Equilibrium unfolding of a small low-potential cytochrome, cytochrome c_{553} from *Desulfovibrio vulgaris*. *Protein Sci. 8*, 1523-1529.

[52] Roncone, R., Monzani, E., Labo, S., Sanangelantoni, A. M., and Casella, L. (2005) Catalytic activity, stability, unfolding, and degradation pathways of engineered and reconstituted myoglobins. *J. Biol. Inorg. Chem 10*, 11-24.

[53] Swint, L., and Robertson, A. D. (1993) Thermodynamics of unfolding for turkey ovomucoid third domain: Thermal and chemical denaturation. *Protein Sci. 2*, 2037-2049.

[54] Dutton, P. L. (1978) Redox potentiometry: Determination of midpoint potentials of oxidation-reduction components of biological electron-transfer systems. *Methods Enzymol. 54*, 411-435.

[55] Du, J., Sono, M., and Dawson, J. H. (2011) The H93G myoglobin cavity mutant as a versatile scaffold for modeling heme iron coordination structures in protein active sites and their characterization with magnetic circular dichroism spectroscopy. *Coord. Chem. Rev. 255*, 700-716.

[56] Perera, R., Sono, M., Sigman, J. A., Pfister, T. D., Lu, Y., and Dawson, J. H. (2003) Neutral thiol as a proximal ligand to ferrous heme iron: Implications for heme proteins that lose cysteine thiolate ligation on reduction. *Proc. Natl. Acad. Sci. USA 100*, 3641-3646.

[57] Lukat-Rodgers, G. S., Rodgers, K. R., Caillet-Saguy, C., Izadi-Pruneyre, N., and Lecroisey, A. (2008) Novel heme ligand displacement by CO in the soluble hemophore HasA and its proximal ligand mutants: Implications for heme uptake and release. *Biochemistry 47*, 2087-2098.

[58] Izadi, N., Henry, Y., Haladjian, J., Goldberg, M. E., Wandersman, C., Delepierre, M., and Lecroisey, A. (1997) Purification and characterization of an extracellular heme-binding protein, HasA, involved in heme iron acquisition. *Biochemistry 36*, 7050-7057.

[59] Kloer, D. P., Hagel, C., Heider, J., and Schulz, G. E. (2006) Crystal structure of ethylbenzene dehydrogenase from *Aromatoleum aromaticum*. *Structure 14*, 1377-1388.

[60] Creevey, N. L., McEwan, A. G., Hanson, G. R., and Bernhardt, P. V. (2008) Thermodynamic characterization of the redox centers within dimethylsulfide dehydrogenase. *Biochemistry 47,* 3770-3776.

[61] McDevitt, C. A., Hanson, G. R., Noble, C. J., Cheesman, M. R., and McEwan, A. G. (2002) Characterization of the redox centers in dimethyl sulfide dehydrogenase from *Rhodovulum sulfidophilum*. *Biochemistry 41,* 15234-15244.

[62] Akbas, N., Draganova, E. B., Block, D. R., Sook, B. R., Chan, Y. F., Zhuo, J., Eichenbaum, Z., Rodgers, K. R., and Dixon, D. W. (2015) Heme-bound SiaA from *Streptococcus pyogenes*: Effects of mutations and oxidation state on protein stability. *J. Inorg. Biochem.*

[63] Zhu, H., Xie, G., Liu, M., Olson, J. S., Fabian, M., Dooley, D. M., and Lei, B. (2008) Pathway for heme uptake from human methemoglobin by the iron-regulated surface determinants system of *Staphylococcus aureus*. *J. Biol. Chem. 283,* 18450-18460.

[64] O'Keeffe, D. T., and Anthony, C. (1980) The interaction between methanol dehydrogenase and the autoreducible cytochromes c of the facultative methylotroph *Pseudomonas* AM1. *Biochem. J 190,* 481-484.

[65] Nunn, D. N., and Anthony, C. (1988) The nucleotide sequence and deduced amino acid sequence of the cytochrome cL gene of *Methylobacterium extorquens* AM1, a novel class of c-type cytochrome. *Biochem. J 256,* 673-676.

[66] Anthony, C. (1992) The *c*-type cytochromes of methylotrophic bacteria. *Biochimica et Biophysica Acta-Bioenergetics 1099,* 1-15.

[67] Williams, P., Coates, L., Mohammed, F., Gill, R., Erskine, P., Bourgeois, D., Wood, S. P., Anthony, C., and Cooper, J. B. (2006) The 1.6 Å X-ray structure of the unusual c-type cytochrome, cytochrome c(L), from the methylotrophic bacterium *Methylobacterium extorquens*. *J. Mol. Biol. 357,* 151-162.

[68] Afolabi, P. R., Mohammed, F., Amaratunga, K., Majekodunmi, O., Dales, S. L., Gill, R., Thompson, D., Cooper, J. B., Wood, S. P., Goodwin, P. M., and Anthony, C. (2001) Site-directed mutagenesis and X-ray crystallography of the PQQ-containing quinoprotein methanol dehydrogenase and its electron acceptor, cytochrome c(L). *Biochemistry 40,* 9799-9809.

[69] Read, J., Gill, R., Dales, S. L., Cooper, J. B., Wood, S. P., and Anthony, C. (1999) The molecular structure of an unusual cytochrome c(2) determined at 2.0 Å; the cytochrome c(H) from *Methylobacterium extorquens*. *Protein Sci. 8,* 1232-1240.

[70] Matsuno, T., Morishita, N., Yamazaki, K., Inoue, N., Sato, Y., Ichise, N., Hara, I., Hoshino, T., Matsuyama, H., Yoshimune, K., and Yumoto, I. (2007) Cytochrome c-552 from gram-negative alkaliphilic *Pseudomonas alcaliphila* AL15-21(T) alters the redox properties at high pH. *J. Biosci. Bioeng. 103,* 247-254.

[71] Campos, A. P., Aguiar, A. P., Hervas, M., Regalla, M., Navarro, J. A., Ortega, J. M., Xavier, A. V., De la Rosa, M. A., and Teixeira, M. (1993) Cytochrome c(6) from *Monoraphidium braunii*. A cytochrome with an unusual heme axial coordination. *Eur. J. Biochem 216*, 329-341.

[72] Tanaka, K., Takahashi, M. A., and Asada, K. (1978) Isolation of monomeric cytochrome f from Japanese radish and a mechanism of autoreduction. *jbc 253*, 7397-7403.

[73] Volkov, A. N., Ferrari, D., Worrall, J. A., Bonvin, A. M., and Ubbink, M. (2005) The orientations of cytochrome c in the highly dynamic complex with cytochrome b(5) visualized by NMR and docking using HADDOCK. *Protein Sci. 14*, 799-811.

[74] Moench, S. J., and Satterlee, J. D. (1995) A comparison of spectral and physicochemical properties of yeast iso-1 cytochrome c and Cys 102-modified derivatives of the protein. *J. Protein Chem 14*, 567-582.

[75] Chen, L., Mathews, F. S., Davidson, V. L., Tegoni, M., Rivetti, C., and Rossi, G. L. (1993) Preliminary crystal structure studies of a ternary electron transfer complex between a quinoprotein, a blue copper protein, and a c-type cytochrome. *Protein Sci. 2*, 147-154.

[76] Epstein, L. M., Straub, D. K., and Maricond, C. (1967) Mössbauer spectra of some porphyrin complexes with pyridine, piperidine, and imidazole. *Inorg. Chem. 6*, 1720-&.

[77] Radonovich, L. J., Hoard, J. L., and Bloom, A. (1972) Stereochemistry of low-spin iron porphyrins. 2. Bis(piperidine)-alpha,beta,gamma,delta-tetraphenylporphinatoiron(II). *J. Am. Chem. Soc. 94*, 2073-2078.

[78] Straub, D. K., and Connor, W. M. (1973) Mössbauer spectra of hemichromes and hemochromes derived from alpha beta gamma delta-tetraarylporphins. *Ann. N. Y. Acad. Sci. 206*, 383-396.

[79] Del Gaudio, J., and La Mar, G. N. (1976) Mechanism of autoreduction of ferric porphyrins and activation of coordinated ligands - detection of one-electron oxidized substrates. *J. Am. Chem. Soc. 98*, 3014-3015.

[80] Del Gaudio, J., and La Mar, G. N. (1978) Magnetic resonance investigation of autoreduction of tetraphenylporphinatoiron(iii) chloride in presence of piperidine. *J. Am. Chem. Soc. 100*, 1112-1119.

[81] Connor, W. M., and Straub, D. K. (1979) Mössbauer spectra of substituted pyridine hemes. *Inorg. Chem. 18*, 866-867.

[82] Srivatsa, G. S., and Sawyer, D. T. (1985) Hydroxide-Induced Reduction of (Tetraphenylporphinato)Iron(II) in Pyridine. *Inorg. Chem. 24*, 1732-1734.

[83] Castro, C. E., Jamin, M., Yokoyama, W., and Wade, R. (1986) Ligation and reduction of iron(III) porphyrins by amines - A model for cytochrome P-450 monoamine oxidase. *J. Am. Chem. Soc. 108*, 4179-4187.

[84] Shin, K., Kramer, S. K., and Goff, H. M. (1987) Base-promoted autoreduction of iron(III) porphyrins in dimethylsulfoxide solution - magnetic-resonance spectroscopy of hydroxoiro(II) porphyrin complexes. *Inorg. Chem. 26*, 4103-4106.

[85] Balch, A. L., Noll, B. C., Olmstead, M. M., and Phillips, S. L. (1996) Structural and spectroscopic characterization of iron(III) dioxoporphodimethene complexes and their autoreduction to an iron(II) complex in pyridine. *Inorg. Chem 35*, 6495-6506.

[86] Zhong, X. H., Feng, Y. Y., Huang, J. S., and Shen, P. W. (1996) A new method for preparation of iron(II) porphyrin complex - Isolation and characterization of amine complex of ferrous porphyrin. *Chin. Chem. Lett. 7*, 185-186.

[87] Zhong, X. H., Huang, J. S., Sheng, P. W., and Feng, Y. Y. (1996) A new method of preparation of iron(II) porphyrin complexes - Isolation and characterization of amine complexes of ferrous porphyrin. *Polyhedron 15*, 2677-2679.

[88] Pittman, M. S., Corker, H., Wu, G., Binet, M. B., Moir, A. J., and Poole, R. K. (2002) Cysteine is exported from the *Escherichia coli* cytoplasm by CydDC, an ATP-binding cassette-type transporter required for cytochrome assembly. *J. Biol. Chem 277*, 49841-49849.

[89] Pittman, M. S., Robinson, H. C., and Poole, R. K. (2005) A bacterial glutathione transporter (*Escherichia coli* CydDC) exports reductant to the periplasm. *J. Biol. Chem 280*, 32254-32261.

[90] Shepherd, M. (2015) The CydDC ABC transporter of Escherichia coli: new roles for a reductant efflux pump. *Biochem. Soc. Trans. 43*, 908-912.

[91] Messens, J., and Collet, J. F. (2006) Pathways of disulfide bond formation in *Escherichia coli*. *Int. J. Biochem. Cell Biol. 38*, 1050-1062.

[92] Schafer, F. Q., and Buettner, G. R. (2001) Redox environment of the cell as viewed through the redox state of the glutathione disulfide/glutathione couple. *Free Radical Biol. Med. 30*, 1191-1212.

[93] Reedy, C. J., Kennedy, M. L., and Gibney, B. R. (2003) Thermodynamic characterization of ferric and ferrous haem binding to a designed four-α-helix protein. *Chem. Commun.*, 570-571.

[94] Umbreit, J. (2007) Methemoglobin - It's not just blue: A concise review. *Am. J. Hematol. 82*, 134-144.

[95] Lu, C. M., Xie, G., Liu, M. Y., Zhu, H., and Lei, B. F. (2012) Direct heme transfer reactions in the group A *Streptococcus* heme acquisition pathway. *PLoS One 7*.

[96] Ran, Y. C., Zhu, H., Liu, M. Y., Fabian, M., Olson, J. S., Aranda, R. I., Phillips, G. N., Dooley, D. M., and Lei, B. (2007) Bis-methionine ligation to heme iron in the

streptococcal cell surface protein Shp facilitates rapid hemin transfer to HtsA of the HtsABC transporter. *J. Biol. Chem. 282*, 31380-31388.

[97] Murray, S. G., and Hartley, F. R. (1981) Coordination chemistry of thioethers, selenoethers, and telluroethers in transition-metal complexes. *Chem. Rev. 81*, 365-414.

[98] Smith, M., and McLendon, G. (1981) Comparative NMR Studies of Cytochrome c and Its Active Site Octapeptide. *J. Am. Chem. Soc.*, 4912-4921.

[99] Martell, J. D., Li, H. Y., Doukov, T., Martasek, P., Roman, L. J., Soltis, M., Poulos, T. L., and Silverman, R. B. (2010) Heme-Coordinating Inhibitors of Neuronal Nitric Oxide Synthase. Iron-Thioether Coordination Is Stabilized by Hydrophobic Contacts without Increased Inhibitor Potency. *J. Am. Chem. Soc. 132*, 798-806.

9 GENERAL CONCLUSIONS

This dissertation investigated the biophysical and biochemical characteristics of heme-binding proteins in heme uptake pathways found in *Corynebacterium diphtheriae* and *Streptococcus pyogenes.* These studies contribute to the growing field of heme protein structure/function determination. Many pathogenic bacteria which utilize the human as a host, including antibiotic resistant pathogens, require iron to survive and commonly obtain the needed iron in the form of heme *(1, 2)*. Studies have shown the deletion of bacterial heme uptake pathways can diminish the survival of these pathogens. It is of increasing interest to understand these proteins in more detail in order to potentially design therapeutic agents as an alternative to antibiotics.

Many reviews have highlighted studies of *b*-type heme transfer proteins from Gram-positive, Gram-negative, and other types of bacteria *(1-11)*. These studies utilize a combination of site-directed mutagenesis, UV-visible absorption, fluorescence, circular dichroism (CD), magnetic circular dichroism (MCD), resonance Raman (rR) and electron paramagnetic resonance spectroscopies, along with mass spectrometry (MS) and X-ray crystallography to shed light on the mechanism of heme binding and transfer. These proteins have shown to utilize a variety of

heme binding motifs, commonly ligating the heme iron in a six-coordinate fashion with a combination of His, Tyr, or Met with the His/Tyr coordination being the most rare. Five-coordinate Tyr-ligated proteins have also been observed *(12)*. Based on the emerging themes of heme ligation, it was of importance to investigate other proteins which could lead to new insights into bacterial heme uptake.

Chapters 2 – 4 provided a detailed look into the important amino acid residues involved in heme binding of the substrate binding protein HmuT from *C. diphtheriae*. This protein was studied using various spectroscopic techniques such as UV-visible absorption, CD, MCD, and rR spectroscopies. Other techniques including site-directed mutagenesis, electrospray ionization mass spectrometry (ESI-MS), chemical and thermal unfolding, pH titrations, and heme reconstitution were also performed. Initial sequence alignment and homology modeling of HmuT indicated the protein to utilize a His/Tyr motif which is not a common binding system for heme proteins; only four others have been studied to our knowledge *(13)*. In addition, HmuT utilizes a histidine from the N-terminal region of the protein and a tyrosine from the C-terminal end of the protein which is opposite to what other His/Tyr heme proteins use. In light of these findings, HmuT was studied in detail to add to the growing types of heme transfer protein studies.

Chapter 2 was a detailed spectroscopic look at the heme axial ligation of HmuT *(13)*. A combination of site-directed mutagenesis, UV-visible absorption, MCD, and rR spectroscopies showed the heme to be ligated by H136 and Y235. HmuT was studied in both the ferric and ferrous oxidation states, as well as the ferrous-carbonyl (Fe-CO) state. Reduction of WT HmuT was only possible in the presence of CO and dithionite indicating a very negative reduction potential; another characteristic of tyrosine-ligated heme proteins. It was also shown through

hemoglobin-iron utilization studies that Y235 is essential for HmuT heme uptake. Additionally, WT HmuT was not affected by changes in pH, while the axial ligand mutant Y235A was altered by pH and gave a pK_a of 6.3 ± 0.1. MCD of this mutant indicated a water bound in place of the tyrosine and was the lowest known pK_a for *b*-type heme proteins with a water bound *trans* to a histidine.

The studies performed in Chapter 2 shed light on other amino acids which although are not directly binding to the heme, may be of importance to the protein and were therefore investigated in Chapter 3. HmuT and mutants (axial ligands and other residues) were studied with site-directed mutagenesis, UV-visible absorption spectroscopy, rR spectroscopy, thermal unfolding, and collision-induced heme dissociation experiments via mass spectrometry. The pH studies performed in Chapter 2 indicated the possibility of a hydrogen-bonding amino acid residue to the axial tyrosine. Based on conservation, R237, Y272, and M292 were mutated to alanine and studied. In addition, a conserved tyrosine, Y349, was also studied although not predicted to be near the heme pocket. Thermal unfolding showed Y235A (axial ligand mutant), R237A (predicted hydrogen-bonding partner), and Y349A (predicted to be involved in protein folding) were most affected by temperature with reduced melting temperature differences of ~10, 13, and 17 degrees, respectively, compared to the WT.

Collision-induced heme dissociation with ESI-MS complemented the thermal unfolding results showing R237A to lose heme in a similar fashion compared to one of the axial ligand mutants, H136A. Heme-bound Y235A was not detected by the MS, indicating the importance of this residue as a heme axial ligand. This study also showed the removal of M292 effected heme binding. This is the first example of a collision-induced heme dissociation study on a heme transfer protein. A similar study has been performed on myoglobin and cytochrome b_5 *(14)*.

This collision mass spectrometry experiment could potentially be an easier method to estimate the relative contribution of amino acids in heme protein binding pockets.

A recent crystal structure of holo-HmuT from *C. glutamicum* has been resolved and confirmed the His/Tyr heme axial ligation determined by our spectroscopic studies in *C. diphtheriae (15)*. The structure also indicated that an arginine residue is most likely the hydrogen-bonding partner to the axial tyrosine. Two different heme orientations were also detected for the structure. Contrary to the crystal structures of the sister proteins *Pseudomonas aeruginosa* PhuT *(16)* and *Shigella dysenteriae* ShuT *(16)*, the heme propionates of *C. glutamicum* HmuT do not appear to form any hydrogen bonds with other residues in the pocket which may be allowing the multiple orientations of the heme in the pocket. Overall, these findings were in line with the spectroscopic evidence presented in our work on *C. diphtheriae* HmuT.

Proteins from the streptococcal iron acquisition (sia) heme uptake pathway in *S. pygoenes* were also investigated. Chapters 5 and 6 examined the SiaA heme protein which is similar to HmuT in that both are substrate binding proteins to the respective ABC transporters. SiaA differs from HmuT in heme axial ligation by using a His/Met binding motif rather than a His/Tyr *(17)*. The SiaA protein has been shown to take a very long time to unfold, as indicated by chemical time-scale unfolding studies *(18)*. These same studies showed that SiaA unfolds in two phases, rather than one. The two unfolding phases are indicative of the heme bound to the protein in two different orientations. Differences in heme orientation have been seen in other heme proteins such as horse heart myoglobin *(19)* and cytochrome b_5 *(20)*. The half-lives of the fast and slow phases for the WT SiaA and non-axial ligand mutants ranged from 1 – 3 h and 8 – 50 h, respectively, indicating the importance of other amino acids in respect to the heme binding of

these proteins. This slow process of unfolding may assist in the heme transfer process which allows a change of conformation sufficient to release the heme without the risk of the protein proceeding along an unfolding pathway that could leave it dysfunctional.

Chapters 7 and 8 discussed the first and second NEAT domains from the Shr (streptococcal hemoprotein receptor) protein in *S. pyogenes*. Shr delivers heme to the protein Shp which in turn transfers heme to SiaA. NEAT (near iron transporter) domains are conserved groups of 150 amino acids which share similar secondary structure *(21, 22)*. These domains are mainly β-stranded and include a 3_{10} α-helix in which a serine residue extends and hydrogen-bonds with a heme propionate. Characterized NEAT proteins studied to date show the domains utilize a conserved YxxxY heme binding motif in which the first tyrosine binds to the heme and the second tyrosine hydrogen-bonds to the first *(21)*. A detailed bioinformatics study in 2014 by Honsa et al. indicated other NEAT heme-binding motifs are likely to be discovered and therefore it was of interest to characterize the NEAT domains of *S. pyogenes*.

Our work on Shr-NEAT1 (Shr-N1) and Shr-NEAT2 (Shr-N2) showed the first example of NEAT domain proteins which utilize a bismethionine axial ligation, rather than a five-coordinate tyrosine in a YxxxY motif. A combination of site-directed mutagenesis, UV-visible absorption, MCD, and rR spectroscopies, along with spectroelectrochemical and pH titrations were used to determine this novel ligand set. Both proteins were isolated as a mixture of ferric and ferrous forms with the coordination number of the heme sensitive to pH e.g. Shr-N1 is six-coordinate methionine in acidic pH and five-coordinate methionine in alkaline conditions.

Shr-N2 exhibited a rare phenomenon of heme autoreduction in which the protein converts bound ferric heme to ferrous heme, even in the presence of oxygen. Downstream of the *sia* operon, in which Shr is encoded, are the genes which encode for a cysteine and glutathione

exporter which, proposed in a similar system in *E. coli*, acts as a redox regulator *(23).* It could be the case that the facile reduction of Shr-N2 may be controlled by this exporter *in vivo*. Ouattara et al. have proposed through kinetic studies that the role of Shr-N2 is to store heme for use by the pathogen in low heme environments. It is known that methionine ligands bind tighter to ferrous iron rather than ferric *(24).* A control of the Shr-N2 reduction by the exporter could be linked to the need to either store or release heme in this protein based on the environmental availability of heme to the pathogen.

The work on both HmuT and SiaA has shown that heme binding is not only dictated by the amino acids which bind directly to the heme, but is also influenced by other nearby residues. In addition to spectroscopy and unfolding studies, the collision energy voltage mass spectrometry experiment performed on HmuT and mutants provided a novel method to estimate the relative contribution of amino acids to heme binding in heme transfer proteins. The unfolding studies of SiaA added to the examples of heme proteins which can bind heme in different orientations and showed that heme protein unfolding can be very slow.

This dissertation has exemplified the variety of heme binding motifs heme transfer proteins are able to employ. Although SiaA utilizes a commonly known His/Met ligand system, HmuT uses a rarer His/Tyr ligand set, yet the proteins are similar in function. In the case of the NEAT proteins from *S. pyogenes*, a look into the literature would lead to the assumption that the heme is most likely coordinated with a tyrosine. In contrast, our work has shown that these proteins use a novel bismethionine coordination, rather than the canonical YxxxY motif. Although common heme binding ligands for heme transfer proteins include His, Tyr, and Met, it could be the case that other amino acids such as Cys or Lys may be discovered in the future as axial ligands for heme transfer proteins.

9.1 References

[1] Rodgers, K. R., and Lukat-Rodgers, G. S. (2014) Biophysical perspectives on the acquisition, transport, and trafficking of heme in bacteria. *Handbook of porphyrin science with applications to chemistry, physics, materials science, engineering, biology and medicine, vol. 30: Heme proteins, part II 30*, 249-309.

[2] Wilks, A., and O'Neill, M. J. (2014) Extracellular heme uptake and metabolism in bacterial pathogenesis, In *Handbook of porphyrin science with applications to chemistry, physics, materials science, engineering, biology and medicine, vol 26: Heme biochemistry* (Ferreira, G. C., Kadish, K. M., Smith, K. M., and Guilard, R., Eds.), pp 267-315, World Scientific, Hackensack, NJ.

[3] Contreras, H., Chim, N., Credali, A., and Goulding, C. W. (2014) Heme uptake in bacterial pathogens. *Curr. Opin. Chem. Biol. 19*, 34-41.

[4] Benson, D. R., and Rivera, M. (2013) Heme uptake and metabolism in bacteria. *Met. Ions Life Sci 12*, 279-332.

[5] Nobles, C. L., and Maresso, A. W. (2011) The theft of host heme by Gram-positive pathogenic bacteria. *Metallomics 3*, 788-796.

[6] Runyen-Janecky, L. J. (2013) Role and regulation of heme on acquisition in gram-negative pathogens. *Front. Cell. Infect. Microbiol. 3*, 55.

[7] Fang, Z., Sampson, S. L., Warren, R. M., van Pittius, N. C. G., and Newton-Foot, M. (2015) Iron acquisition strategies in mycobacteria. *Tuberculosis 95*, 123-130.

[8] Smith, A. D., and Wilks, A. (2012) Extracellular heme uptake and the challenges of bacterial cell membranes. *Curr. Top. Membr. 69*, 359-392.

[9] Braun, V., and Hantke, K. (2011) Recent insights into iron import by bacteria. *Curr. Opin. Chem. Biol. 15*, 328-334.

[10] Farrand, A. J., and Skaar, E. P. (2014) Heme and infectious diseases, In *Handbook of porphyrin science with applications to chemistry, physics, materials science, engineering, biology and medicine, vol 26: Heme biochemistry* (Ferreira, G. C., Kadish, K. M., Smith, K. M., and Guilard, R., Eds.) 26 ed., pp 317-377, World Scientific, Hackensack, NJ.

[11] Honsa, E. S., and Maresso, A. W. (2011) Mechanisms of iron import in anthrax. *BioMetals 24*, 533-545.

[12] Grigg, J. C., Ukpabi, G., Gaudin, C. F., and Murphy, M. E. (2010) Structural biology of heme binding in the *Staphylococcus aureus* Isd system. *J. Inorg. Biochem. 104*, 341-348.

[13] Draganova, E. B., Akbas, N., Adrian, S. A., Lukat-Rodgers, G. S., Collins, D. P., Dawson, J. H., Allen, C. E., Schmitt, M. P., Rodgers, K. R., and Dixon, D. W. (2015) Heme binding by *Corynebacterium diphtheriae* HmuT: Function and heme environment. *Biochemistry 54*, 6598-6609.

[14] Hunter, C. L., Mauk, A. G., and Douglas, D. J. (1997) Dissociation of heme from myoglobin and cytochrome *b*(5): Comparison of behavior in solution and the gas phase. *Biochemistry 36*, 1018-1025.

[15] Muraki, N., and Aono, S. (2016) Structural basis for heme recognition by HmuT responsible for heme transport to the heme transporter in *Corynebacterium glutamicum*. *Chem. Lett. 45*, 24-26.

[16] Ho, W. W., Li, H. Y., Eakanunkul, S., Tong, Y., Wilks, A., Guo, M. L., and Poulos, T. L. (2007) Holo-and apo-bound structures of bacterial periplasmic heme-binding proteins. *J. Biol. Chem. 282*, 35796-35802.

[17] Sook, B. R., Block, D. R., Sumithran, S., Montañez, G. E., Rodgers, K. R., Dawson, J. H., Eichenbaum, Z., and Dixon, D. W. (2008) Characterization of SiaA, a streptococcal heme-binding protein associated with a heme ABC transport system. *Biochemistry 47*, 2678-2688.

[18] Akbas, N., Draganova, E. B., Block, D. R., Sook, B. R., Chan, Y. F., Zhuo, J., Eichenbaum, Z., Rodgers, K. R., and Dixon, D. W. (2015) Heme-bound SiaA from *Streptococcus pyogenes*: Effects of mutations and oxidation state on protein stability. *J. Inorg. Biochem.*

[19] Moczygemba, C., Guidry, J., and Wittung-Stafshede, P. (2000) Heme orientation affects holo-myoglobin folding and unfolding kinetics. *FEBS Lett. 470*, 203-206.

[20] Pochapsky, T. C., Sligar, S. G., McLachlan, S. J., and La Mar, G. N. (1990) Relationship between heme binding site structure and heme orientations of two ferrocytochrome b_5s. A study in prosthetic group recognition. *J. Am. Chem. Soc 112*, 5258-5263.

[21] Honsa, E. S., Maresso, A. W., and Highlander, S. K. (2014) Molecular and evolutionary analysis of NEAr-iron Transporter (NEAT) domains. *PLoS One 9*.

[22] Andrade, M. A., Ciccarelli, F. D., Perez-Iratxeta, C., and Bork, P. (2002) NEAT: A domain duplicated in genes near the components of a putative Fe(3+) siderophore transporter from Gram-positive pathogenic bacteria. *Genome Biol. 3*, RESEARCH0047.

[23] Shepherd, M. (2015) The CydDC ABC transporter of Escherichia coli: new roles for a reductant efflux pump. *Biochem. Soc. Trans. 43*, 908-912.

[24] Martell, J. D., Li, H. Y., Doukov, T., Martasek, P., Roman, L. J., Soltis, M., Poulos, T. L., and Silverman, R. B. (2010) Heme-Coordinating Inhibitors of Neuronal Nitric Oxide Synthase. Iron-Thioether Coordination Is Stabilized by Hydrophobic Contacts without Increased Inhibitor Potency. *J. Am. Chem. Soc. 132*, 798-806.